Technical Report CHL-98-29
September 1998

US Army Corps of Engineers
Waterways Experiment Station

Assessment of Channel Deepening in the Delaware River and Bay

A Three-Dimensional Numerical Model Study

by Keu W. Kim, Billy H. Johnson

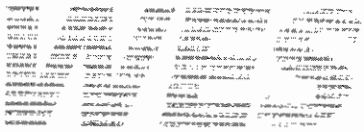

Prepared for U.S. Army Engineer District, Philadelphia

Technical Report CHL-98-29
September 1998

Assessment of Channel Deepening in the Delaware River and Bay

A Three-Dimensional Numerical Model Study

by Keu W. Kim, Billy H. Johnson

U.S. Army Corps of Engineers
Waterways Experiment Station
3909 Halls Ferry Road
Vicksburg, MS 39180-6199

Final report

Approved for public release; distribution is unlimited

Prepared for U.S. Army Engineer District, Philadelphia
Philadelphia, PA 19107-3390

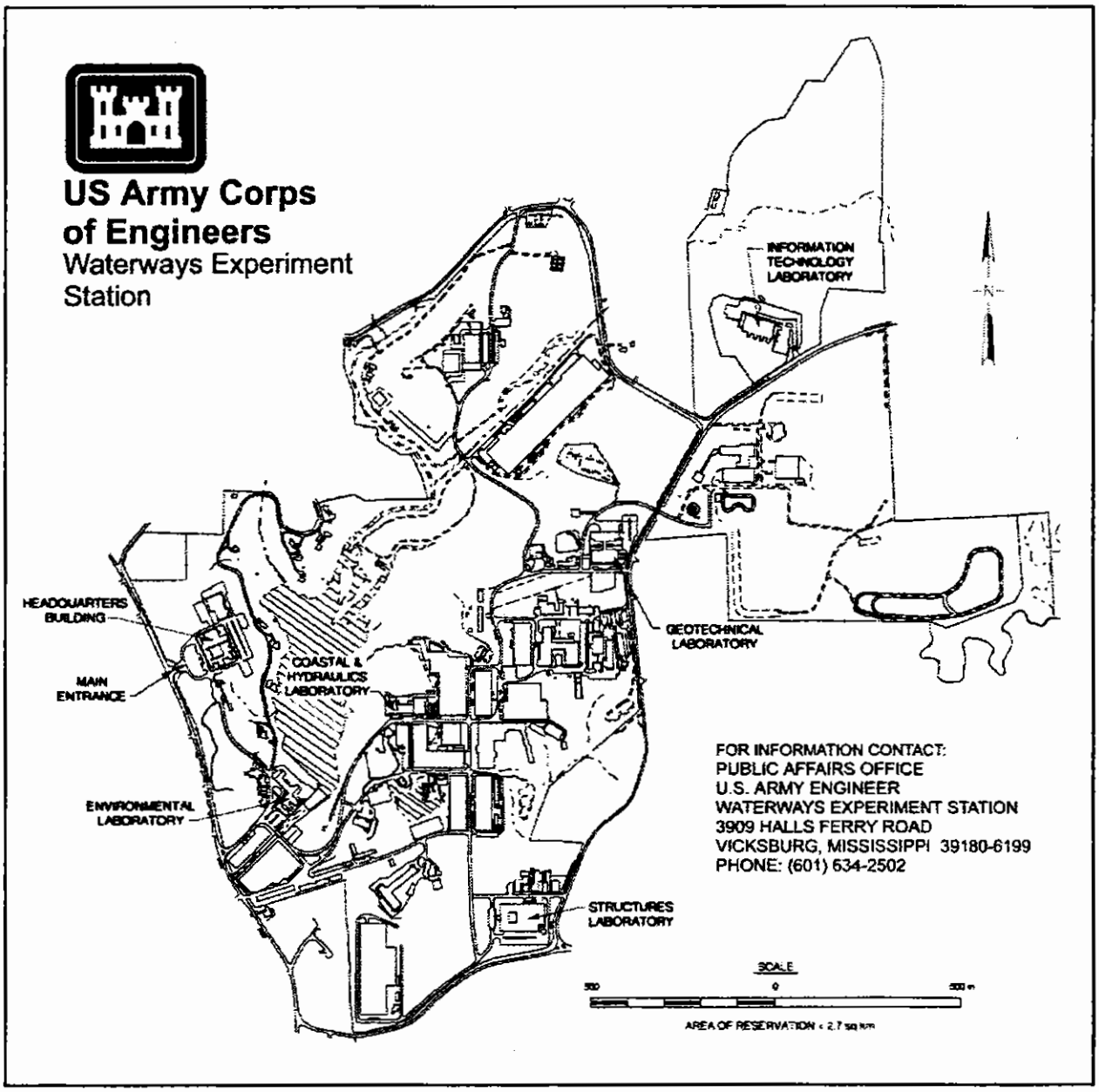

Waterways Experiment Station Cataloging-in-Publication Data

Kim, Keu W.

Assessment of channel deepening in the Delaware River and Bay : a three-dimensional numerical model study / by Keu W. Kim, Billy H. Johnson ; prepared for U.S. Army Engineer District, Philadelphia.

224 p. : ill. ; 28 cm. — (Technical report ; CHL-98-29)

Includes bibliographic references.

1. Delaware Bay (Del. and N.J.) 2. Chesapeake and Delaware Canal (Del. and Md.) 3. Chesapeake Bay (Md. and Va.) 4. Salinity — Evaluation. 5. Hydrodynamics — Testing. I. Johnson, Billy H. II. United States. Army. Corps of Engineers. Philadelphia District. III. U.S. Army Engineer Waterways Experiment Station. IV. Coastal and Hydraulics Laboratory (U.S. Army Engineer Waterways Experiment Station) V. Title. VI. Series: Technical report (U.S. Army Engineer Waterways Experiment Station) ; CHL-98-29.

TA7 W34 no.CHL-98-29

Contents

List of Figures

Preface

The study described herein was conducted during 1993-1997 for the U.S. Army Engineer District, Philadelphia, by personnel of the Hydraulics Laboratory (HL), U.S. Army Engineer Waterways Experiment Station (WES), under the general supervision of Mr. Frank A. Herrmann, Jr., Director, HL; Mr. Richard A. Sager, Acting Director, HL; and Mr. W. H. McAnally, Chief of the Waterways and Estuaries Division (WD), HL.

Drs. Keu W. Kim, WD, and Billy H. Johnson, HL, conducted the study and prepared this report.

This report is being published by the WES Coastal and Hydraulics Laboratory (CHL). The CHL was formed in October 1996 with the merger of the WES Coastal Engineering Research Center and Hydraulics Laboratory. Dr. James R. Houston is the Director of the CHL, and Mr. Charles C. Calhoun, Jr., is Assistant Director.

During the preparation and publication of this report, Director of WES was Dr. Robert W. Whalin. Commander was COL Robin R. Cababa, EN.

This report should be cited as follows:

Kim, K. W., and Johnson, B. H. (1998). "Assessment of Channel Deepening in the Delaware River and Bay; A Three-Dimensional Numerical Model Study," Technical Report CHL-98-29, U.S. Army Engineer Waterways Experiment Station, Vicksburg, MS.

1 Introduction

Background

Delaware Bay and River (Figure 1) is a major coastal plain estuary located on the east coast of the United States. The Delaware Bay and River extends for about 200 km from its connection to the Atlantic Ocean to the head of tide at Trenton, NJ. The system has a funnel shape with a relatively wide and shallow lower bay and a narrow upstream channel. The mean depth is about 25 ft[1] (7.62 m) with a dredged navigation channel of 40 ft (12.20 m) below mean lower low water (MLLW) maintained.

The Delaware River, gauged at Trenton, contributes about 60 percent of the total freshwater discharge into the bay with the Schuylkill River entering at Philadelphia, PA, contributing about 15 percent. Many other small streams contribute the remaining freshwater flow, with none contributing more than 5 percent. Mean annual flow from the two major contributors are 11,650 cfs (330 m^3/sec) and 2,950 cfs (84 m^3/sec), respectively. The total average annual inflow is about 20,350 cfs (577 m^3/sec). Tides are dominated by the semidiurnal M2 tide with the total tide range at the mouth being about 4 ft (1.22 m) but increasing to about 8 ft (2.44 m) at the head of tide at Trenton.

During low to average inflow periods, the Delaware Bay and River system is almost vertically mixed. Typical differences in salinity over the water column from top to bottom are about 1 ppt in the bay. However, during high-inflow periods significant stratification can develop. Thus, depending upon inflow conditions, Delaware Bay ranges from being classified as a well-mixed estuary to a partially stratified one.

The U. S. Army Engineer District, Philadelphia, has proposed deepening the existing 40-ft (12.22-m) navigation channel in Delaware Bay and River to 45 ft (13.72 m) below mean lower low water from the mouth of Delaware Bay and River to the Philadelphia and Camden, NJ, harbors. The proposed project would reduce waterborne transportation costs by minimizing the need for light loading

[1] All elevations and stages cited herein are referenced to the National Geodetic Vertical Datum (NGVD) unless otherwise specified. All depths are referenced to mean lower low water.

and lightering of bulk shipments and by encouraging the use of larger and more efficient transport vessels.

An environmental concern with the proposed deepening project is the potential for change in the estuary's salinity regime. While salinities fluctuate seasonally and from year to year, a permanent shift in salinity patterns could adversely impact water supplies in the Philadelphia-Camden area. These consist of water directly withdrawn from the river as well as water supplies obtained from adjacent aquifers that are in part recharged by river water. In addition, depending upon their magnitude, permanent changes in salinity patterns could adversely impact bay ecosystems. An example is the oyster beds located in the lower bay.

To address the issue of the impact of channel deepening on saltwater intrusion, the U.S. Army Engineer Waterways Experiment Station (WES) proposed the development of a three-dimensional (3-D) numerical hydrodynamic model of the bay. Since studies such as those by Wong (1990) have shown that a substantial fraction of the subtidal volume exchange in the Delaware estuary is associated with the exchange through the Chesapeake and Delaware (C&D) Canal, the model would need to include not only the Delaware Bay and River but also the C&D Canal and a portion of the Upper Chesapeake Bay.

Overview of Previous 3-D Model Studies of the Delaware-Chesapeake Bays System

WES has recently conducted two numerical modeling studies in the Chesapeake-Delaware Bay area. One involved the development of a 3-D hydrodynamic model of only the Chesapeake Bay and its major tributaries by Johnson et al. (1991) to provide flow fields to a 3-D water quality model developed during the same study by Cerco and Cole (1994). No coupling between the two bays was allowed, i.e., the C&D Canal was closed. The water quality model is being used by the Chesapeake Bay Program to determine

a. The relationship between nutrient loading and anoxia in Chesapeake Bay.

b. Critical nutrient(s) in control of eutrophication and anoxia.

c. Whether both point and nonpoint sources should be controlled.

d. The degree of control needed.

e. Which controls should be implemented first.

f. The length of time it will take for Chesapeake Bay water to improve once controls are implemented.

A follow-up study is now being conducted with the focus on water quality modeling in the major tributaries of the bay, e.g., James, York, etc.

The second study involved the development of a 3-D hydrodynamic model of the Upper Chesapeake Bay-C&D Canal-Delaware Bay and River system by Hsieh, Johnson, and Richards (1993) to provide insight into the direction and magnitude of net flows through the C&D Canal over various time periods. Since that study focused on the C&D Canal, there was not enough detail for use in this study.

Other 3-D modeling studies of Delaware Bay include those of Galperin and Mellor (1990) and Walters (1992). Galperin and Mellor developed a 3-D, time-dependent numerical model of the coupled bay and continental shelf. However, computed water-surface elevations at the mouth were replaced each time-step with observed data. There is concern over this type of simplistic data assimilation. In addition, grid resolution was quite coarse. Walters' model employs a finite-element spatial discretization with a harmonic decomposition in time, i.e., a spectral approach. Such models do not allow for aperiodic forcing of tide and salinity boundary conditions that are influenced by transient wind and freshwater events.

Approach and Scope

As previously noted, although during low-inflow periods the Delaware Bay and River are relatively well-mixed, a 3-D model of the Delaware-C&D Canal-Chesapeake system has been employed in the study since the system is partially stratified during some periods. Of course, in addition to density effects, wind forcing can also create vertical variations in the flow field. The same model applied in the previous studies by Johnson et al. (1991) and Hsieh, Johnson, and Richards (1993) has been applied. This model is referred to as CH3D-WES (Curvilinear Hydrodynamics in Three-Dimensions-WES).

The study consists of both the 3-D modeling component as well as an intensive one-year field data collection effort to provide data for the model. Before the model was applied to these data, several sensitivity studies were conducted with the model. These included grid and computational time-step convergence tests, as well as a sensitivity test to assess the impact of channel deepening on conditions at the mouth of the Delaware Bay.

At the conclusion of the sensitivity tests, the model was verified using the collected field data, along with data from a drought period in 1965. The model was subsequently applied with and without channel deepening to assess the impact on salinity intrusion and circulation. These impacts were determined for inflows ranging from those occurring during the drought of record in 1965 to extremely high inflows that occurred during April-May 1993. Other uses of the model were to assess the impact of a sea level rise and the impact of closing the C&D Canal on the hydrodynamics of both Delaware Bay and the Upper Chesapeake Bay.

As a final note, after the initial model study was completed and results were furnished to the District, it was discovered that portions of the bathymetric representation of the system were in error. Previously the 40-ft (12.20-m) channel was modeled as extending to Trenton. In reality, the 40-ft channel extended only to River Mile (RM) 127 with the depth being about 25 ft (7.62 m) from RM 127 to RM 132 and about 10 ft (3.05 m) from RM 132 to the head of tide at Trenton. In addition, even though the navigation channel is referred to as a 40-ft (12.20-m) channel, an inspection of historical channel surveys revealed several localized areas with depths exceeding 40 ft (12.20 m) for both the 1965 channel and the 1992-93 channel.

Further, in the initial 1965 verification effort, the C&D Canal was taken to be 25 ft (7.62 m) deep with a width of 400 ft (121.95 m). However, the actual channel in 1965 was 27 ft (8.23 m) by 250 ft (76.21 m), giving a flow area of 6,750 ft^2 (627.42 m^2). Thus, in the final 1965 verification presented herein, in addition to the bathymetric changes already noted, depths in the C&D Canal were set to yield a flow area more closely matching the actual flow area. For the 1992-93 verification and all subsequent production runs, the C&D depths were returned to 40 ft (12.20 m).

One additional change between the results presented herein and those previously given to the District concerns the number of freshwater inflows and background concentrations of nonsea salts attached to those inflows. In the earlier effort, which employed the bathymetry data that were in error, only seven inflow points were specified and the concentration of each was set to zero. In the results presented herein, 21 inflow points are prescribed with nonzero concentrations attached to the flow at Trenton and the flow from the Schuylkill River. Utilizing the additional inflow points provides for a better representation of the time and space distribution of freshwater inflows. These points were selected and flow data were provided by the Delaware River Basin Commission (DRBC).

2 Numerical Model

As previously noted, the particular hydrodynamic computer model employed is called CH3D-WES. The basic model (CH3D) was developed by Sheng[1] for WES but was extensively modified in its application to Chesapeake Bay. These modifications have consisted of different basic formulations as well as substantial recoding for more efficient computing. As its name implies, CH3D-WES makes hydrodynamic computations on a curvilinear or boundary-fitted planform grid. Physical processes impacting baywide circulation and vertical mixing that are modeled include tides, wind, density effects (salinity and temperature), freshwater inflows, turbulence, and the effect of the earth's rotation. Adequately representing the vertical turbulence is crucial to a successful simulation of stratification/destratification. A second-order turbulence model based upon the assumption of local equilibrium of turbulence is employed. The boundary-fitted coordinates feature of the model provides enhancement to fit the deep navigation channel and irregular shoreline configuration of the bay and permits adoption of an accurate and economical grid schematization. The solution algorithm employs an external mode consisting of vertically averaged equations to provide the solution for the free surface to the internal mode consisting of the full 3-D equations.

Basic Equations

The basic equations for an incompressible fluid in a right-handed Cartesian coordinate system (x, y, z) are[2]:

$$\frac{\partial u}{\partial x} + \frac{\partial v}{\partial y} + \frac{\partial w}{\partial z} = 0 \tag{1}$$

[1] Y. P. Sheng. (1986). "A three-dimensional mathematical model of coastal, estuarine and lake currents using boundary-fitted grid," Report No. 585, A.R.A.P. Group of Titan Research and Technology, Princeton, NJ.

[2] For convenience, symbols and unusual abbreviations are listed and defined in the Notation (Appendix A).

$$\frac{\partial u}{\partial t} + \frac{\partial u^2}{\partial x} + \frac{\partial uv}{\partial y} + \frac{\partial uw}{\partial z} = fv - \frac{1}{\rho}\frac{\partial p}{\partial x} + \frac{\partial}{\partial x}\left(A_H \frac{\partial u}{\partial x}\right)$$

$$+ \frac{\partial}{\partial y}\left(A_H \frac{\partial u}{\partial y}\right) + \frac{\partial}{\partial z}\left(A_v \frac{\partial u}{\partial z}\right) \qquad (2)$$

$$\frac{\partial v}{\partial t} + \frac{\partial uv}{\partial x} + \frac{\partial v^2}{\partial y} + \frac{\partial vw}{\partial z} = -fu - \frac{1}{\rho}\frac{\partial p}{\partial y} + \frac{\partial}{\partial x}\left(A_H \frac{\partial v}{\partial x}\right)$$

$$+ \frac{\partial}{\partial y}\left(A_H \frac{\partial v}{\partial y}\right) + \frac{\partial}{\partial z}\left(A_v \frac{\partial v}{\partial z}\right) \qquad (3)$$

$$\frac{\partial p}{\partial z} = -\rho g \qquad (4)$$

$$\frac{\partial T}{\partial t} + \frac{\partial uT}{\partial x} + \frac{\partial vT}{\partial y} + \frac{\partial wT}{\partial z}$$

$$= \frac{\partial}{\partial x}\left(K_H \frac{\partial T}{\partial x}\right) + \frac{\partial}{\partial y}\left(K_H \frac{\partial T}{\partial y}\right) + \frac{\partial}{\partial z}\left(K_v \frac{\partial T}{\partial z}\right) \qquad (5)$$

$$\frac{\partial S}{\partial t} + \frac{\partial uS}{\partial x} + \frac{\partial vS}{\partial y} + \frac{\partial wS}{\partial z}$$

$$= \frac{\partial}{\partial x}\left(K_H \frac{\partial S}{\partial x}\right) + \frac{\partial}{\partial y}\left(K_H \frac{\partial S}{\partial y}\right) + \frac{\partial}{\partial z}\left(K_v \frac{\partial S}{\partial z}\right) \qquad (6)$$

$$\rho = \rho\,(T,S) \qquad (7)$$

where

(u, v, w) = velocities in x-, y-, z-directions

t = time

f = Coriolis parameter defined as $2\Omega \sin \phi$ where Ω is the rotational speed of the earth and ϕ = latitude

ρ = density

p = pressure

A_H , K_H = horizontal turbulent eddy coefficients

A_v , K_v = vertical turbulent eddy coefficients

g = gravitational acceleration

T = temperature

S = salinity

Equation 4 implies that vertical accelerations are negligible. Thus, the pressure is hydrostatic.

Various forms of the equation of state can be used for Equation 7. In the present model, Equation 8 is used:

$$\rho = P/(\alpha + 0.698P) \tag{8}$$

where

$$P = 5890 + 38T - 0.375T^2 + 3S$$

$$\alpha = 1779.5 + 11.25T - 0.0745T^2$$

and T is in degrees Celsius, S is in parts per thousand, and ρ is in grams per cubic centimeter.

Nondimensionalization of Equations

Working with the dimensionless form of the governing equations makes it easier to compare the relative magnitude of various terms in the equations. Therefore, the following dimensionless variables are used:

$$(u^*, v^*, w^*) = (u, v, wX_r/Z_r)/U_r$$

$$(x^*, y^*, z^*) = (x, y, zX_r/Z_r)/X_r$$

$$(\tau_x^*, \tau_y^*) = (\tau_x^w, \tau_y^w)/\rho_o f Z_r U_r$$

$$t* = tf$$

$$\zeta^* = g\zeta/fU_rX_r = \zeta/S_r$$

$$\rho^* = (\rho - \rho_o)/(\rho_r - \rho_o)$$

$$T^* = (T - T_o)/(T_r - T_o)$$

$$A_H^* = A_H/A_{Hr}$$

$$A_v^* = A_v/A_{vr}$$

$$K_H^* = K_H/K_{Hr}$$

$$K_v^* = K_v/K_{vr}$$

where

(τ_x^w, τ_y^w) = wind stress in x-, y-directions

ζ = water-surface elevation

ρ_0, T_0 = typical values for the water density and temperature

and S_r, T_r, U_r, ρ_r, X_r, Z_r, A_{Hr}, A_{vr}, K_{Hr}, and K_{vr} are arbitrary reference values of the salinity, temperature, velocity, density, horizontal dimension, vertical dimension, horizontal viscosity, vertical viscosity, horizontal diffusion, and vertical diffusion. This then yields the following dimensionless parameters in the governing equations:

a. Vertical Ekman number:

$$E_v = A_{vr}/fZ_r^2$$

b. Lateral Ekman number:

$$E_H = A_{Hr}/fX_r^2$$

c. Vertical Prandtl (Schmidt) number:

$$Pr_v = A_{vr}/K_{vr}$$

d. Lateral Prandtl (Scmidt) number:

$$Pr_H = A_{Hr}/K_{Hr}$$

e. Froude number:

$$F_r = U_r/(gZ_r)^{1/2}$$

f. Rossby number:

$$R_o = U_r/fX_r$$

g. Densimetric Froude number:

$$Fr_D = F_r / \sqrt{\epsilon}$$

where

$$\epsilon = (\rho_r - \rho_o)/\rho_o$$

External-Internal Modes

The basic equations (Equations 1-4) can be integrated over the depth to yield a set of vertically integrated equations for the water surface, ζ, and unit flow rates U and V in the x- and y-directions. Using the dimensionless variables (asterisks have been dropped) and the parameters previously defined, the vertically integrated equations constituting the external mode are:

$$\frac{\partial \zeta}{\partial t} + \beta \left(\frac{\partial U}{\partial x} + \frac{\partial V}{\partial y} \right) = 0 \tag{9}$$

$$\frac{\partial U}{\partial t} = - H \frac{\partial \zeta}{\partial x} + \tau_{sx} - \tau_{bx} + V$$

$$- R_o \left[\frac{\partial}{\partial x} \left(\frac{UU}{H} \right) + \frac{\partial}{\partial y} \left(\frac{UV}{H} \right) \right]$$

$$+ E_H \left[\frac{\partial}{\partial x} \left(A_H \frac{\partial U}{\partial x} \right) + \frac{\partial}{\partial y} \left(A_H \frac{\partial U}{\partial y} \right) \right]$$

$$- \frac{R_o}{Fr_D^2} \frac{H^2}{2} \frac{\partial \rho}{\partial x} \tag{10}$$

$$\frac{\partial V}{\partial t} = - H \frac{\partial \zeta}{\partial y} + \tau_{sy} - \tau_{by} - U$$

$$- R_o \left[\frac{\partial}{\partial x} \left(\frac{UV}{H} \right) + \frac{\partial}{\partial y} \left(\frac{VV}{H} \right) \right]$$

$$+ E_H \left[\frac{\partial}{\partial x} \left(A_H \frac{\partial V}{\partial x} \right) + \frac{\partial}{\partial y} \left(A_H \frac{\partial V}{\partial y} \right) \right]$$

$$- \frac{R_o}{Fr_D^2} \frac{H^2}{2} \frac{\partial \rho}{\partial y} \qquad (11)$$

where

$$\beta = gZ_r/f^2X_r^2 = (R_o/F_r)^2$$

H = total depth

τ_s, τ_b = surface and bottom shear stresses.

As will be discussed later, the major purpose of the external mode is to provide the updated water-surface field.

The dimensionless form of the internal mode equations from which the 3-D velocity, salinity, and temperature fields are computed are:

$$\frac{\partial hu}{\partial t} = - h \frac{\partial \zeta}{\partial x} + E_v \frac{\partial}{\partial z} \left(A_v \frac{\partial hu}{\partial z} \right) + hv$$

$$- R_o \left(\frac{\partial huu}{\partial x} + \frac{\partial huv}{\partial y} + \frac{\partial huw}{\partial z} \right)$$

$$+ E_H \left[\frac{\partial}{\partial x} \left(A_H \frac{\partial hu}{\partial x} \right) + \frac{\partial}{\partial y} \left(A_H \frac{\partial hu}{\partial y} \right) \right]$$

$$- \frac{R_o}{Fr_D^2} \left(\int_z^\zeta \frac{\partial \rho}{\partial x} dz \right) \qquad (12)$$

$$\frac{\partial hv}{\partial t} = - h \frac{\partial \zeta}{\partial y} + E_v \frac{\partial}{\partial z}\left(A_v \frac{\partial hv}{\partial z}\right) - hu$$

$$- R_o \left(\frac{\partial hvu}{\partial x} + \frac{\partial hvv}{\partial y} + \frac{\partial hvw}{\partial z}\right)$$

$$+ E_H \left[\frac{\partial}{\partial x}\left(A_H \frac{\partial hv}{\partial x}\right) + \frac{\partial}{\partial y}\left(A_H \frac{\partial hv}{\partial y}\right)\right]$$

$$- \frac{R_o}{Fr_D^2}\left(\int_z^\zeta \frac{\partial \rho}{\partial y}\, dz\right) \qquad (13)$$

$$w_{k+1/2} = w_{k-1/2} - \left(\frac{\partial uh}{\partial x} + \frac{\partial vh}{\partial y}\right) \qquad (14)$$

$$\frac{\partial hT}{\partial t} = \frac{E_v}{Pr_v}\frac{\partial}{\partial z}\left(K_v \frac{\partial T}{\partial z}\right) - R_o\left(\frac{\partial huT}{\partial x} + \frac{\partial hvT}{\partial y} + \frac{\partial hwT}{\partial z}\right)$$

$$+ \frac{E_H}{Pr_H}\left[\frac{\partial}{\partial x}\left(K_H \frac{\partial hT}{\partial x}\right) + \frac{\partial}{\partial y}\left(K_H \frac{\partial hT}{\partial y}\right)\right] \qquad (15)$$

$$\frac{\partial hS}{\partial t} = \frac{E_v}{Pr_v}\frac{\partial}{\partial z}\left(K_v \frac{\partial S}{\partial z}\right) - R_o\left(\frac{\partial huS}{\partial x} + \frac{\partial hvS}{\partial y} + \frac{\partial hwS}{\partial z}\right)$$

$$+ \frac{E_H}{Pr_H}\left[\frac{\partial}{\partial x}\left(K_H \frac{\partial hS}{\partial x}\right) + \frac{\partial}{\partial y}\left(K_H \frac{\partial hS}{\partial y}\right)\right] \qquad (16)$$

In these equations h is the thickness of an internal layer, w is the vertical component of the velocity, and k+1/2 and k-1/2 represent the top and bottom, respectively, of the k^{th} vertical layer.

Boundary-Fitted Equations

To better resolve complex geometries in the horizontal directions, the CH3D-WES makes computations on the boundary-fitted or generalized curvilinear

planform grid shown in Figure 2. This necessitates the transformation of the governing equations into boundary-fitted coordinates (ξ,η). If only the x- and y-coordinates are transformed, a system of equations similar to those solved by Johnson (1980) for vertically averaged flow fields is obtained. However, in CH3D-WES not only are the x- and y-coordinates transformed into the (ξ,η) curvilinear system, but also the velocity is transformed such that its components are perpendicular to the (ξ,η) coordinate lines; i.e., contravariant components of the velocity are computed. This is accomplished by employing the following definitions for the components of the Cartesian velocity (u, v) in terms of contravariant components $\bar{u}$ and $\bar{v}$

$$u = x_\xi \bar{u} + x_\eta \bar{v}$$

$$v = y_\xi \bar{u} + y_\eta \bar{v}$$

along with the following expressions for replacing Cartesian derivatives

$$f_x = \frac{1}{J}\left[(fy_\eta)_\xi - (fy_\xi)_\eta \right]$$

$$f_y = \frac{1}{J}\left[- (fx_\eta)_\xi + (fx_\xi)_\eta \right]$$

where J is the Jacobian of the transformation defined as

$$J = x_\xi y_\eta - x_\eta y_\xi$$

With the governing equations written in terms of the contravariant components of the velocity, boundary conditions can be prescribed on a boundary-fitted grid in the same manner as on a Cartesian grid since $\bar{u}$ and $\bar{v}$ are perpendicular to the curvilinear cell faces (e.g., at a land boundary, either $\bar{u}$ or $\bar{v}$ is set to zero).

Initially the vertical dimension was handled through the use of what is commonly called a sigma-stretched grid. Such a grid is illustrated in Figure 3. However, with a sigma-stretched grid, the bottom layer in one column communicates with the bottom layer in an adjacent column. Thus, if depth changes are rather coarsely resolved, channel stratification cannot be maintained. As a result, the governing equations, Equations 17-21, presented for solution on the Cartesian or z-plane in the vertical direction are the ones constituting the internal mode.

With both the Cartesian coordinates and the Cartesian velocity transformed, the following boundary-fitted equations for $\bar{u}$, $\bar{v}$, w, S, and T to be solved in each vertical layer are obtained.

$$\frac{\partial h\bar{u}}{\partial t} = -h\left(\frac{G_{22}}{J^2}\frac{\partial\zeta}{\partial\xi} - \frac{G_{12}}{J^2}\frac{\partial\zeta}{\partial\eta}\right) + \frac{h}{J}\left(G_{12}\,\bar{u} + G_{22}\,\bar{v}\right) + \frac{R_o x_\eta}{J^2}\left[\frac{\partial}{\partial\xi}\left(Jy_\xi h\bar{u}\,\bar{u}\right.\right.$$

$$\left. + Jy_\eta h\bar{u}\,\bar{v}\right) + \frac{\partial}{\partial\eta}\left(Jy_\xi h\bar{u}\,\bar{v} + Jy_\eta h\bar{v}\,\bar{v}\right)\Big] - \frac{R_o y_\eta}{J^2}\left[\frac{\partial}{\partial\xi}\left(Jx_\xi h\bar{u}\,\bar{u} + Jx_\eta h\bar{u}\,\bar{v}\right)\right.$$

$$\left. + \frac{\partial}{\partial\eta}\left(Jx_\xi h\bar{u}\bar{v} + Jx_\eta h\bar{v}\bar{v}\right)\right] - R_o\left[\left(w\bar{u}\right)_{top} - \left(w\bar{u}\right)_{bot}\right]$$

$$+ E_v\left[\left(A_v\frac{\partial\bar{u}}{\partial z}\right)_{top} - \left(A_v\frac{\partial\bar{u}}{\partial z}\right)_{bot}\right] - \frac{R_o h}{Fr_D^2}\left[\int_z^\zeta\left(\frac{G_{22}}{J^2}\frac{\partial\rho}{\partial\xi}\right.\right.$$

$$\left.\left. - \frac{G_{12}}{J^2}\frac{\partial\rho}{\partial\eta}\right)dz\right] + \text{Horizontal Diffusion} \qquad (17)$$

$$\frac{\partial h\bar{v}}{\partial t} = -h\left(-\frac{G_{21}}{J^2}\frac{\partial\zeta}{\partial\xi} + \frac{G_{11}}{J^2}\frac{\partial\zeta}{\partial\eta}\right) - \frac{h}{J}\left(G_{11}\,\bar{u} + G_{21}\,\bar{v}\right) - \frac{R_o x_\xi}{J^2}\left[\frac{\partial}{\partial\xi}\left(Jy_\xi h\bar{u}\bar{u}\right.\right.$$

$$\left. + Jy_\eta h\bar{u}\bar{v}\right) + \frac{\partial}{\partial\eta}\left(Jy_\xi h\bar{u}\bar{v} + Jy_\eta h\bar{v}\bar{v}\right)\Big] + \frac{R_o y_\xi}{J^2}\left[\frac{\partial}{\partial\xi}\left(Jx_\xi h\bar{u}\,\bar{u} + Jx_\eta h\bar{u}\,\bar{v}\right)\right.$$

$$\left. + \frac{\partial}{\partial\eta}\left(Jx_\xi h\bar{u}\bar{v} + Jx_\eta h\bar{v}\bar{v}\right)\right] - R_o\left[\left(w\bar{v}\right)_{top} - \left(w\bar{v}\right)_{bot}\right]$$

$$+ E_v\left[\left(A_v\frac{\partial\bar{v}}{\partial z}\right)_{top} - \left(A_v\frac{\partial\bar{v}}{\partial z}\right)_{bot}\right] - \frac{R_o h}{Fr_D^2}\left[\int_z^\zeta\left(-\frac{G_{21}}{J^2}\frac{\partial\rho}{\partial\xi} + \frac{G_{11}}{J^2}\frac{\partial\rho}{\partial\eta}\right)dz\right]$$

$$+ \text{Horizontal Diffusion} \qquad (18)$$

$$w_{top} = w_{bot} - \frac{1}{J}\left(\frac{\partial J\bar{u}h}{\partial\xi} + \frac{\partial J\bar{v}h}{\partial\eta}\right) \qquad (19)$$

$$\frac{\partial hS}{\partial t} = \frac{E_v}{Pr_v}\left[\left(K_v \frac{\partial S}{\partial z}\right)_{top} - \left(K_v \frac{\partial S}{\partial z}\right)_{bot}\right] - \frac{R_o}{J}\left(\frac{\partial hJ\bar{u}S}{\partial \xi} + \frac{\partial hJ\bar{v}S}{\partial \eta}\right)$$

$$- R_o\left[(wS)_{top} - (wS)_{bot}\right] + \text{Horizontal Diffusion} \qquad (20)$$

$$\frac{\partial hT}{\partial t} = \frac{E_v}{Pr_v}\left[\left(K_v \frac{\partial T}{\partial z}\right)_{top} - \left(K_v \frac{\partial T}{\partial z}\right)_{bot}\right] - \frac{R_o}{J}\left(\frac{\partial hJ\bar{u}T}{\partial \xi} + \frac{\partial hJ\bar{v}T}{\partial \eta}\right)$$

$$- R_o\left[(wT)_{top} - (wT)_{bot}\right] + \text{Horizontal Diffusion} \qquad (21)$$

where

$$G_{11} = x_\xi^2 + y_\xi^2$$

$$G_{22} = x_\eta^2 + y_\eta^2$$

$$G_{12} = G_{21} = x_\xi x_\eta + y_\xi y_\eta$$

Similarly, the transformed external mode equations become:

$$\frac{\partial \zeta}{\partial t} + \beta\left(\frac{\partial \bar{U}}{\partial \xi} + \frac{\partial \bar{V}}{\partial \eta}\right) = 0 \qquad (22)$$

$$\frac{\partial \bar{U}}{\partial t} = -\frac{H}{J^2}\left(G_{22}\frac{\partial \zeta}{\partial \xi} - G_{12}\frac{\partial \zeta}{\partial \eta}\right)$$

$$+ \frac{1}{J}\left(G_{12}\bar{U} + G_{22}\bar{V}\right) + \frac{R_o x_\eta}{J^2 H}\left[\frac{\partial}{\partial \xi}\left(Jy_\xi \bar{U}\bar{U} + Jy_\eta \bar{U}\bar{V}\right) + \frac{\partial}{\partial \eta}\left(Jy_\xi \bar{U}\bar{V} + Jy_\eta \bar{V}\bar{V}\right)\right]$$

$$- \frac{R_o y_\eta}{J^2}\left[\frac{\partial}{\partial \xi}\left(Jx_\xi \bar{U}\bar{U} + Jx_\eta \bar{U}\bar{V}\right) + \frac{\partial}{\partial \eta}\left(Jx_\xi \bar{U}\bar{V} + Jx_\eta \bar{V}\bar{V}\right)\right]$$

$$+ \tau_{s\xi} - \tau_{b\xi} - \frac{R_o}{Fr_D^2}\frac{H^2}{2}\left(G_{22}\frac{\partial \rho}{\partial \xi} - G_{12}\frac{\partial \rho}{\partial \eta}\right)$$

+ Horizontal Diffusion (23)

$$\frac{\partial \overline{V}}{\partial t} = -\frac{H}{J^2}\left(-G_{21}\frac{\partial \zeta}{\partial \xi} + G_{11}\frac{\partial \zeta}{\partial \eta}\right) - \frac{1}{J}\left(G_{11}\overline{U} + G_{21}\overline{V}\right)$$

$$-\frac{R_o x_\xi}{J^2 H}\left[\frac{\partial}{\partial \xi}\left(Jy_\xi \overline{U}\overline{U} + Jy_\eta \overline{U}\overline{V}\right) + \frac{\partial}{\partial \eta}\left(Jy_\xi \overline{U}\overline{V} + Jy_\eta \overline{V}\overline{V}\right)\right]$$

$$+\frac{R_o y_\xi}{J^2 H}\left[\frac{\partial}{\partial \xi}\left(Jx_\xi \overline{U}\overline{U} + Jx_\eta \overline{U}\overline{V}\right) + \frac{\partial}{\partial \eta}\left(Jx_\xi \overline{U}\overline{V} + Jx\eta \overline{V}\overline{V}\right)\right]$$

$$+\tau_{s\eta} - \tau_{b\eta} - \frac{R_o}{Fr_D^2}\frac{H^2}{2}\left(-G_{21}\frac{\partial \rho}{\partial \xi} + G_{11}\frac{\partial \rho}{\partial \eta}\right)$$

+ Horizontal Diffusion (24)

where $\overline{U}$ and $\overline{V}$ are contravariant components of the vertically averaged velocity.

Equations 22-24 are solved first to yield the water-surface elevations, which are then used to evaluate the water-surface slope terms in the internal mode equations. The horizontal diffusion terms are quite lengthy and are given by Johnson et al. (1991).

Boundary Conditions

The boundary conditions at the free surface are

$$A_v\left(\frac{\partial \overline{u}}{\partial z}, \frac{\partial \overline{v}}{\partial z}\right) = \left(\tau_{s_\xi}, \tau_{s_\eta}\right)/\rho = \left(CW_\xi^2, CW_\eta^2\right) \quad (25)$$

$$\frac{\partial T}{\partial z} = \frac{Pr}{E_v} K(T - T_e) \quad (26)$$

$$\frac{\partial S}{\partial z} = 0 \quad (27)$$

whereas the boundary conditions at the bottom are

$$A_v \left(\frac{\partial \bar{u}}{\partial z} , \frac{\partial \bar{v}}{\partial z} \right) = \left(\tau_{b_\xi} , \tau_{b_\eta} \right) / \rho = \frac{U_r}{A_{vr}} Z_r C_d \left(\bar{u}_1^2 + \bar{v}_1^2 \right)^{1/2} \left(\bar{u}_1, \bar{v}_1 \right) \quad (28)$$

$$\frac{\partial T}{\partial z} = 0 \quad (29)$$

$$\frac{\partial S}{\partial z} = 0 \quad (30)$$

where

C = surface drag coefficient

W = wind speed

K = surface heat exchange coefficient

T_e = equilibrium temperature

C_d = bottom friction coefficient

$\bar{u}_1, \bar{v}_1$ = values of the horizontal velocity components next to the bottom

With z_1 equal to one-half the bottom layer thickness, C_d is given by

$$C_d = k^2 \left[\ln \left(z_1 / z_o \right) \right]^{-2} \quad (31)$$

where

k = von Karman constant

z_o = bottom roughness height

Manning's formulation is employed for the bottom friction in the external mode equations if the model is used purely to compute vertically averaged flow fields. As presented by Garratt (1977), the surface drag coefficient is computed from

$$C = (0.75 + 0.067W) \times 10^{-3} \quad (32)$$

with the maximum allowable value being 0.003. As discussed by Edinger, Brady, and Geyer (1974), the surface heat exchange coefficient, K, and the equilibrium

temperature, T_e, are computed from the meteorological data (wind speed, cloud cover, wet and dry bulb air temperatures, and relative humidity).

Along the shoreline where river inflow occurs, the freshwater inflow and its temperature are prescribed and the salinity is normally assumed to be zero. However, as previously noted, in the Delaware Model, nonzero nonsea salt concentrations are prescribed for Delaware and Schuylkill riverflows. All other freshwater inflows are considered to be lateral inflows with a zero salt concentration. At an ocean boundary, the water-surface elevation is prescribed along with time-varying vertical distributions of salinity and temperature. During flood, the specified values of salinity and temperature are employed, whereas during ebb, interior values are advected out of the grid. Along a solid boundary, the normal component of the velocity and the viscosity and diffusivity are set to zero.

Initial Conditions

At the start of a model run, the values of ζ, $\overline{u}$, $\overline{v}$, w, $\overline{U}$ and $\overline{V}$ are all set to zero. Values of the salinity and temperature are read from input files. These initial fields are generated from known data at a limited number of locations. Once the values in individual cells are determined by interpolating from the field data, the resulting 3-D field is smoothed several times. Generally, the salinity and temperature fields are frozen for the first few days of a simulation.

Numerical Grid

A staggered grid is used in both the horizontal and vertical directions of the computational domain. In the horizontal directions, a unit cell consists of a ζ-point in the center ($\zeta_{i,j}$), a U-point on its left face ($U_{i,j}$), and a V-point on its bottom face ($V_{i,j}$). In the vertical direction, the vertical velocities are computed at the "full" grid points. Horizontal velocities, temperature, salinity, and density are computed at the "half" grid points (half grid spacing below the full points).

Numerical Solution Algorithm

Finite differences are used to replace derivatives in the governing equations, resulting in a system of linear algebraic equations to be solved in both the external and internal modes.

The external mode solution consists of the surface displacement and vertically integrated contravariant unit flows $\overline{U}$ and $\overline{V}$. All of the terms in the transformed vertically averaged continuity equation are treated implicitly whereas only the water-surface slope terms in the transformed vertically averaged momentum equations are treated implicitly. If the external mode is used purely as a vertically averaged model, the bottom friction is also treated implicitly. Those terms treated

implicitly are weighted between the new and old time-steps. The resulting finite difference equations are then factored such that a ξ-sweep followed by an η-sweep of the horizontal grid yields the solution at the new time-step.

Writing Equations 9-11 as

$$\frac{\partial \zeta}{\partial t} + \beta \left(\frac{\partial \overline{U}}{\partial \xi} + \frac{\partial \overline{V}}{\partial \eta} \right) = 0 \tag{33}$$

$$\frac{\partial \overline{U}}{\partial t} + \frac{H}{J^2} G_{22} \frac{\partial \zeta}{\partial \eta} = M \tag{34}$$

$$\frac{\partial \overline{V}}{\partial t} + \frac{H}{J^2} G_{11} \frac{\partial \zeta}{\partial \eta} = N \tag{35}$$

where M and N are the remaining terms in Equations 10 and 11, the ξ-sweep is

$$\xi\text{-sweep} \Rightarrow \zeta_{ij}^{*} + \frac{\beta\theta\Delta t}{\Delta\xi} \left(\overline{U}_{i+1,j}^{*} - \overline{U}_{ij}^{*} \right)$$

$$= \zeta_{ij}^{n} (1-\theta) \frac{\Delta t}{\Delta \xi} \left(\overline{U}_{i+1,j}^{n} - \overline{U}_{ij}^{n} \right) \frac{\Delta t}{\Delta \eta} \left(\overline{V}_{ij+1}^{n} - \overline{V}_{ij}^{n} \right) \tag{36}$$

where θ is a parameter determining the degree of implicitness and

$$\overline{U}_{ij}^{n+1} + \frac{\theta \Delta t H G_{22}}{\Delta \xi J^2} \left(\zeta_{ij}^{*} - \zeta_{i-1,j}^{*} \right) = \overline{U}_{ij}^{n} - (1 - \theta) \frac{\Delta t H G_{22}}{\Delta \xi J^2} \left(\zeta_{ij}^{n} - \zeta_{i-1,j}^{n} \right) + \Delta t \, M^{n} \tag{37}$$

The η-sweep then provides the updated ζ and $\overline{V}$ at the $n + 1$ time level.

$$\eta\text{-sweep} \Rightarrow \zeta_{ij}^{n+1} + \frac{\beta\theta\Delta t}{\Delta\eta} \left(\overline{V}_{i,j+1}^{n+1} - \overline{V}_{ij}^{n+1} \right) = \zeta_{i,j}^{*}$$

$$- (1 - \theta) \frac{\Delta t}{\Delta \eta} \left(\overline{V}_{i,j+1}^{n} - \overline{V}_{i,j}^{n} \right) + \frac{\Delta t}{\Delta \eta} \left(\overline{V}_{i,j+1}^{n} - \overline{V}_{i,j}^{n} \right) \tag{38}$$

and

$$\overline{V}_{i,j}^{n+1} + \frac{\theta \Delta t HG_{11}}{\Delta \eta \, J^2} \left(\zeta_{i,j+1}^{n+1} - \zeta_{i,j}^{n+1} \right)$$

$$= V_{i,j}^{n} - (1 - \theta) \frac{\Delta t HG_{11}}{\Delta \eta \, J^2} \left(\zeta_{i,j+1}^{n} - \zeta_{i,j}^{n} \right) + \Delta t \, N^{n} \qquad (39)$$

A typical value of θ of 0.55 yields stable and accurate solutions.

The internal mode consists of computations from Equations 17-21 for the three velocity components $\bar{u}$, $\bar{v}$, and w, salinity, and temperature. The only terms treated implicitly are the vertical diffusion terms in all equations and the bottom friction and surface slope terms in the momentum equations. Values of the water-surface elevations from the external mode are used to evaluate the surface slope terms in Equations 17 and 18. As a result, the extremely restrictive speed of a free-surface gravity wave is removed from the stability criteria. Roache's second upwind differencing is used to represent the convective terms in the momentum equations, whereas a spatially third-order scheme developed by Leonard (1979) called QUICKEST is used to represent the advective terms in Equations 20 and 21 for salinity and temperature, respectively. For example, if the velocity on the right face of a computational cell is positive, then with QUICKEST the value of the salinity used to compute the flux through the face is

$$S_R = \frac{1}{2} \left(S_{i,j,k} + S_{i+1,j,k} \right) - \frac{1}{6} \left[1 - \left(\frac{\overline{U}_{i+1,j,k} \, \Delta t}{\Delta \xi} \right)^2 \right] \left(S_{i+1,j,k} - 2S_{i,j,k} + S_{i-1,j,k} \right)$$

$$- \frac{1}{2} \frac{U_{i+1,j,k} \, \Delta t}{\Delta \xi} \left(S_{i+1,j,k} - S_{i,j,k} \right) \qquad (40)$$

Turbulence Parameterization

Vertical turbulence is modeled using the concept of eddy viscosity and diffusivity to represent the velocity and density correlation terms that arise from a time averaging of the governing equations. These eddy coefficients are computed from mean flow characteristics using a simplified second-order closure model originally developed by Donaldson (1973). The closure model has been further developed and applied to various types of flows by Lewellen (1977) and Sheng (1982). A discussion of the implementation of the turbulence model taken from

Sheng[1] follows. For more details, consult these references and Johnson et al. (1991).

Assuming local equilibrium of turbulence, i.e., there is no time evolution or spatial diffusion of the second-order correlations, an equation relating the turbulent kinetic energy and the macroscale of turbulence to the mean flow shear and stratification (given by the Richardson number Ri) can be derived as

$$3A^2b^2sQ^4 + A[(bs + 3b + 7b^2s)\,Ri - Abs(1 - 2b)]Q^3 + b(s + 3 + 4bs)Ri^2 + (bs - A)(1 - 2b)\,Ri = 0 \tag{41}$$

where

$A = 0.75$

$b = 0.125$

$s = 1.8$

and

$$Q = \frac{q}{\Lambda\sqrt{(\partial\bar{u}/\partial z)^2 + (\partial\bar{v}/\partial z)^2}} \tag{42}$$

In this expression, q is defined as

$$q = \left(\overline{u'u'} + \overline{v'v'} + \overline{w'w'}\right)^{1/2}$$

and Λ is the macroscale of turbulence, u', v', and w' are the turbulent velocity fluctuations, and the overbar indicates time averaging.

It can also be shown that the following relations hold:

$$\overline{u'w'} = -\frac{\dfrac{\partial\bar{u}}{\partial z}\,\Lambda}{q}\,\frac{1 + \dfrac{\bar{\omega}}{A}}{1 - \omega}\,\overline{w'w'} \tag{43}$$

---

[1] Y. P. Sheng. (1990). "A simplified second order closure model of turbulent transport," unpublished paper prepared for the U.S. Army Engineer Waterways Experiment Station, Vicksburg, MS.

$$\overline{v'w'} = -\frac{\frac{\partial \bar{v}}{\partial z}\Lambda}{q}\frac{1+\frac{\bar{\omega}}{A}}{1-\omega}\overline{w'w'} \tag{44}$$

$$q^2 b = \left[\frac{\left(1+\frac{\bar{\omega}}{A}\right)}{Q^2(1-\omega)} + \bar{\omega}\right]\overline{w'w'} \tag{45}$$

where

$$\omega = \frac{Ri}{AQ^2}$$

and

$$\bar{\omega} = \frac{\omega}{1-\frac{\omega}{bs}}$$

Thus, after the velocity shear and flow stratification are determined, q can be computed from Equations 41 and 42. $\overline{w'w'}$ is then determined from

$$\overline{w'w'} = \frac{\frac{q^2}{2} - q^2 b}{\frac{3}{2}(1-2\omega)} \tag{46}$$

Finally, after Λ is prescribed, $\overline{u'w'}$ and $\overline{v'w'}$ can be computed from Equations 43 and 44 and the vertical eddy coefficients can be determined from

$$A_v = \frac{\overline{-u'w'}}{\frac{\partial \bar{u}}{\partial z}} = \frac{\Lambda}{q}\frac{A+\bar{\omega}}{A(1-\omega)}\overline{w'w'} \tag{47}$$

$$K_v = \frac{\overline{-\rho'w'}}{\frac{\partial \rho}{\partial z}} = \frac{\Lambda}{q}\frac{bs}{(bs-\omega)A}\overline{w'w'} \tag{48}$$

where ρ' is the turbulent density fluctuation.

In addition to setting $\Lambda = 0.65z$ near boundaries, three basic constraints are used to compute Λ at a vertical position z:

$$\left|\frac{d\Lambda}{dz}\right| \leq 0.65 \tag{49}$$

$$\Lambda \leq \frac{q}{N} = \frac{q}{\left(-\frac{g}{\rho}\frac{\partial \rho}{\partial z}\right)^{0.5}} \tag{50}$$

$$\Lambda \leq Q_{cut}\left(z_{q=qmax} - z_{q=qmax/2}\right) \tag{51}$$

where N is the Brunt-Vaisala frequency. Equation 51 states that Λ is less than a fraction of the spread of turbulence as measured by the distance between the location of a maximum q^2 to where q^2 is equal to 25 percent of the maximum. The coefficient Q_{cut} is on the order of 0.15 to 0.25.

3 Field Data Collection Program

A successful verification of the 3-D hydrodynamic model of the Delaware Bay-C&D Canal-Chesapeake Bay system requires field data. These data must contain freshwater inflows; tides at the bay entrance and at Annapolis, MD, as well as at various interior stations; wind data at one or more stations from which the surface wind stress can be determined; and currents and salinity at several locations throughout the bay. With the modeled system being so large, there is a lack of synoptic data throughout the Delaware Bay, the C&D Canal, and the upper Chesapeake Bay. Therefore, to provide data for the numerical model study, WES and the Philadelphia District conducted a detailed field data collection program that began in October 1992 and concluded in October 1993. Details of the data collection program are presented in Fagerburg and Benson (1995).

The field data collection program consisted of both short-term and long-term continuous recording of tide, velocity, and salinity data. The two short-term (2 weeks) field data sets covered 12-25 October 1992 and 19-30 April 1993. The data collection stations were positioned at various locations from Wilmington, DE, to the entrance of Delaware Bay, as well as within the C&D Canal and in Upper Chesapeake Bay. As illustrated in Figure 4, a total of seven data collection ranges with two to four stations per range were monitored for current and salinity at three to five depths.

During the long-term data collection, a total of 13 stations were maintained at various times throughout the Delaware Bay, C&D Canal, and Upper Chesapeake Bay to provide data on water-surface elevations, velocity, and salinity at an interval of 15 minutes. The locations of these stations are shown in Figure 5. Due to equipment problems, as well as the loss of several instruments, all stations did not record data for the complete year. Table 1 gives the recording history of the stations illustrated in Figure 5.

Although these data were used primarily to verify that the 3-D model could reproduce observed conditions in the bay, the data were also used in the assessment of channel deepening on salinity intrusion. During most of the October 1992-October 1993 period, freshwater inflows were close to average inflow conditions. However, during April-May 1993 a large spring runoff event

occurred. Data collected at the model boundaries during this time were used to assess the impact of channel deepening during periods of high freshwater inflow (see Chapter 6).

Table 1
Recording History of Long-Term Meters

Station No.	Instrument Type	Data Collected	Depth of Deployment	Latitude/ Longitude	Period of Deployment
S0.8	ENDECO 1152	Water levels Salinity	Near-surface	38° 47' 22" 75° 06' 10"	10/92-10/93
S1.2	DATASONDE 3	Salinity	20% of depth 80% of depth	38° 56' 12" 75° 03' 27"	11/92-01/93
S1.3	DATASONDE 3	Salinity	20% of depth 50% of depth 80% of depth	38° 41' 13" 75° 07' 11"	10/92-02/93
S1.4	DATASONDE 3	Salinity	20% of depth 50% of depth 80% of depth	38° 52' 11" 75° 06' 54"	03/93-04/93 06/93-10/93 03/93-07/93
S1.8	DATASONDE 3	Salinity	20% of depth 50% of depth 80% of depth	39° 09' 31" 75° 06' 54"	10/92-11/92 04/93-10/93
	ENDECO 174	Velocity Direction Salinity	60% of depth		
S3.2	DATASONDE 3	Salinity	20% of depth 80% of depth	39° 27' 35" 75° 34' 14"	04/93
S3.5	DATASONDE 3	Salinity	20% of depth 80% of depth	39° 33' 31" 75° 34' 23"	10/92-10/93
	ENDECO 174	Velocity Direction Salinity	60% of depth	39° 33' 31" 75° 34' 23"	10/92-10/93
S3.9	DATASONDE 3	Salinity	80% of depth	39° 32' 30" 75° 44' 30"	10/92-10/93
	ENDECO 174	Velocity Direction Salinity	60% of depth		
	ENDECO 1029	Water level	Near-surface		
S4.8	DATASONDE 3	Salinity	20% of depth 80% of depth	39° 31' 45" 75° 51' 43"	01/93-10/93
	ENDECO 174	Velocity Direction Salinity	60% of depth		

(Continued)

Table 1 (Concluded)

Station No.	Instrument Type	Data Collected	Depth of Deployment	Latitude/ Longitude	Period of Deployment
S4.9	DATASONDE 3	Salinity	20% of depth 80% of depth	39° 31' 08" 75° 52' 47"	10/92-12/92
	ENDECO 174	Velocity Direction Salinity	60% of depth		
S6.2	DATASONDE 3	Salinity	20% of depth	38° 59' 38" 76° 23' 18"	10/92-12/92 05/93-10/93
			50% of depth		10/92-12/92
			80% of depth		06/93-10/93
			99% of depth		10/92-12/92
S6.3	DATASONDE 3	Salinity	20% of depth 50% of depth 99% of depth	38° 59' 07" 76° 21' 13"	10/92-12/92 03/93-10/93
S6.4	ENDECO 1029	Water level	Near-surface	38° 58' 48" 76° 2' 09"	10/92-10/93

4 Model Sensitivity Results

This chapter presents results from grid convergence runs, time-step convergence runs, and model runs and assesses the impact of channel deepening on flow conditions at the bay mouth. Boundary conditions for the convergence runs and part of the boundary conditions for the run to investigate conditions at the mouth were provided by Hsieh, Johnson, and Richards (1993). These data were for September 1984.

Grid Convergence Results

The initial planform boundary-fitted grid generated for the modeled system is shown in Figure 6. This grid was generated to force grid lines to follow navigation channels in both the Delaware and Upper Chesapeake Bays and to represent the geometry in a reasonable fashion while keeping the total number of grid cells to a minimum. Although, based upon past experience, the grid was considered adequate for the study, an integral part of grid generation for any numerical model study is to assess the impact that the grid has on the computed solution. In other words, as the grid is refined, does the solution being computed upon the grid significantly change?

To address this basic question, the grid resolution in Figure 6 was doubled in the lower bay (Figure 7) with the results computed using this grid then compared with those obtained using the initial grid. As illustrated in Figures 8 and 9, computed water-surface elevations and velocity from both grids at the location labeled *A* on Figure 7 were virtually identical. Similar results were obtained at all other locations where results were compared. However, as illustrated in Figure 10, small differences in the computed salinity occurred. Thus, based upon the grid convergence runs, the grid shown in Figure 6 was considered questionable for the study. In addition, through consultation with various environmental groups in the Delaware Bay community, it was decided that additional resolution was desirable in the lower bay near the eastern shore where oyster beds exist, as well as in the vicinity of Philadelphia where water intakes exist. Thus, the grid presented in Figure 2 is the final grid used in the study. With this grid density, grid effects are minimal.

The final grid contains about 3,500 planform cells. With a maximum of 18 layers in the vertical, the total number of computational cells is about 13,000. Each of the vertical layers is 5 ft (1.52 m) except for the top layer, which varies in thickness with the tide. Typical horizontal dimensions of the grid in the Delaware River are 400 ft (122 m) by 1,000 ft (305 m), whereas those in the lower Delaware Bay are 1,000 ft (305 m) by 3,000 ft (915 m).

Time-Step Convergence Results

As with any numerical solution scheme, the solution scheme employed in CH3D-WES contains truncation errors associated with not only the spatial discretization but also the computational time-step. As with the grid convergence exercise described in the previous section, there is a need in any numerical modeling study to assess the impact of the time-step on the solution being computed. This was accomplished by making model runs with decreasing time-steps and comparing computed results at several locations throughout the computational grid. Figures 11-13 illustrate the impact of decreasing the time-step from 2 minutes to 1 minute at location *A* in Figure 7. Results showed that there is a noticeable difference between the solution generated using a 4-minute time-step and that generated using a time-step of 2 minutes. However, the solutions generated using a 2-minute step and a 1-minute time-step are virtually identical. Results were similar at several other locations where comparisons were made. Therefore, all computations were subsequently made using a 2minute time-step.

Impact of Channel Deepening on Conditions at the Bay Mouth

The field data collection discussed in Chapter 3 provided data for model verification. In addition, researchers wanted to be able to use these data at the model boundaries for assessing the impact of channel deepening on salinity conditions in the system. However, before the observed data at the bay mouth could be used to drive model runs with and without the deepening project, the impact of the deepening on conditions at the mouth had to be determined.

To provide insight, computations were made on the numerical grid shown in Figure 14 with and without the proposed channel deepening. Computed results from the two simulations were then compared at locations across the bay mouth.

As previously noted, September 1984 data obtained from Hsieh, Johnson, and Richards (1993) were used to partially drive the model. However, the water-surface elevation time-series used to drive the model's open water boundaries were derived from harmonic analysis using Schwiderski's Global Ocean Random-Point Tide (RPTIDE) program (Schwiderski and Szeto 1981). Tidal elevations along the cross-shore boundaries were linearly interpolated between tidal elevations at the coast and the offshore boundary. Constant salinities were

specified along the open ocean boundaries. These boundary conditions are considered adequate to address the impact of channel deepening on conditions at the bay mouth.

Comparisons of the water-surface elevation, velocity, and salinities at the bay mouth with and without the deepened channel are presented in Figures 15-17, respectively. The maximum difference in the velocity is 0.41 cm/sec with the maximum difference in the salinity being 0.06 ppt. As for the water surface, the impact of the deepened channel on velocity and salinity at the bay mouth is negligible. These results imply that since the deepening project does not extend to the bay mouth (terminates about 15 km above the bay entrance) the impact on existing flow conditions at the mouth is negligible. Therefore, the numerical grid shown in Figure 2, without the ocean segment, with the bay mouth driven by observed data was employed for model verification and for subsequently assessing the impact of channel deepening on salinity intrusion and circulation in the Delaware Bay. In addition, the impacts of a sea level rise and the closing of the C&D Canal have been addressed by driving the model at the mouth.

5 Model Verification

Field data collected during October 1992 and April 1993, along with data from the drought period of June-November 1965, have been used to verify the 3-D numerical model. This chapter presents results from the simulations with each of these data sets.

As previously discussed, these results reflect the changes made to the model bathymetry after the initial study to more accurately reflect actual conditions during both 1992-93 and 1965 and the additional freshwater inflows. Areas below Philadelphia, PA, where depths are greater than 40 ft (13.20 m) are given in Table 2. Delaware Bay and River Miles (RM) are shown in Figure 18.

Table 2
Depths Greater than 40 ft (12.20 m)

Location, RM	1965 Depth, ft	1992-93 Depth, ft
77.7 - 76.7	45	45
70.0 - 69.0	50	55
69.0 - 68.0	40	45
57.7 - 56.7	45	50
56.7 - 55.7	50	50
50.4 - 49.0	45	45
41.4 - 40.4	50	50
40.4 - 39.4	50	55
39.4 - 37.4	45	55
37.4 - 32.4	45	45
32.4 - 31.4	45	50
31.4 - 30.4	50	50
30.4 - 30.0	40	50
30.0 - 29.0	45	50
28.0 - 27.0	45	50
10.7 - 8.7	45	45
8.7 - 7.7	40	45

The locations of the 21 inflow points employed in the model are given in Table 3.

Table 3
Freshwater Inflows

Name	Location, RM
Susquehanna River	Inflow to Chesapeake Bay
Delaware River at Trenton	135
Crosswicks Creek	129.3
Neshaminy Creek	115.80
Rancocas Creek	111.8
Pennsauken Creek	105.0
Cooper River	102.3
Timber Creek	95.6
Schuylkill River	Enters Delaware River at 92.5
Mantua Creek	88.9
Chester Creek	83.5
Raccoon Creek	80.8
Oldsmans Creek	78.1
Christina River	71.4
Salem Creek	59.2
Alloway and Augustine Creek	55.2
Cohansey River	39.0
Leipsic River	35.0
St. Jones River	22.4
Maurice River	20.0
Mispillion River	12.3

Time-varying background chlorinity concentrations prescribed at Trenton were normally at or below 15 ppm, whereas those on the Schuylkill were higher, e.g., in the 20- to 30-ppm range. Chlorinity concentrations of all other inflows were set to zero. This has essentially no impact since the flow rates of those inflows are quite small.

The major parameter available for model calibration is the bottom drag coefficient. The final values selected are given in Table 4. These values were determined to yield the best match of computed and observed data throughout the

Table 4 Bottom Drag Coefficients	
Location	**Value**
Upper Chesapeake Bay	0.0025
C&D Canal	0.0035
Delaware Bay RM 0-RM 25	0.0025
RM 25-RM 83	0.0017
RM 83-RM 100	0.0022
RM 100-Trenton	0.0025

modeled system. The range of values agrees well with typical values employed by other researchers, e.g., Walters (1992).

October 1992 Simulation

The October 1992 period represented an inflow that was slightly below the long-term average inflow for this month. Inflows on the Delaware, Schuylkill, and Susquehanna Rivers for this period are presented in Figures 19-21, respectively, whereas water-surface elevations at the Delaware Bay mouth and Annapolis are presented in Figures 22 and 23. An analysis of the tidal records at Cape May and Cape Henlopen did not reveal a tilt in the water surface across the bay mouth, so the record shown in Figure 22 was specified in each cell across the mouth. The tide at Annapolis was similarly applied there.

The surface and bottom salinity boundary conditions at the Delaware Bay mouth and Annapolis are shown in Figures 24 and 25. Values at other depths were determined using a linear interpolation. Field data indicate that generally the salinity is higher by about 2 ppt at the northern end of the bay mouth. Thus, the salinities shown in Figure 24 were applied at the southernmost end of the Delaware Bay mouth and then linearly increased across the Delaware Bay mouth by 2 ppt at the northernmost end to approximately represent observed lateral variations. There was no lateral variation prescribed in the salinity at the Annapolis boundary. Note that little stratification is observed at the Delaware Bay mouth, whereas salinity differences between the surface and bottom of the water column at Annapolis are about 5 ppt.

Wind data were available at four locations, namely, Wilmington International Airport, Baltimore-Washington International Airport (BWI), Dover Air Force Base, and Millville, NJ. Plots of the wind records at these locations are presented in Figures 26-29. It is important to note that these data are for winds over land. Factors to convert the BWI data to winds over water were obtained from Johnson et al. (1991). Factors for the other stations were not available. Thus, after

experimentation with various combinations of wind fields it was decided to apply one wind field over the entire grid that was an average of all of the records. The factors for conversion of overland winds to overwater winds were selected to be 2.0 for the north-south component and 1.0 for the east-west component. The average wind field for October 1992 is presented in Figure 30.

To initiate numerical solutions, the initial state of the system must be specified. As discussed in Chapter 2, generally the water surface is taken to be flat without fluid motion. These conditions are not important since they are "flushed" from the system at the speed of a free-surface gravity wave, i.e., the square root of the water depth times the acceleration of gravity. However, since the 3-D model is a variable density model, salinity is modeled and directly coupled with the solution for the fluid motion through the water density. Thus, the initial salinity field must also be specified. More care must be taken here since the effect of initial conditions is removed from the system at basically the speed of the residual flow velocity, which is typically on the order of 5-10 cm/sec. Therefore, to reduce the "spin-up" time required, the initial salinity field is constructed using available field data to represent the true salinity as accurately as possible.

With these boundary forcings and an initial salinity field that was constructed from the available field data and held constant for the first 5 days of the simulation to allow the flow field to adjust to the initial density field, the 3-D numerical model was run for the month of October 1992. Model results for water-surface elevations, velocities, and salinities were then compared with the field data collected at the locations shown in Figure 4.

Water surfaces are compared in Figures 31-33. Although there is a slight setup in the computed results, it can be seen that the model reproduces the tide within the C&D Canal and computes the proper phasing and amplification of the tide in the upper reaches of the Delaware River.

Computed tidal velocities are compared with field data in Figures 34-37. In the C&D Canal, positive values reflect flow toward Delaware Bay. It should be noted that the current meter at station S 1.8 began to malfunction near the end of the month, and the meter at S 3.5 began malfunctioning by the middle of the month. Although the observed data are point values, whereas the computed values are averages over large cells, it can be seen that the model does an excellent job of reproducing the currents in the Delaware Bay-C&D Canal-Upper Chesapeake Bay system. Of particular importance is the fact that Figure 36 illustrates that the exchange between the two bays is computed well.

Comparisons of computed and observed salinities during October 1992 at several locations shown in Figure 4 are presented in Figures 38-43. The magnitude of the salinity is reproduced well as is the proper intrusion distance. For these inflow conditions, which are about half of the mean average annual, maximum salt concentrations of about 3-4 ppt occur at Range 7, which is located at about RM 69. This corresponds well with the data collected for this period as

well as with observations noted by other researchers, e.g., Cohen and McCarthy (1962).

April 1993 Simulation

Inflow conditions for April 1993 were quite high. Flow hydrographs on the Delaware, Susequehanna, and Schuylkill Rivers for this period are presented in Figures 44-46. It can be seen that the peak freshwater inflow at Trenton is about 5 times the average annual flow of 11,650 cfs (330 m^3/sec). Tidal boundary conditions and salinity boundary conditions are illustrated in Figures 47-50. Unlike the October 1992 conditions, it can be seen that Delaware Bay is partially stratified during April 1993, with the Upper Chesapeake Bay being highly stratified. The average wind employed for this simulation is shown in Figure 51. All of the previous discussion concerning lateral variations in the boundary conditions and the manner for specifying initial flow and salinity fields apply for this simulation also.

Water-surface elevations and velocities at several locations (Figure 4) are compared in Figures 52-56. It can be seen that these results are comparable to those obtained for the case of inflow conditions more representative of average conditions, i.e., the October 1992 simulation.

Salinity comparisons are given in Figures 57-59. The impact of the high-flow event is obvious. Salinity levels are pushed far below their location in October 1992, with a resulting much sharper horizontal salinity gradient. The decreased intrusion that results from high-inflow events can be seen by comparing Figures 57 and 40. These results demonstrate that the numerical model responds properly to changing freshwater inflows.

June-November 1965 Simulation

The final flow event reproduced for model verification was the drought period of June-November 1965. As can be seen from the discharge hydrographs on the Susquehanna, Delaware, and Schuylkill Rivers presented in Figures 60-62, extremely low flows occurred that were about 20 percent of the average annual flows. Such conditions result in the movement of salinity upriver to the vicinity of Philadelphia. Reproducing a low-flow event such as this is important since the major concern about the impact of a deepened channel on the salinity regime and how it might impact water supplies is for such low-flow occurrences.

Tides specified at Annapolis and at the Delaware Bay mouth are shown in Figures 63 and 64 and the average wind field is given in Figure 65. Salinity boundary conditions at the Delaware Bay mouth were provided by the DRBC and are shown in Figure 66. Salinity conditions at Annapolis were not available for this period. Therefore, approximate salinities were specified to be 19 ppt near the bottom and 15 ppt near the surface by using computed results from the full

Chesapeake Bay numerical model of Johnson et al. (1991) for flow conditions approximating these. No lateral variation in salinities was prescribed at either boundary.

Interior data for comparison with model results were limited for this simulation. A comparison of the water-surface elevations during July 1965 at Philadelphia is given in Figure 67. These results are similar to those for the October 1992 and April 1993 simulations, although the phasing does not appear to be reproduced as well. An inspection of results before the data gap around 3 July shows excellent matching of the phase. It is suspected that a problem with the timing of the recorded data rather than the computed results is responsible for the phase difference after 4 July. No current velocity data were available. Near-surface salinity/chlorinity comparisons at two locations (Marcus Hook and Ben Franklin Bridge, Figure 18) in the upper river are shown in Figures 68 and 69. The salinities labeled observed were actually constructed from chlorinities that were computed from observed conductivity measurements using the following expressions:

Specific Conductance Range, *K*	Equation
0 - 249.6	$Cl = 8.092*10^{-4}(K)^{1.7687}$
249.7 - 525.7	$Cl = 3.326*10^{-5}(K)^{2.3518}$
525.8 - 5,477	$Cl = 2{,}686*10^{-2}(K)^{1.2789}$
5,478 - above	United Nations Educational, Scientific, and Cultural Organization relationships
Note: K = mhos at 25 degrees Celcius and *Cl* is in ppm.	

Salinity is then determined from

$$S = 0.03 + 1.805\ Cl \qquad (52)$$

It can be seen that the model reproduces the movement of salinity up the river during extremely low flow periods quite well, especially trends in the salt movement as well as events such as those around 8 October and 18 November.

In summary, model verification has covered a wide range of inflow conditions ranging from extremely high inflows during April 1993 to record low levels during 1965 along with variable wind and tide conditions. The model has been shown to reproduce water levels, flow velocities, and salinities well over this range of events. The major parameter varied during this verification was bottom friction. Values for the drag coefficient were determined during the October 1992 simulation and were not changed for the other two verification simulations nor during the productions runs to be discussed later. With the model considered verified, it was then employed to address the issue of the impact of channel deepening on the salinity regime in Delaware Bay. In addition, the model was also used to determine the impact of a 1.0-ft (0.30-m) sea level rise and the

impact of closing the C&D Canal on salinity conditions and subtidal circulation in the Delaware and Upper Chesapeake Bays. It should be noted that the model run with the C&D Canal closed was made merely to provide insight into the effect of the canal. No one has proposed closing the canal.

6 Impact of 45-ft Channel

Several data sets have been used in the 3-D model to address the impact of channel deepening on salinity conditions and subtidal circulation in Delaware Bay. These include the June-November 1965 low-flow period, the same data set but with the Delaware flows adjusted to represent flows that would have occurred with today's regulation plan, June-November wind and tide forcings with monthly averaged inflows prescribed, and the high-flow transition period of April-May 1993. Each of these periods was simulated first with the existing 40-ft (12.2-m) channel and then with the proposed 45-ft (13.72-m) channel. Results for each data set were then compared between the two runs.

Initial conditions were constructed as previously discussed. It should be remembered that the channel deepening plan terminates about 15 km inside the bay. When model runs are made with the deepened channel in place, the initial salinity field is constructed by assuming that the salinity in the additional vertical layer at the bottom is the same as that in the layer above.

Several types of model output are presented to aid in the analysis of the impact of channel deepening. These include time series plots of salinity at several locations throughout the modeled system (Figure 18); a time-history of the 30-day average salinities (chlorinities) at RM 98; the location of the 30-day average 180-ppm and 7-day average 250-ppm chloride fronts as a function of time; the location of monthly averaged salinity contours of 0.25 ppt, 5.0 ppt, 10.0 ppt, and 15.0 ppt; and subtidal circulation plots. However, not all plots were generated for all simulations.

Since salinity rather than chlorinity is computed in the 3-D model, to provide chlorinity plots at the upper river locations, the computed salinities were converted to chlorinity by the use of Equation 52. The reason for converting salinity to chlorinity at upstream locations such as RM 98 is because the DRBC's reservoir flow regulation plan is based upon the location of the 7-day average 250-ppm chloride front (isochlor) as well as the 30-day average chlorinity at RM 98.

June-November 1965 Simulation

The boundary forcings for this data set have previously been discussed. Interest in the simulation of this data set to assess channel deepening is because this flow period is the low flow of record on the Delaware River. Therefore, if there is an impact on salinity conditions in the vicinity of the water intakes and areas of groundwater recharge from the river near Philadelphia due to channel deepening, it should show up in these simulations as well as those discussed in the next section using regulated 1965 flows on the Delaware River.

Figures 70-77 illustrate the impact of the deepening on salinity at RM's 42, 54, and 69, and chlorinity at RM 98 for the last 2 months of the simulation, i.e., October and November. The maximum impact of the deepening occurs near the end of the simulation after the prolonged low-flow period on the Delaware River. Therefore, only results for the last 2 months are presented. Note that not only is the magnitude of the salinity at each location shown but difference plots are presented to demonstrate the impact of the deepened channel more clearly.

These results illustrate that the greatest impact of the deepened channel occurs in the middle portion of the estuary. For example, the deepened channel results in increases of about 0.5 ppt near the surface at RM 54 and increases of as much as 2.0 ppt near the bottom of the water column. Chlorinity in the upper river at RM 98 increased by 50-75 ppm. It should be noted that the maximum instantaneous chlorinity at RM 98 is about 300 ppm with the deepened channel and above 200 ppm without the deepening. The deepened channel increases the chlorinity by less than 50 percent. Thus, for the actual flow conditions that occurred during June-November 1965, maximum chlorinities exceeded the target of 180 ppm with the 40-ft (12.20-m) channel. However, it should be noted that existing flow management (reservoir regulation) precludes such flows happening today.

One question raised during the model study concerned the magnitude of the volume transport through the C&D Canal. Figure 78 shows the volume transport through the canal for July-September 1965. It can be seen that transport as high as 105,000 cfs (3,000 m^3/sec) can occur, with the maximum difference between the existing channel and the deepened channel in place being about 875 cfs (25 m^3/sec). The negative sign indicates a net flow from Delaware Bay to Chesapeake Bay. Therefore, deepening the navigation channel in Delaware Bay will result in more flow moving from Delaware Bay into Upper Chesapeake Bay for the conditions modeled. With more net flow diverted to the Upper Chesapeake Bay, down-estuary residual currents are slightly lower. As a result, salinity is allowed to move farther upstream. This is one of the factors contributing to the computed increase in salinity due to channel deepening at locations such as RM 98.

Other reasons include the fact that the deeper channel allows higher salinities to be transported into the estuary from the ocean. Thus, the overall salt content of the system is greater. The salt is then advected and diffused throughout the system by tidal currents. Long-term distribution of the salinity is controlled

primarily by the long-term residual or subtidal currents. Another reason is that salt in the lower portion of the estuary is driven upstream due to the baroclinic component of the horizontal pressure gradient. The baroclinic component is the vertical integral of the horizontal density gradient. Thus, with a deeper channel, this term becomes greater. Therefore, deepening a navigation channel increases salinities in the system. Finally, with the deeper channel the conveyance area for the freshwater inflow increases. With the increased conveyance area, residual currents due to the freshwater inflow, which help to retard the upstream migration of the salinity, decrease. Thus, the salt is able to move farther upstream.

Regulated June-November 1965 Simulations

These simulations are considered the most crucial of all the simulations to illustrate the impact of channel deepening since they represent flows determined by the DRBC's reservoir regulation plan. A comparison of the regulated flow at Trenton as obtained from DRBC[1] and the observed flows that occurred during this period is presented in Figure 79. All other forcings were the same as in the previous data set. It can be seen that generally when the observed flow is greater than about 3,500 cfs (99 m^3/sec) the regulated flow is lower, whereas when the observed flow drops below about 2,625 cfs (74 m^3/sec) the regulated flow is higher. As will be seen in the results presented in the following paragraphs, with the regulated flow plan, salinity conditions in the upper river are not as severe as those with the observed flows.

Figures 80-91 are time series plots for November 1965 that show the impact of channel deepening on the salinity regime throughout the bay. Results are presented at the same locations as in the previous simulation as well as at several locations in the lower bay over oyster beds. Due to the shallow depths in those areas, surface and bottom salinities are virtually the same. It can be seen that deepening the channel has almost no impact on salinities in the extreme lower bay, i.e., RM 27. It should be remembered that a location of (80,xx) is in the channel, whereas a location such as (85,25) is in the shallows toward the New Jersey side of the bay. At locations over the oyster beds farther up in the bay, i.e., RM 38 and RM 43, the deepened channel does impact salinities slightly. Maximum differences appear to be less than 0.2 ppt. At RM 54, as well as at upstream locations, increases in the salinities due to channel deepening appear to be about the same as with the observed 1965 flows.

A comparison of Figure 91 with Figure 77 shows that salinities at RM 98 are lower for the case of regulated flows in the 40-ft (12.20-m) channel than for observed flows. Maximum near-surface chlorinities for the deepened channel are about 225 ppm, whereas with the 40-ft (12.20-m) channel they are about 175 ppm. Thus, the impact of the deepened channel on this inflow scenario is to increase the chlorinity by about 33 percent.

---

[1] DRBC, 1993, Personal Communication with Dr. Dick Tortoriello, P. O. Box 7360, West Trenton, NJ 08628-0360.

Figure 92 illustrates the location of the 30-day average 180-ppm chloride. The location of this parameter plays a major role in the DRBC's reservoir regulation plan. These results show that even though the location of the 180-ppm chloride is pushed about 5 miles (8,000 m) up the river due to the deepened channel, the location is still below RM 98. Figures 93 and 94 show the 30-day average chlorinity at RM 98. It can be seen that although the deepened channel increases the 30-day average chlorinity from about 100 ppm to 150 ppm at RM 98, the critical value of 180 ppm is never reached. Figure 95 is a plot similar to Figure 92 but for the location of the 7-day average 250-ppm chloride for October and November.

Figure 96 shows the location of the monthly averaged 0.25-2.50 ppt isohalines with and without channel deepening for November. It can be seen that the impact of a channel deepening of 5 ft (1.52 m) is to push these contours upstream.

Figures 97 and 98 illustrate the impact of channel deepening on the residual currents (monthly averaged) over the lower bay. These plots were generated to address environmental concerns over oyster beds. These results show that changes in the residual circulation caused by channel deepening will be less than 1.0 cm/sec out of total residual currents of less than 10.0 cm/sec. The difference is so small it is difficult to draw conclusions.

From these results, it can be seen that even though the channel deepening increases the maximum instantaneous chlorinity at RM 98 from about 175 ppm to 225 ppm by the end of November, the 30-day average chlorinity is still substantially below the critical value of 180 ppm and the location of the 30-day average 180-ppm isochlor is below RM 98. When viewing these results, it should be remembered that the difference plots represent only the impact of channel deepening with any errors associated with numerical effects, forcings, etc., canceled out.

Monthly Averaged Flows with 1965 Forcings Simulations

The previous simulations with the regulated flows representing the low flow of record are extremely important for analyzing the impact of channel deepening on salinities in the upper bay. However, to provide insight on the impact for more normal conditions, model runs were made using the June-November winds, tides, and salinity boundary conditions with monthly averaged inflows. Table 5 lists these inflows for the Delaware, Schuylkill, and Susquehanna Rivers.

Figures 99-118 are time series plots of salinities at many of the same locations for which results have previously been presented. It can be seen that for monthly averaged flows the maximum salinity at RM 69 is less than 1.5 ppt compared to 6-7 ppt for the regulated 1965 flow. There is no ocean-derived salt at RM 98 for the monthly averaged inflow case. Different results in the salinity change due to channel deepening can be seen at the locations over the oyster beds in the lower

Table 5
Monthly Averaged Inflows, cfs (m^3/sec)

Month	Delaware	Schuylkill	Susquehanna
Jan	12160 (344.3)	3278 (92.8)	39310 (1,113.1)
Feb	12850 (363.9)	3666 (103.8)	53190 (1,506.2)
Mar	20590 (583.0)	4692 (132.9)	72260 (2,046.2)
Apr	22060 (624.7)	4190 (118.7)	81220 (2,299.9)
May	14220 (402.7)	3047 (86.3)	49380 (1,398.3)
Jun	9170 (260.0)	2130 (60.3)	37440 (1,060.2)
Jul	7090 (200.8)	1596 (45.2)	26340 (745.9)
Aug	5959 (168.7)	1376 (39.0)	13260 (375.5)
Sept	5801 (164.3)	1378 (39.0)	16350 (463.0)
Oct	6809 (192.8)	1320 (37.4)	24040 (680.7)
Nov	10390 (294.2)	2257 (63.9)	35620 (1,008.7)
Dec	12370 (350.3)	3082 (87.3)	48720 (1,379.6)

bay for these flow conditions compared with the changes computed for the low-flow cases. Horizontal salinity gradients are much greater due to the salinity being pushed down the river by the increased flow with a resulting change in flow patterns. A general conclusion is that deepening the channel will have no impact on salinity conditions in the upper river for more normal monthly averaged inflows since the salt does not intrude that far, but impacts are seen over the oyster beds in the lower bay.

As for the regulated low-flow case discussed previously, the monthly averaged isohalines of 0.25-2.50 ppt are presented in Figure 119 for November. Comparing this plot with Figure 96 shows that monthly averaged flows result in salinity levels moving far downstream from their location for regulated low flows.

Figures 120 and 121 illustrate the impact of channel deepening for monthly average flow events on the residual circulation of lower Delaware Bay over the oyster beds. The impact is similar to that for the low-flow case discussed; i.e., changes in the residual circulation due to channel deepening are less than 1.0 cm/sec.

April-May 1993 Simulations

As previously noted, extremely high freshwater inflow occurred during April 1993 on the Delaware River with a substantial drop in those flows by the end of May. Environmental groups have expressed an interest in analyzing the impact of

channel deepening during this transition flow. Inflows on the Susquehanna, Delaware, and Schuylkill Rivers for this period are given in Figure 122. The average wind field and tides at both the Delaware Bay mouth and Annapolis for May 1993 are presented in Figures 123 and 124. Conditions for April have previously been presented in Figures 47, 48, and 51. Salinity boundary conditions at the Delaware Bay mouth and Annapolis for May are shown in Figure 125. As with the wind and tides, the April salinity boundary conditions have been previously presented in Figures 49 and 50. No lateral variations were prescribed in the water-surface elevations at the bay mouth, but lateral variations in the bay mouth salinities were specified in the manner previously discussed.

Figures 126 and 127 are times series plot of salinities at RM 36. The impact of the large freshwater inflow during most of April and the subsequent transition to a much lower flow during May is clearly seen. Maximum salinities near the surface during the first part of May are about 5 ppt with maximum bottom salinities being about 8 ppt. Minimum salinities occurring during the strength of ebb are essentially zero throughout the water column during this period. As the freshwater inflow begins to drop around the first of May, salinities begin to rise near the middle of May. The impact of the channel deepening results in salinity increases of about 0.2 ppt near the surface and about 0.7 ppt near the bottom toward the end of May. Model results at RM 54 showed no salinity at any time during the simulation. These results also clearly demonstrate the fact that relatively strong stratification can develop in Delaware Bay during high-flow periods.

7 Impact of a 1.0-ft Sea Level Rise

In addition to assessing the impact of channel deepening on salinity conditions in Delaware Bay, the model has been applied to simulate the effect of a 1.0-ft (0.30-m) rise in the mean water level at the mouth of Delaware Bay for the 40-ft (12.20-m) channel. The simulation was made using the regulated June-November 1965 data set, but with the mean tide level at the mouth of Delaware Bay raised 1.0 ft (0.30 m) and the mean level at Annapolis raised 0.90 ft (0.27 m). This value was determined by applying the full Chesapeake Bay model of Johnson et al. (1991) using a September 1983 data set with a 1.0-ft (0.30-m) increase in the tide at the mouth of Chesapeake Bay to determine the resulting increase in water surface at Annapolis. It should be noted, however, that the full Chesapeake Bay model does not allow for the exchange through the C&D Canal.

As illustrated in Figure 128, November salinities are increased 0.2-0.4 ppt at RM 69 at the Delaware Memorial Bridge. Likewise, Figure 129 shows that chlorinities at RM 98 are increased by about 25 ppm. These results, i.e., increases in salt concentration in the upper estuary as a result of a sea level rise, are as expected. However, Figure 130 shows that in the lower bay salt concentrations can actually decrease at some locations with an increase in the mean tide level at the mouth. The reason is not entirely known, but is probably due to a different distribution of the residual circulation over the lateral extent of the lower bay. To accurately model the impact of a sea level rise, the Chesapeake and Delaware Bays should probably be modeled together.

8 Impact of Closing the C&D

To determine the impact on salinity and circulation in Delaware Bay due to the exchange between the Upper Chesapeake Bay and Delaware Bay through the C&D Canal, the June-November 1965 regulated flow data set was run with and without the canal being open. As previously noted, no one has proposed closing the canal. Canal closing was simulated by specifying a zero depth in cells at both ends of the canal. Figures 131-133 reveal that with the canal closed, salinities are reduced by as much as 4.0 ppt near Reedy Point at the eastern end of the canal, and the chlorinity at RM 98 is reduced by about 50 ppm. In the Upper Chesapeake Bay, near the entrance to the canal, salinities are reduced by as much as 5.0 ppt with the canal closed.

The reason for the decrease in the salt concentration on both sides of the canal is that the net direction of flow through the canal during the simulation period is from Delaware Bay to Upper Chesapeake Bay. Thus, with the canal closed, the transport of higher salt concentrations from Delaware Bay into Upper Chesapeake Bay is cut off, resulting in a decrease in salinity in Upper Chesapeake Bay near the entrance to the canal.

The reason for the decrease in Delaware Bay is that since the net flow is from Delaware Bay to Chesapeake Bay, closing the canal results in an increase in the residual flow down Delaware Bay. This is illustrated in Figure 134, which shows the difference in near-surface residual circulation (closed-open) for November. As a result of the increased down-estuary residual circulation, salt is pushed down-estuary.

The general conclusion is that the exchange through the canal has a significant impact on the salinity and subtidal flow regimes in both the Delaware and Upper Chesapeake Bays. Obviously, if the direction of net flow is from the Chesapeake Bay to Delaware Bay, these results would change. Thus, the direction of net flow must be considered when assessing the impact of the C&D Canal on flow and salinity conditions in Delaware Bay.

9 Summary and Conclusions

A 3-D numerical model of the Delaware Bay-C&D Canal-Upper Chesapeake Bay system has been developed to aid in assessing the impact of deepening the navigation channel in Delaware Bay from 40 ft (12.20 m) to 45 ft (13.72 m). In addition, the model has been applied to determine the impact of a sea level rise of 1.0 ft (0.30 m) and to provide insight into the impact of the C&D Canal on the hydrodynamics of both bays. To provide data for model verification, as well as for some deepening runs, a one-year field data collection program was conducted. These data, along with data from the drought of June-November 1965, constituted the study databases.

Before the model was verified, several sensitivity experiments were conducted. These consisted of grid convergence runs, time-step convergence runs, and model runs to investigate the impact of the deepening project on flow conditions at the mouth of Delaware Bay. After the sensitivity runs were completed, the final numerical grid and computational time-step were selected for both model verification and model production runs.

Model verification centered around reproducing the flow events of October 1992, April 1993, and June-November 1965. Inflows in October 1992 were about one half the average annual freshwater inflow, whereas those in April 1993 were much higher. The historical data for June-November 1965 represented a record low-flow event. Reproducing the drought event was considered crucial since water supplies in the upper river may become contaminated by the encroaching salinity during such events.

Results from model runs with a 45-ft (13.72-m) channel were compared with results from the existing 40-ft (12.20-m) channel runs to assess the impact of channel deepening. Typical comparisons consisted of time series plots of salinity at several locations, locations of various isohalines, and the impact on residual circulation patterns over oyster beds. For the regulated 1965 drought conditions, deepening the channel by 5 ft (1.52 m) will result in the maximum instantaneous chlorinity at RM 98 increasing from about 175 ppm to 225 ppm. However, the location of the 30-day average 180-ppm isochlor remains below RM 98. Thus, for such conditions, channel deepening should not exceed DRBC's standards for salinity at RM 98.

In addition to addressing the impact of channel deepening on salinity conditions, the 3-D model was also used to determine the impact of a sea level rise and to assess the impact of the exchange through the C&D Canal on salinity and circulation in Delaware Bay. It was determined that a 1.0-ft (0.30-m) sea level rise in the 40-ft (12.20-m) channel would result in an increase in chlorinity at RM 98 of about 25 ppm. However, depending upon the location in the lower bay, the impact could be to reduce salinities slightly due to a redistribution of the residual circulation over the wide lower bay. The impact of the exchange between Delaware Bay and Upper Chesapeake Bay through the C&D Canal was shown to be significant. For the regulated June-November 1965 flow conditions, salinities near Reedy Point were reduced by as much as 4 ppt with the canal closed. Similarly, salinities in the upper end of Upper Chesapeake Bay were reduced by as much as 5 ppt. Chlorinities at RM 98 in Delaware Bay were reduced by about 50 ppm with the canal closed. These results are dependent upon the fact that the net flow through the canal for the period simulated is from the Delaware Bay to Upper Chesapeake Bay. Different results would be obtained for simulation periods where the wind, tidal forcing, and/or freshwater inflow resulted in the net flow being from Chesapeake Bay to Delaware Bay.

References

Cerco, C. F., and Cole, T. M. (1994). "Three-dimensional eutrophication model of Chesapeake Bay," Technical Report EL-94-4, U.S. Army Engineer Waterways Experiment Station, Vicksburg, MS.

Cohen, B., and McCarthy, L. T. (1962). "Salinity of the Delaware Estuary," Geological Survey Water-Supply Paper 1586-B, Washington, DC.

Donaldson, C., dup. (1973). "Atmospheric turbulence and the dispersal of atmospheric pollutants," *AMS Workshop on Micrometeorology*. D. A. Haugen, ed., Science Press, Boston, 313-390.

Edinger, J. E., Brady, D. K., and Geyer, J. C. (1974). "Heat exchange and transport in the environment," Report 14, EPRI Publication No. 74-049-00-3, prepared for Electric Power Research Institute, Palo Alto, CA.

Fagerburg, T., and Benson, H. (1995). "Delaware Bay field data report," Technical Report HL-95-1, U.S. Army Engineer Waterways Experiment Station, Vicksburg, MS.

Galperin, B., and Mellor, G. L. (1990). "A time-dependent, three-dimensional model of the Delaware Bay and River system, Part I: Description of the model and tidal analysis," *Estuarine, Coastal and Shelf Science* 31, 231-253.

Garratt, J. R. (1977). "Review of drag coefficients over oceans and continents," *Monthly Weather Review* 105, 915-929.

Hsieh, B. B., Johnson, B. H., and Richards, D. R. (1993). "A three-dimensional numerical model study for the Chesapeake and Delaware Canal and adjacent bays," Technical Report HL-93-4, U.S. Army Engineer Waterways Experiment Station, Vicksburg, MS.

Johnson, B. H. (1980). "VAHM - a vertically averaged hydrodynamic model using boundary-fitted coordinates," Miscellaneous Paper HL-80-3, U.S. Army Engineer Waterways Experiment Station, Vicksburg, MS.

Johnson B. H., Kim, K. W., Heath, R. E., and Butler, H. L. (1991). "Verification of a three-dimensional numerical hydrodynamic model of Chesapeake Bay," Technical Report HL-91-7, U.S. Army Engineer Waterways Experiment Station, Vicksburg, MS.

Leonard, B. P. (1979). "A stable and accurate convective modeling procedure based on upstream interpolation," *Computer Methods in Applied Mechanics and Engineering* 19, 59-98.

Lewellen, W. S. (1977). "Use of invariant modeling." *Handbook of Turbulence*, W. Frost, ed., Plenum Publishing, 1, 237-280.

Schwiderski, E. W., and Szeto, L. T. (1981). "The NSWC global ocean tide data tape (GDTD), its features and application, random-point tide program," NSWC TR 81-254, Naval Surface Weapons Center, Dahlgren, VA.

Sheng, Y. P. (1982). "Hydraulic applications of a second-order closure model of turbulence transport." *Applying research to hydraulic practice;* proceedings of the conference, Jackson, MS, August 17-20, 1982. Peter E. Smith, ed. sponsored by the Hydraulics Division of the American Society of Civil Engineers, New York, 106-119.

Walters, R. A. (1992). "A study of salt transport processes in Delaware Bay." *Estuarine and coastal modeling;* Proceedings of the second international conference, Tampa, FL, November 13-15, 1992. Malcolm L. Spaulding et al., ed., American Society of Civil Engineers, New York, 240-251.

Wong K. C. (1990). "The current and sea level variability in the Chesapeake and Delaware Canal," *Journal of Geophysical Research* 95(C10), 18-343 through 18-352.

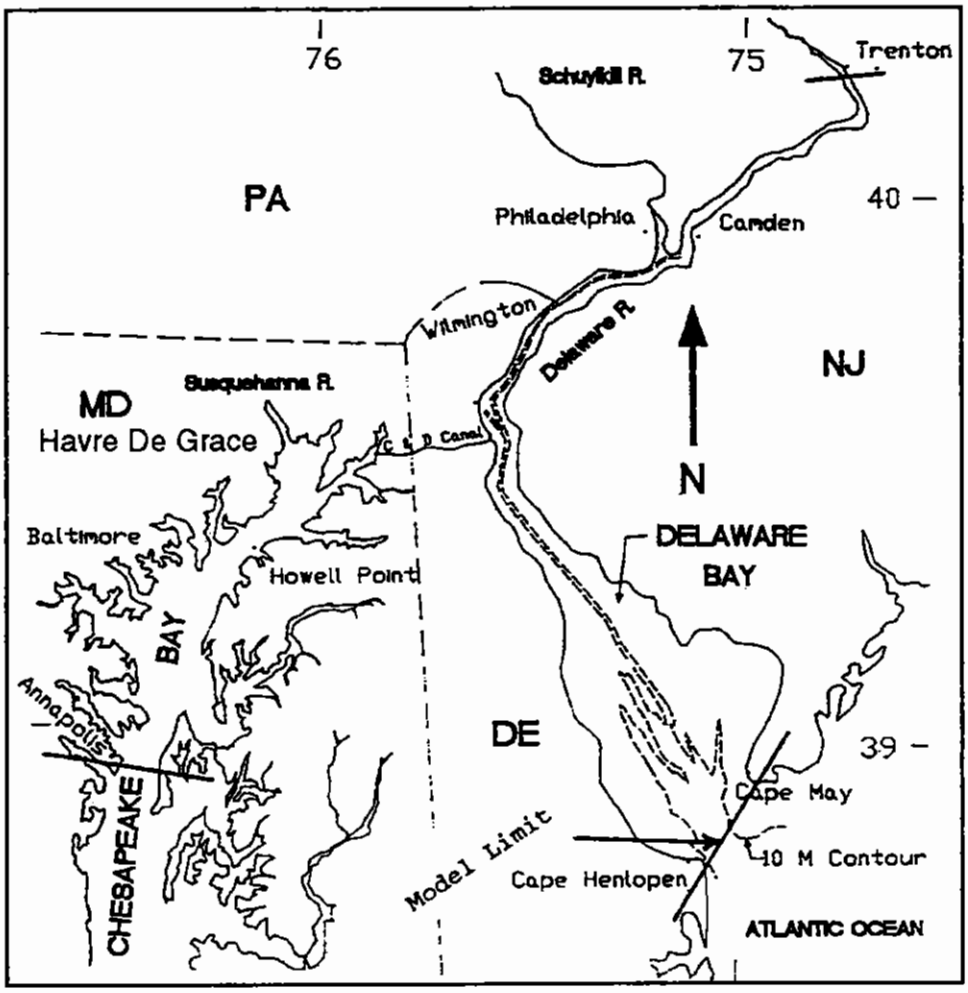

Figure 1. Delaware Bay - C&D Canal - Upper Chesapeake Bay

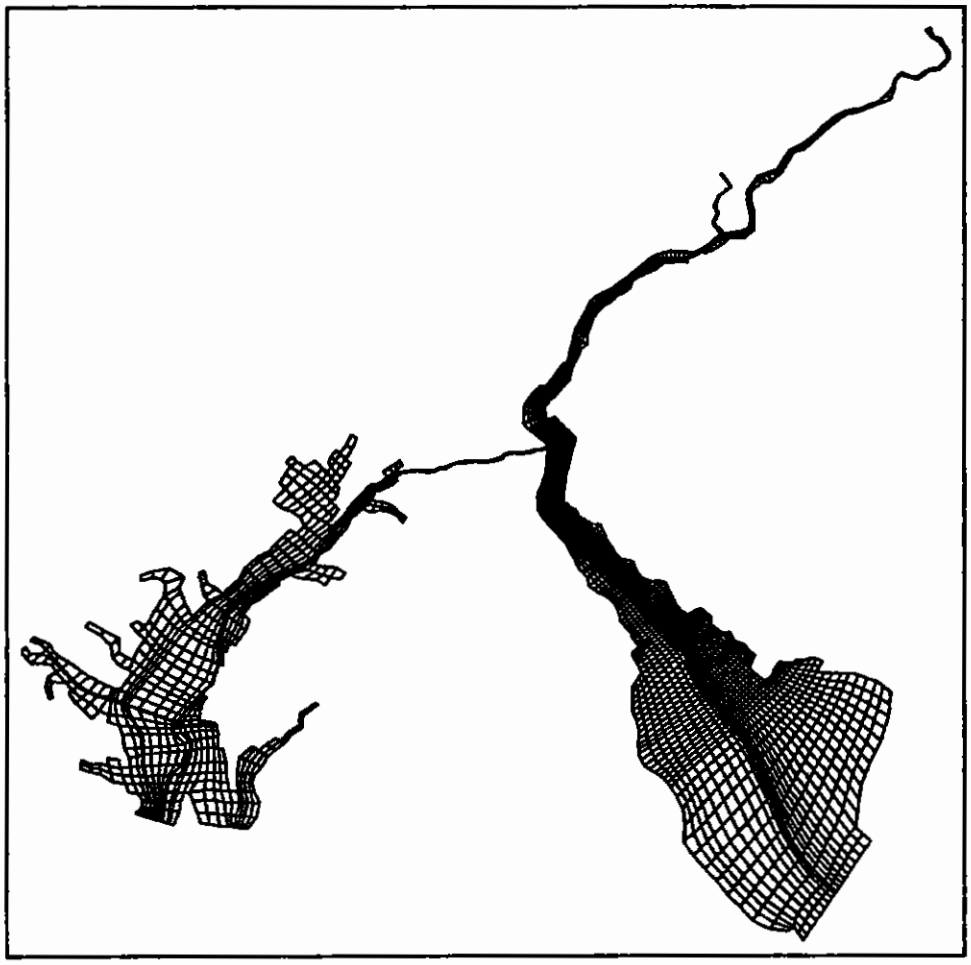

Figure 2. Modified base planform numerical grid

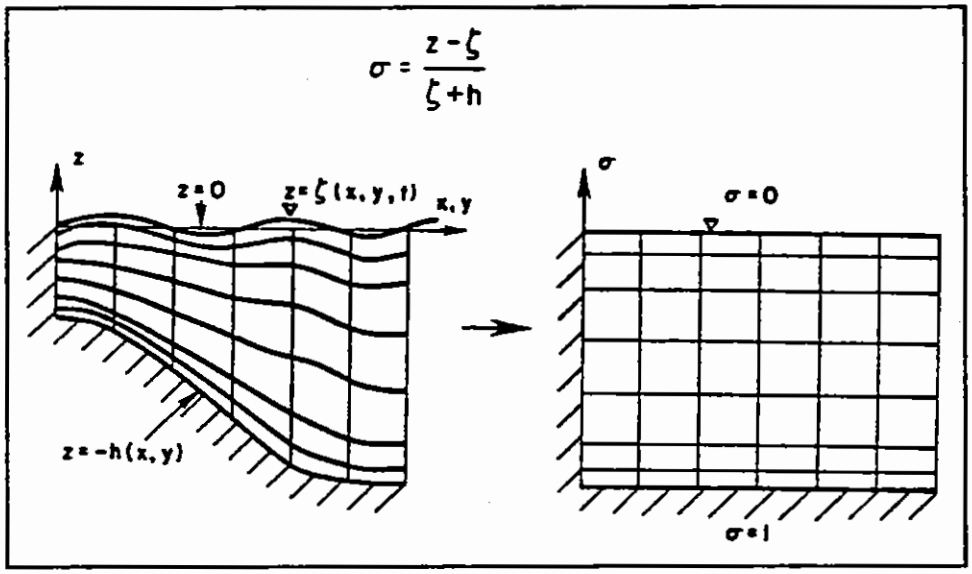

Figure 3. Example of a sigma grid

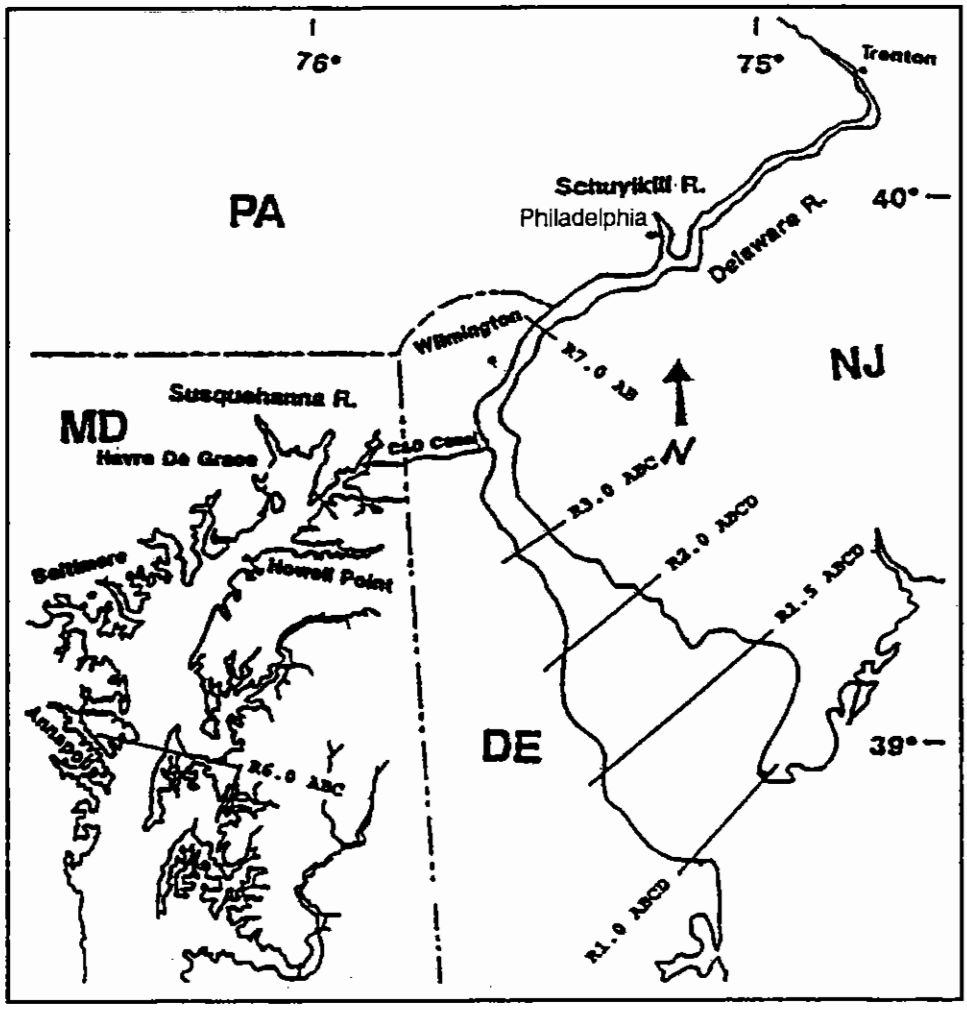

Figure 4. Location of short-term meters

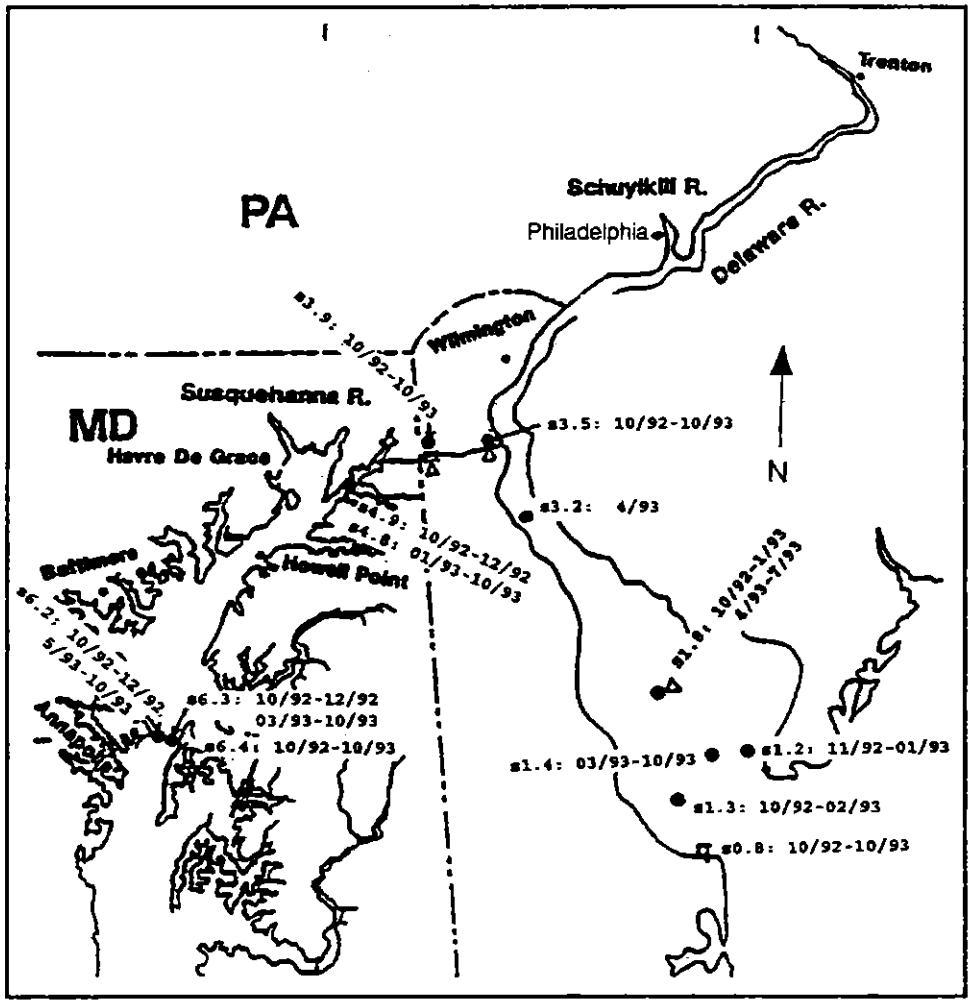

Figure 5. Location of long-term meters

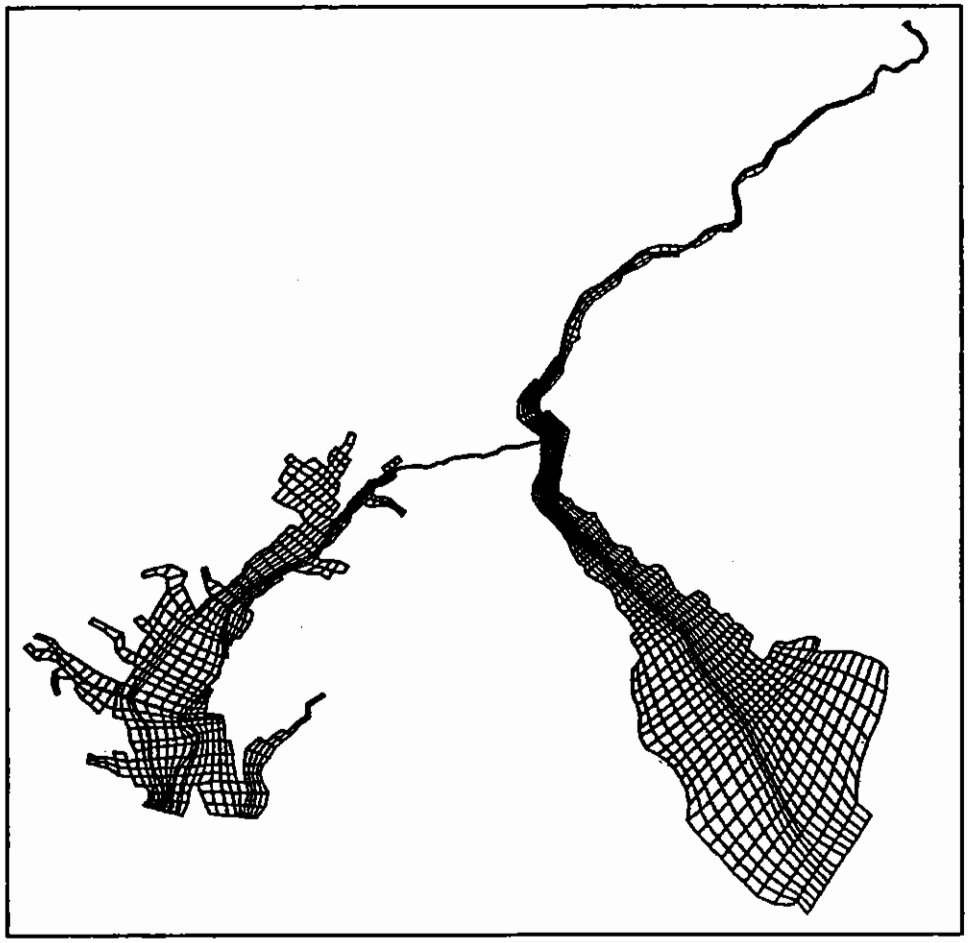

Figure 6. Initial numerical planform grid

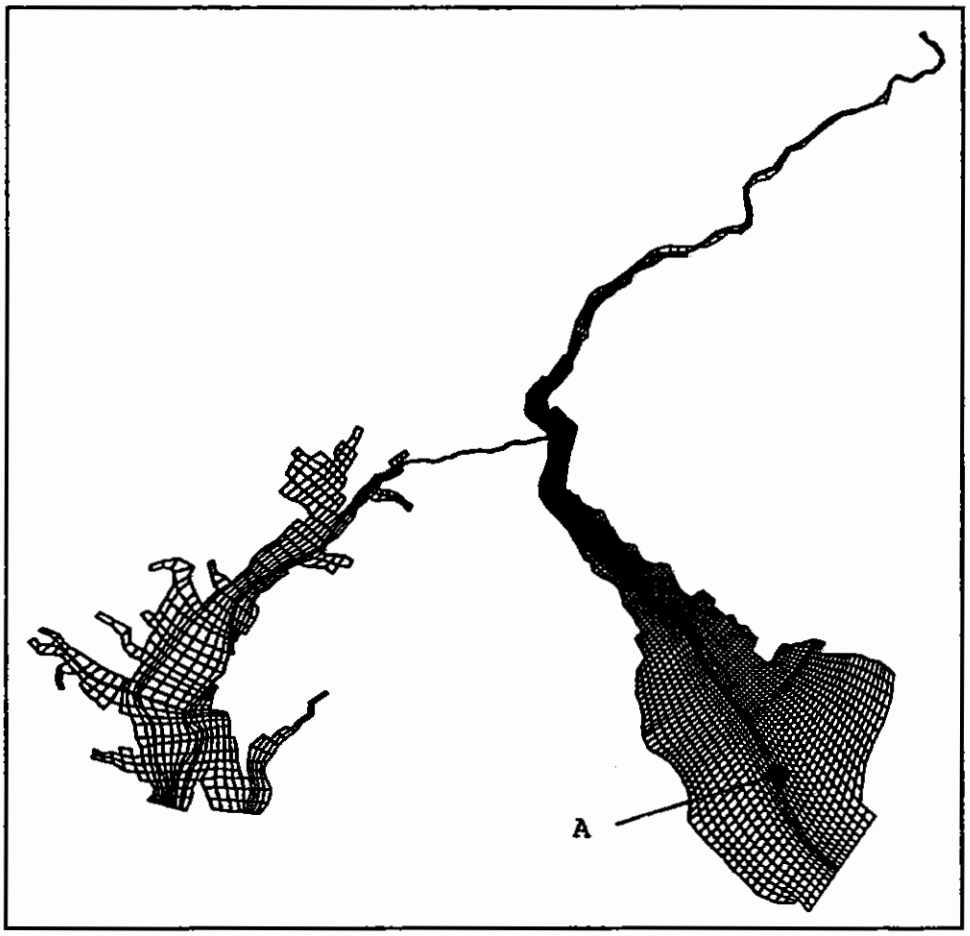

Figure 7. Refined numerical planform grid

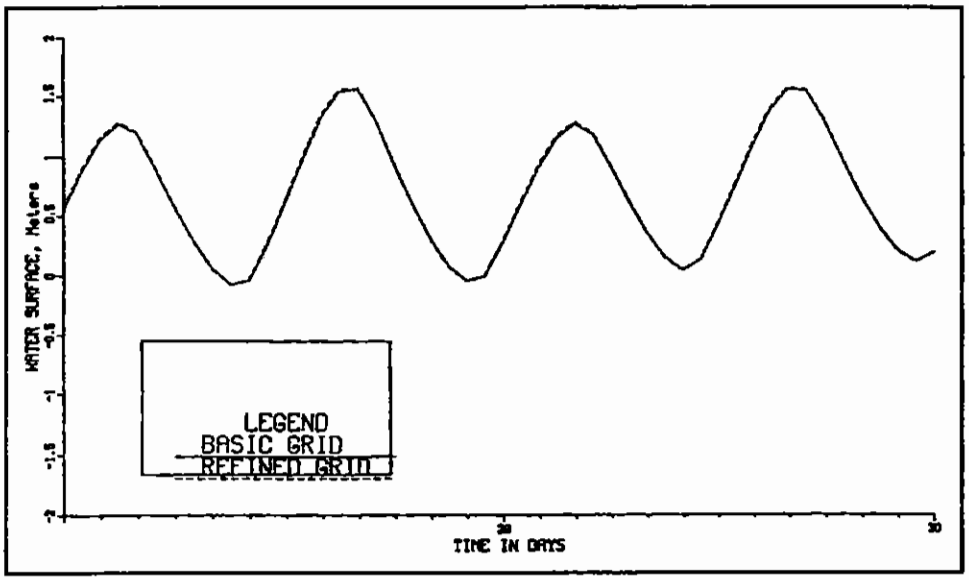

Figure 8. Impact of grid on water-surface elevation, measured at location A in Figure 7

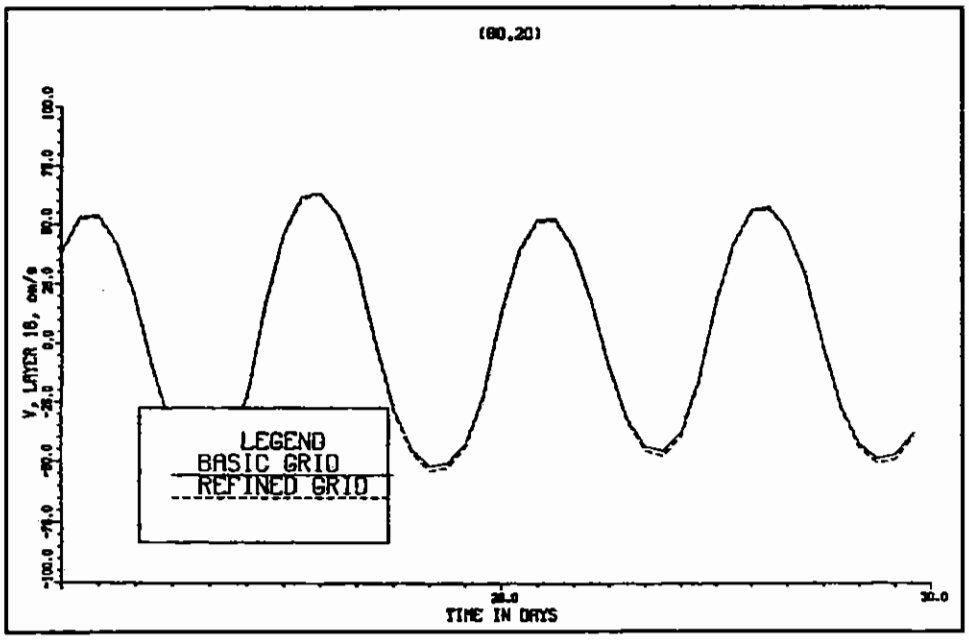

Figure 9. Impact of grid on velocity, measured at location A in Figure 7

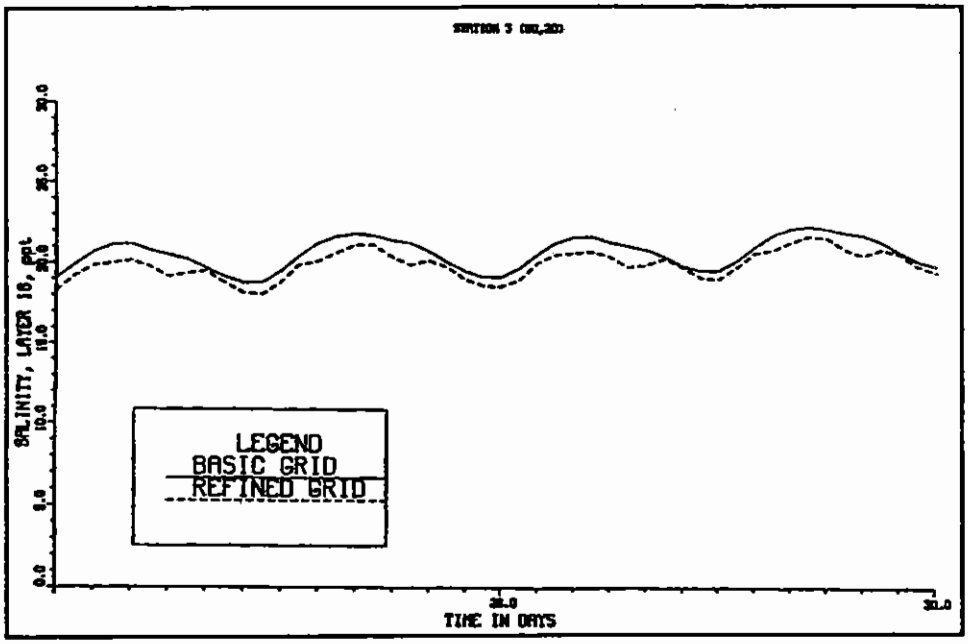

Figure 10. Impact of grid on salinity

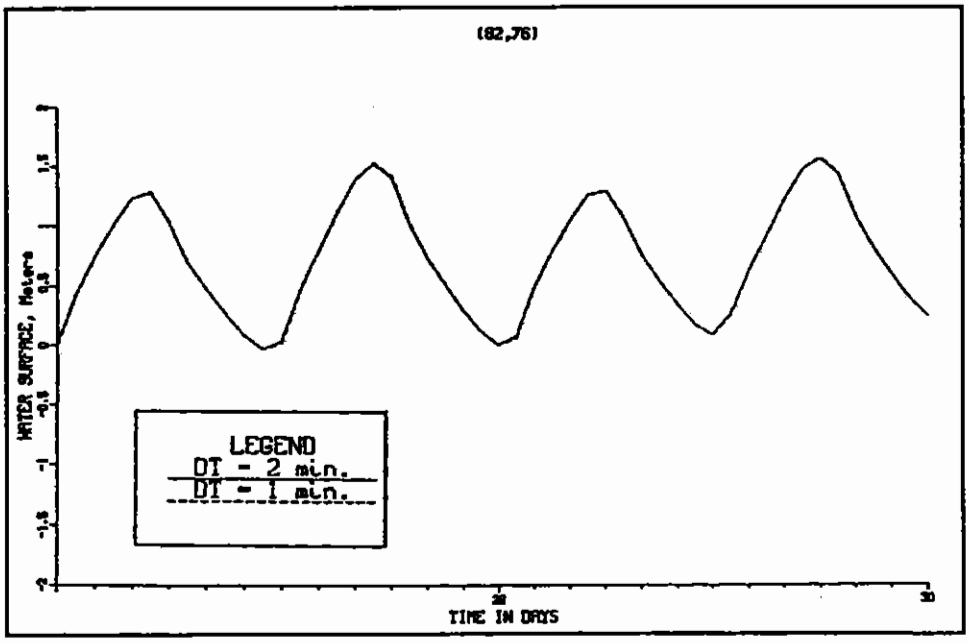

Figure 11. Impact of time-step on water-surface elevation

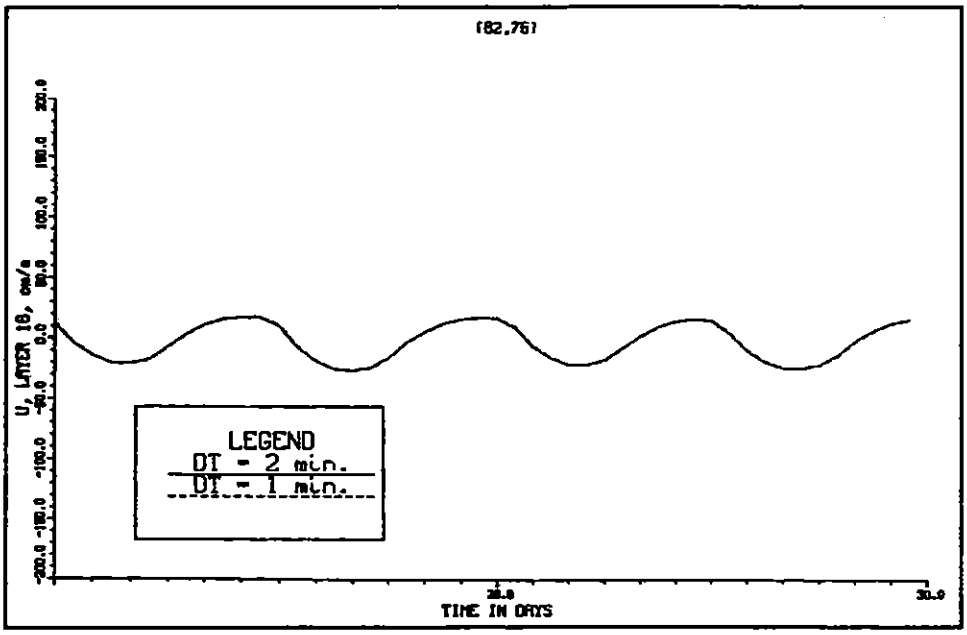

Figure 12. Impact of time-step on velocity

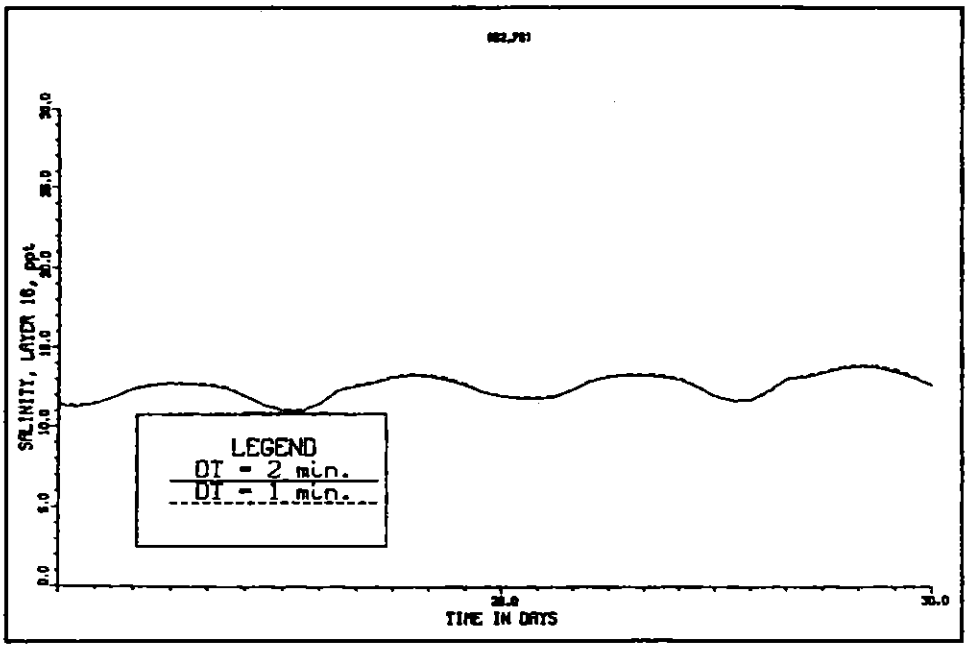

Figure 13. Impact of time-step on salinity

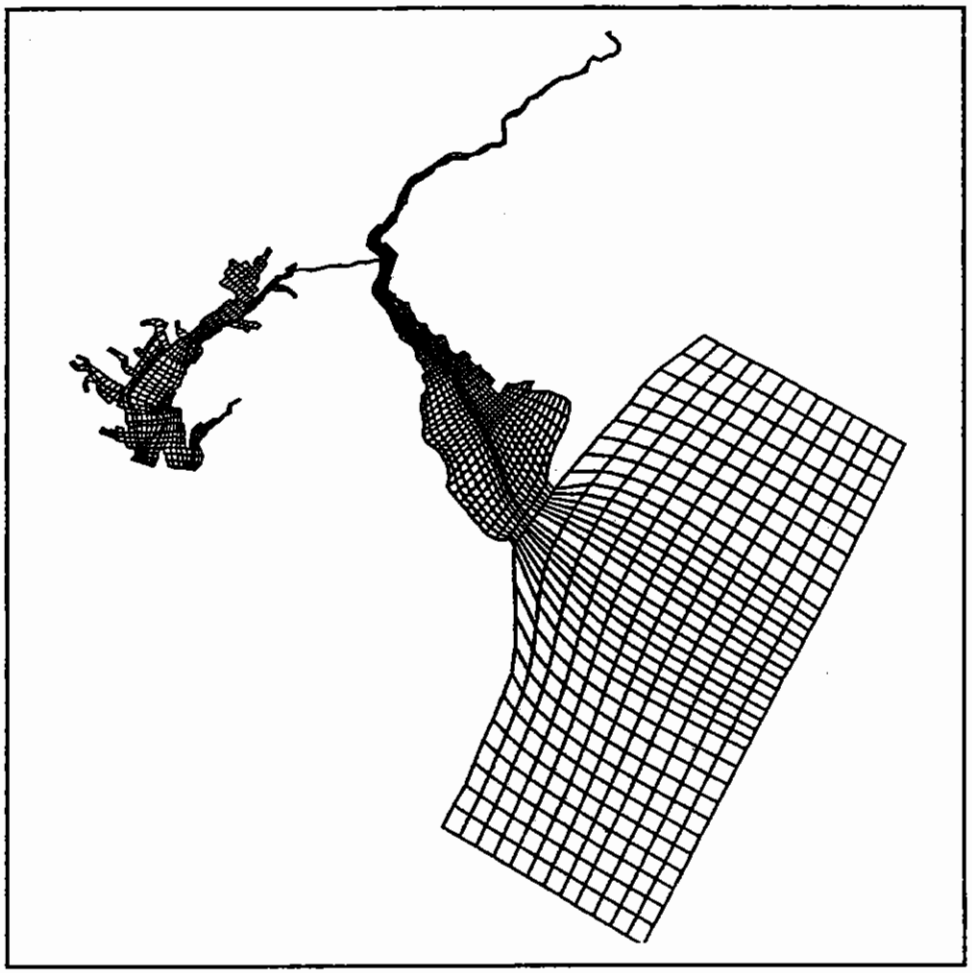

Figure 14. Extended numerical planform grid

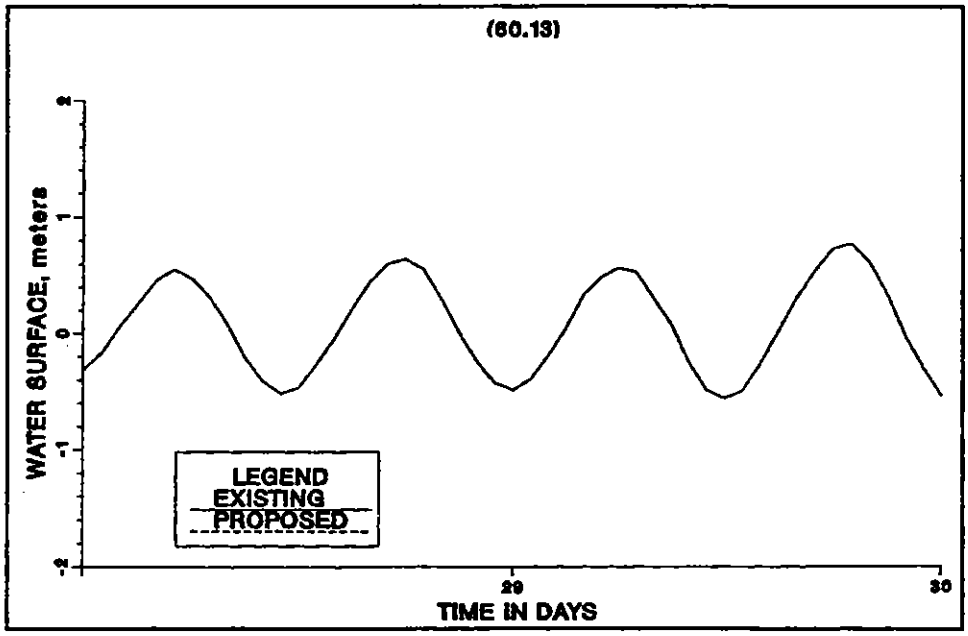

Figure 15. Impact of channel deepening on water surface at bay mouth

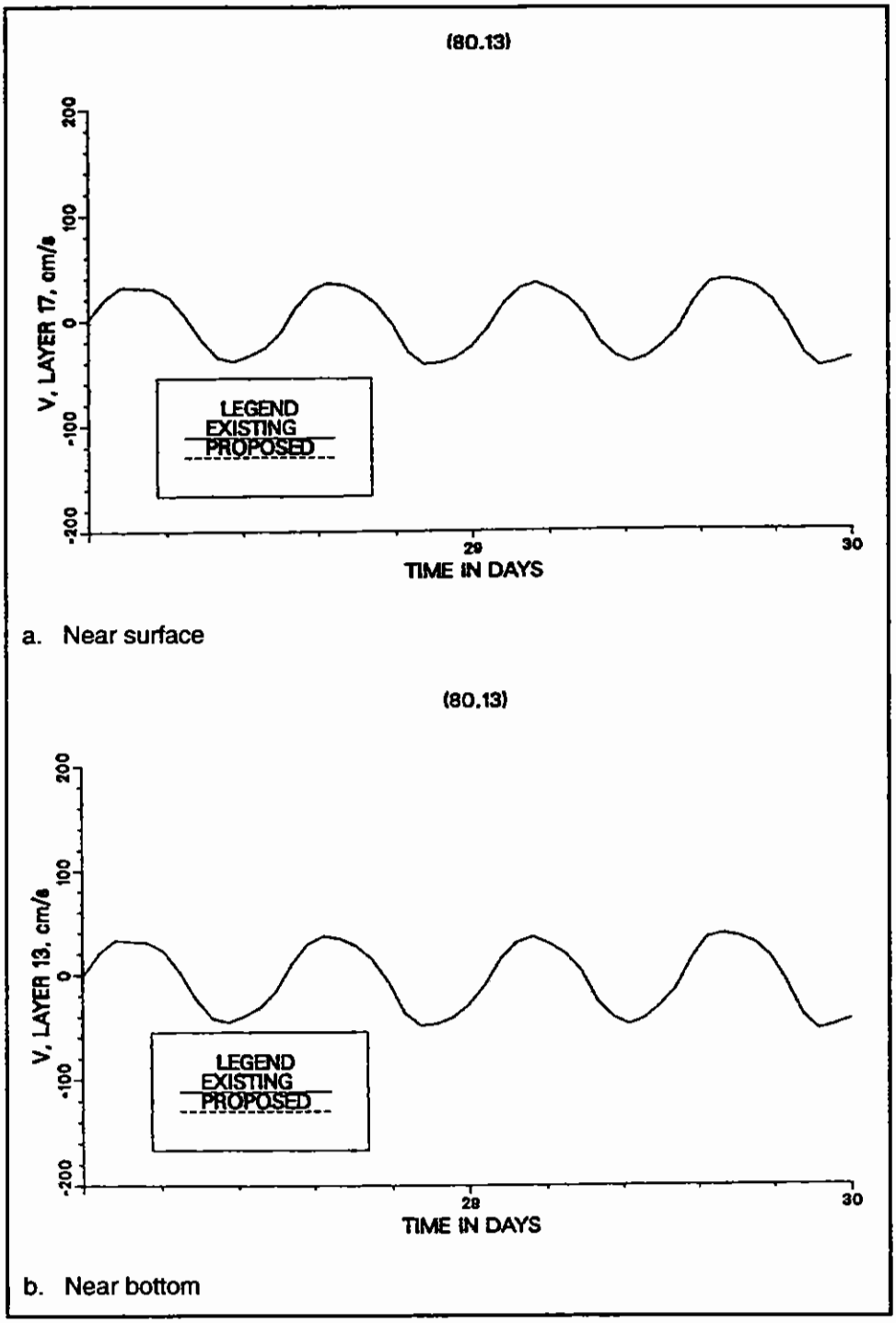

Figure 16. Impact of channel deepening on velocity at bay mouth

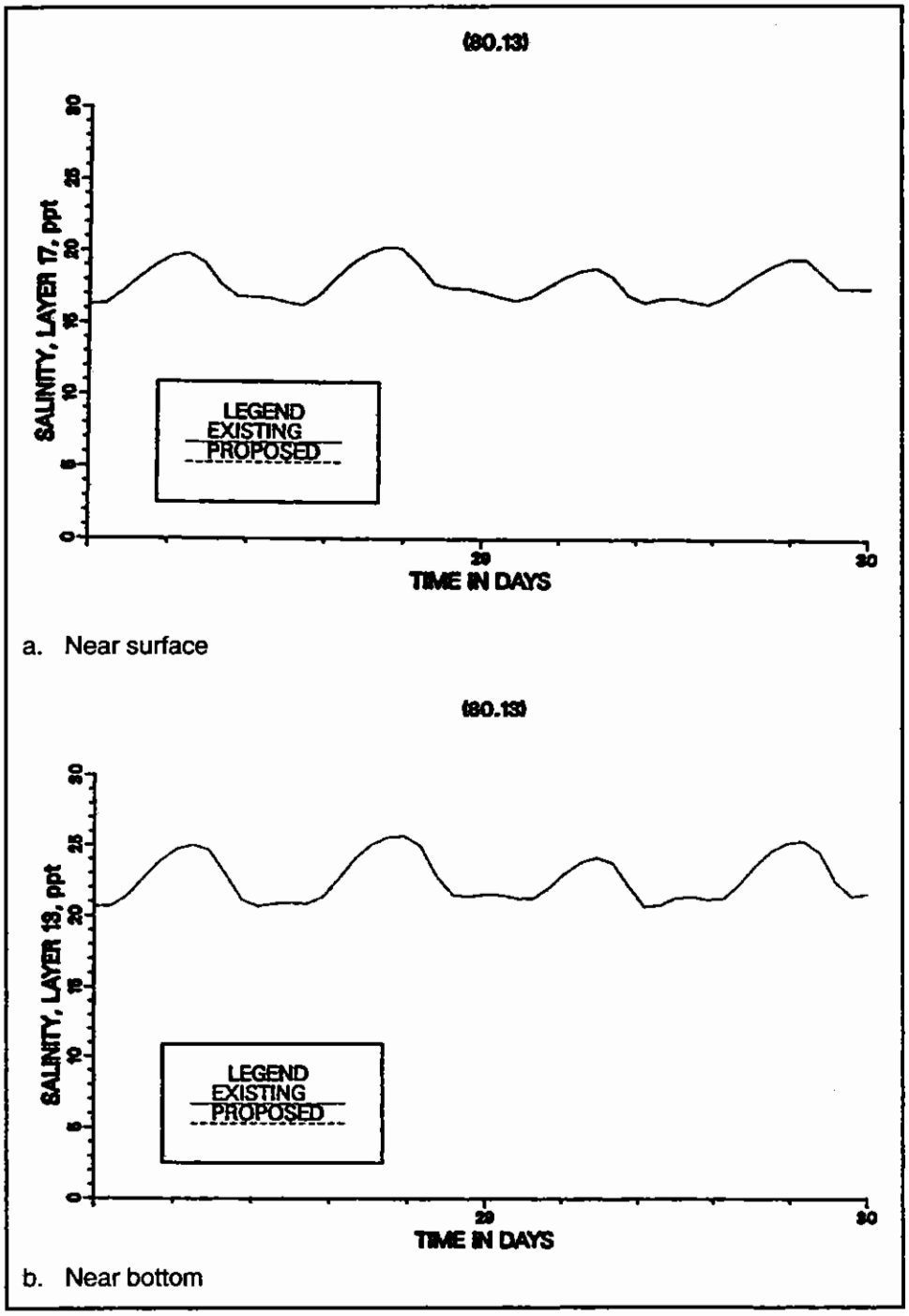

Figure 17. Impact of channel deepening on salinity at bay mouth

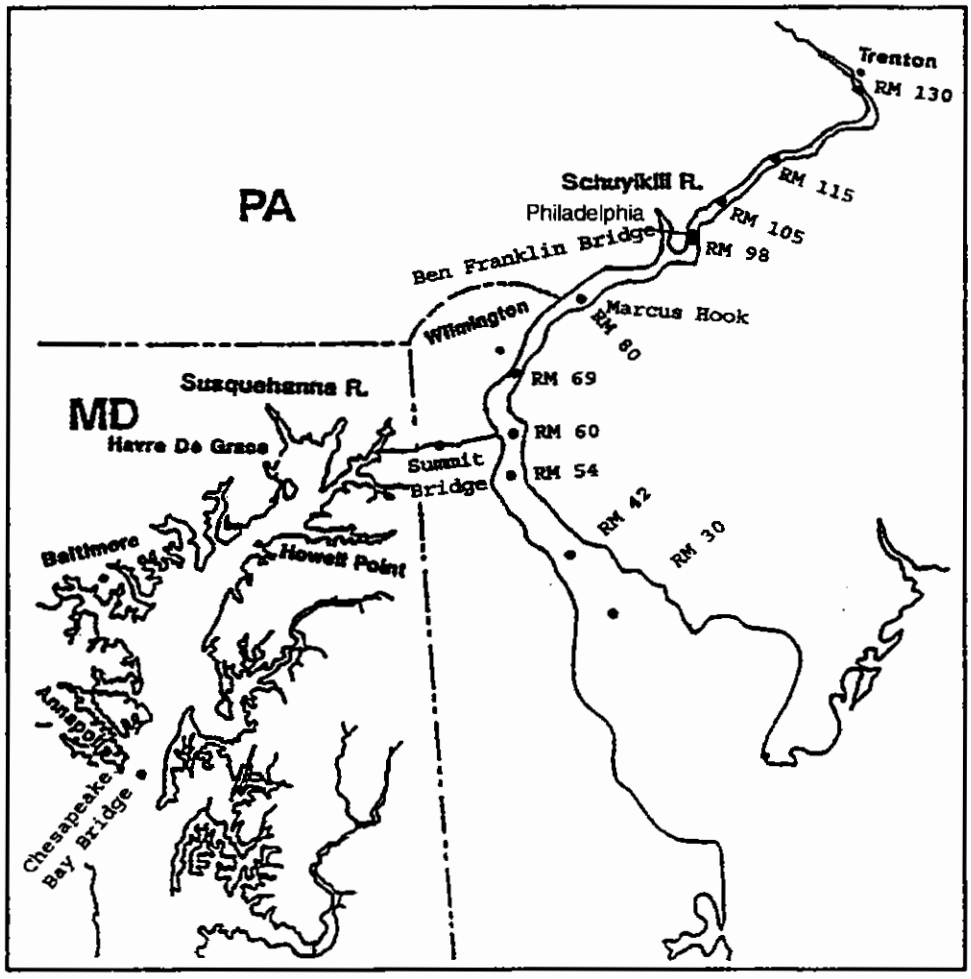

Figure 18. River Miles and station locations

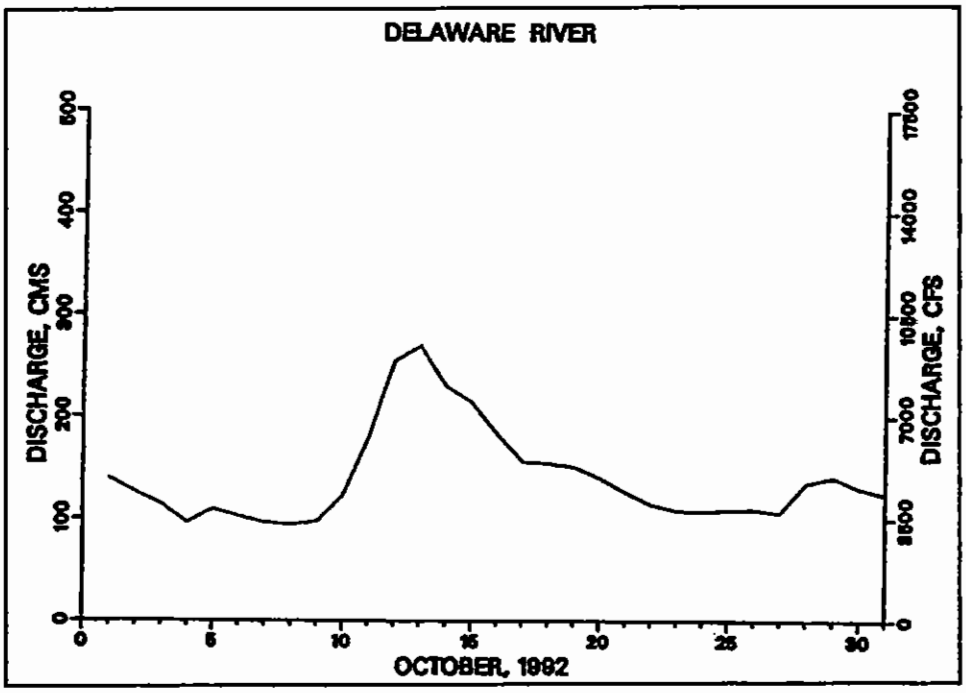

Figure 19. Freshwater inflow on the Delaware River in October 1992

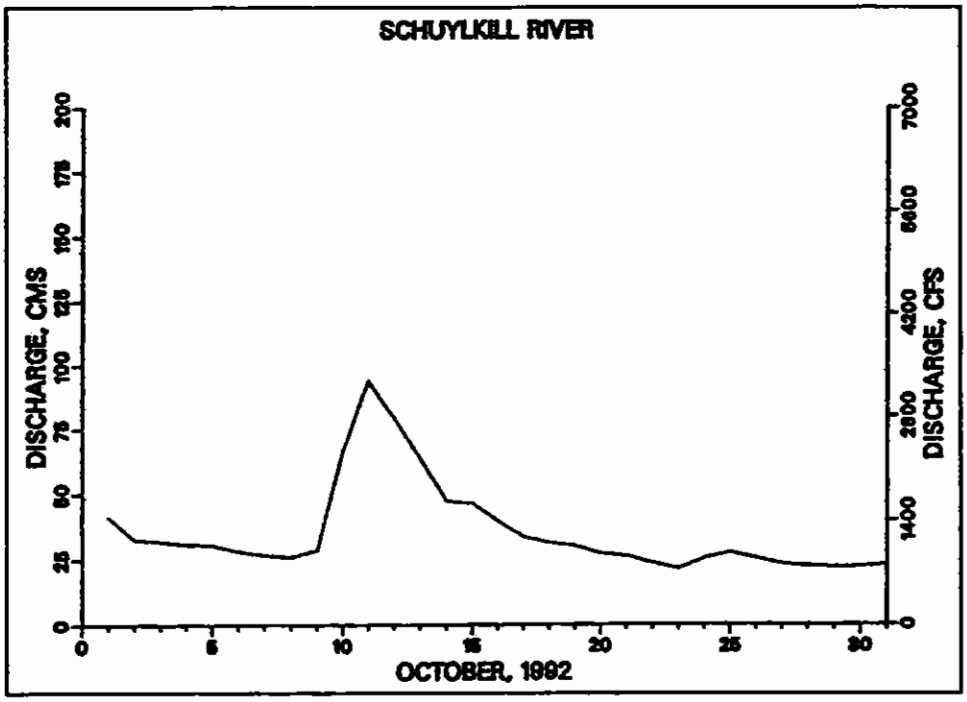

Figure 20. Freshwater inflow on the Schuylkill River in October 1992

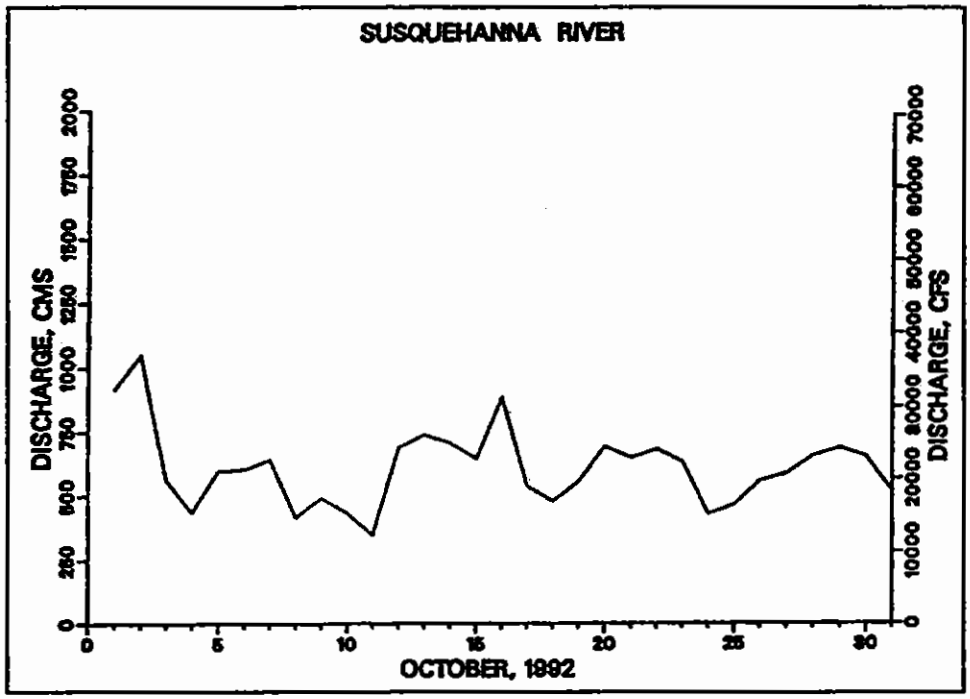

Figure 21. Freshwater inflow on the Susquehanna River in October 1992

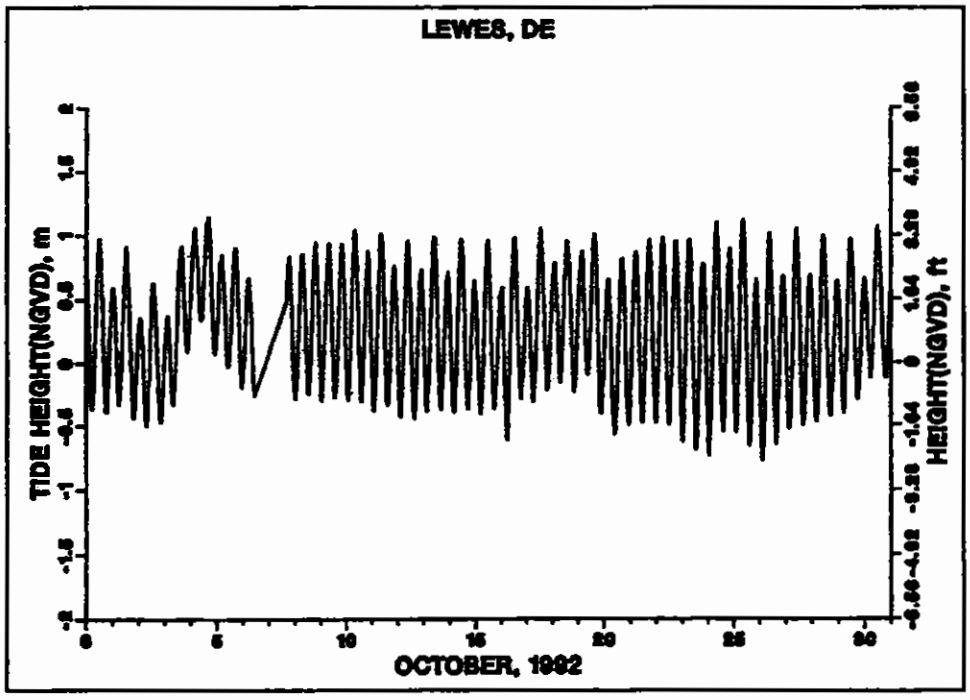

Figure 22. Tide at Delaware Bay mouth, referenced to NGVD, in October 1992

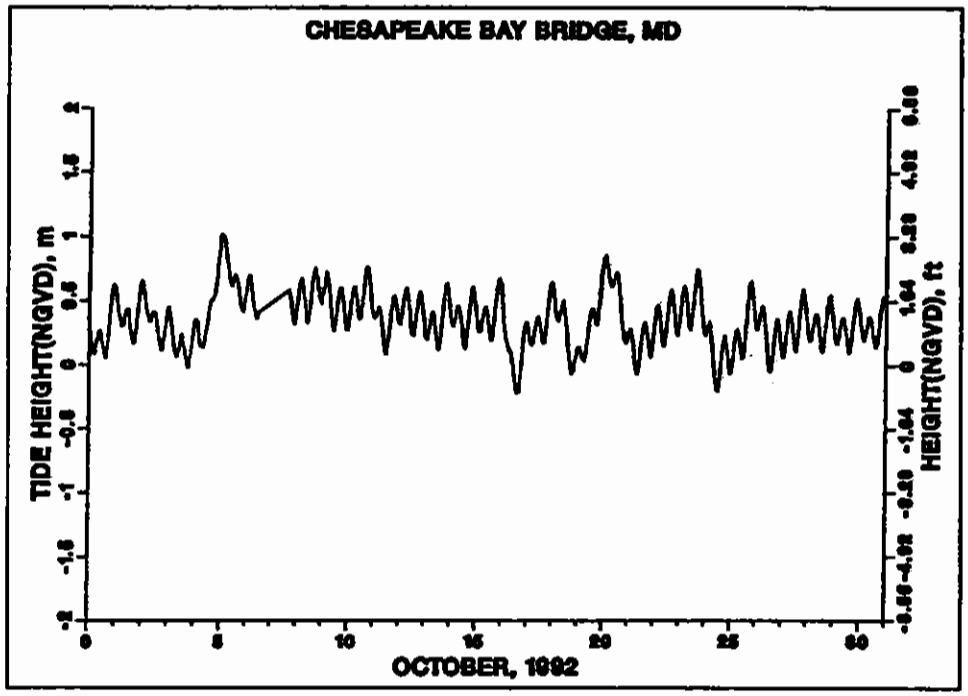

Figure 23. Tide (NGVD) at Annapolis, MD, in October 1992

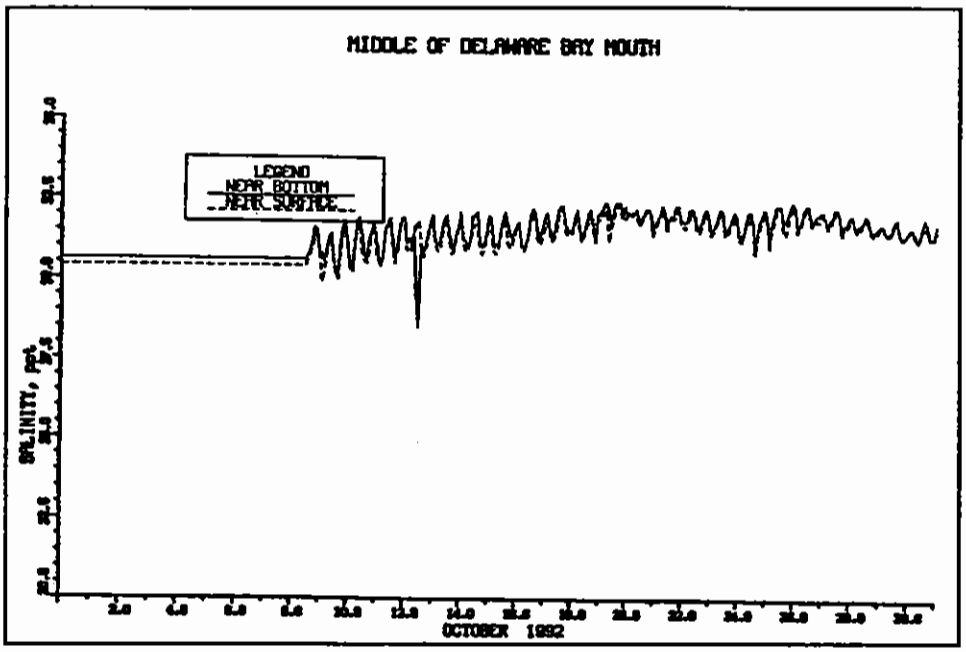

Figure 24. Salinity at Delaware Bay mouth in October 1992

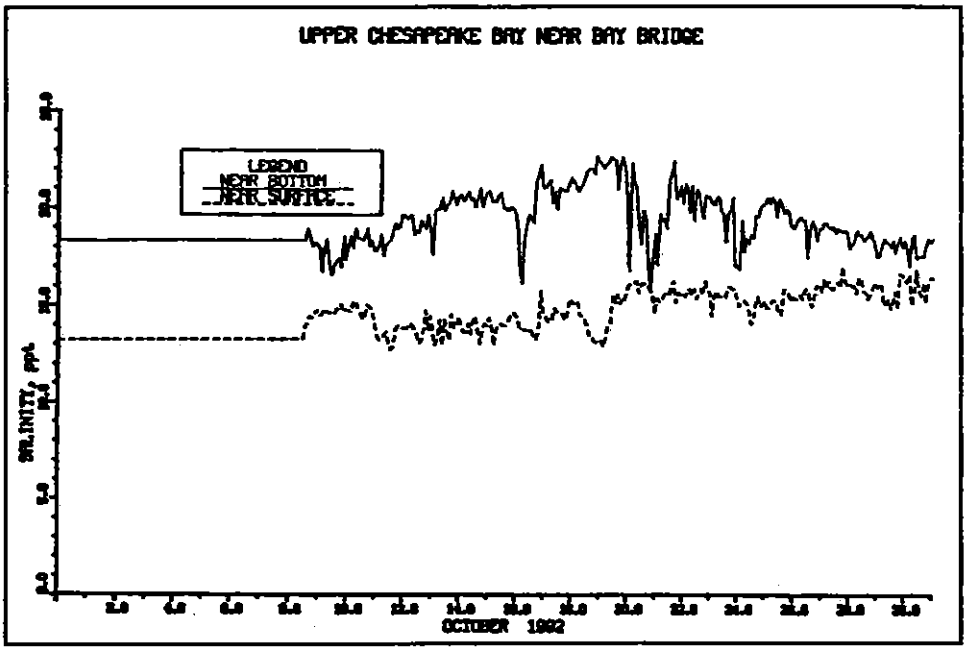

Figure 25. Salinity at Annapolis in October 1992

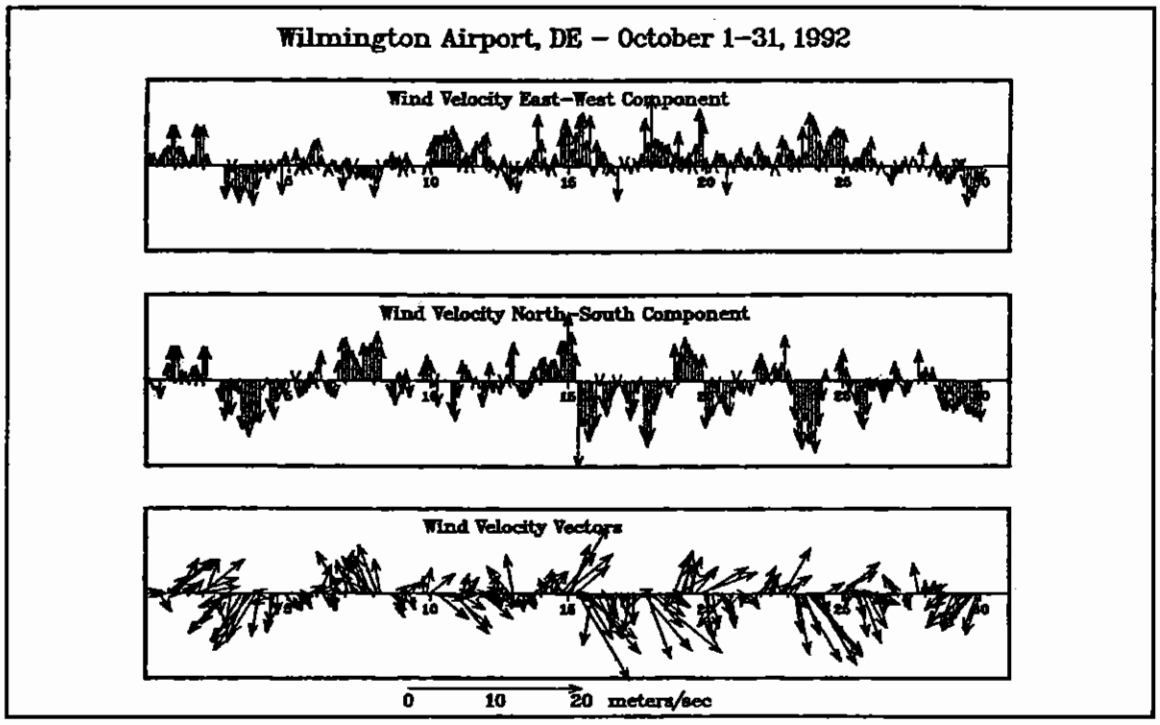

Figure 26. Wind at Wilmington Airport in October 1992

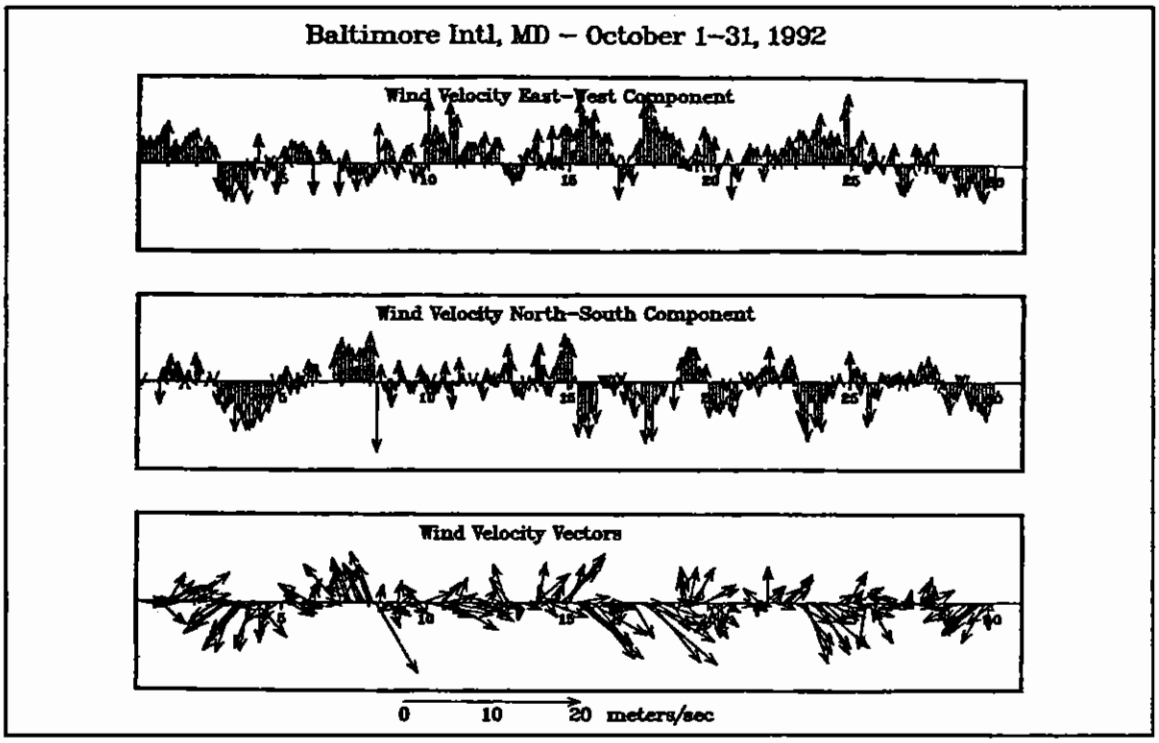

Figure 27. Wind at Baltimore International Airport in October 1992

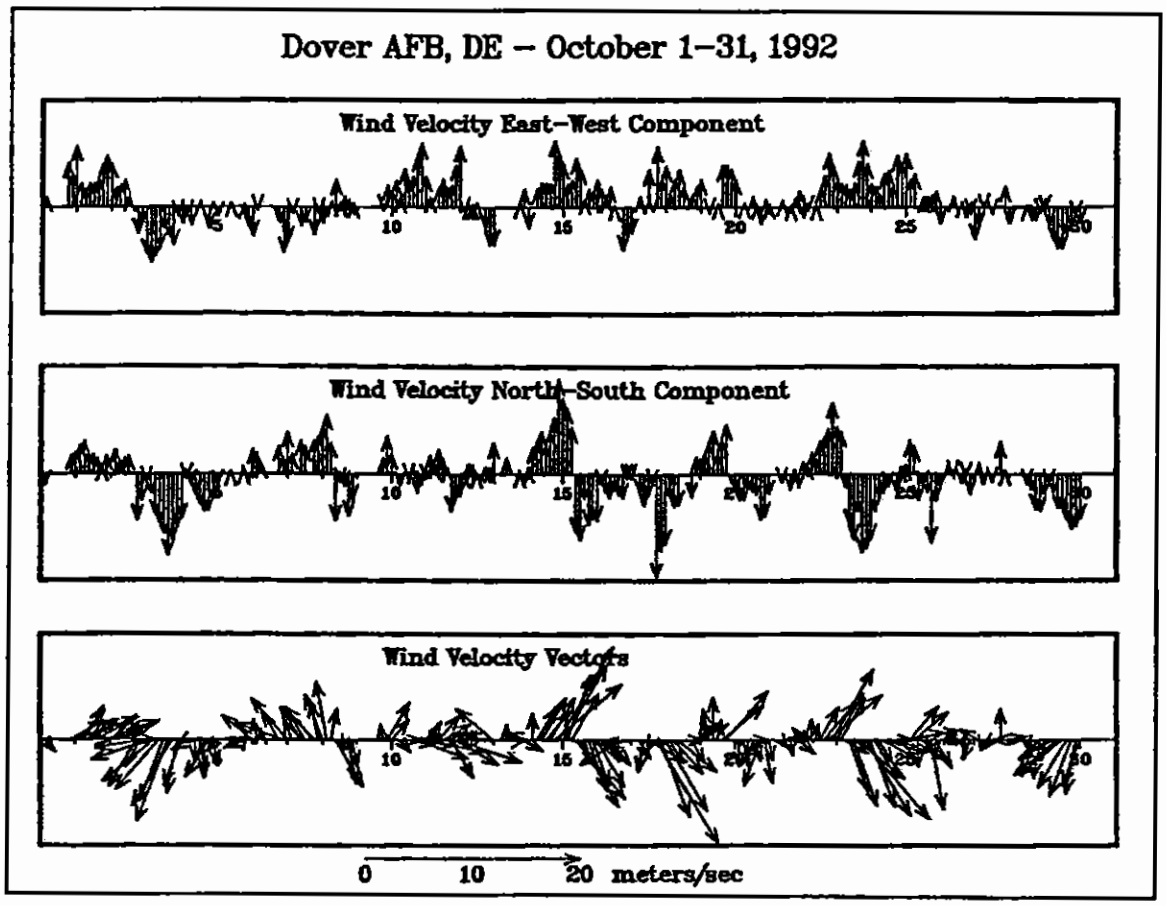

Figure 28. Wind at Dover Air Force Base in October 1992

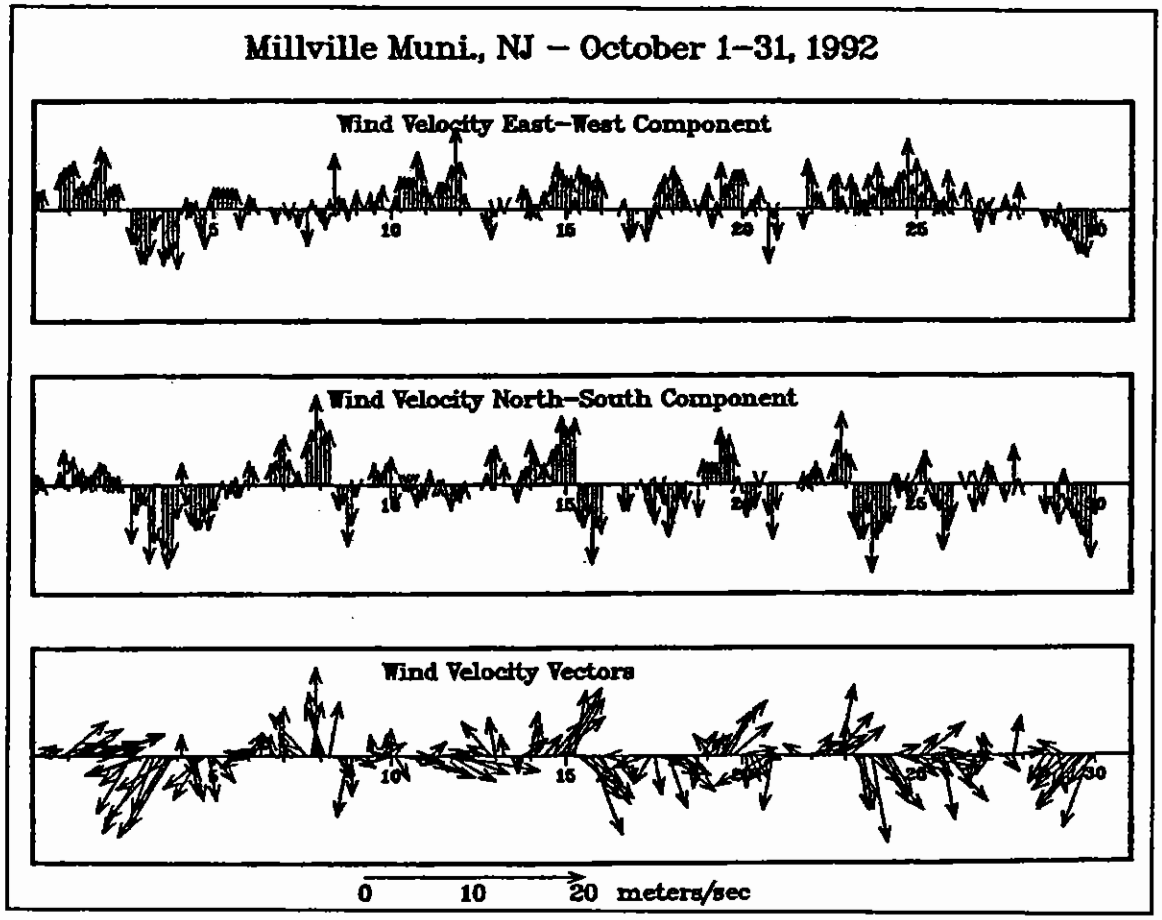

Figure 29. Wind at Millville Muni Station, NJ, in October 1992

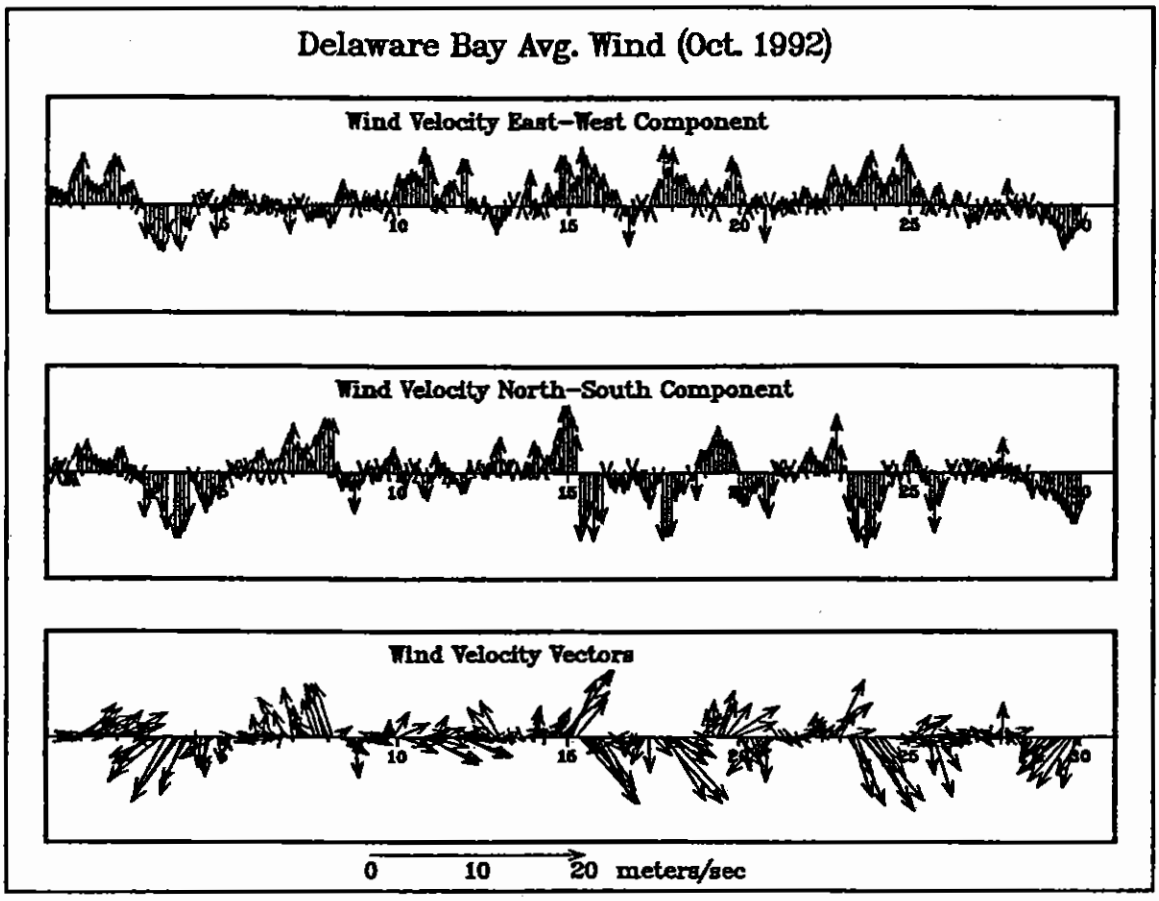

Figure 30. Average wind for October 1992

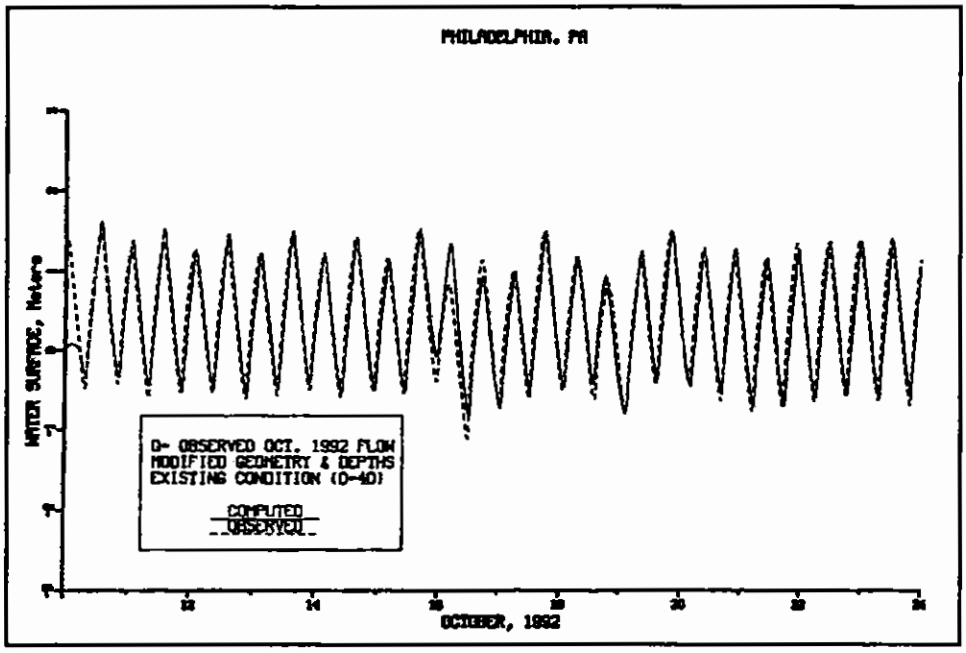

Figure 31. Water-surface elevation (NGVD) at Philadelphia, PA, in October 1992

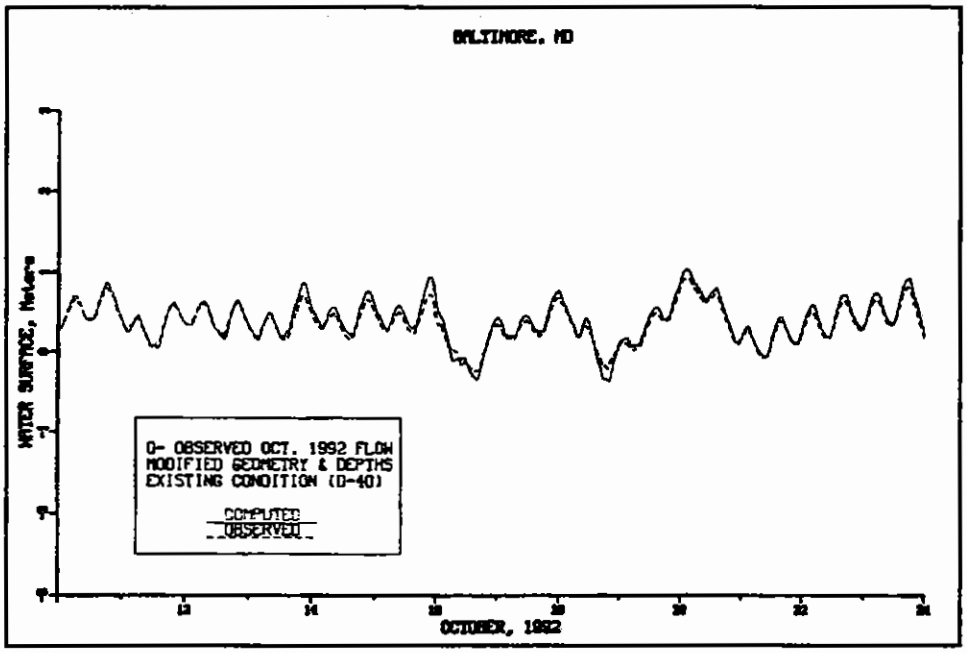

Figure 32. Water-surface elevation (NGVD) at Baltimore, MD, in October 1992

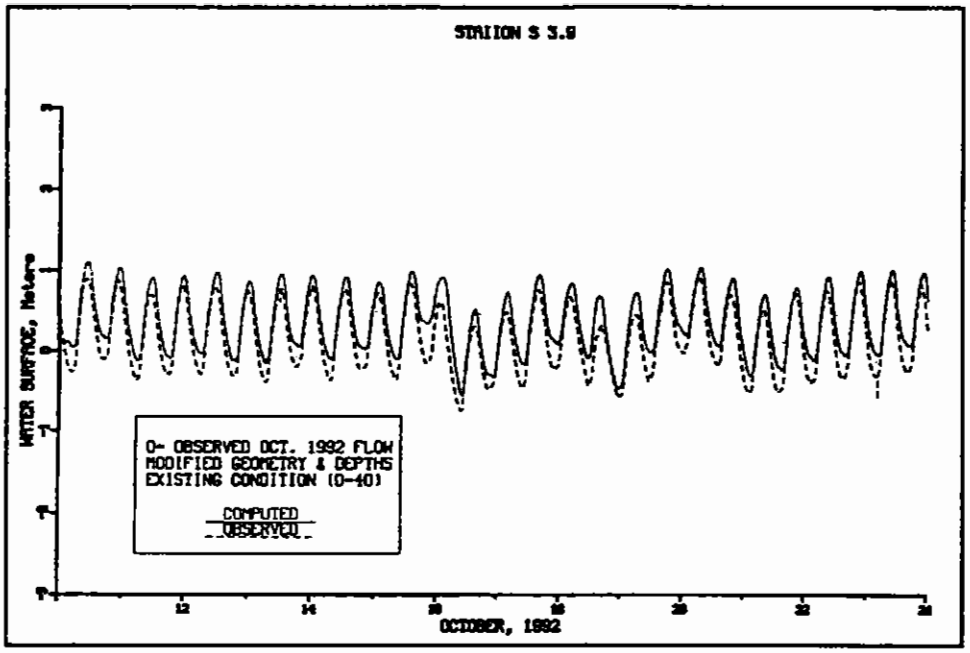

Figure 33. Water-surface elevation (NGVD) at Summit Bridge, MD, in October 1992

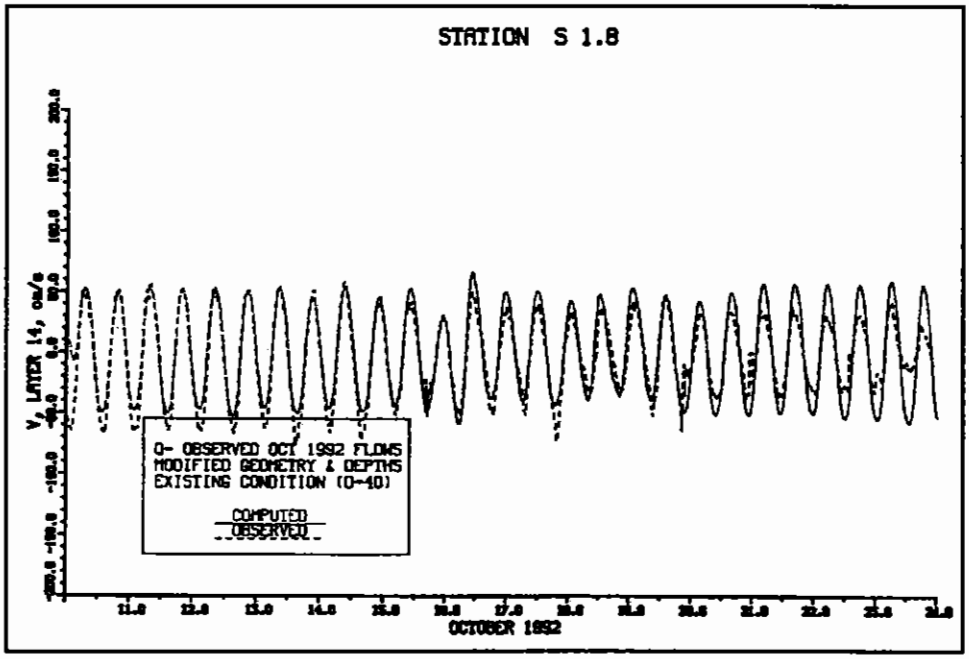

Figure 34. Along-bay velocity at Station S 1.8 in October 1992

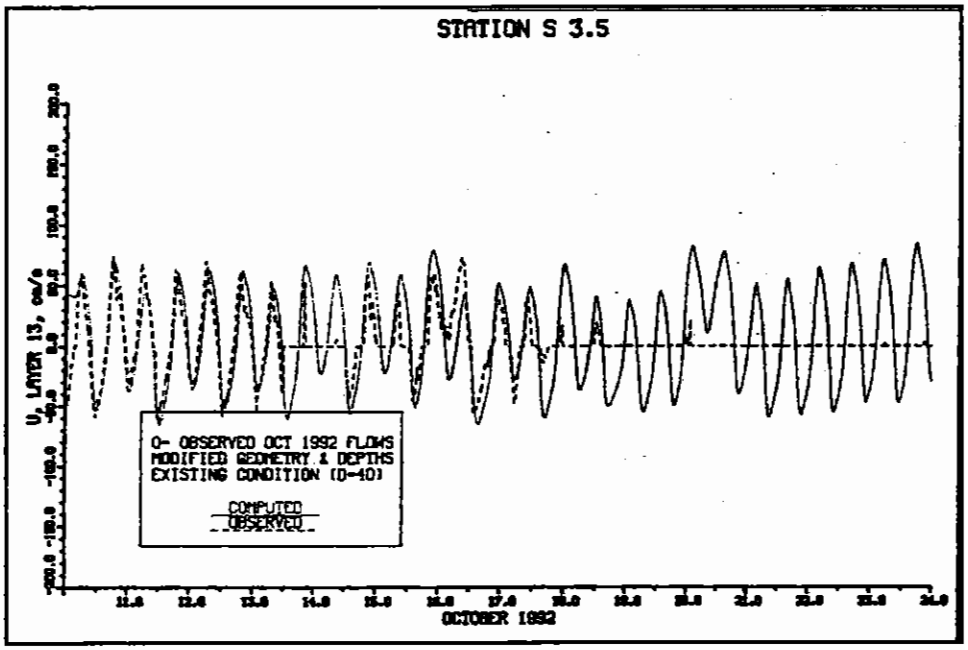

Figure 35. Velocity at Station S 3.5 in October 1992

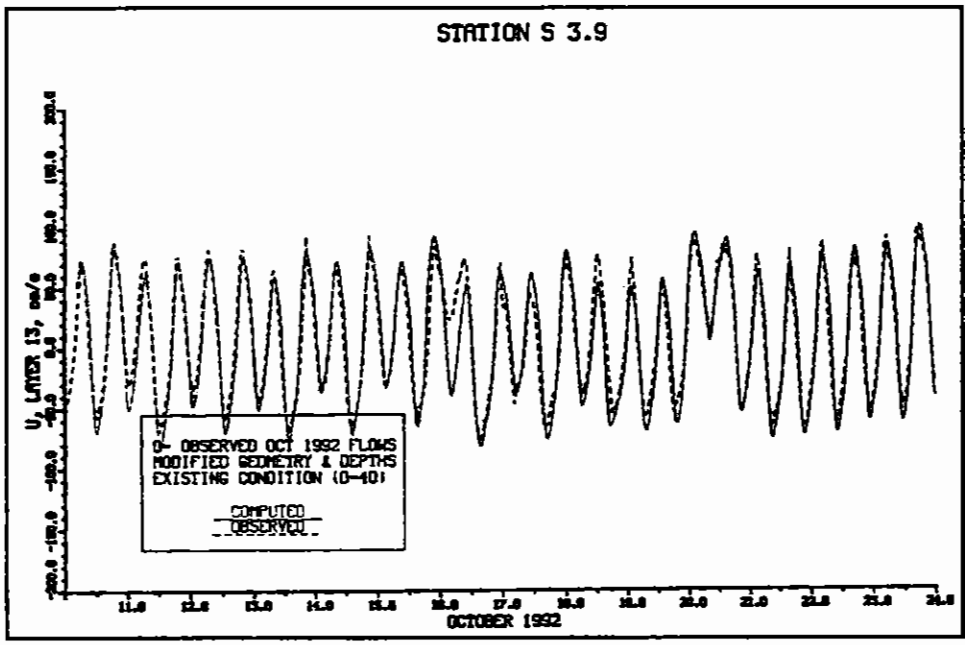

Figure 36. Velocity at Station S 3.9 in October 1992

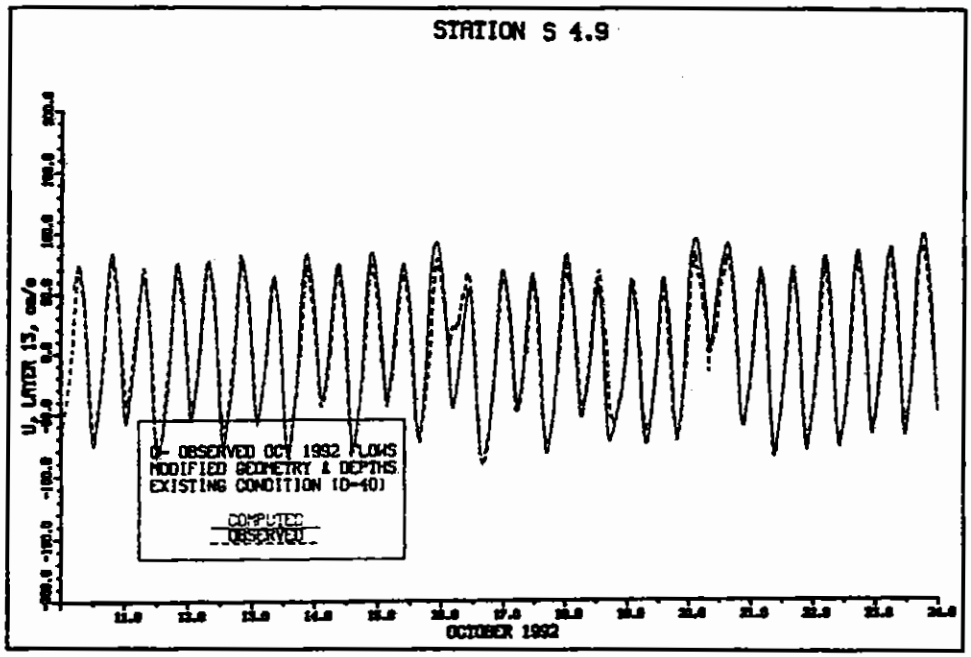

Figure 37. Along-bay velocity at Station S 4.9 in October 1992

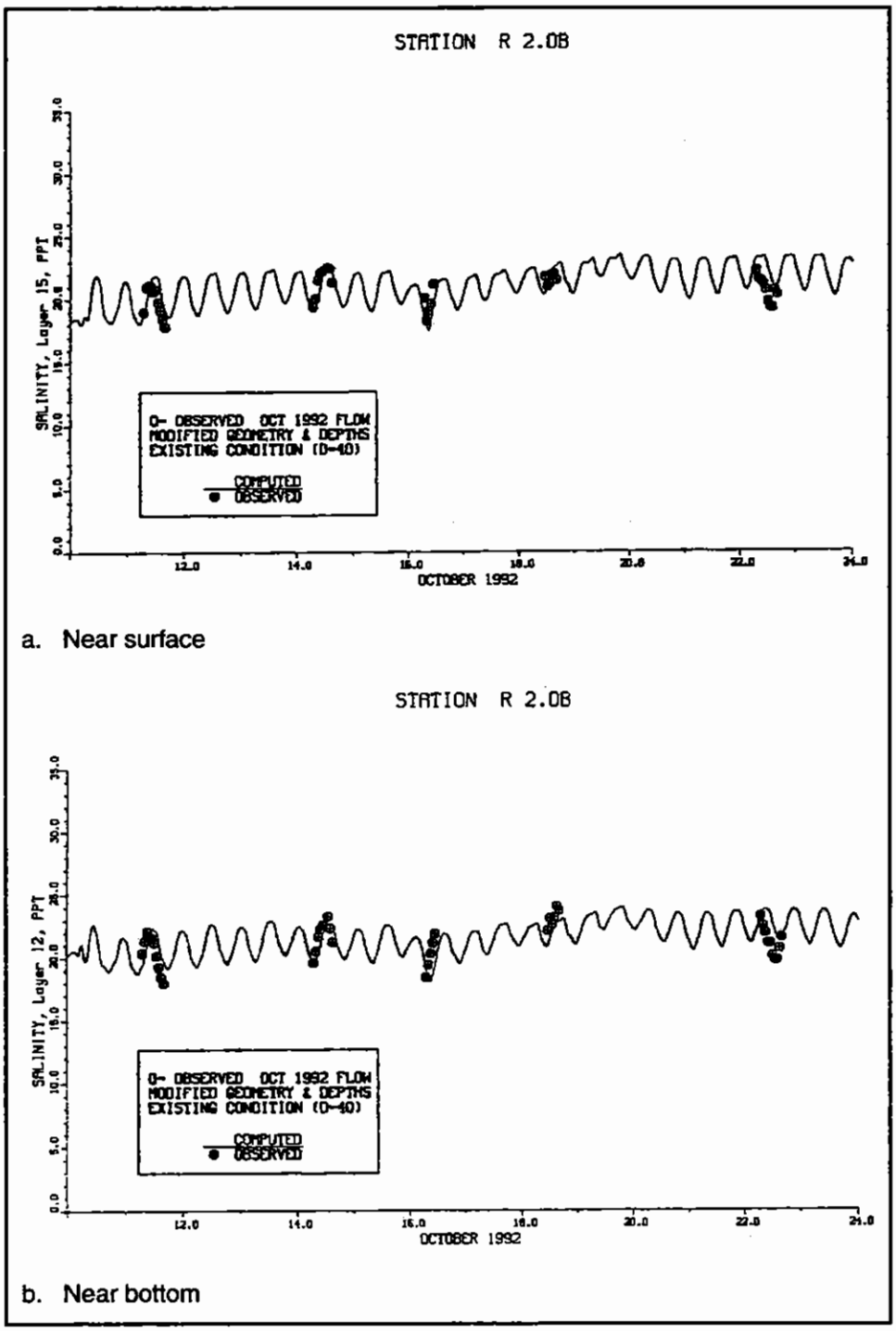

Figure 38. Salinity at Station R 2.0B in October 1992

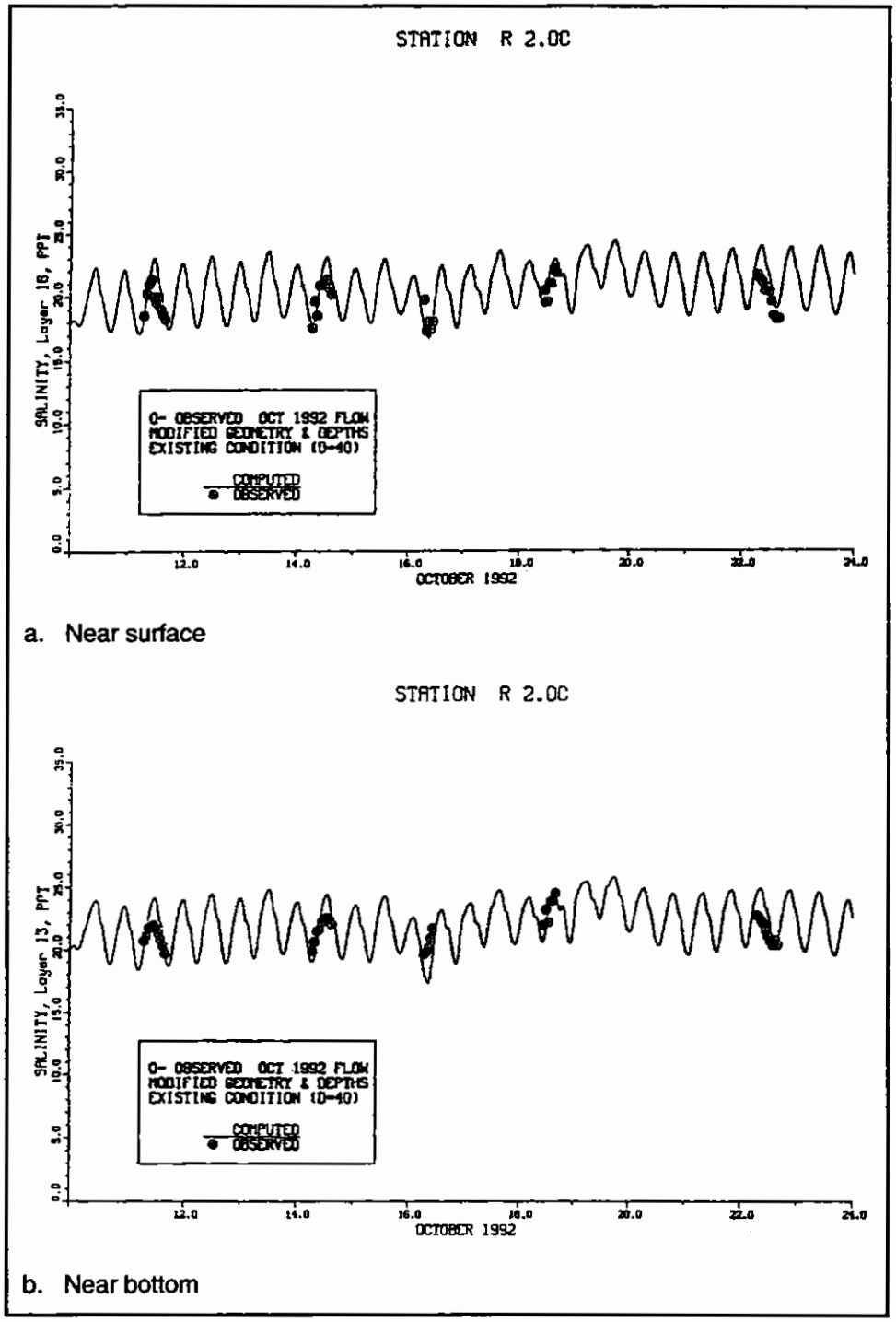

Figure 39. Salinity at Station R 2.0C in October 1992

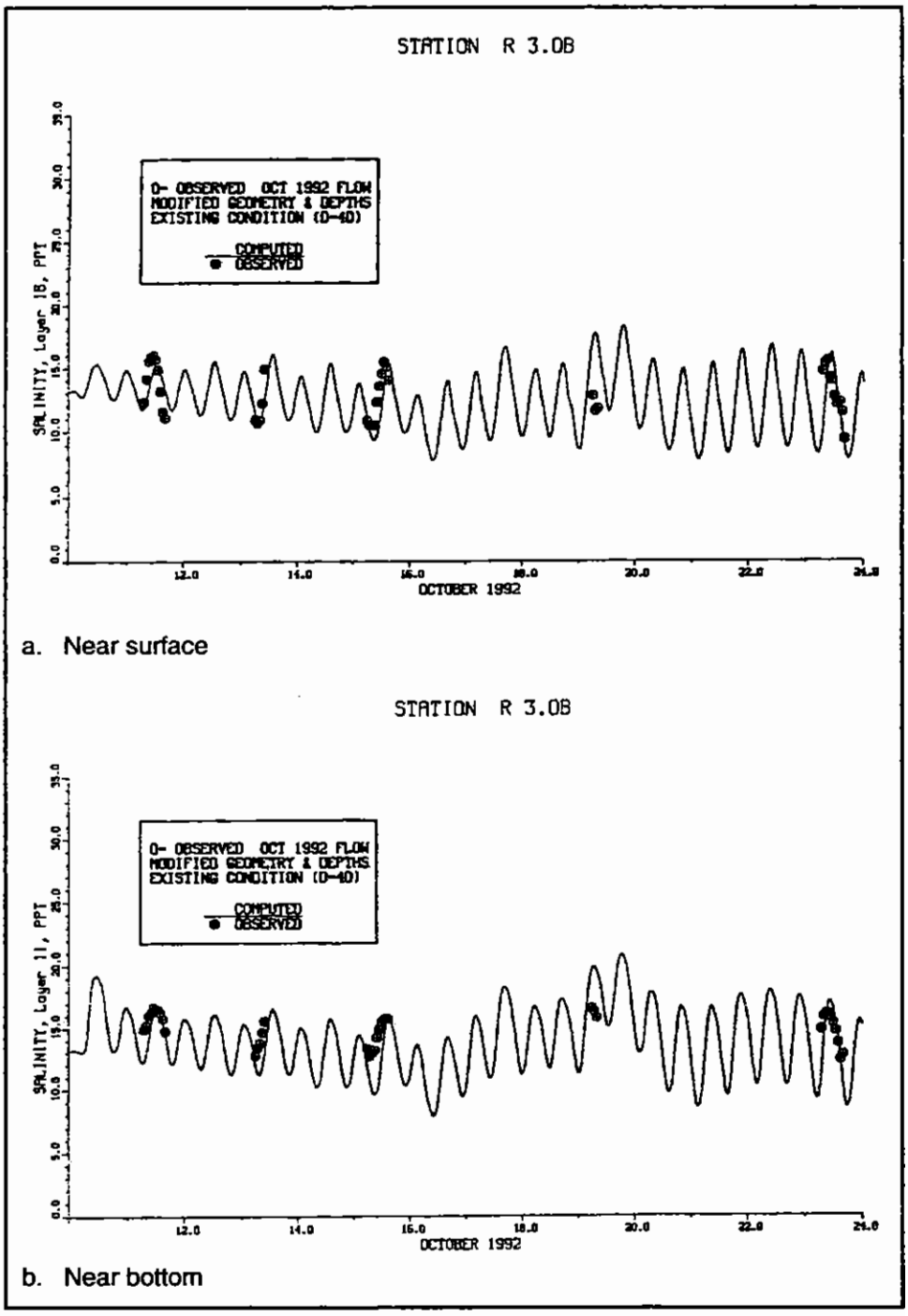

Figure 40. Salinity at Station R 3.0B in October 1992

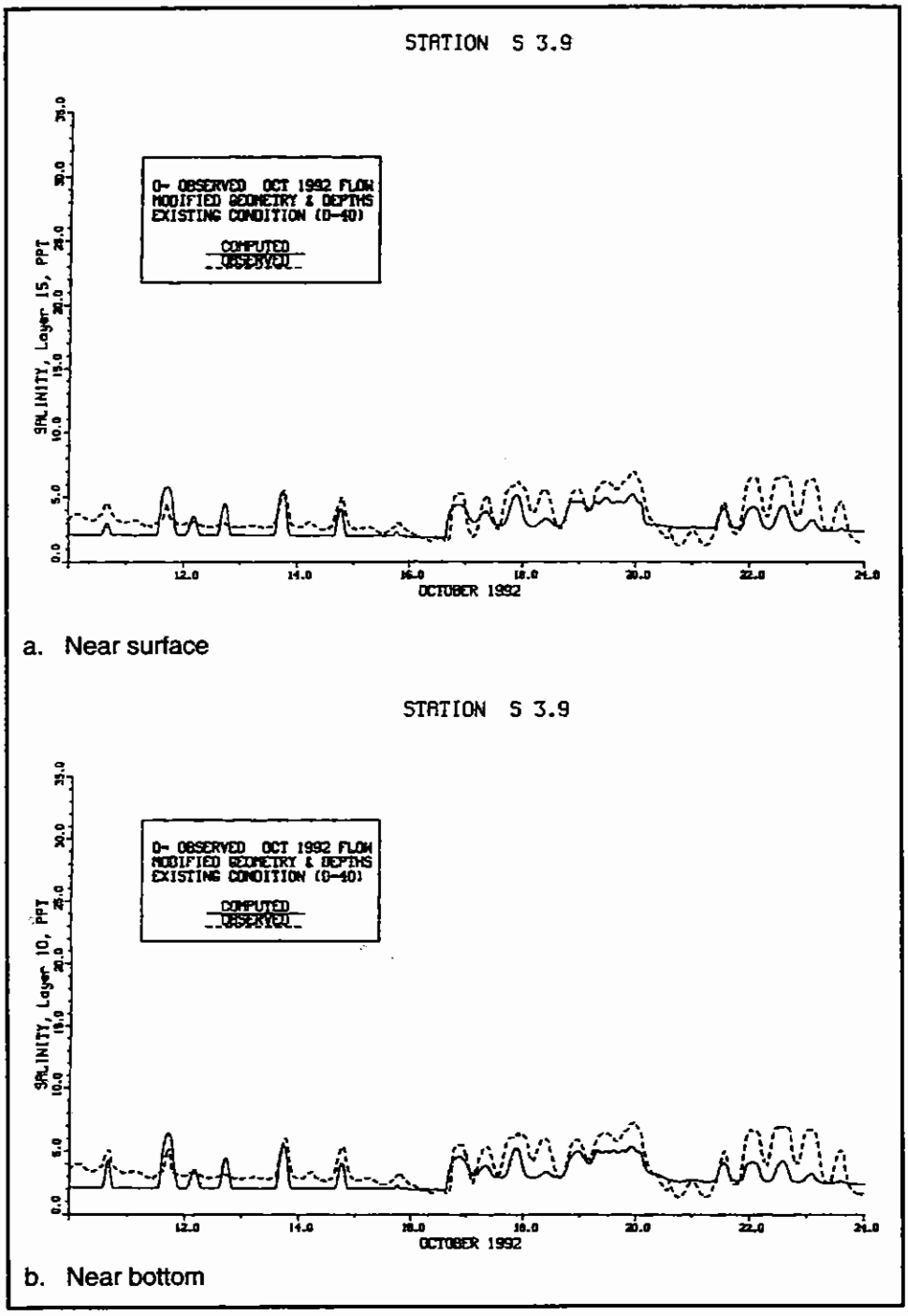

Figure 41. Salinity at Station S 3.9 in October 1992

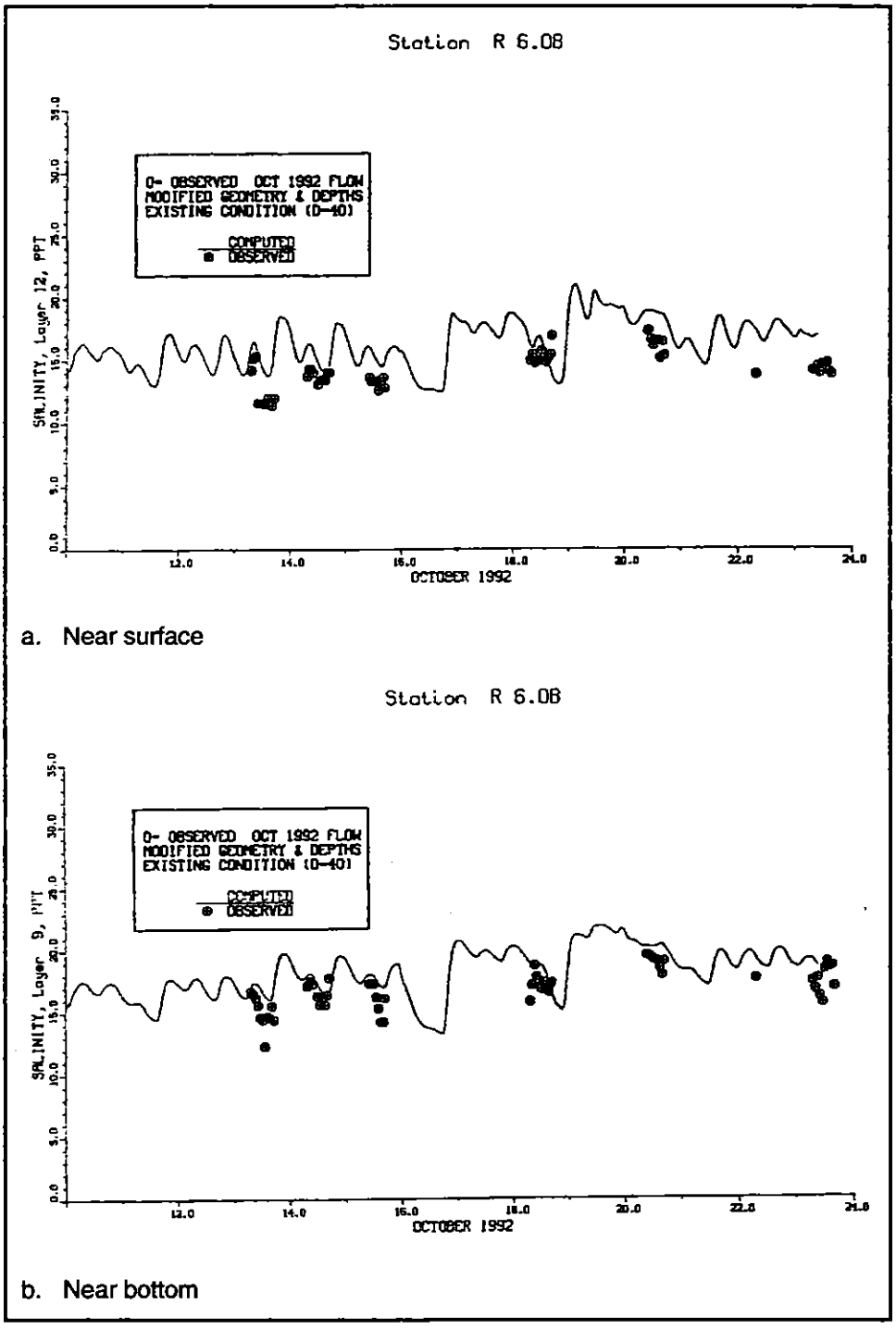

Figure 42. Salinity at Station R 6.0B in October 1992

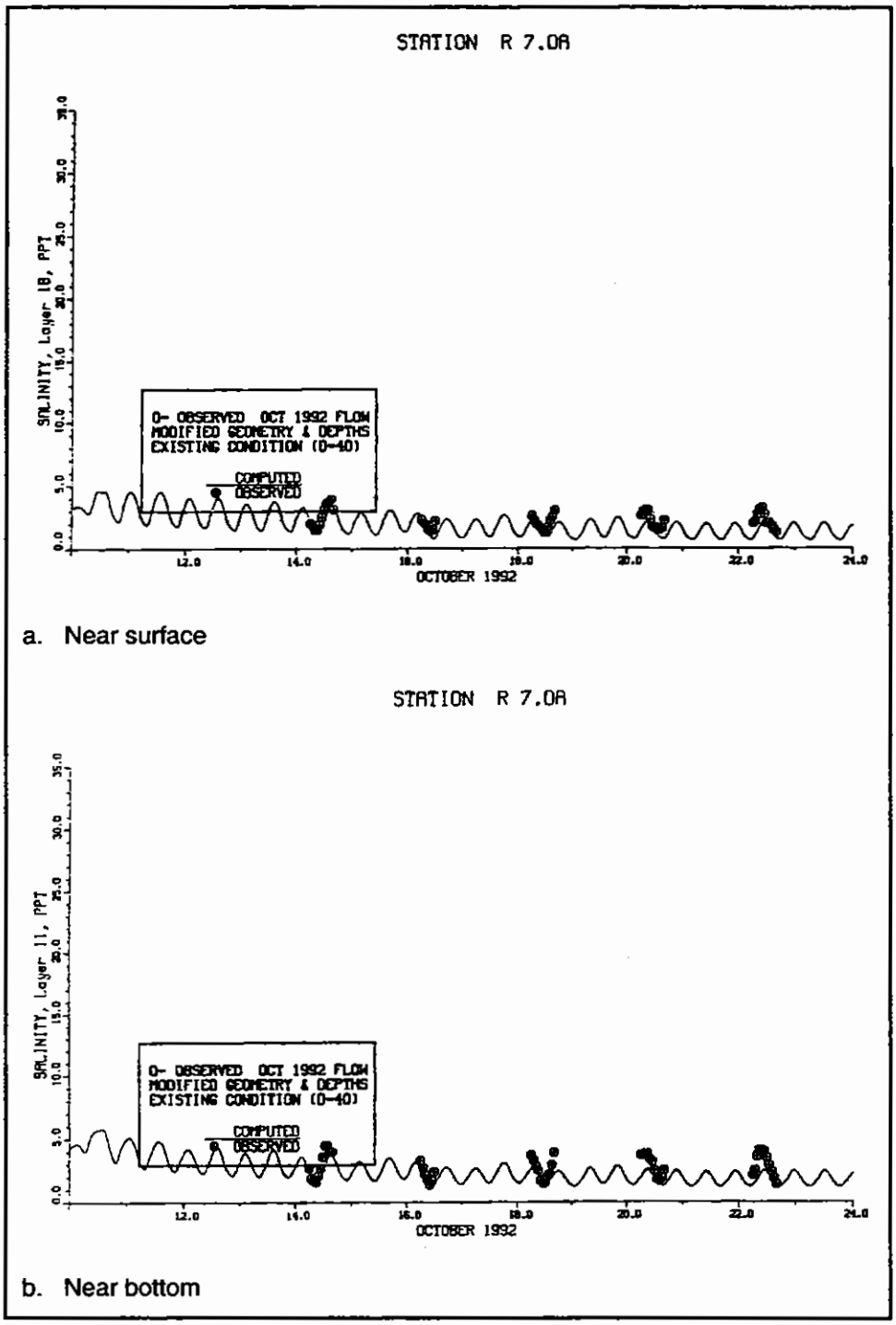

Figure 43. Salinity at Station R 7.0A in October 1992

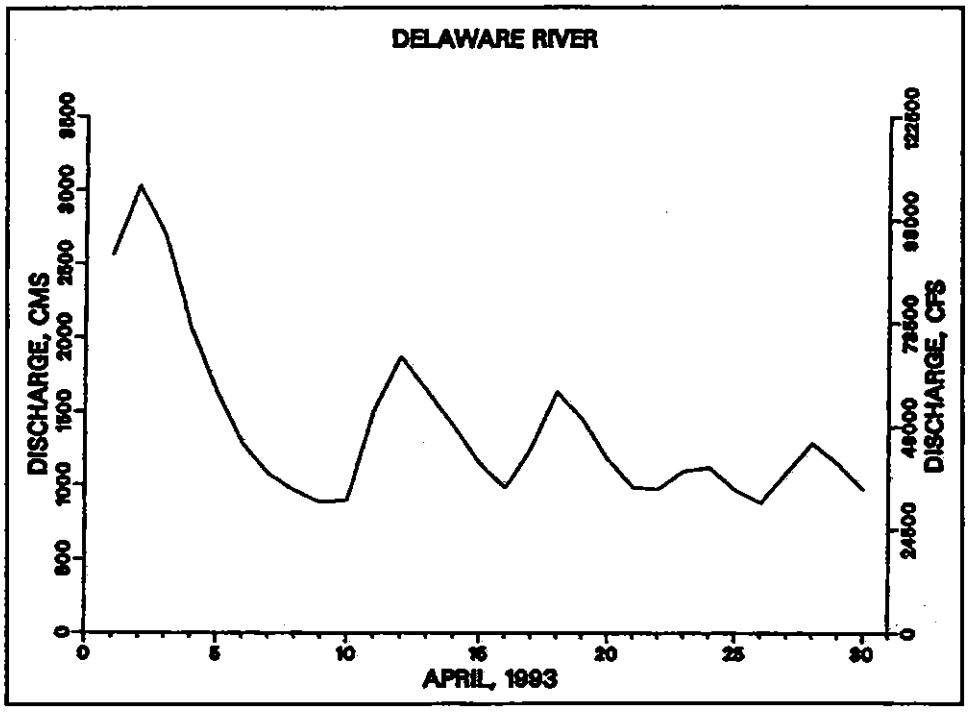

Figure 44. Freshwater inflow on the Delaware River in April 1993

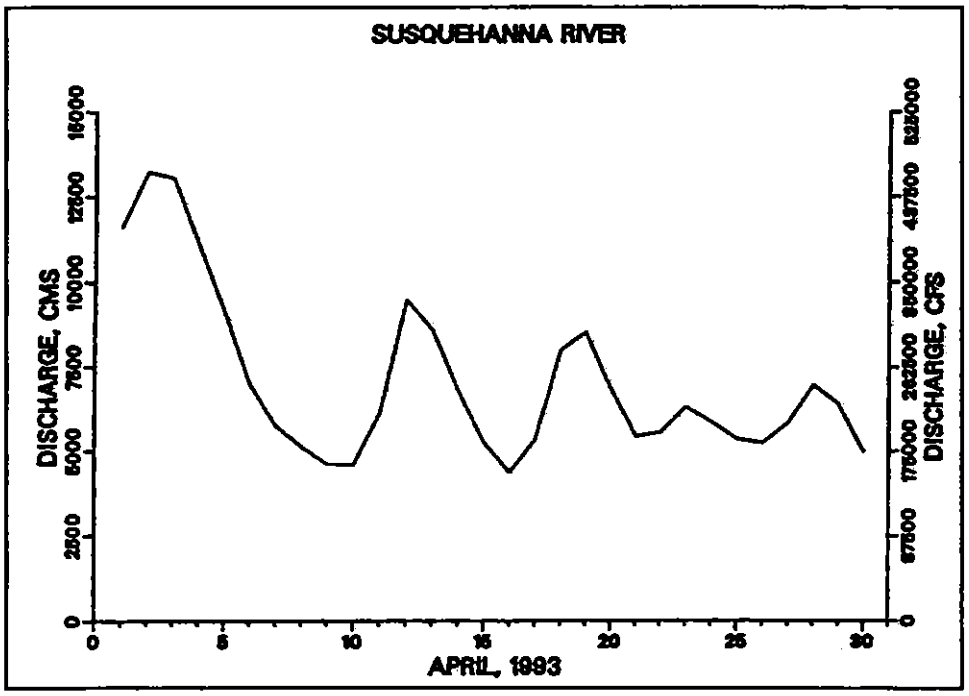

Figure 45. Freshwater inflow on the Susquehanna River in April 1993

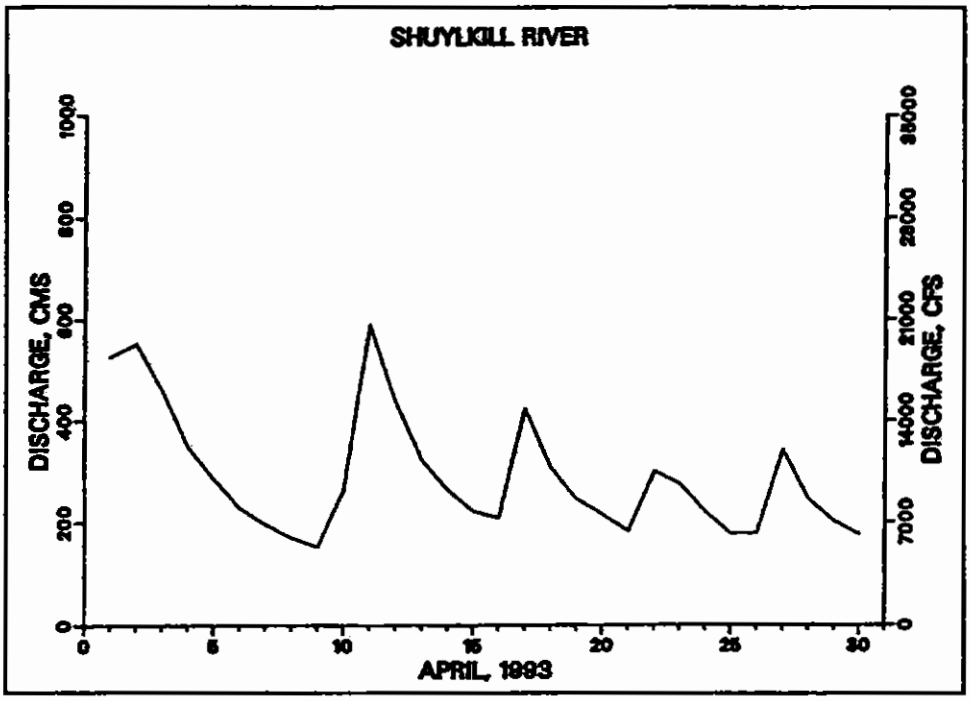

Figure 46. Freshwater inflow on the Schuylkill River in April 1993

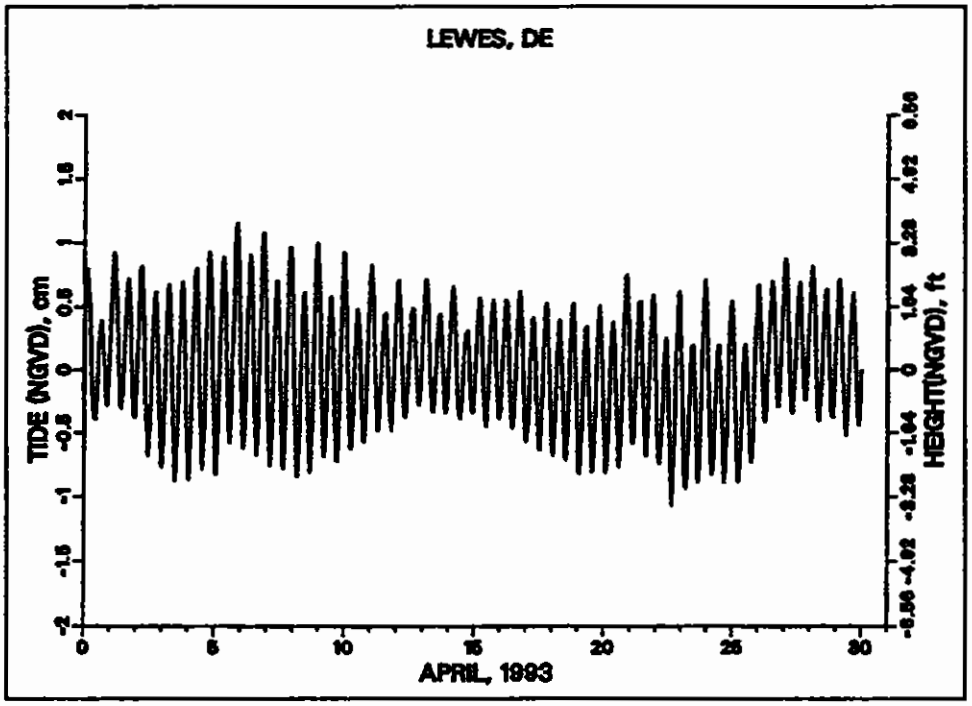

Figure 47. Tide (NGVD) at the Delaware Bay mouth in April 1993

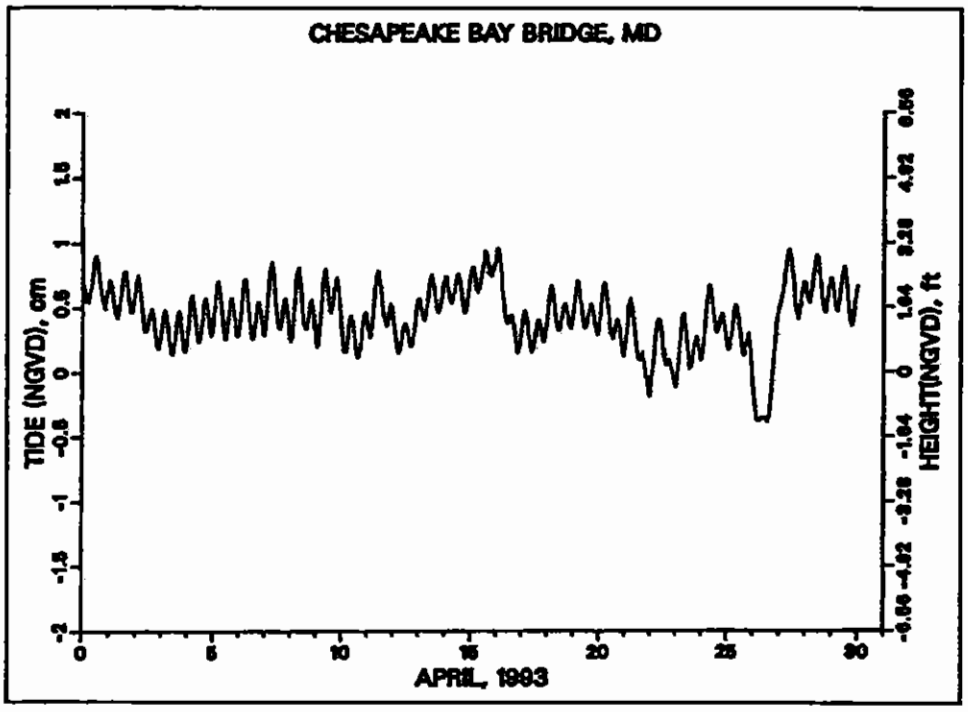

Figure 48. Tide (NGVD) at Annapolis, MD, in April 1993

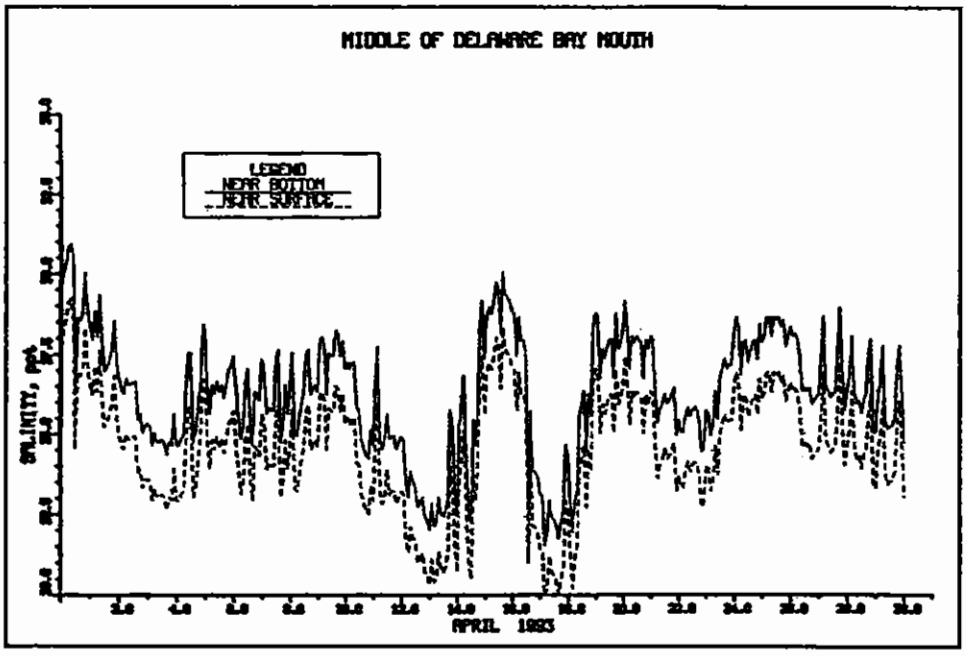

Figure 49. Salinity at Delaware Bay mouth in April 1993

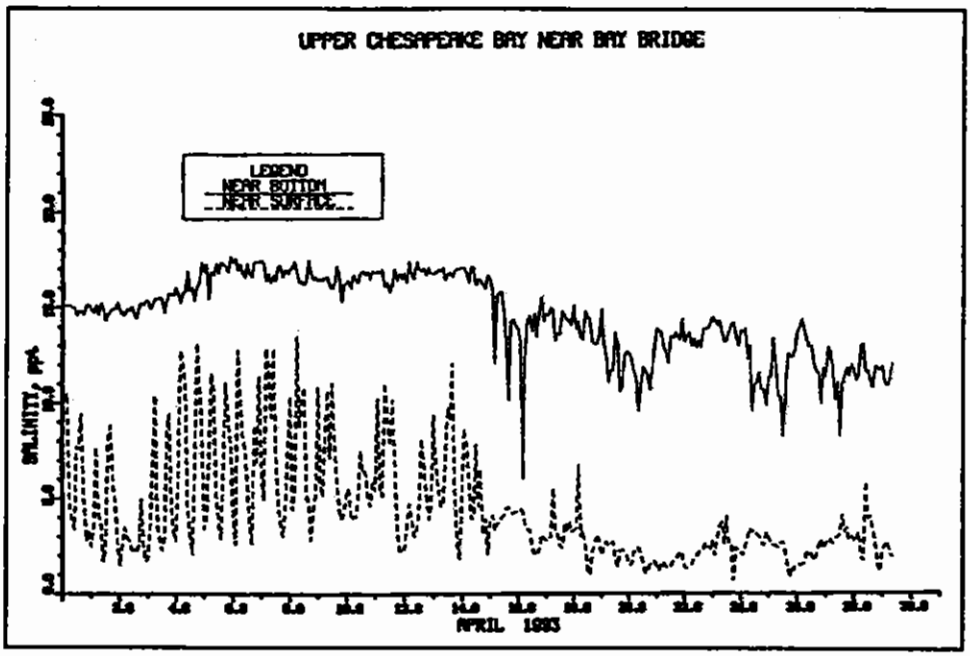

Figure 50. Salinity at Annapolis, MD, in April 1993

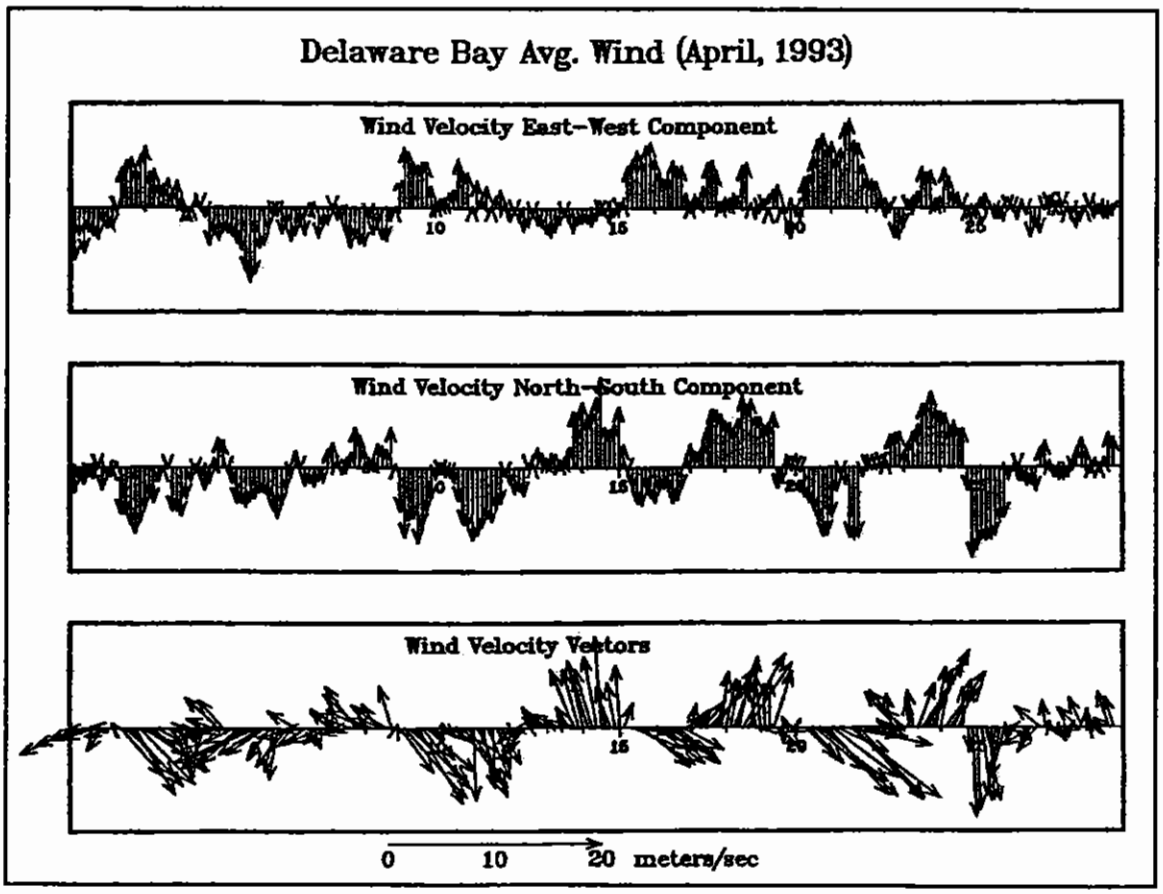

Figure 51. Average wind for April 1993

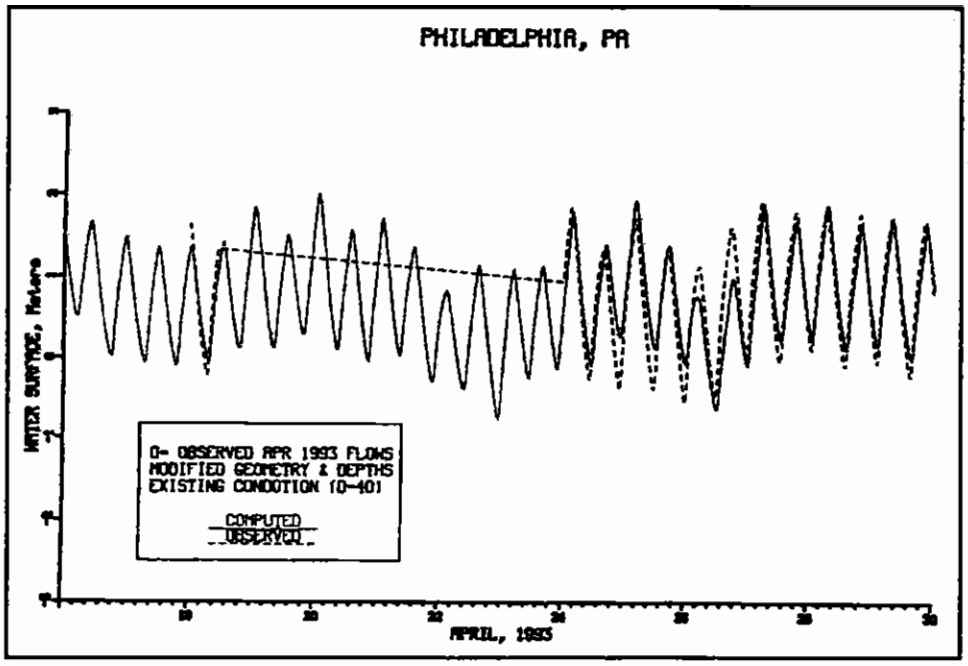

Figure 52. Water-surface elevation (NGVD) at Philadelphia, PA, in April 1993

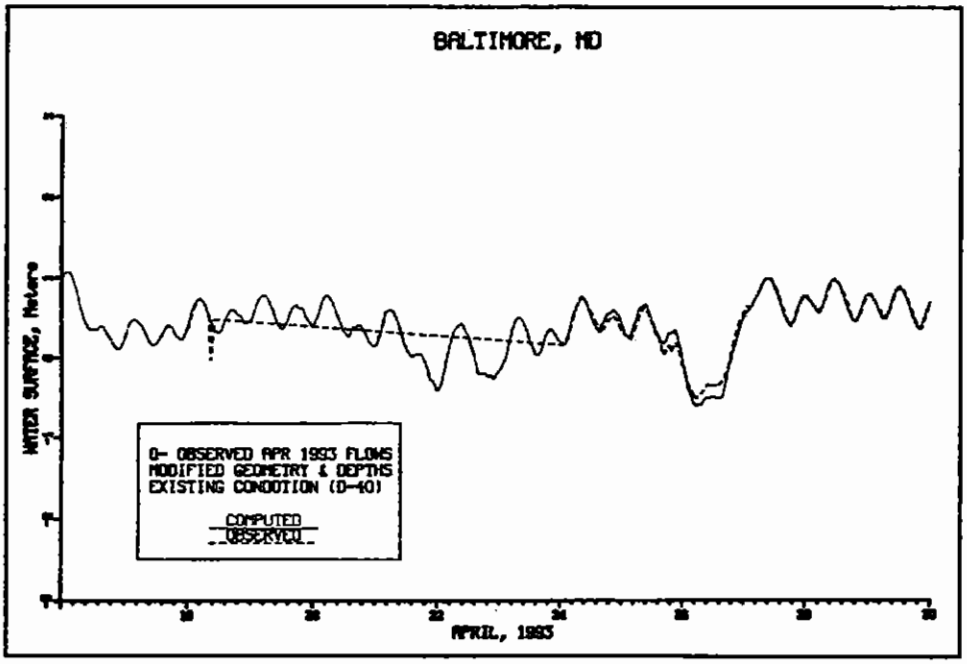

Figure 53. Water-surface elevation (NGVD) at Baltimore, MD, in April 1993

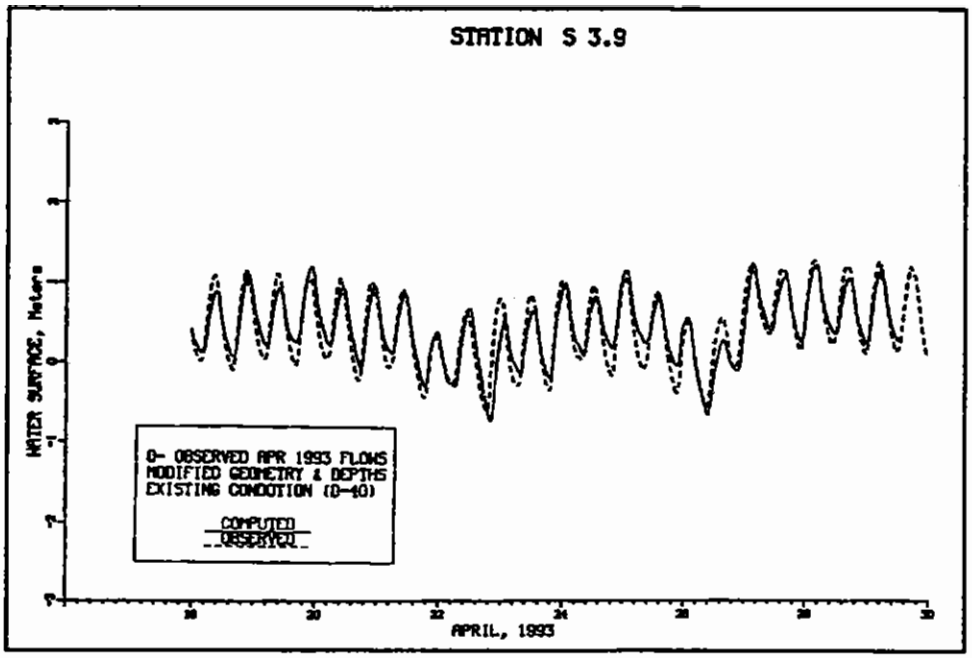

Figure 54. Water-surface elevation (NGVD) at Summit Bridge, MD, in April 1993

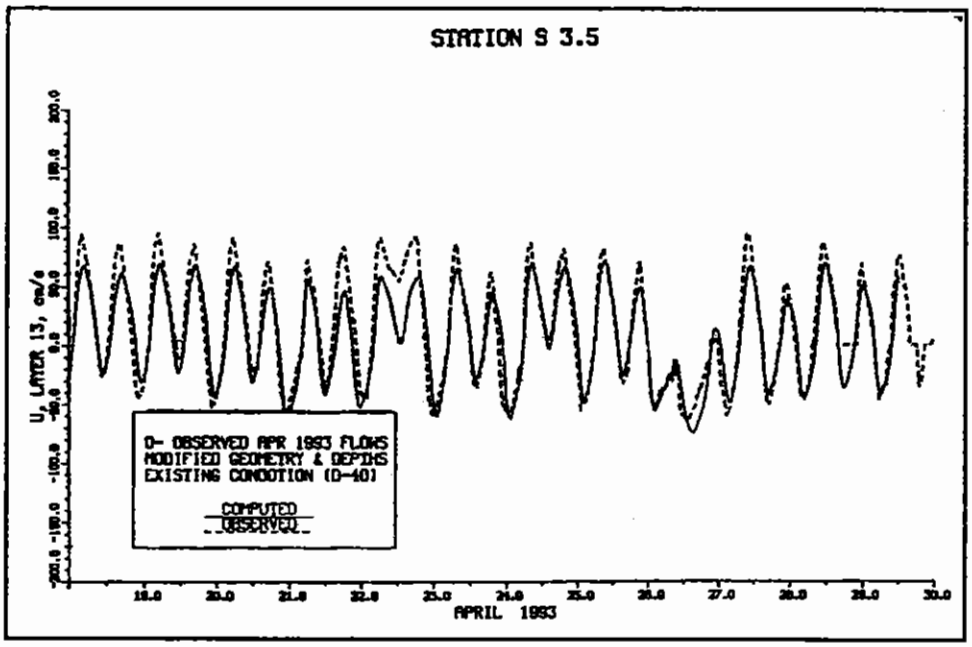

Figure 55. Velocity at Station S 3.5 in April 1993

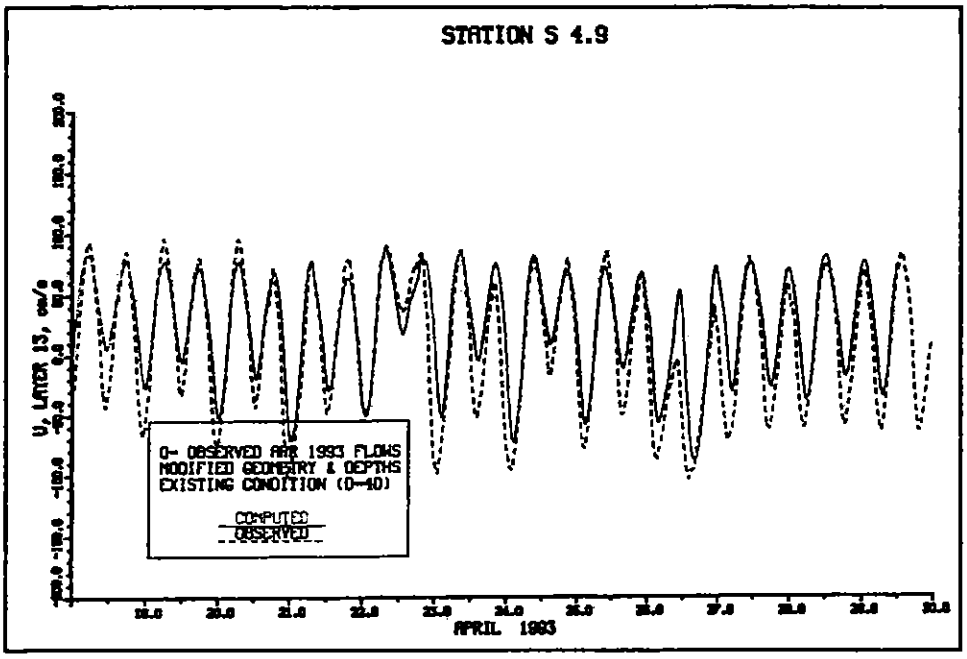

Figure 56. Along-bay velocity at Station S 4.9 in April 1993

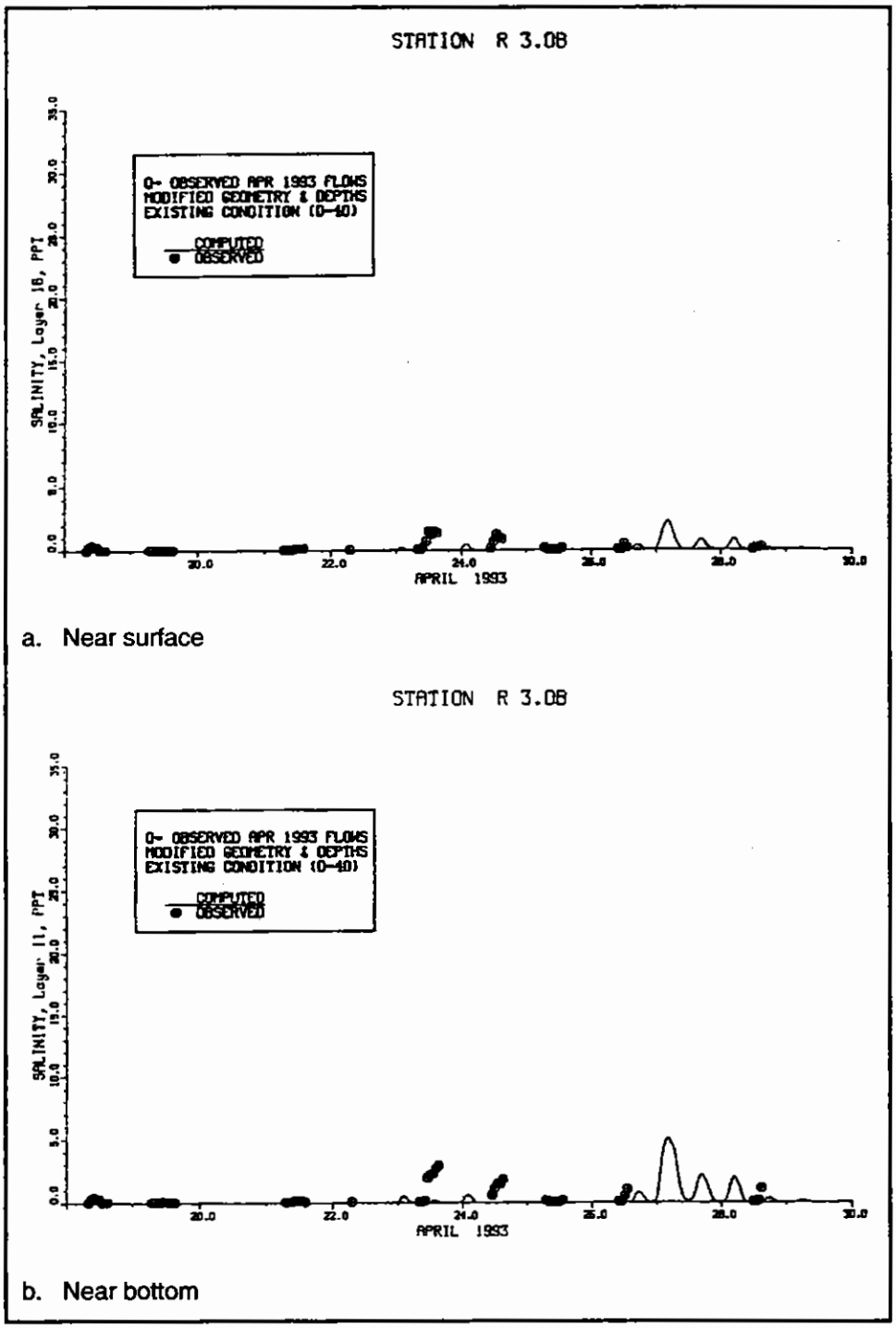

Figure 57. Salinity at Station R 3.0B in April 1993

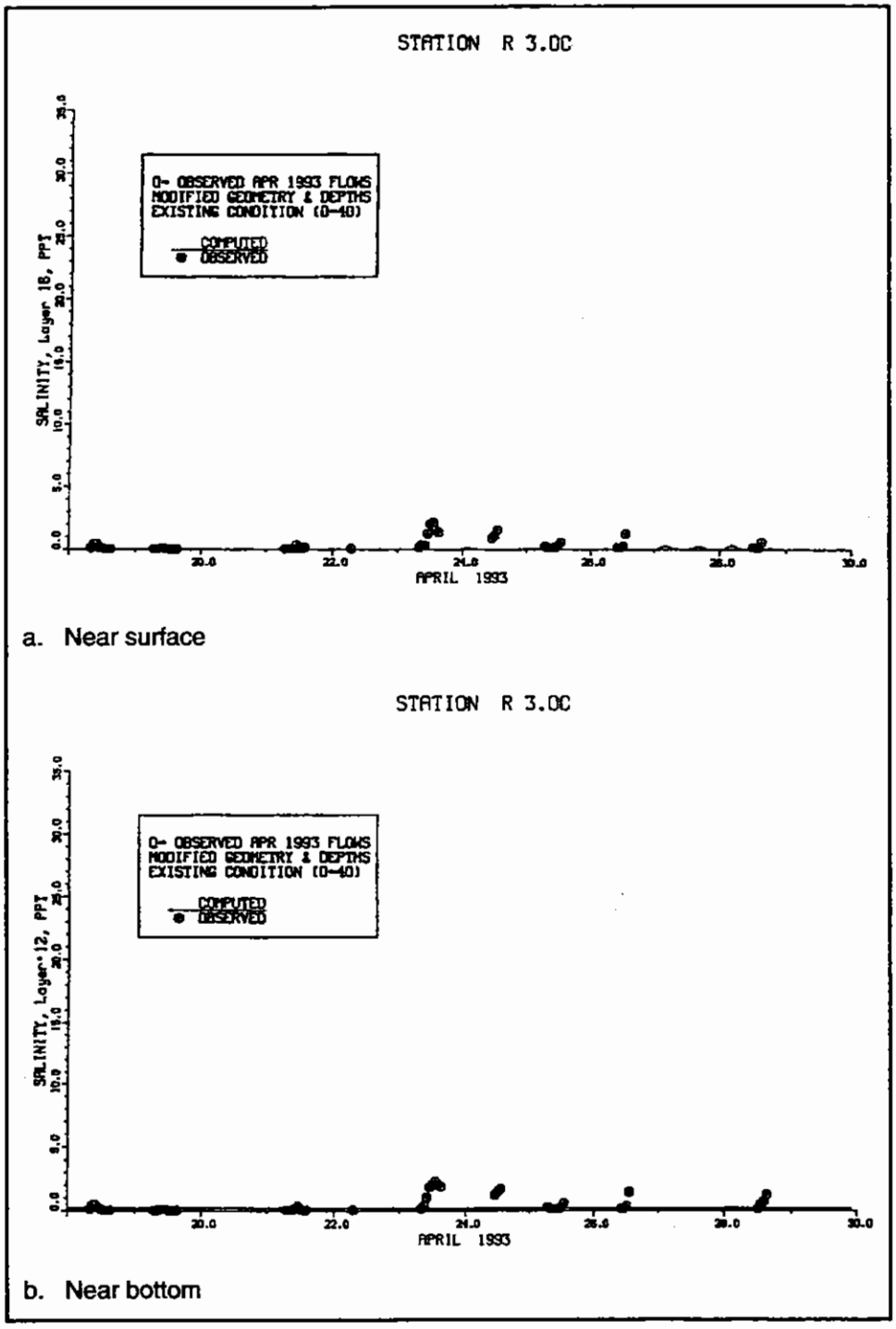

Figure 58. Salinity at Station R 3.0C in April 1993

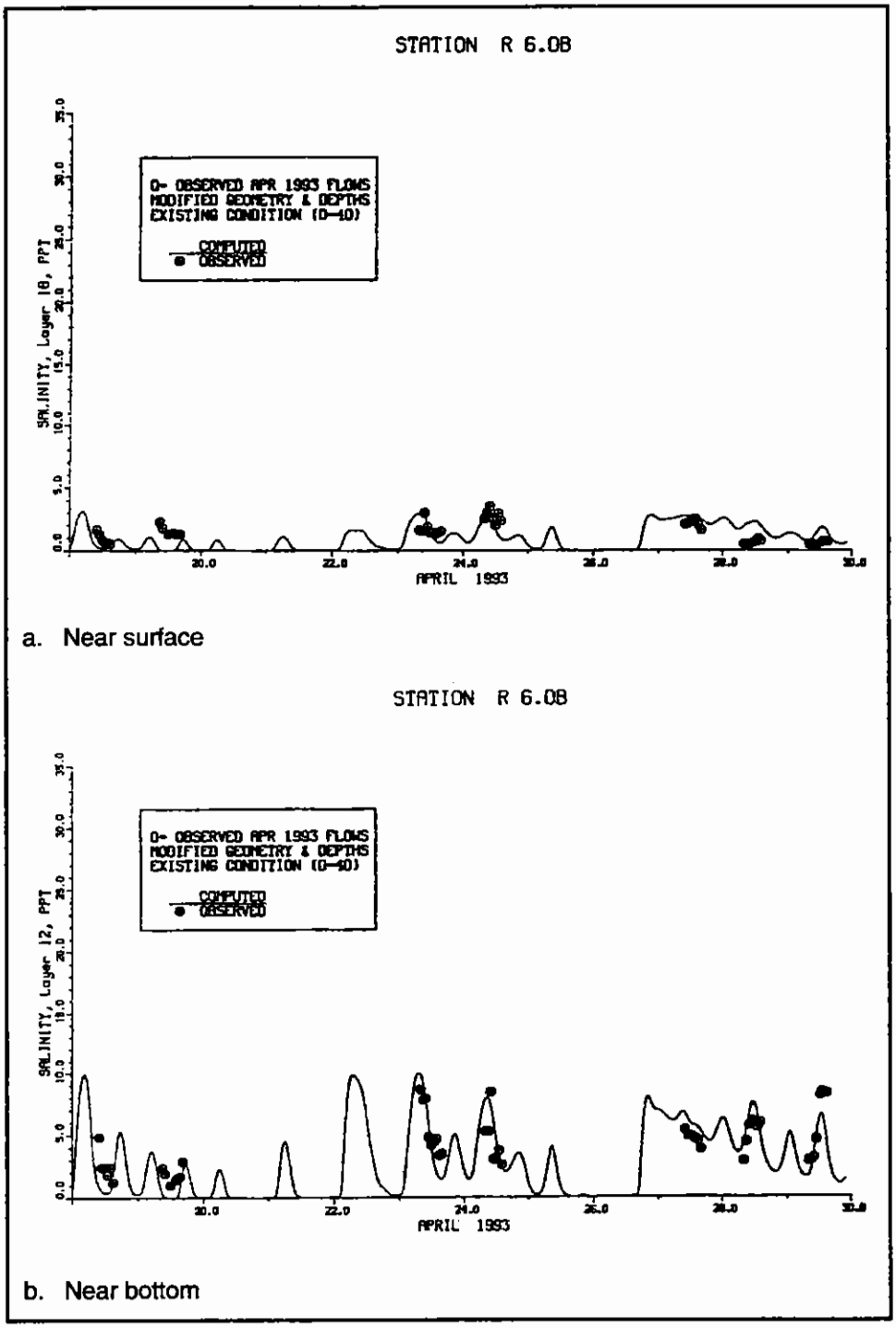

Figure 59. Near-surface salinity at Station R 6.0B in April 1993

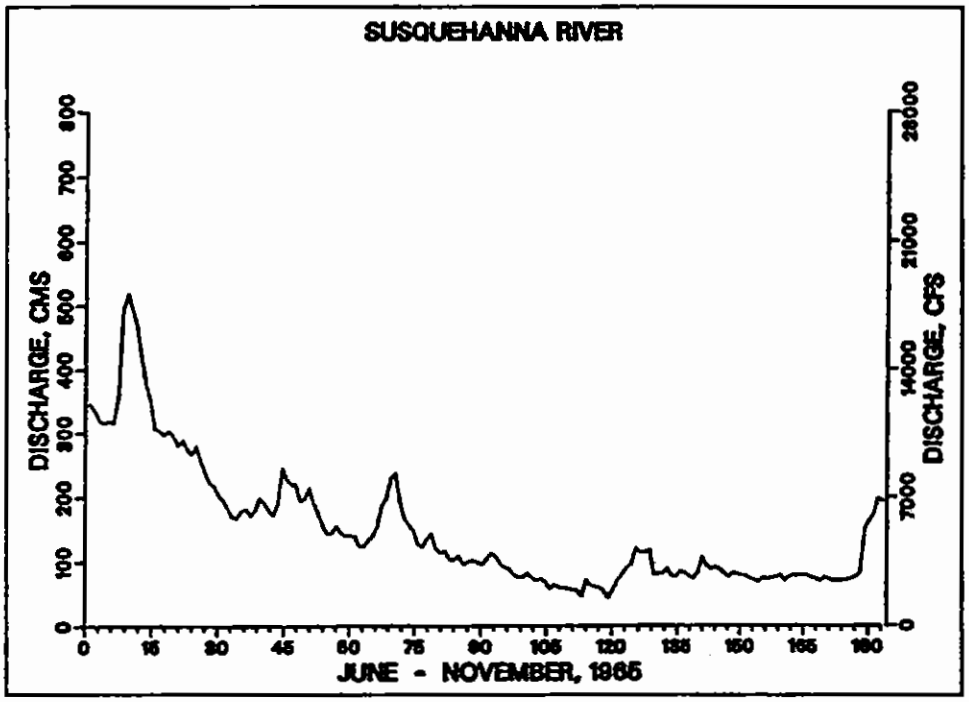

Figure 60. 1965 freshwater inflow on the Susquehanna River

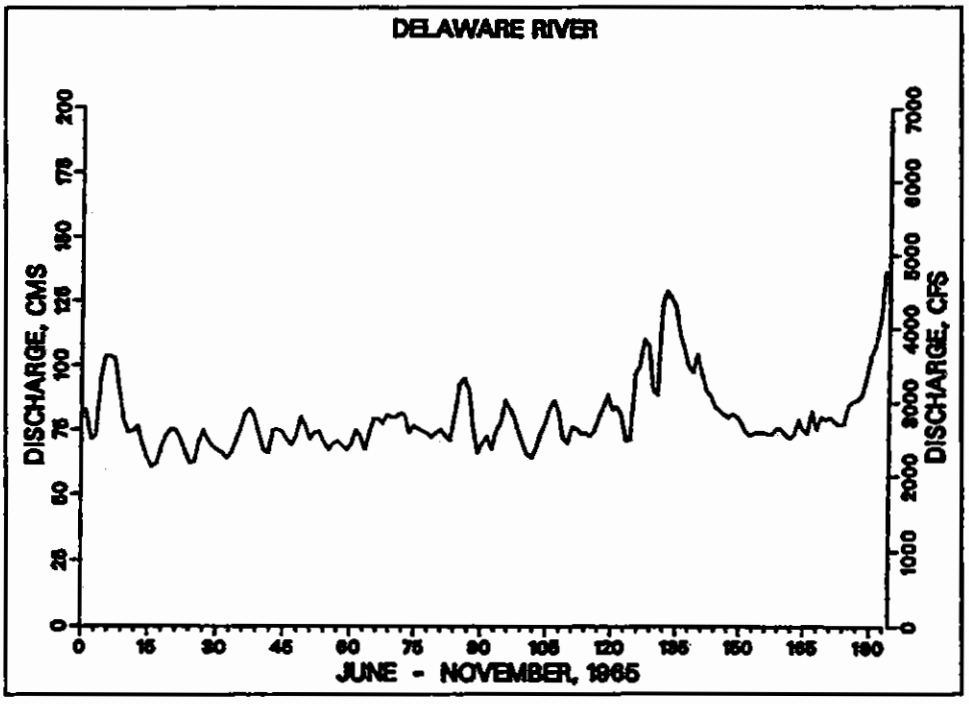

Figure 61. 1965 freshwater inflow on the Delaware River

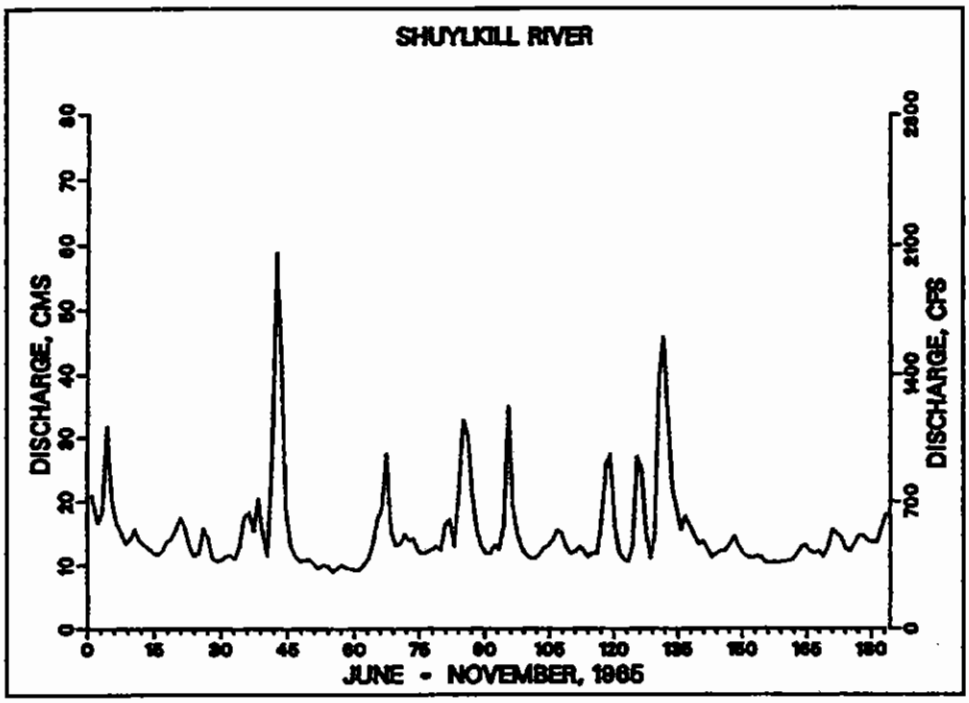

Figure 62. 1965 freshwater inflow on the Schuylkill River

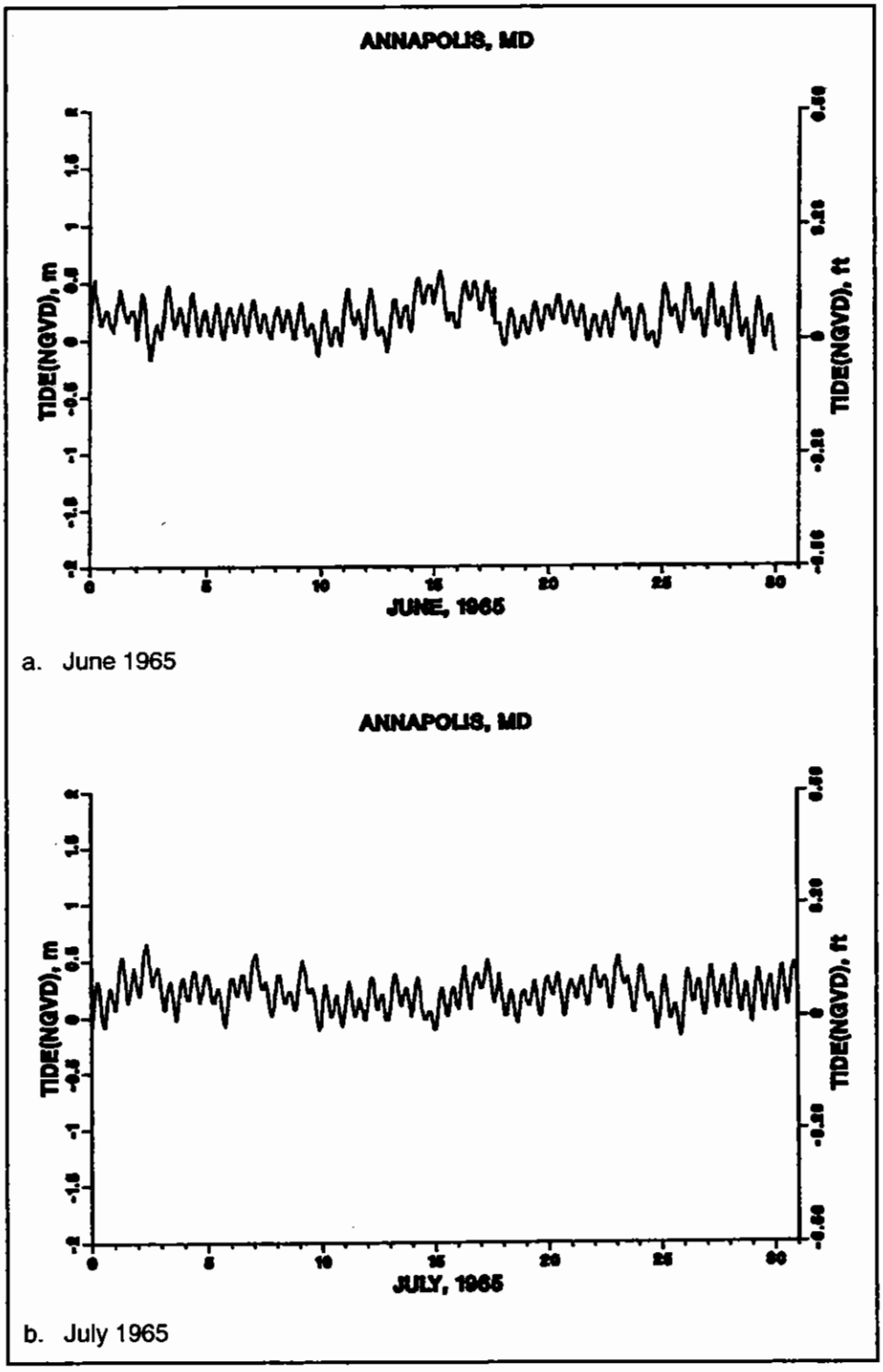

Figure 63. 1965 tide (NGVD) at Annapolis (Sheet 1 of 3)

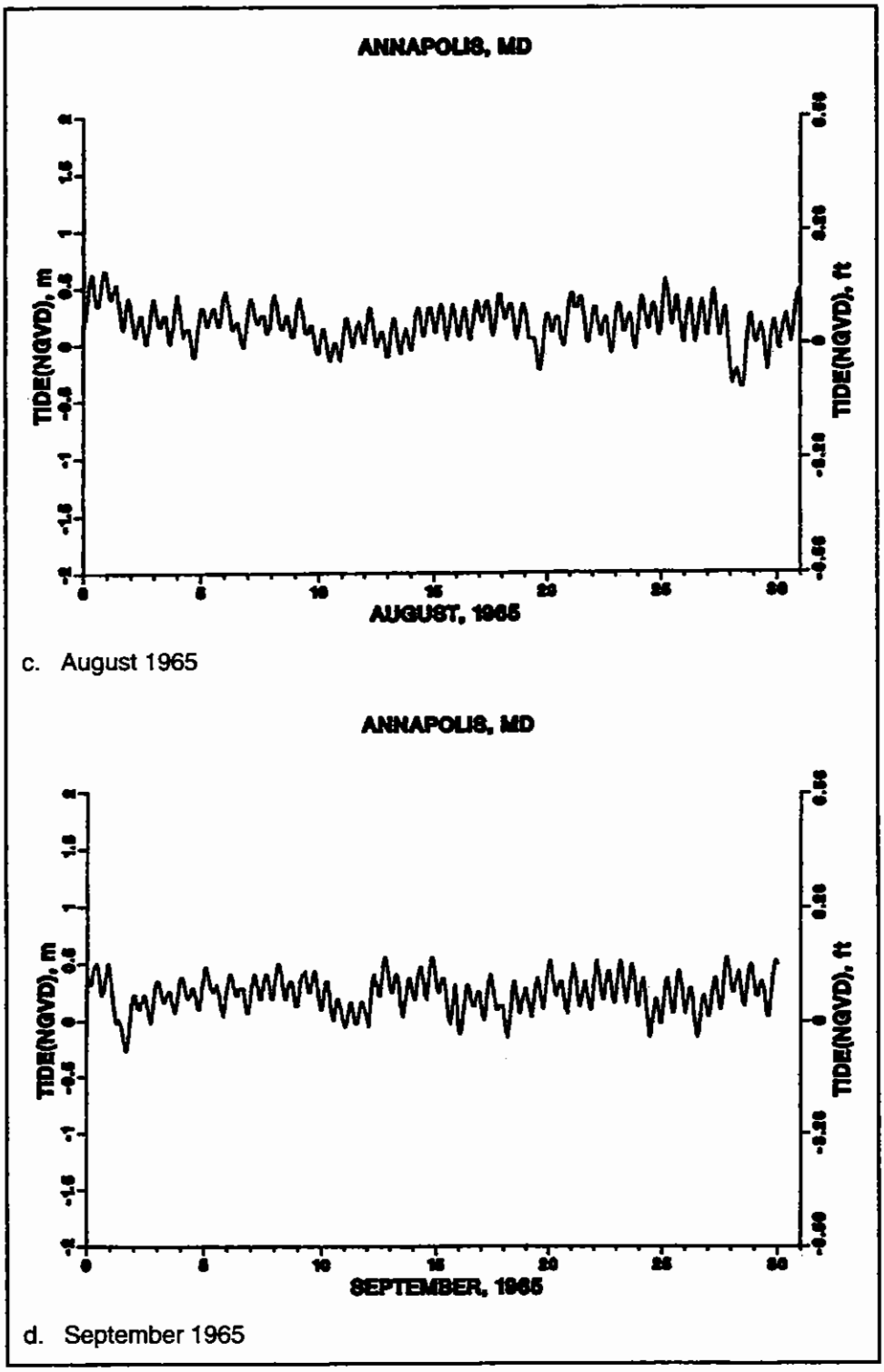

c. August 1965

d. September 1965

Figure 63. (Sheet 2 of 3)

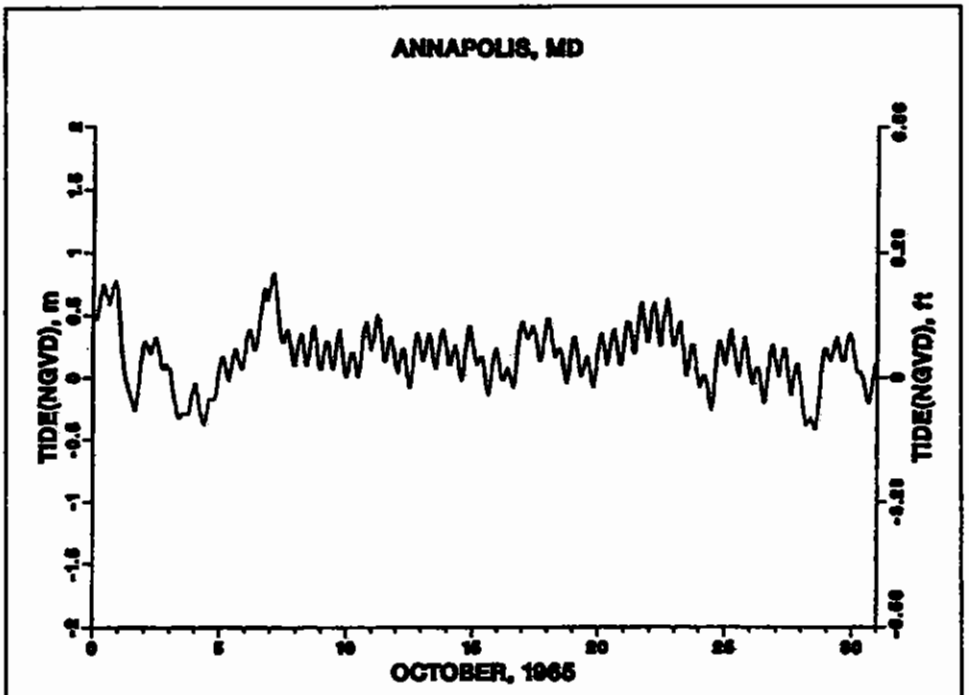

e. October 1965

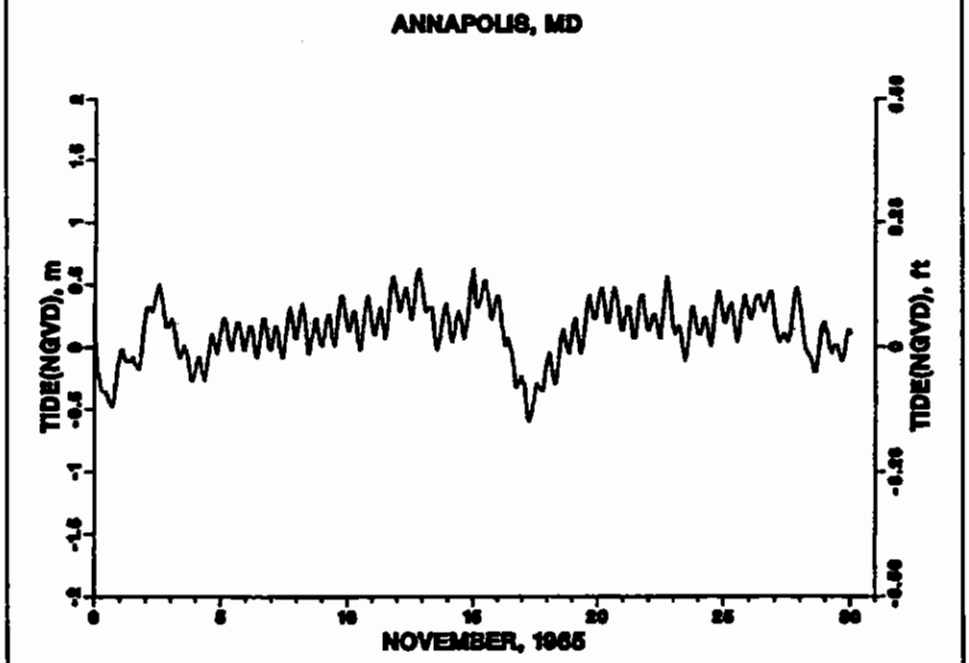

f. November 1965

Figure 63. (Sheet 3 of 3)

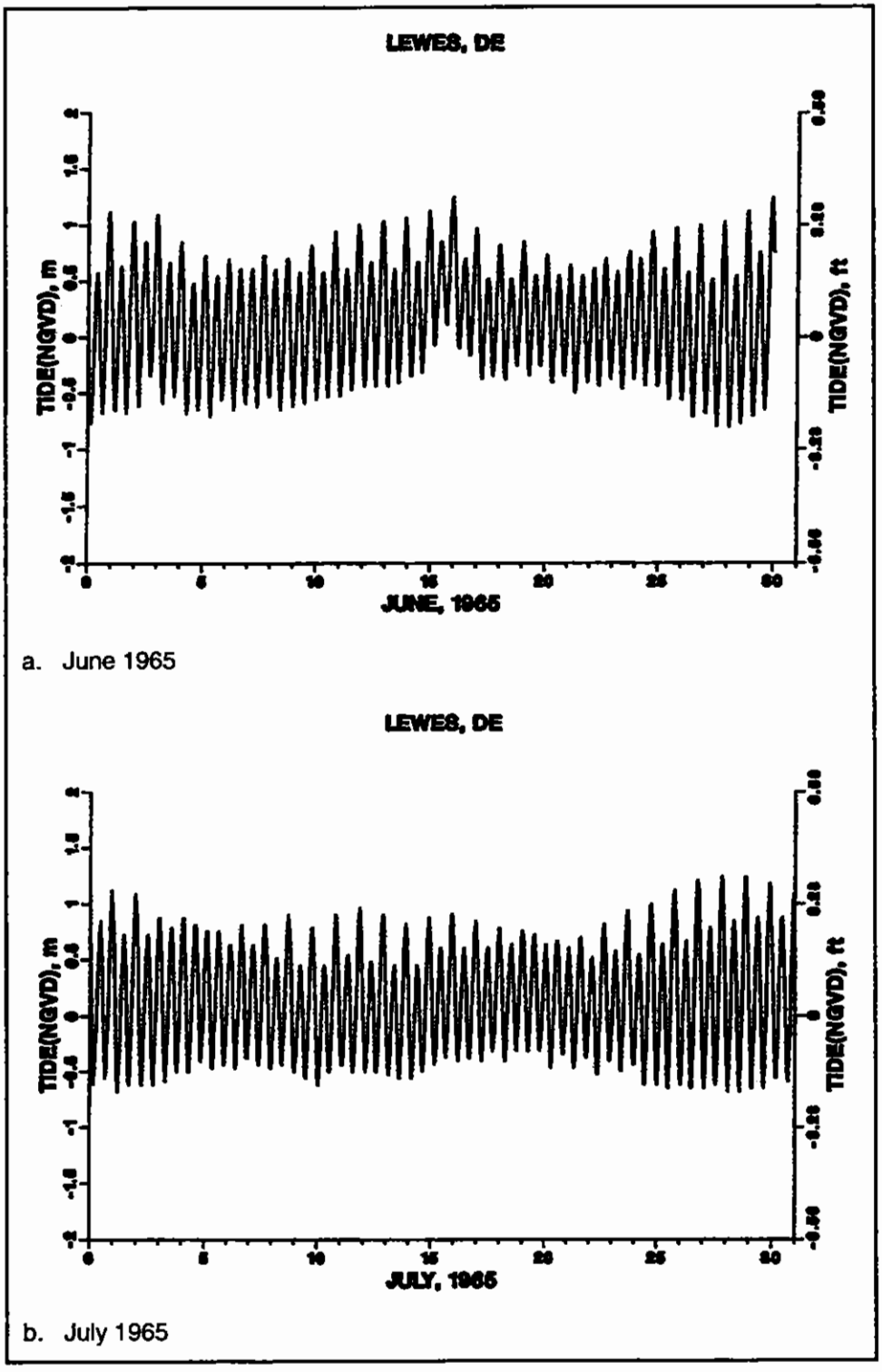

Figure 64. 1965 tide (NGVD) at Delaware Bay mouth (Sheet 1 of 3)

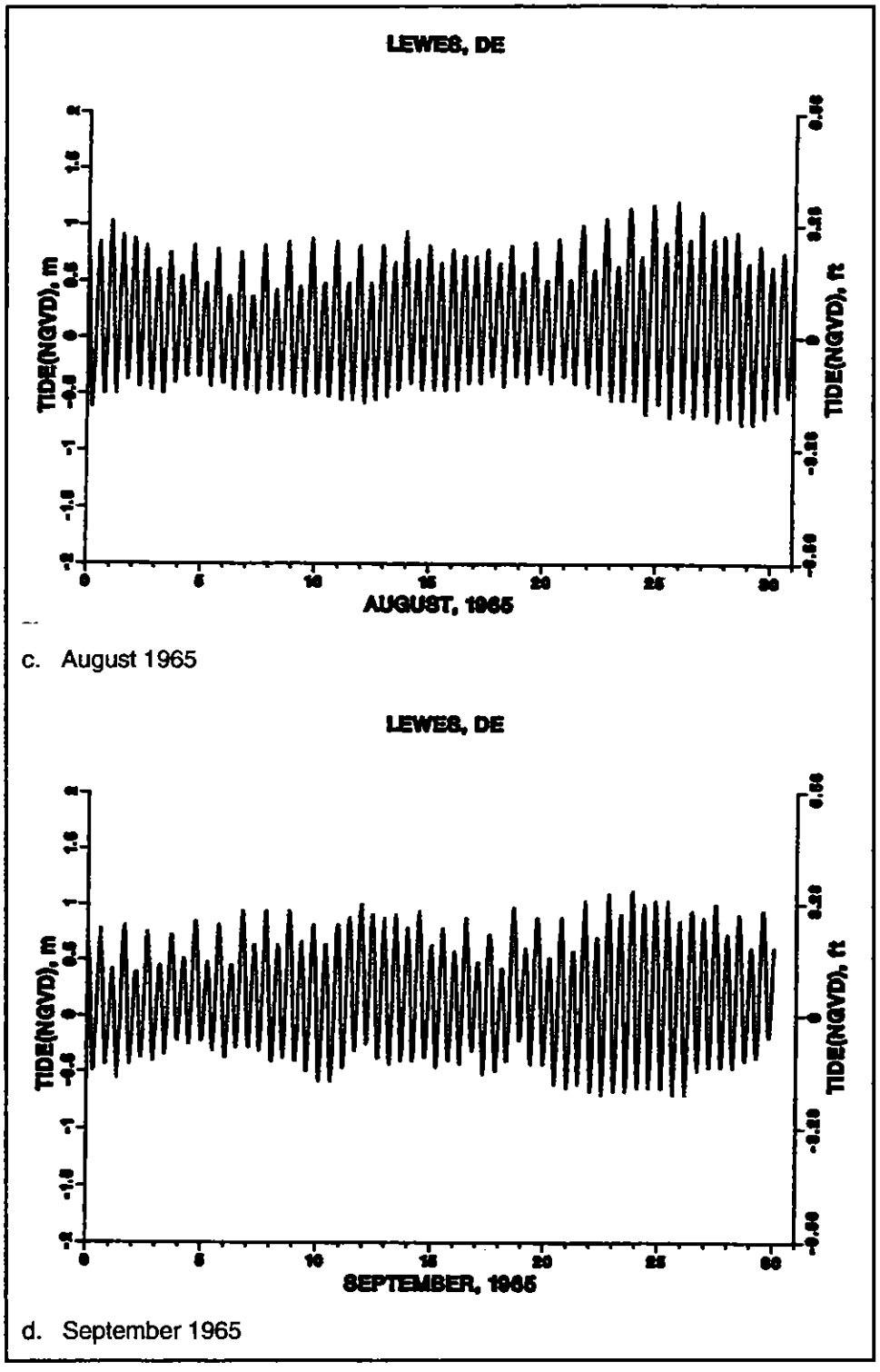

c. August 1965

d. September 1965

Figure 64. (Sheet 2 of 3)

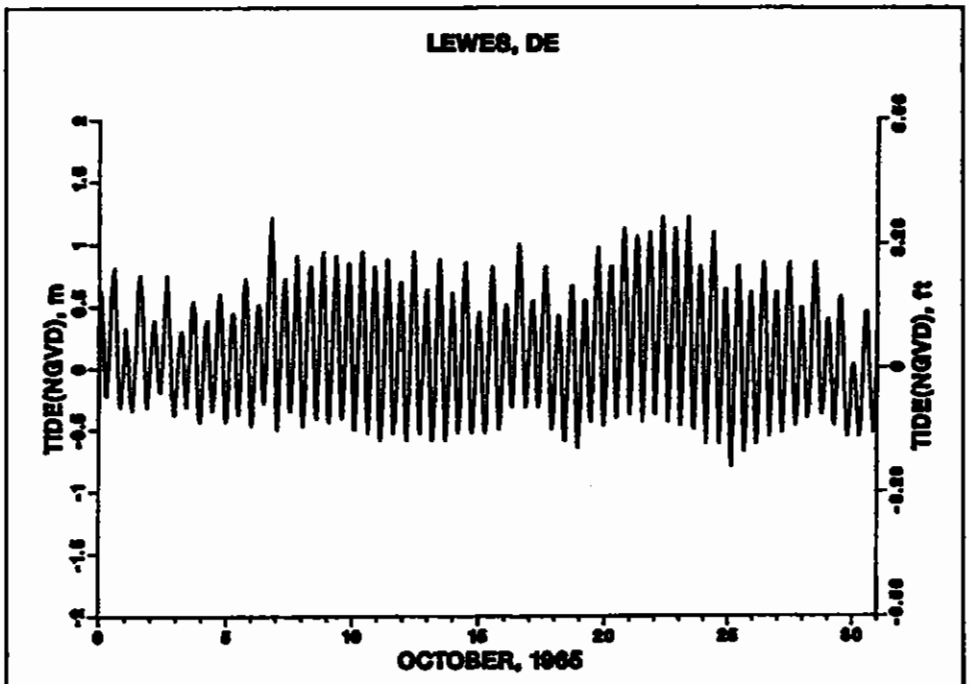

e. October 1965

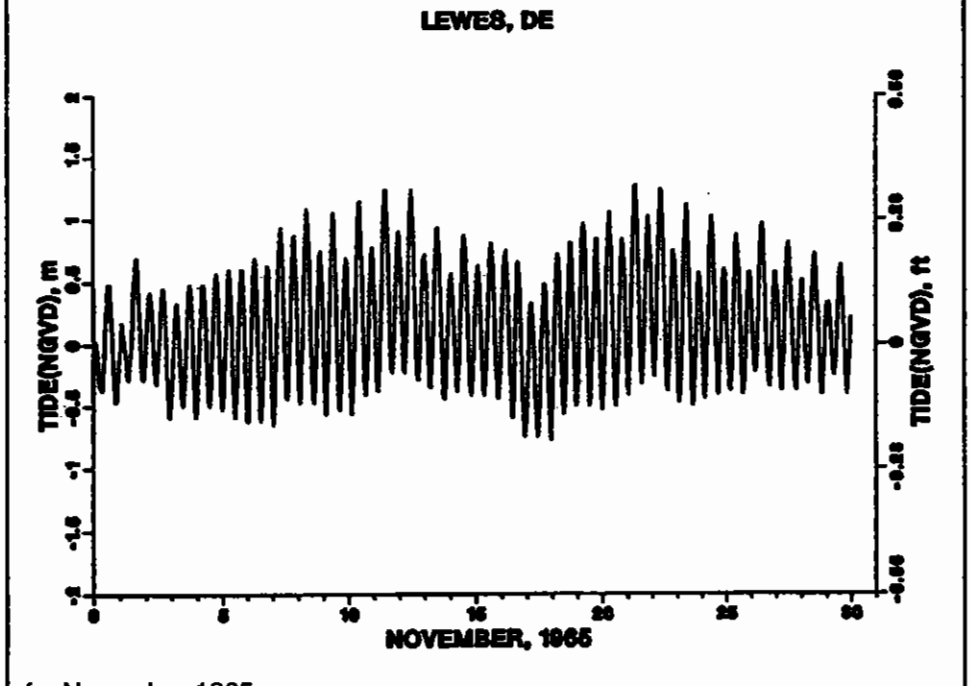

f. November 1965

Figure 64. (Sheet 3 of 3)

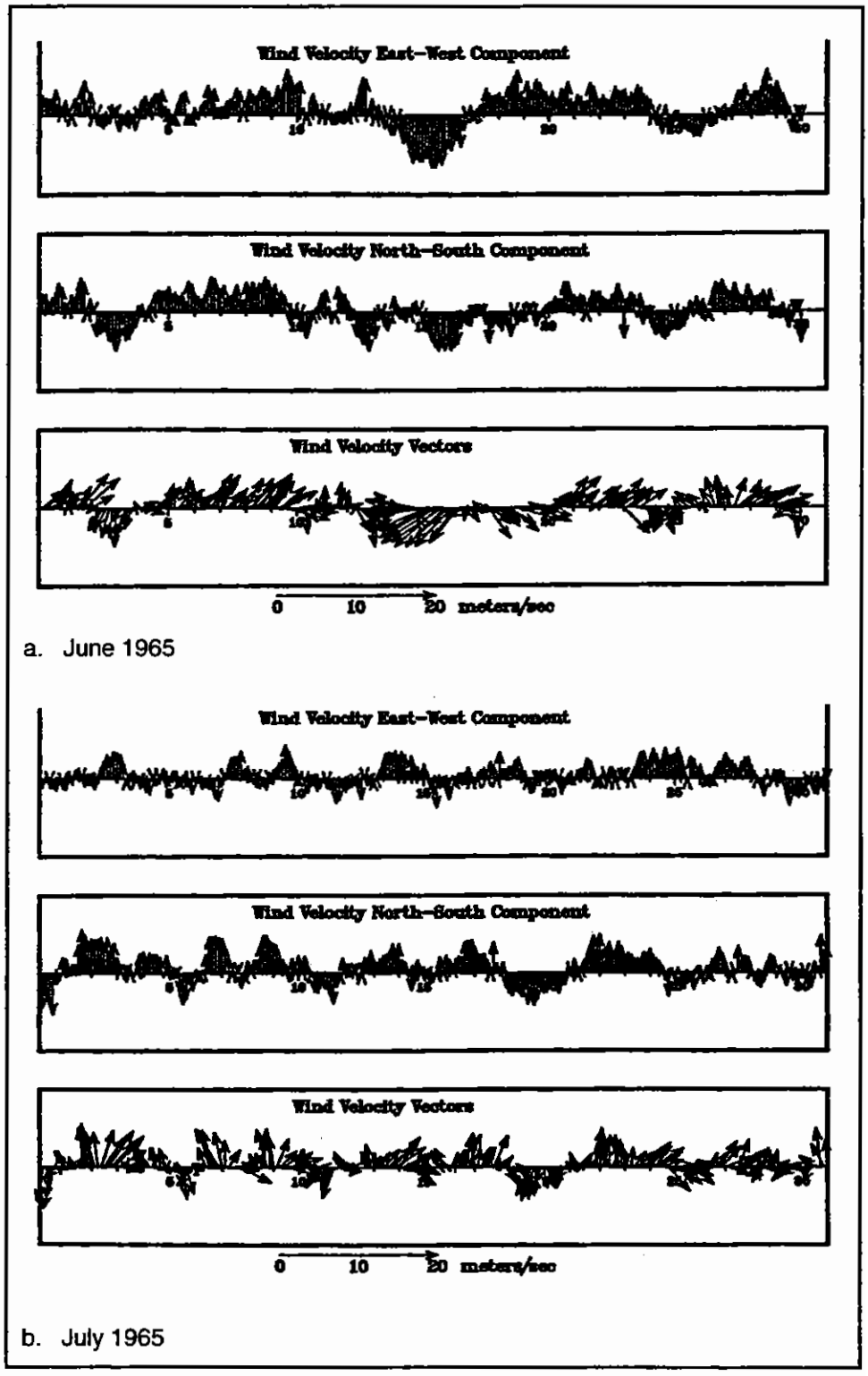

Figure 65. 1965 average wind (Sheet 1 of 3)

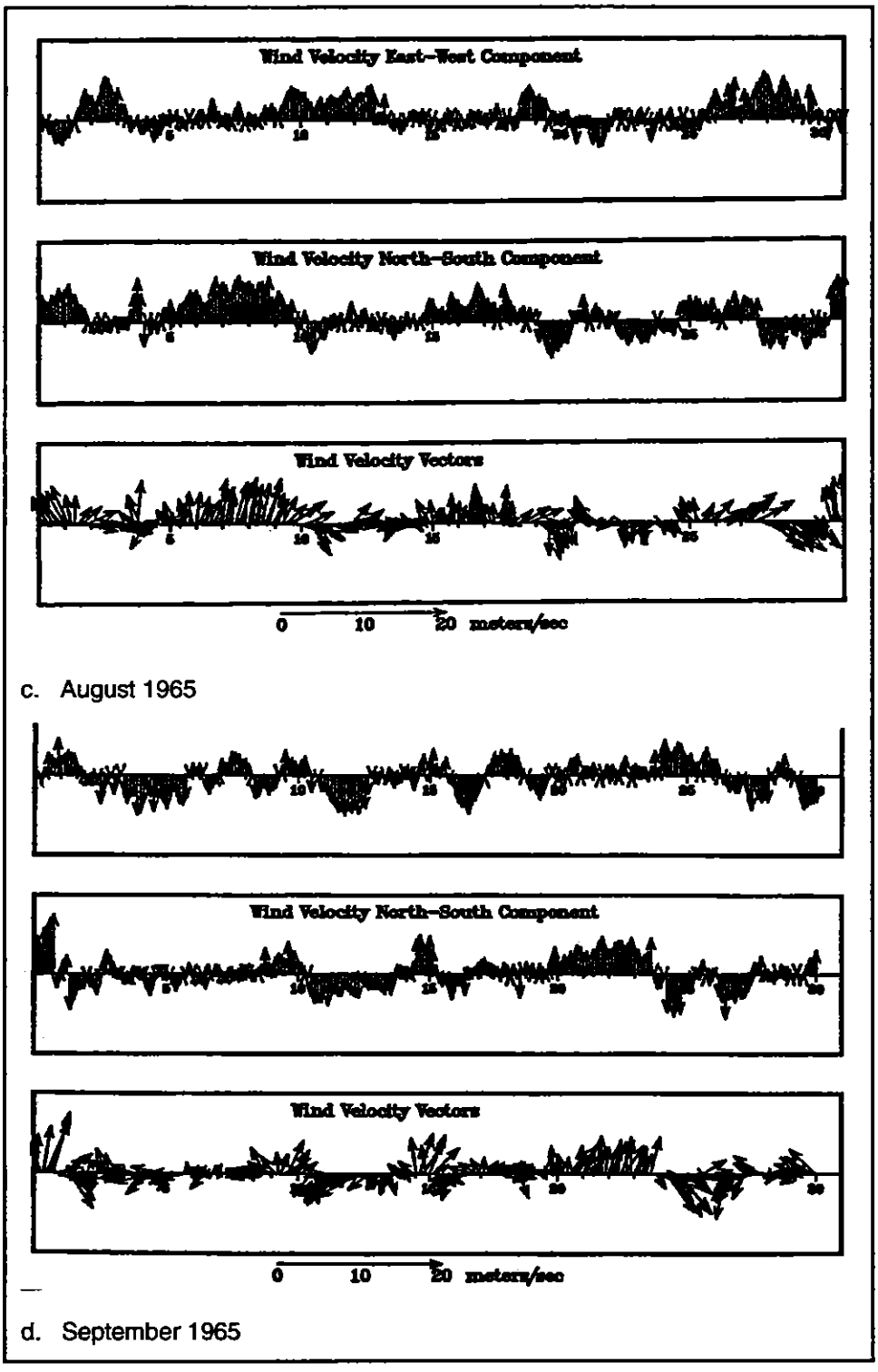

Figure 65. (Sheet 2 of 3)

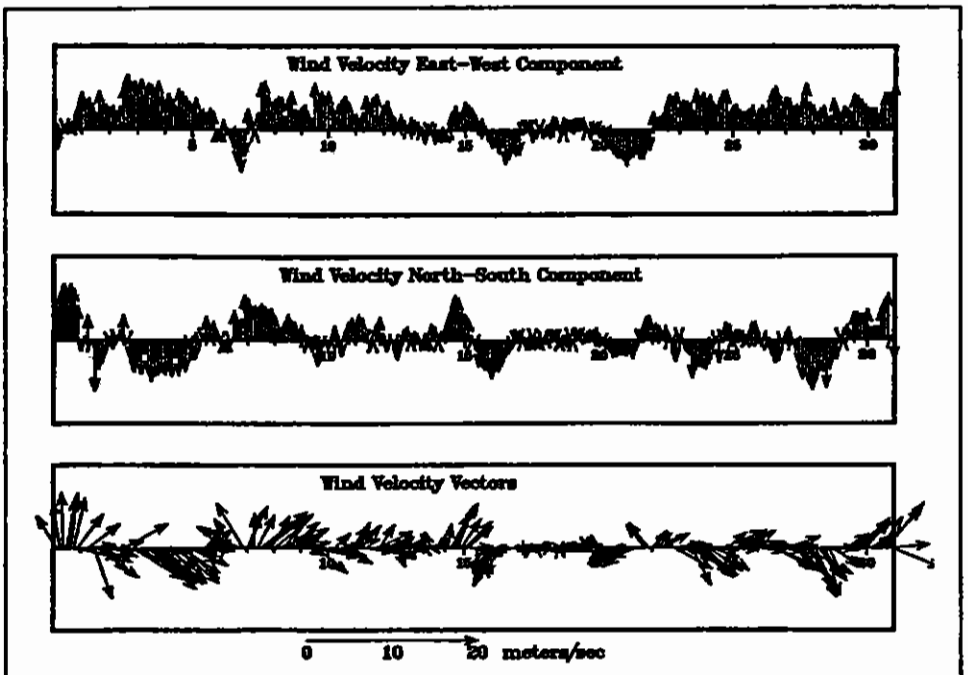

e. October 1965

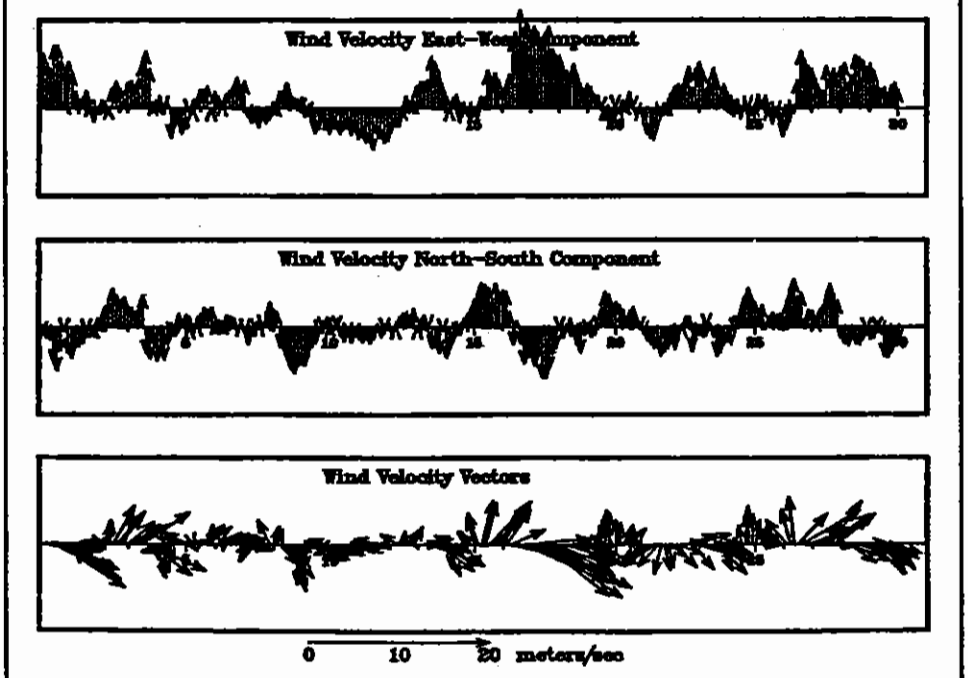

f. November 1965

Figure 65. (Sheet 3 of 3)

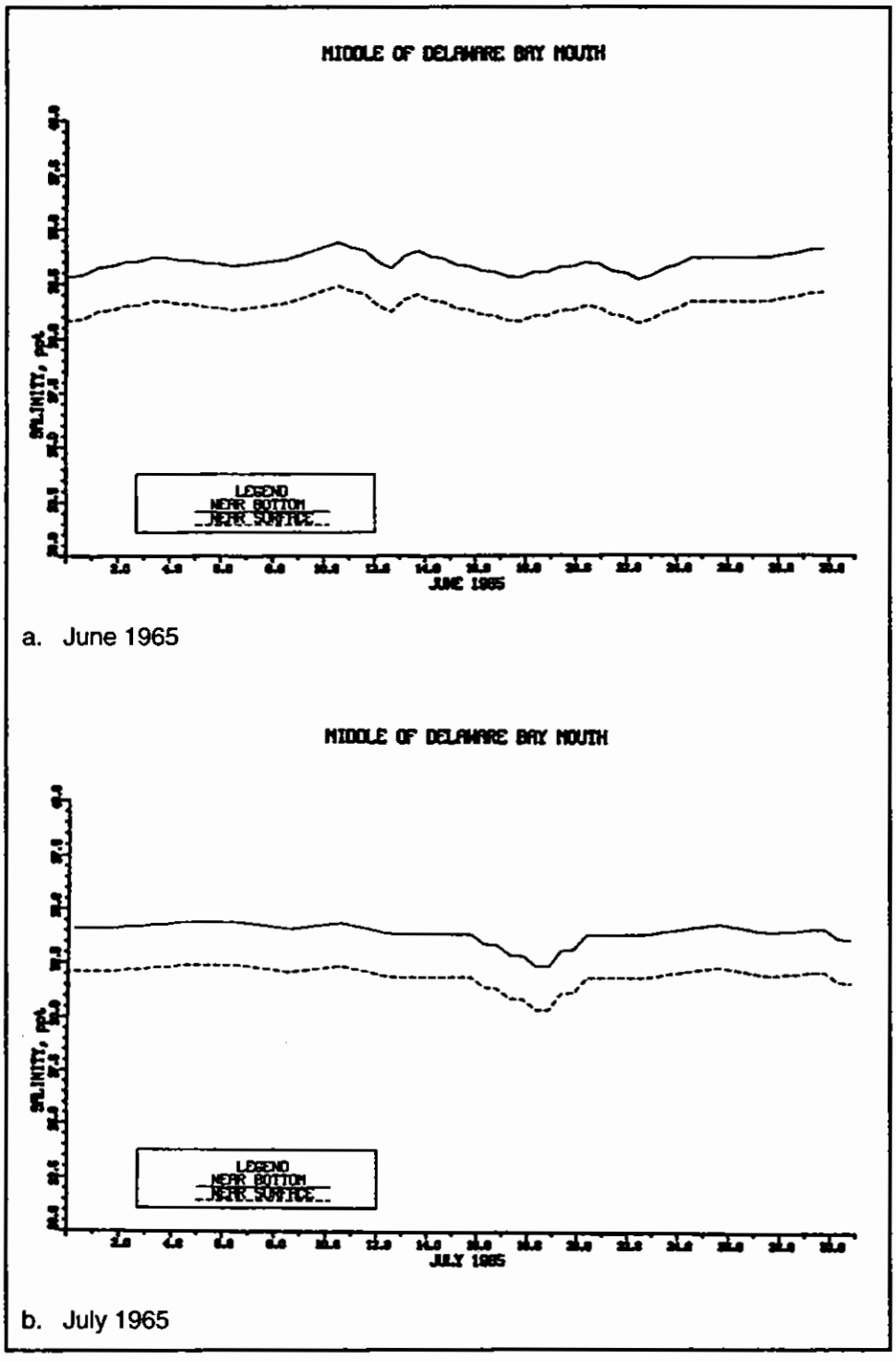

Figure 66. 1965 salinity at the Delaware Bay mouth (Sheet 1 of 3)

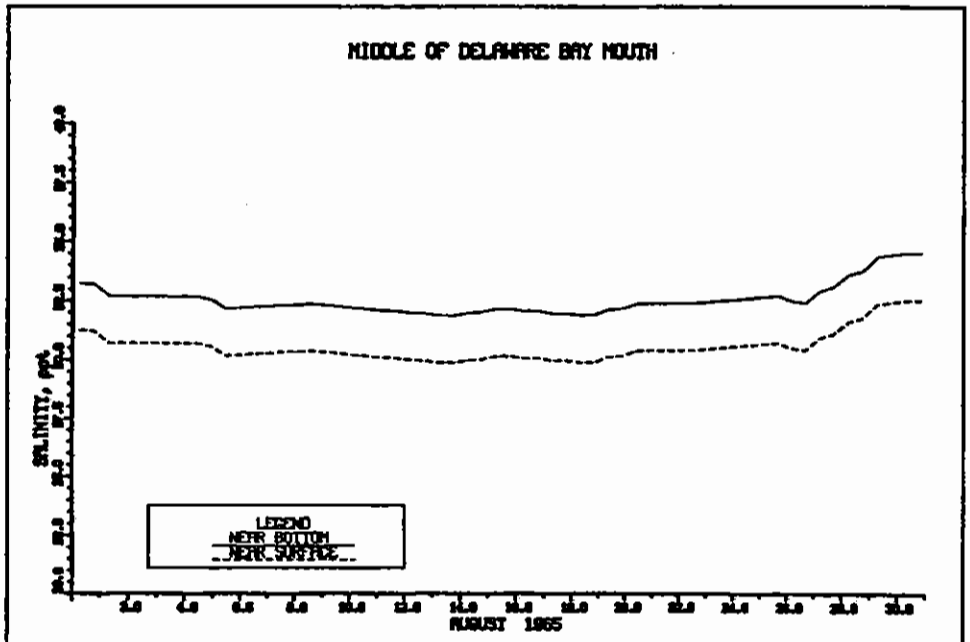

c. August 1965

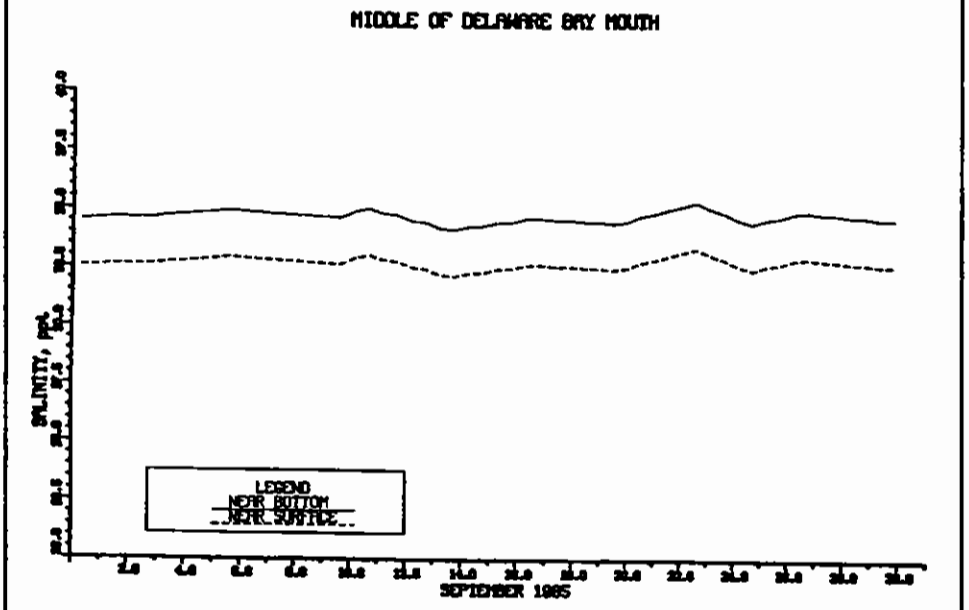

d. September 1965

Figure 66. (Sheet 2 of 3)

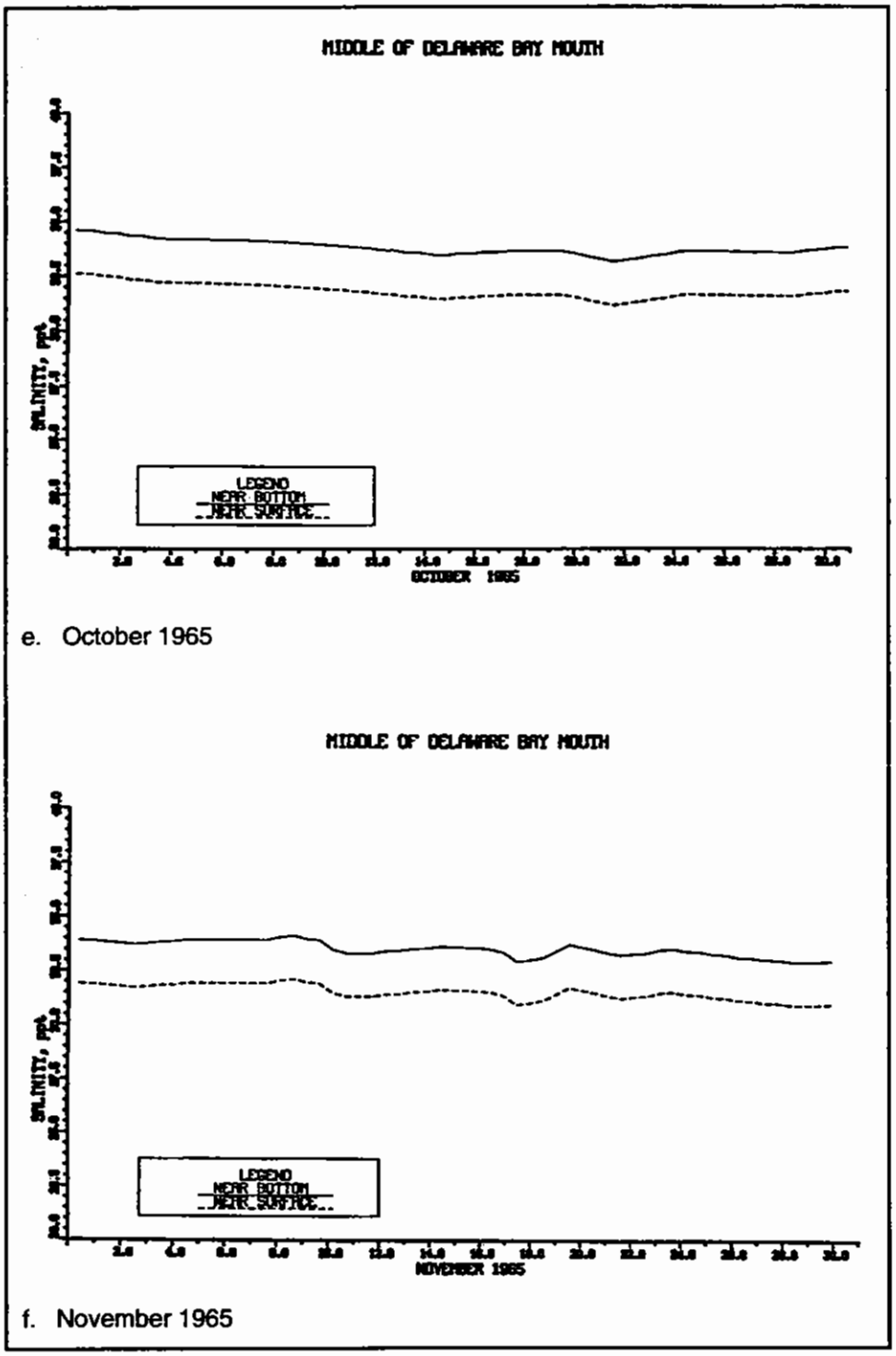

e. October 1965

f. November 1965

Figure 66. (Sheet 3 of 3)

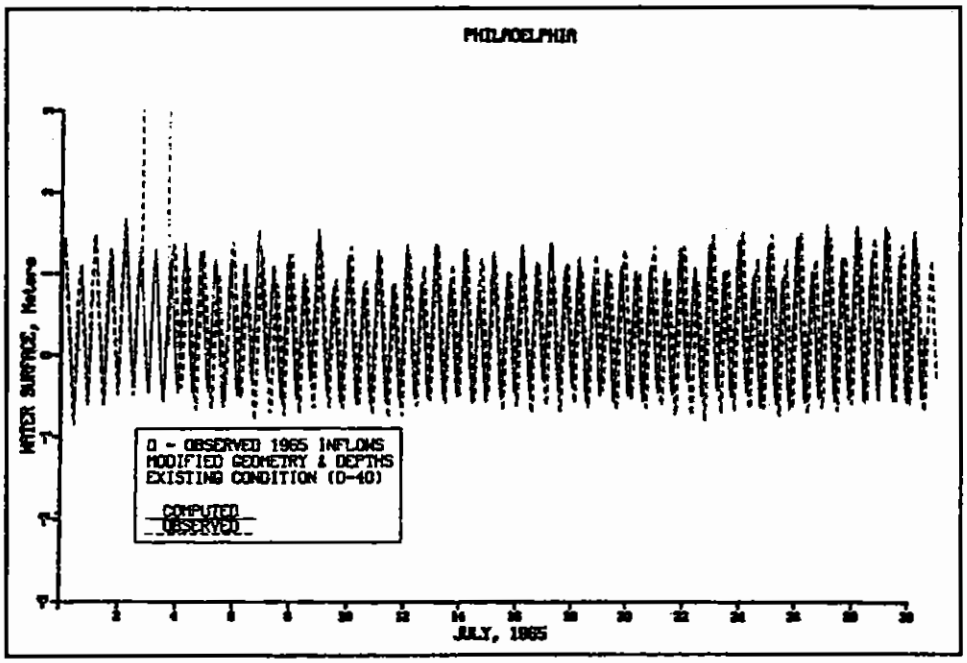

Figure 67. Water-surface elevation (NGVD) at Philadelphia, PA, in July 1965

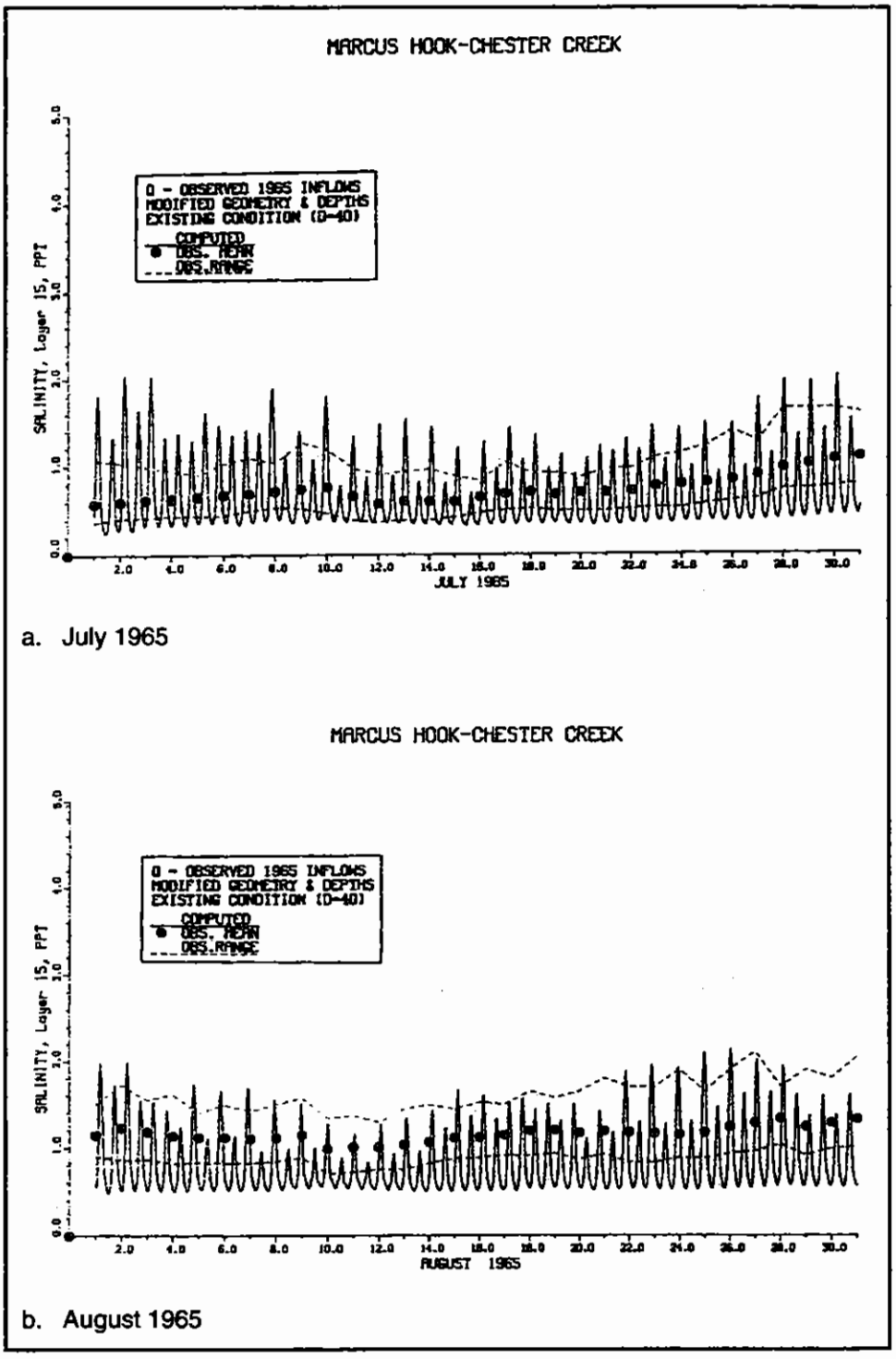

Figure 68. 1965 salinity at Marcus Hook-Chester Creek (Sheet 1 of 3)

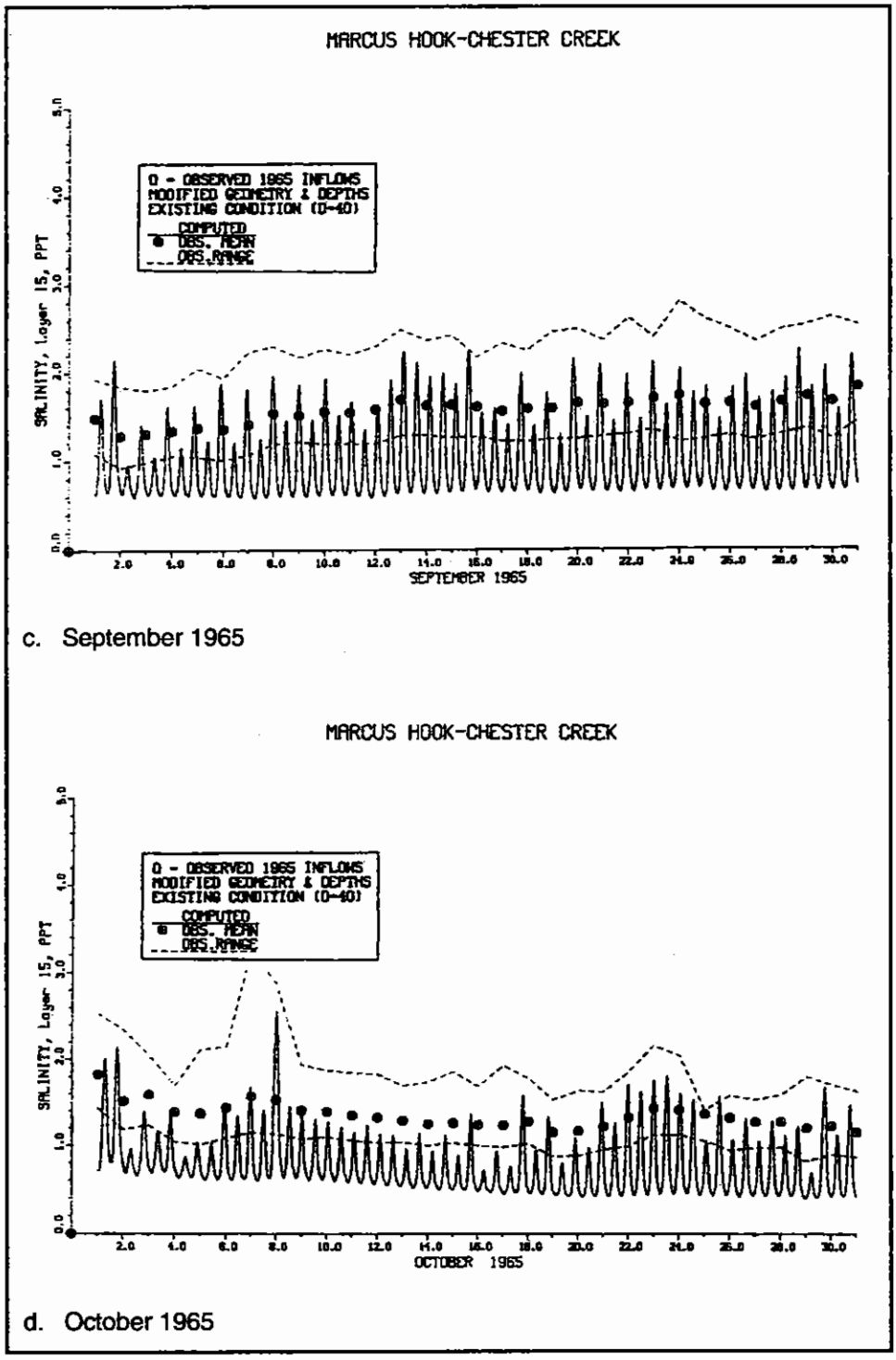

Figure 68. (Sheet 2 of 3)

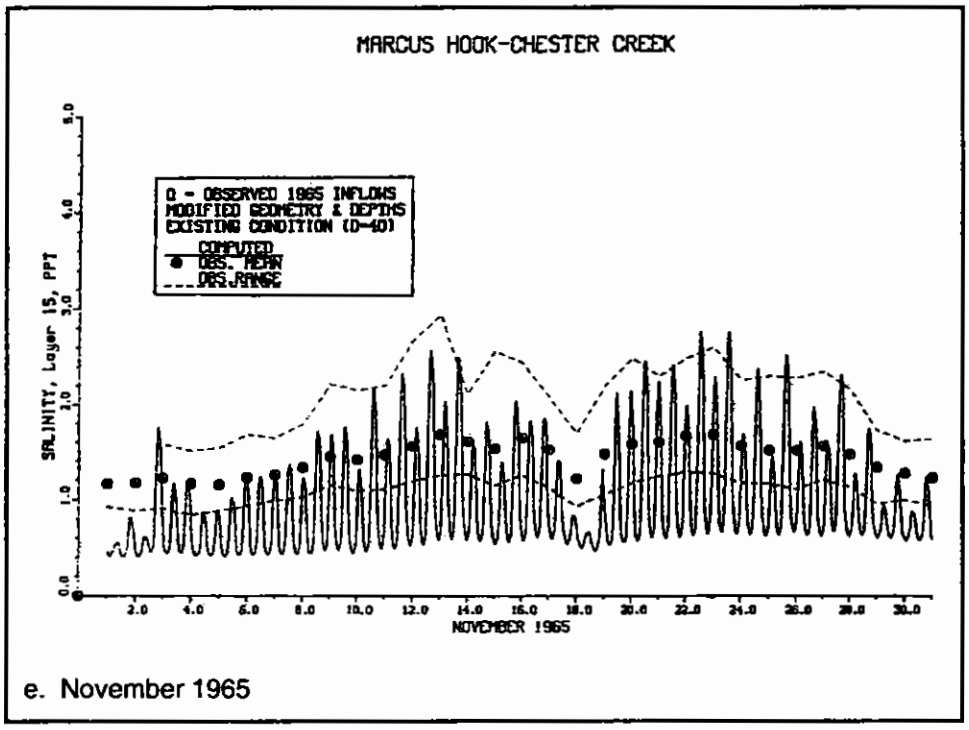

e. November 1965

Figure 68. (Sheet 3 of 3)

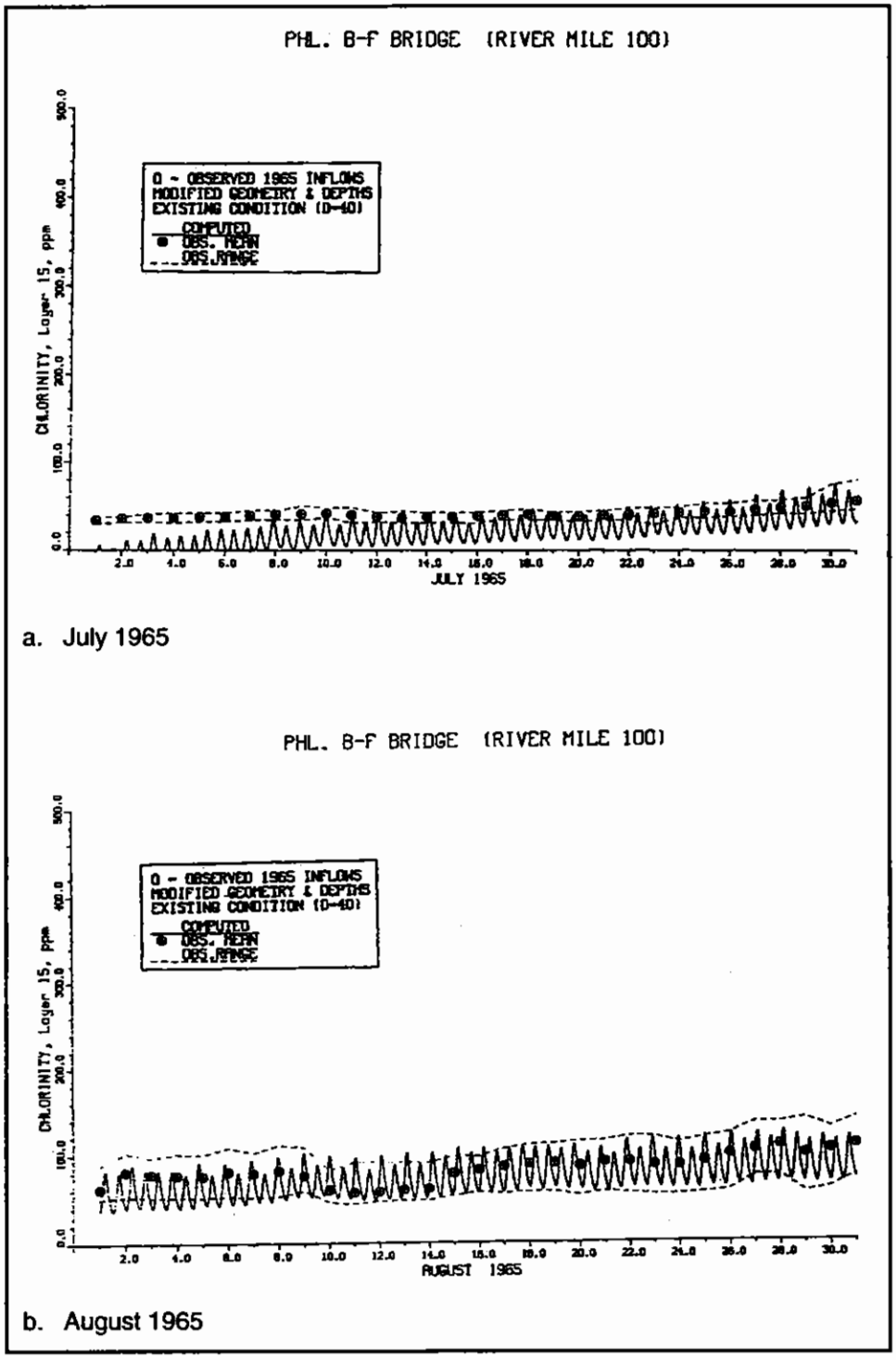

Figure 69. 1965 chlorinity at Benjamin Franklin Bridge (Sheet 1 of 3)

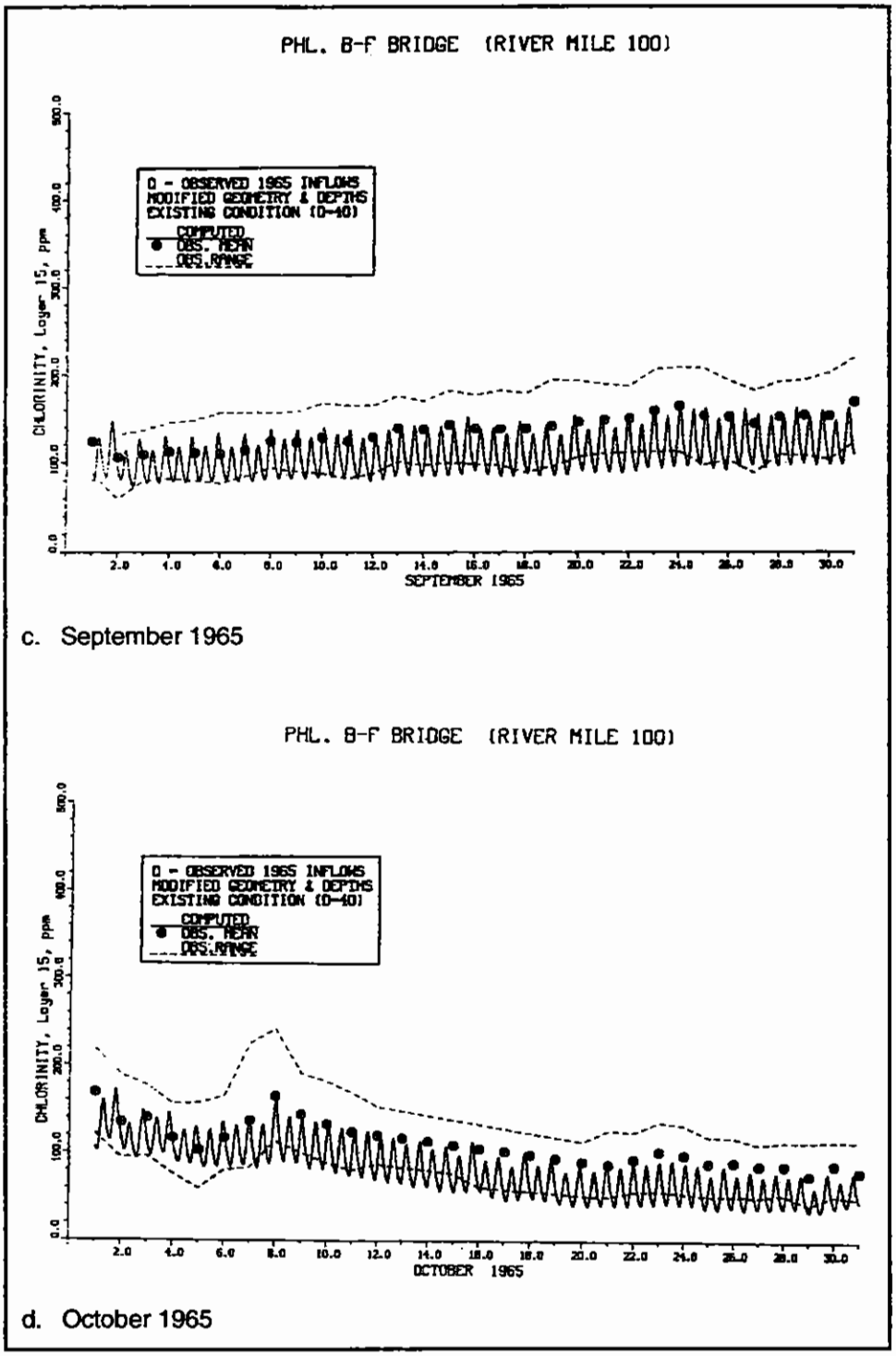

c. September 1965

d. October 1965

Figure 69. (Sheet 2 of 3)

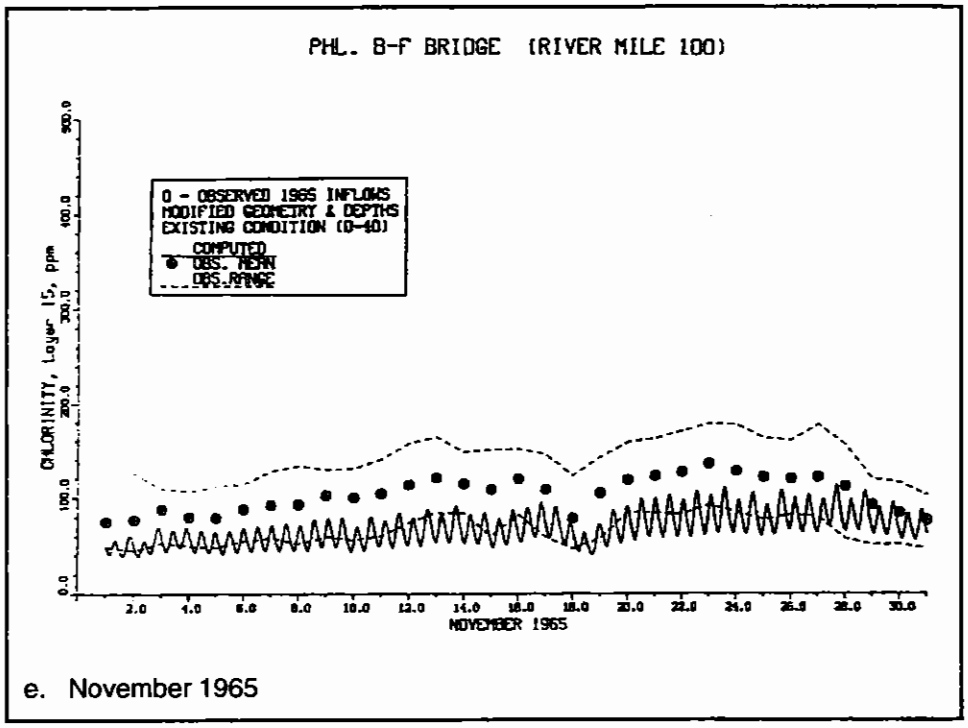

e. November 1965

Figure 69. (Sheet 3 of 3)

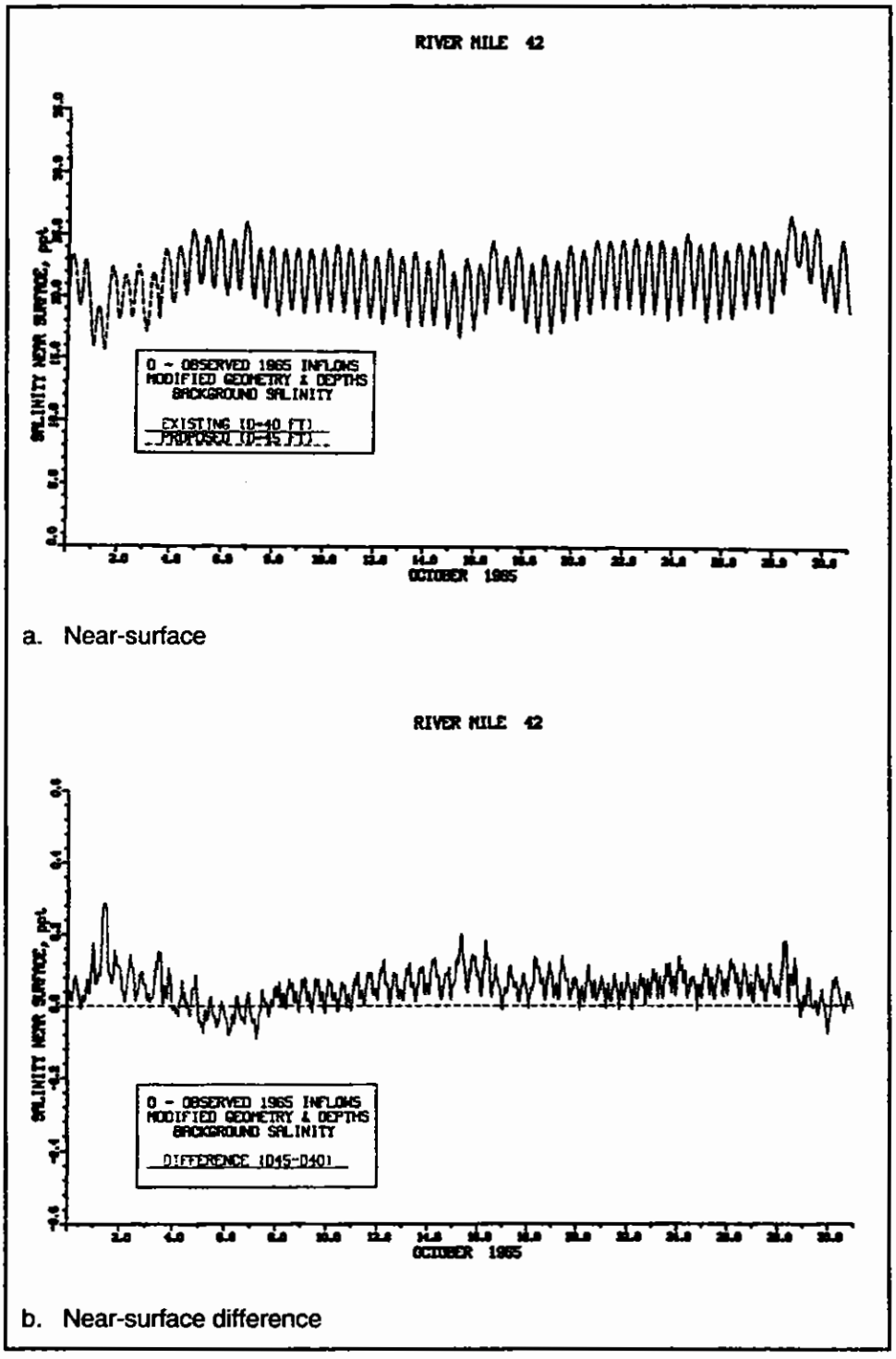

Figure 70. Impact of channel deepening on salinity at RM 42 for October 1965 (Continued)

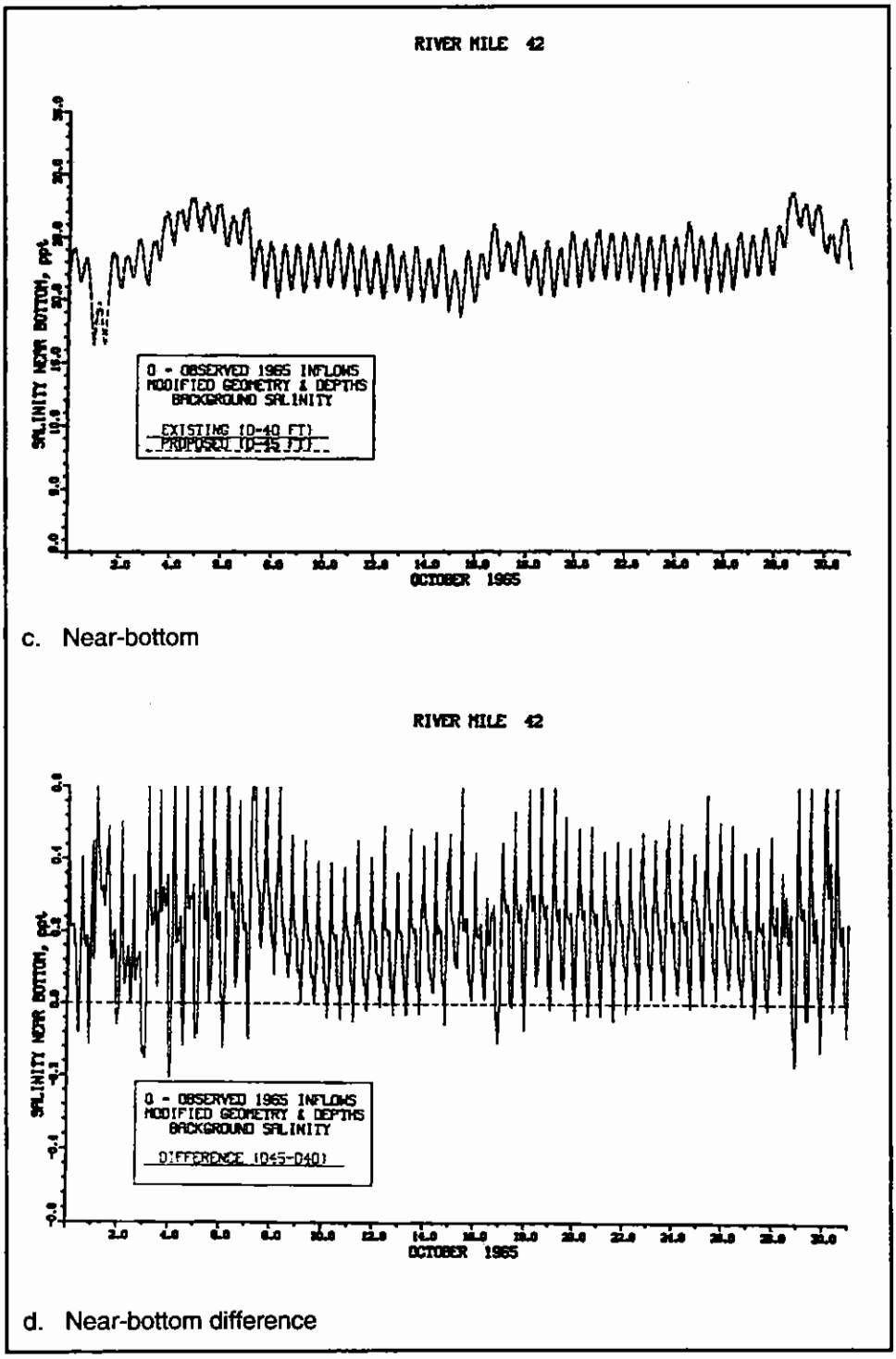

Figure 70. (Concluded)

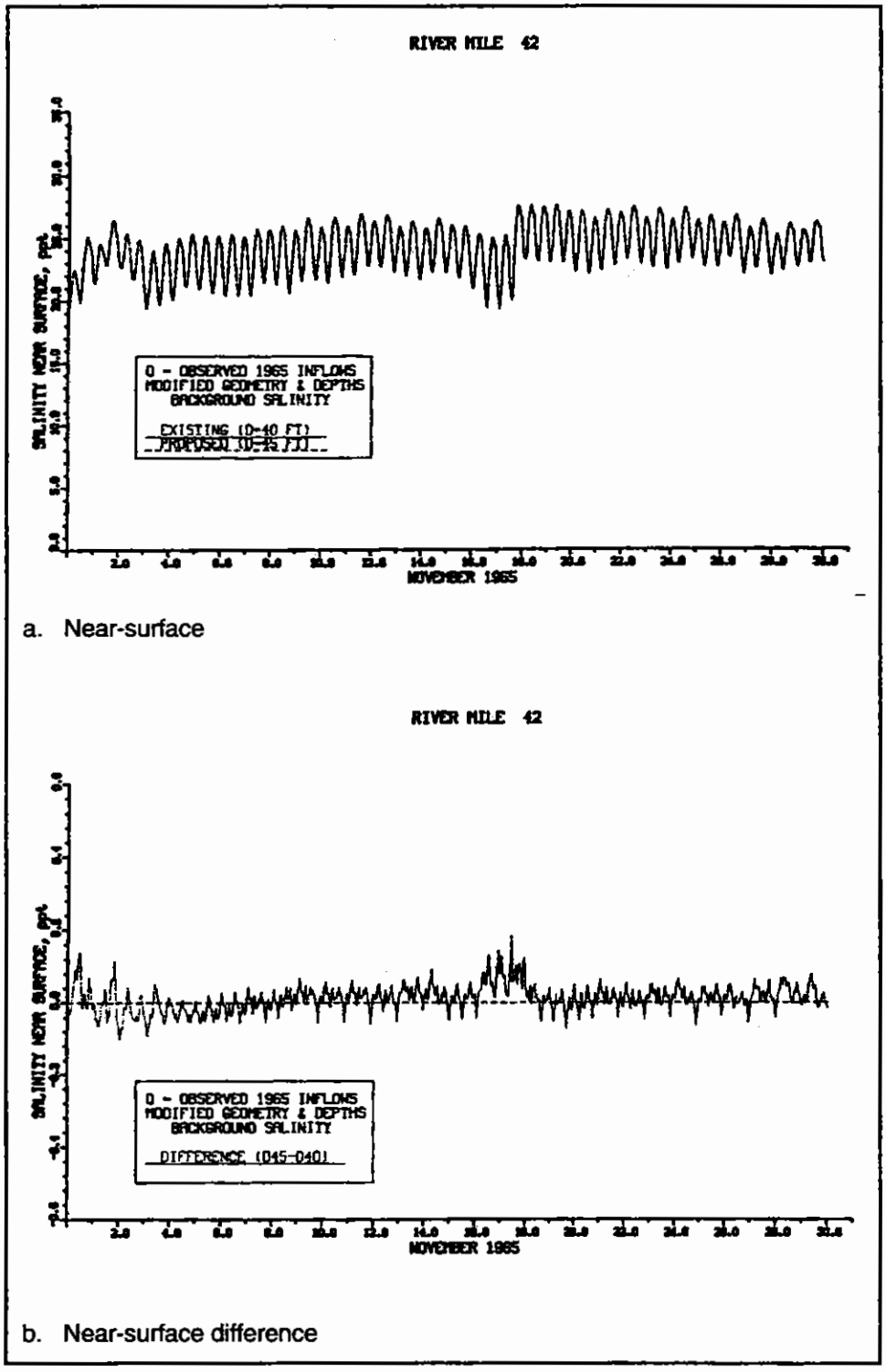

Figure 71. Impact of channel deepening on salinity at RM 42 for November 1965 (Continued)

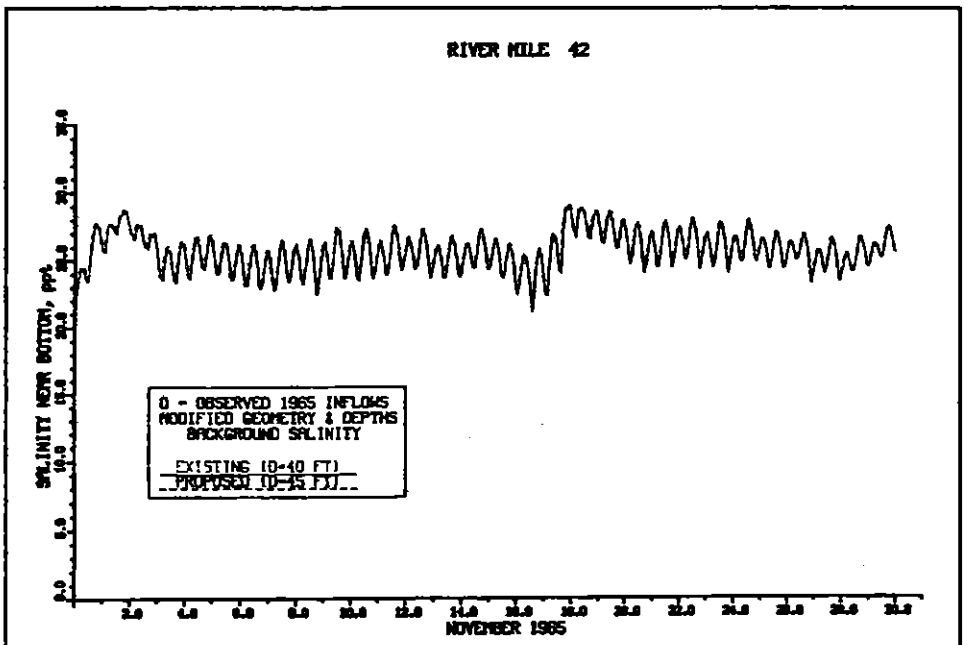

c. Near-bottom

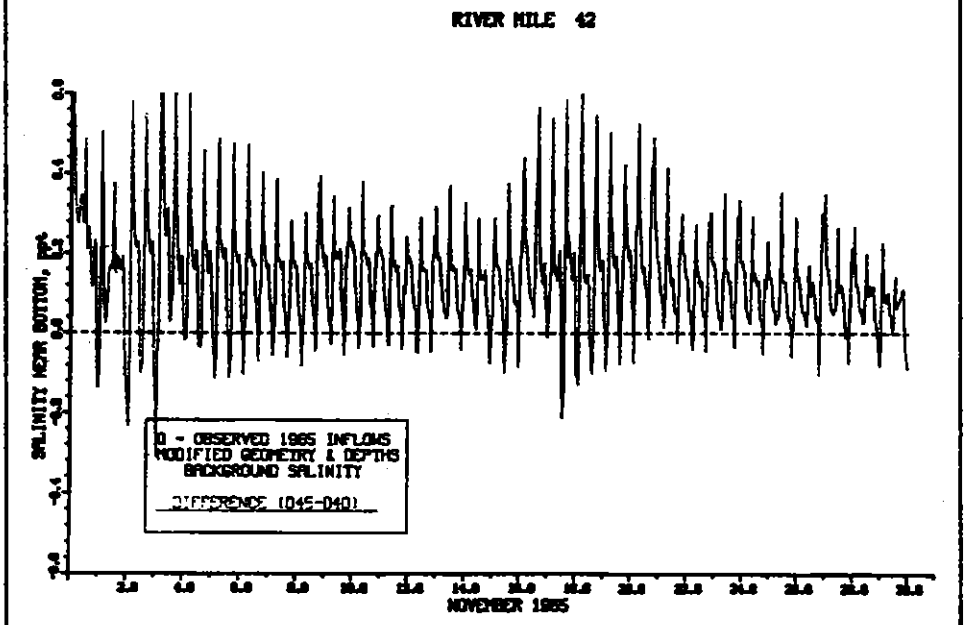

d. Near-bottom difference

Figure 71. (Concluded)

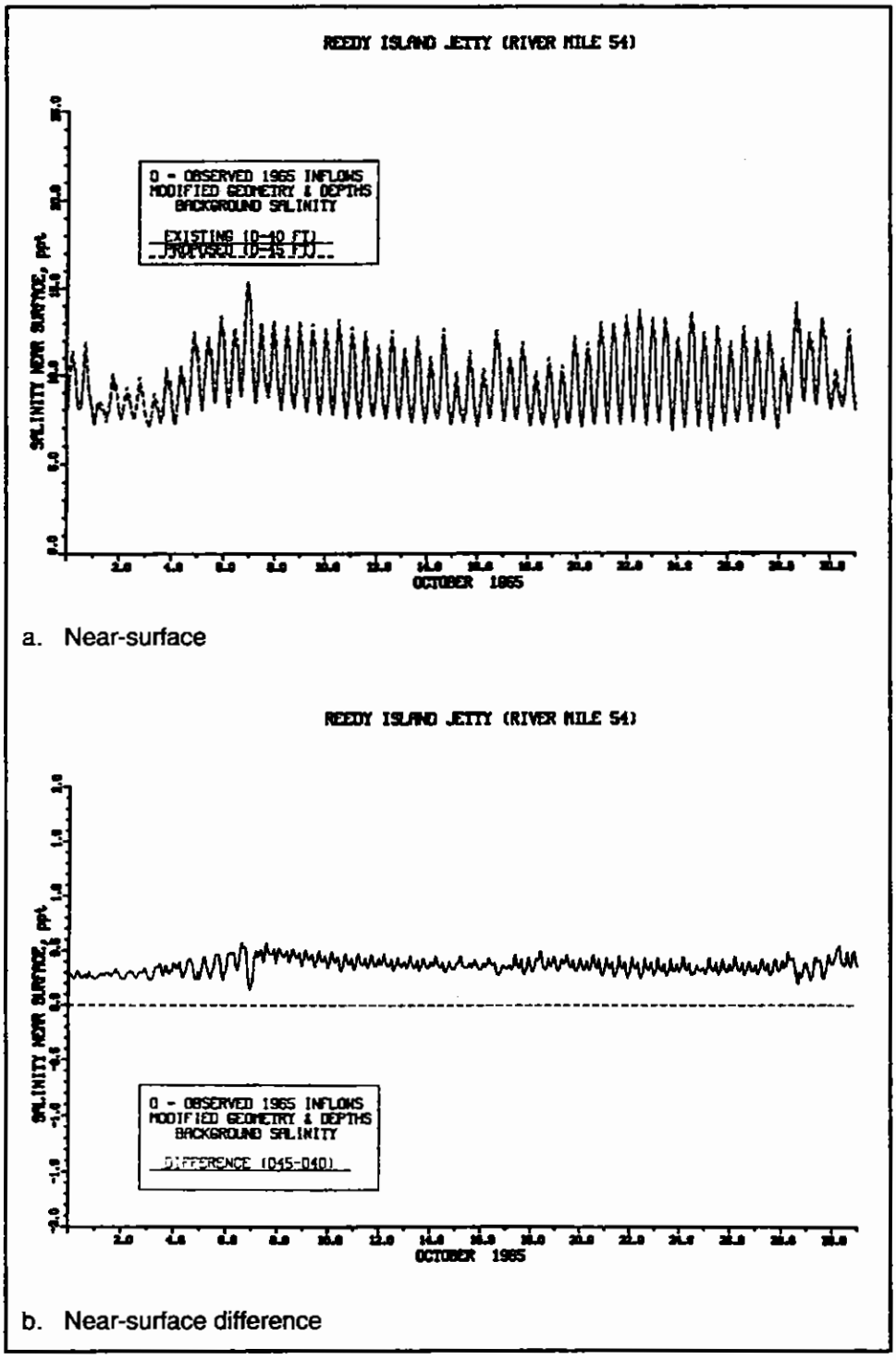

Figure 72. Impact of channel deepening on salinity at RM 54 for October 1965 (Continued)

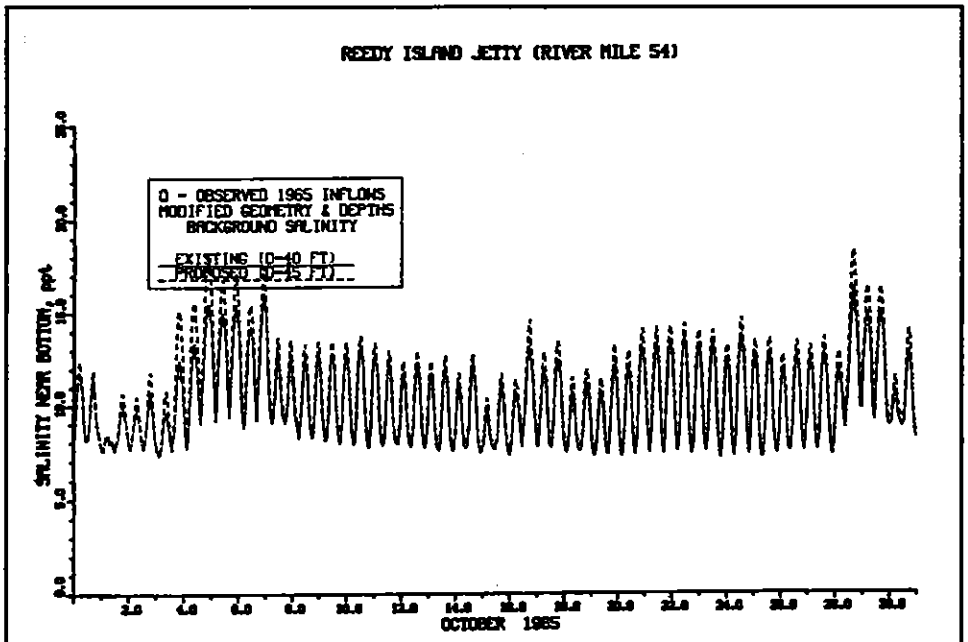

c. Near-bottom

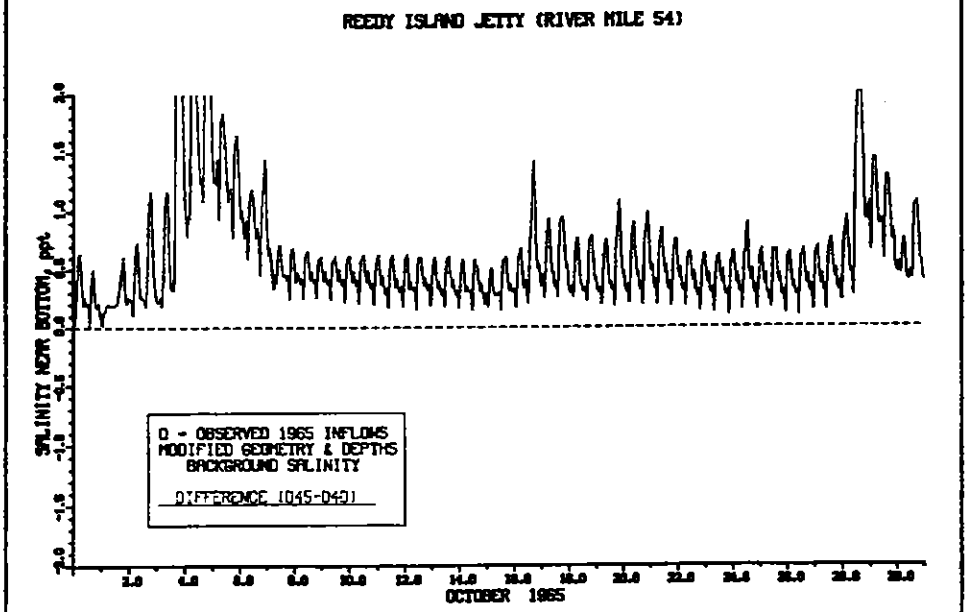

d. Near-bottom difference

Figure 72. (Concluded)

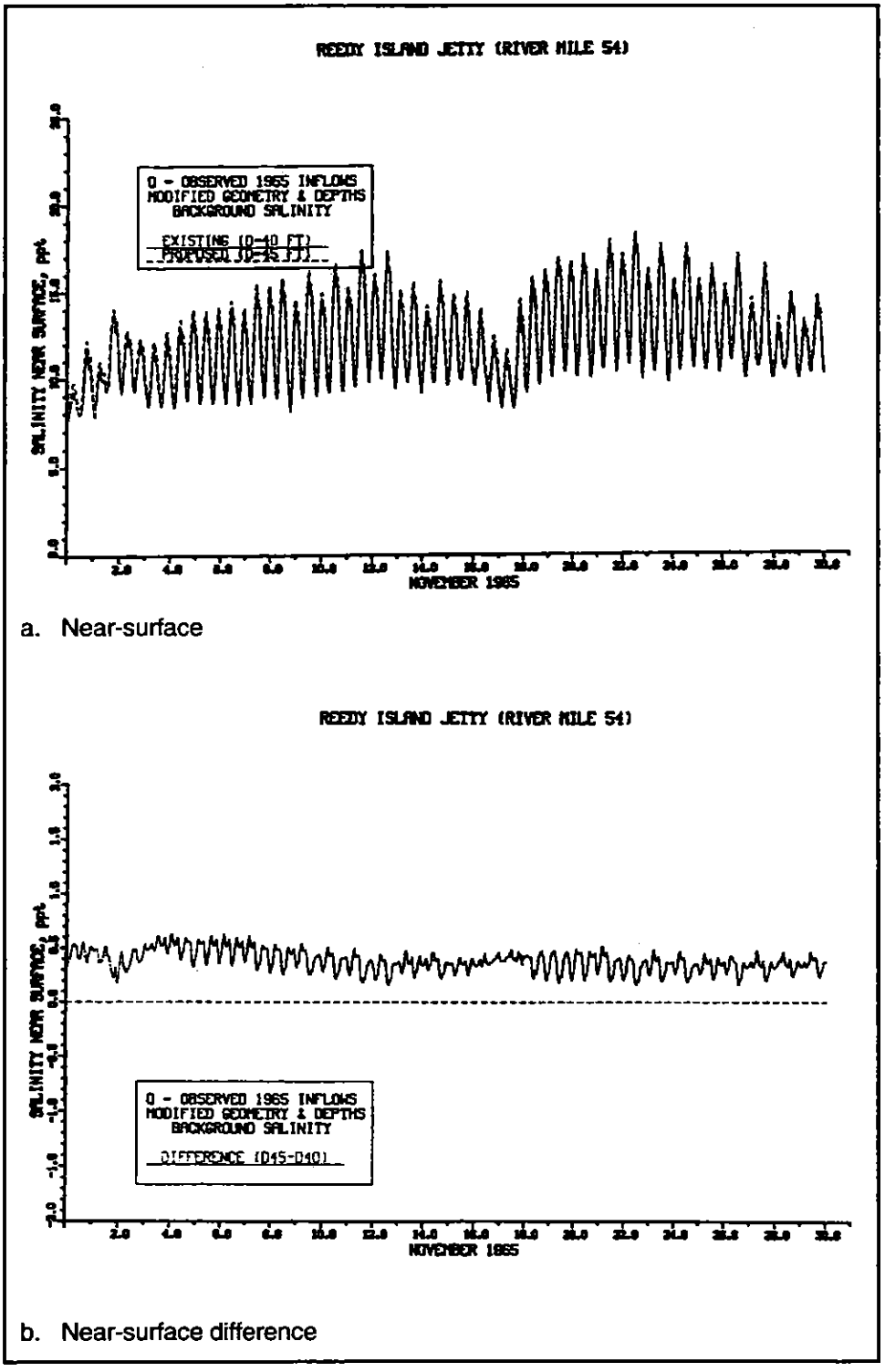

Figure 73. Impact of channel deepening on salinity at RM 54 for November 1965 (Continued)

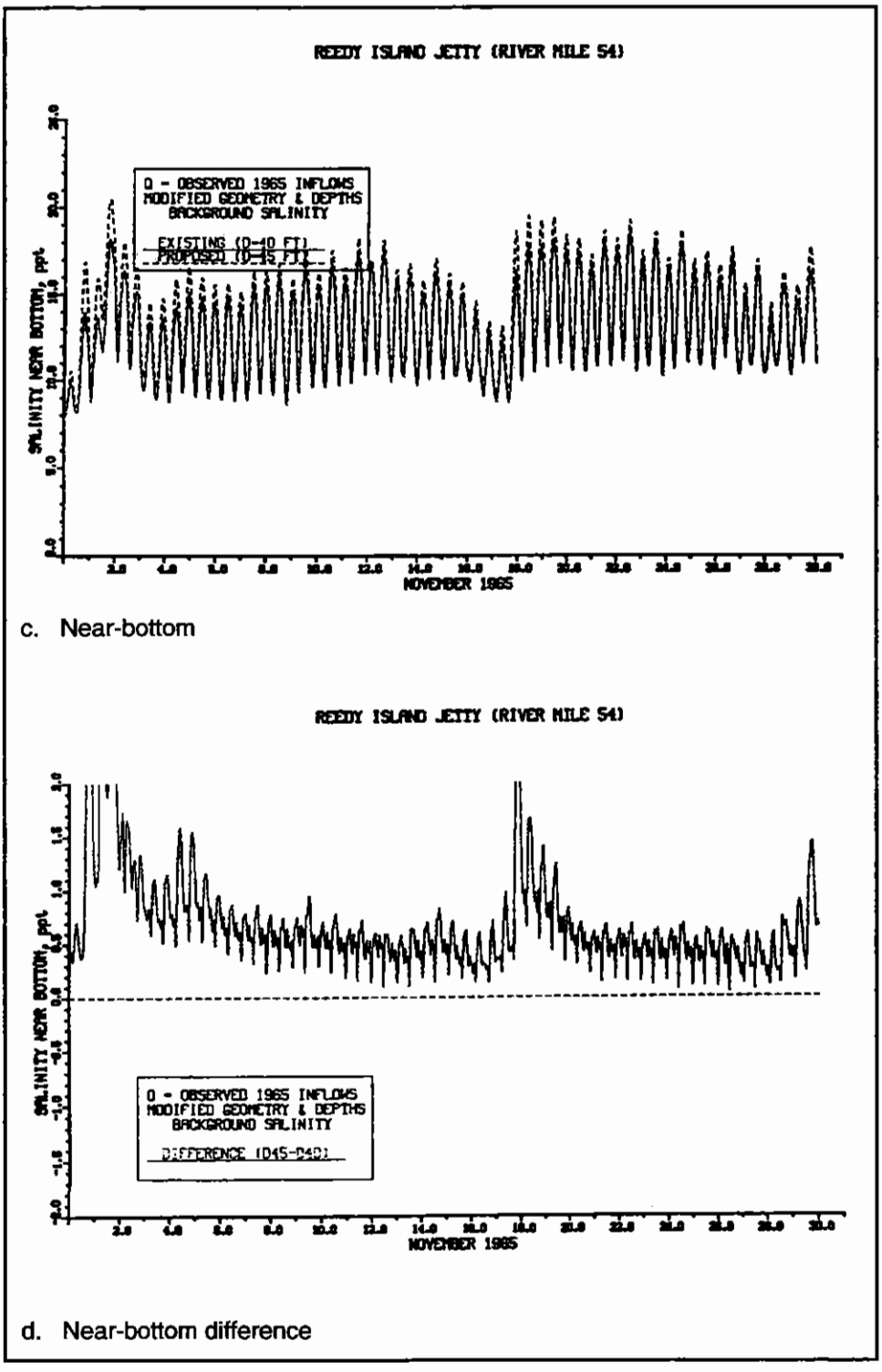

Figure 73. (Concluded)

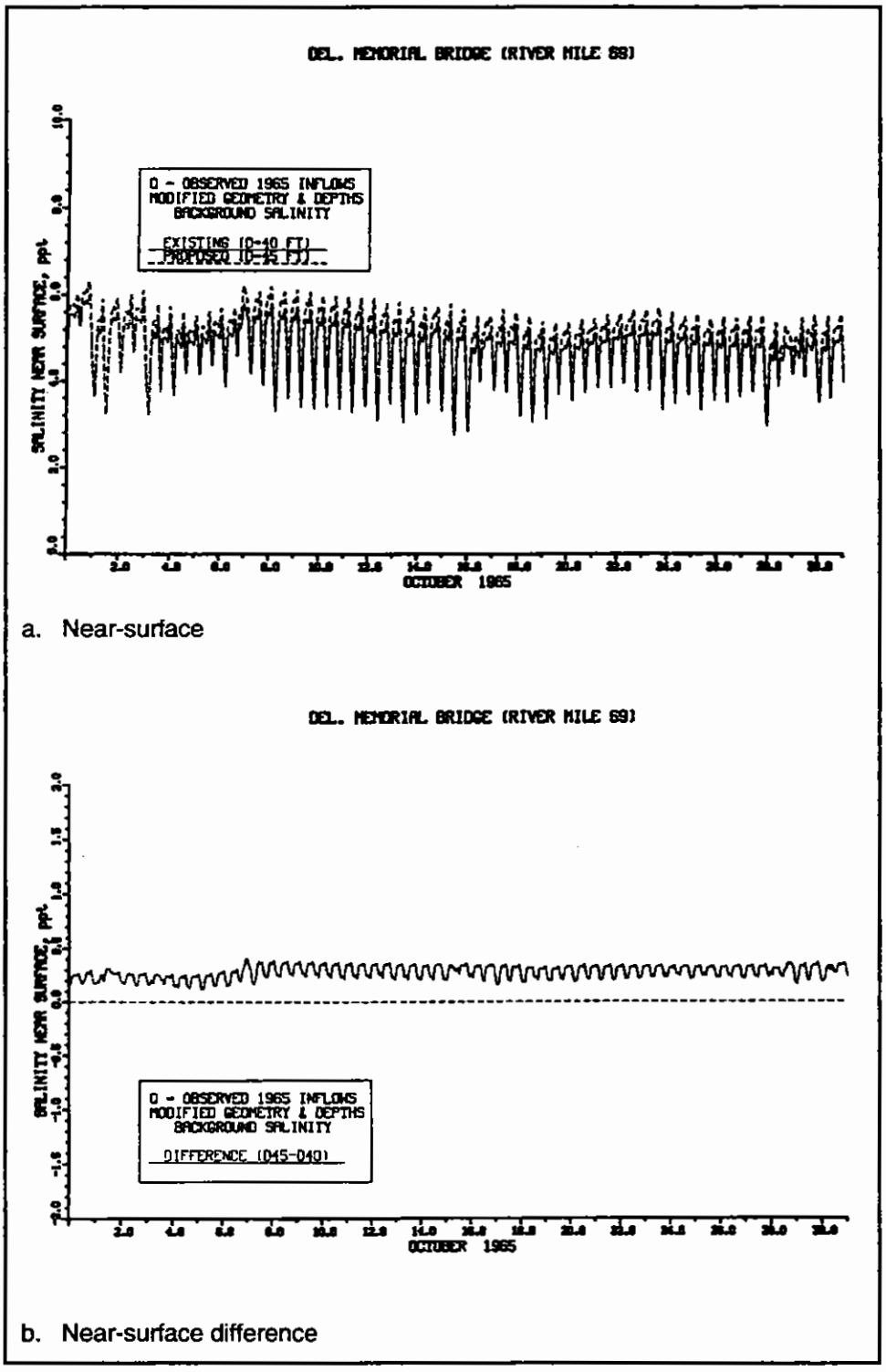

Figure 74. Impact of channel deepening on salinity at RM 69 for October 1965 (Continued)

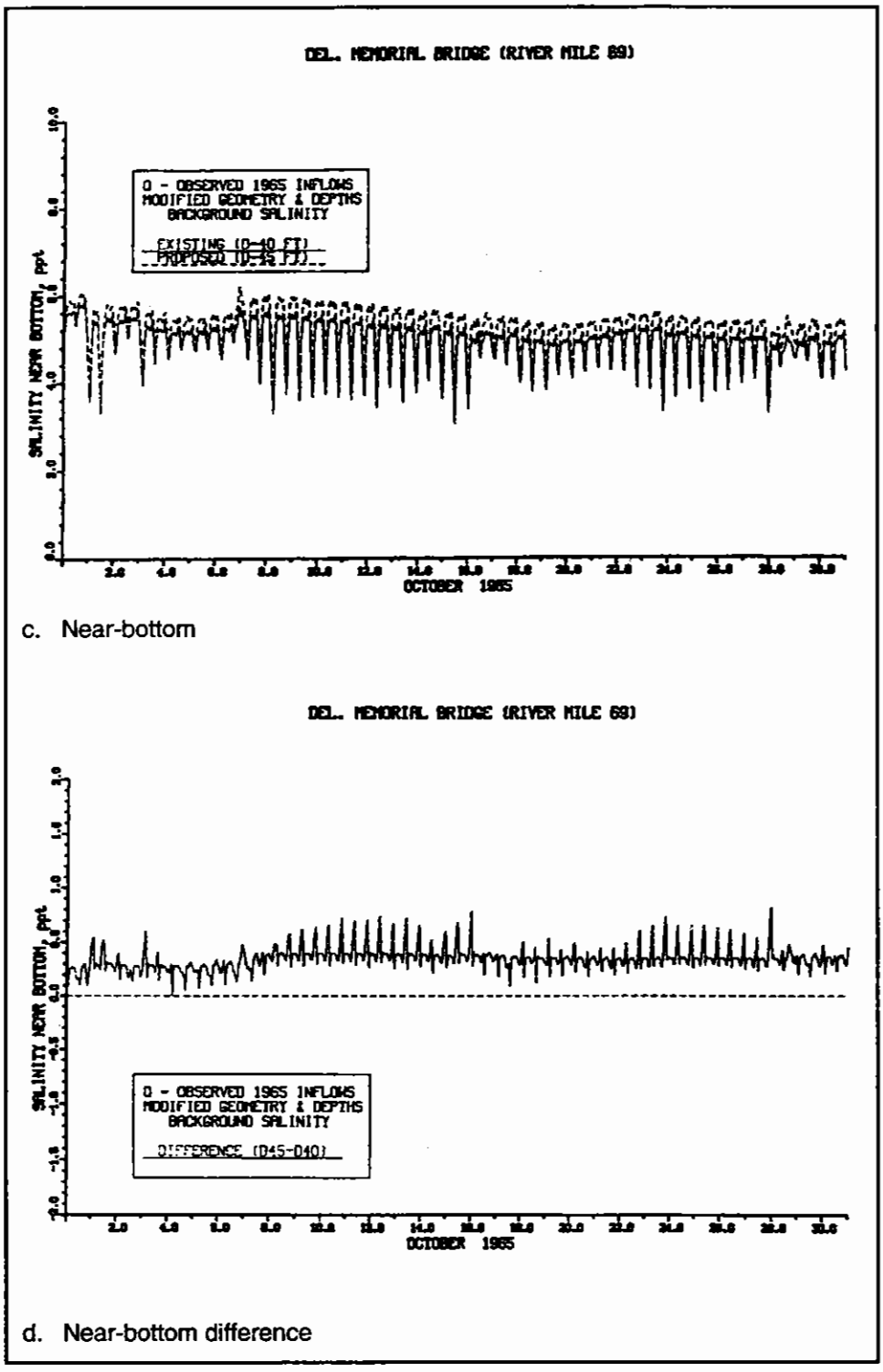

c. Near-bottom

d. Near-bottom difference

Figure 74. (Concluded)

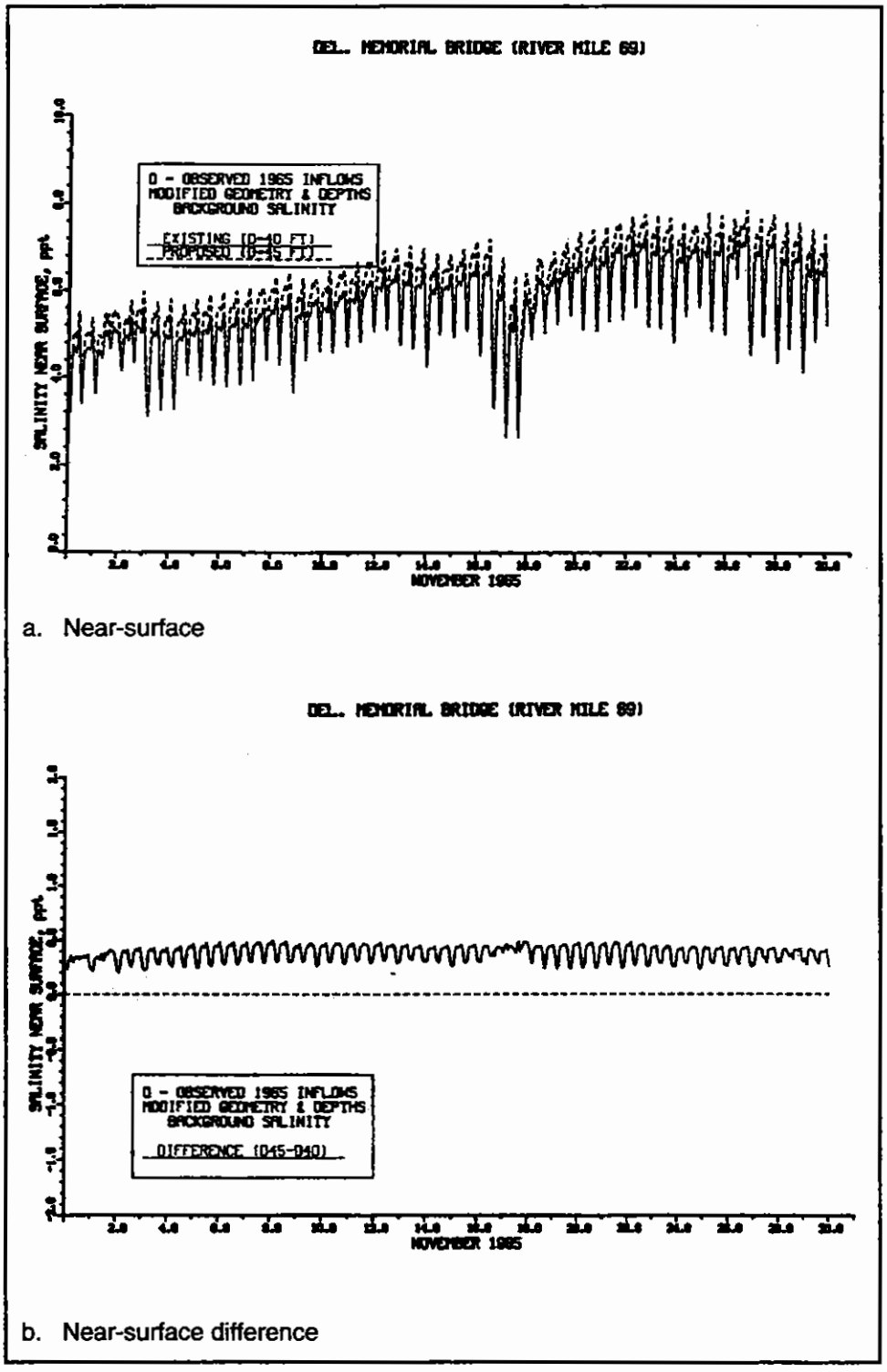

Figure 75. Impact of channel deepening on salinity at RM 69 for November 1965 (Continued)

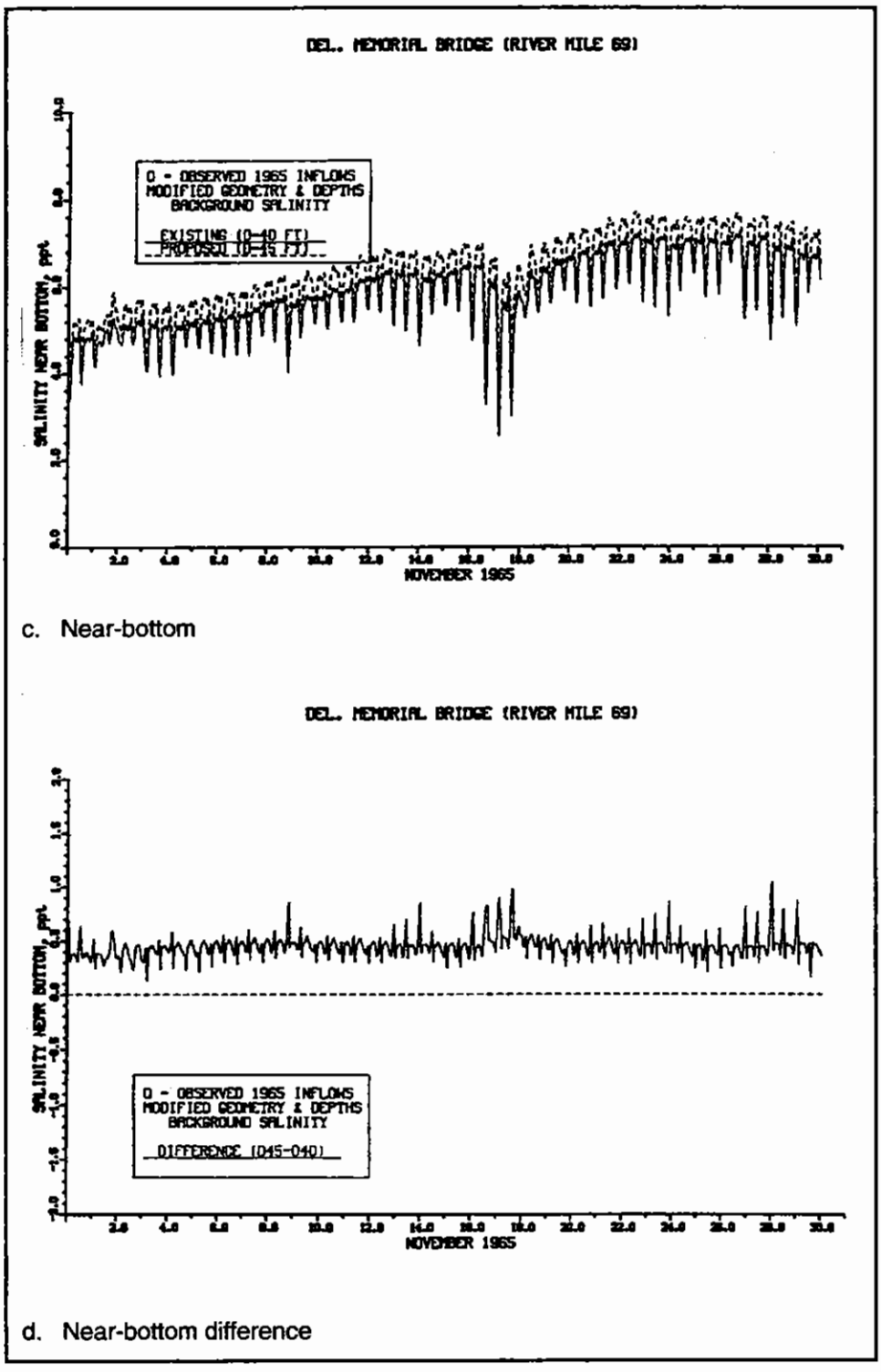

Figure 75. (Concluded)

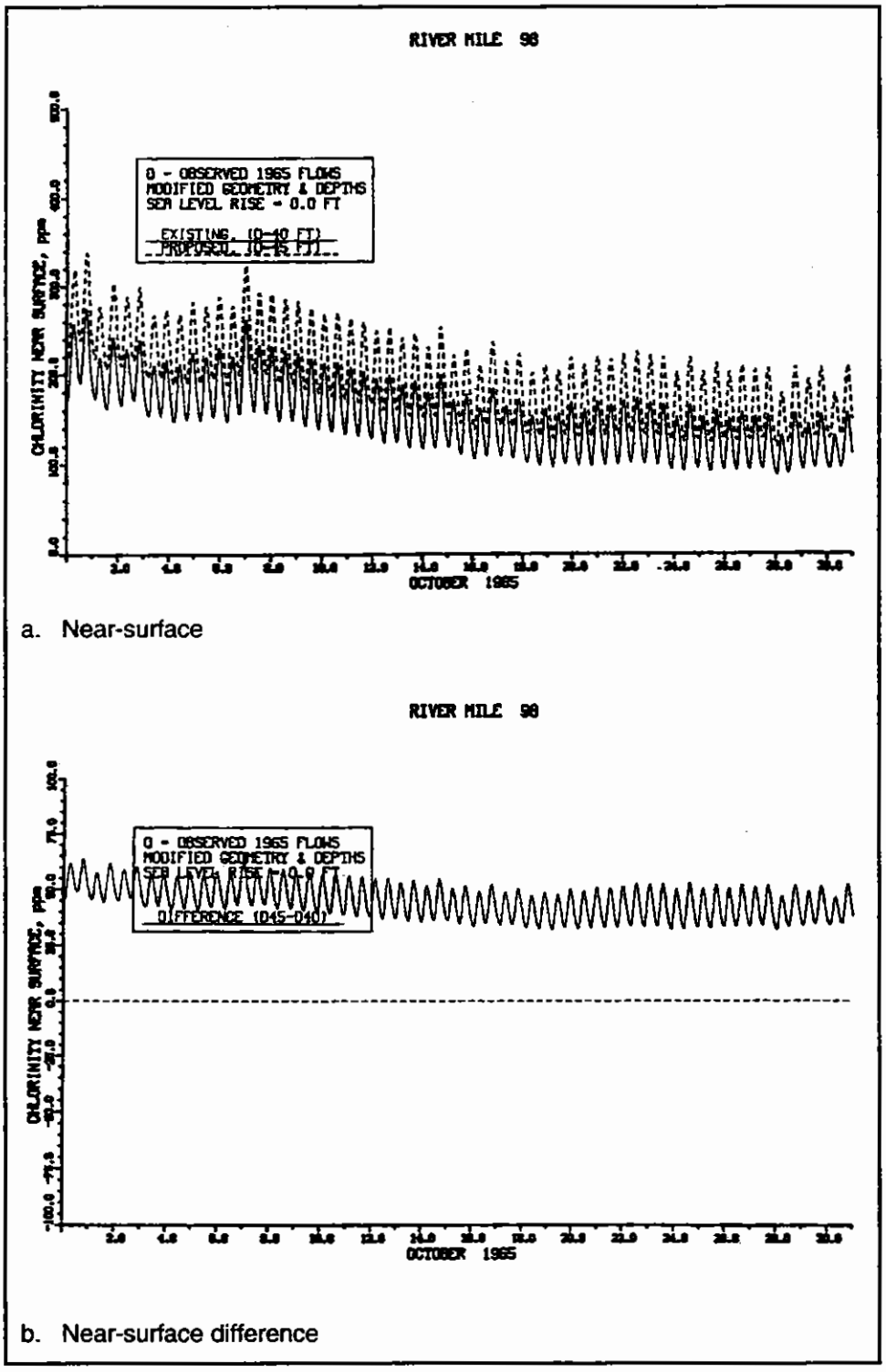

Figure 76. Impact of channel deepening on chlorinity at RM 98 for October 1965 (Continued)

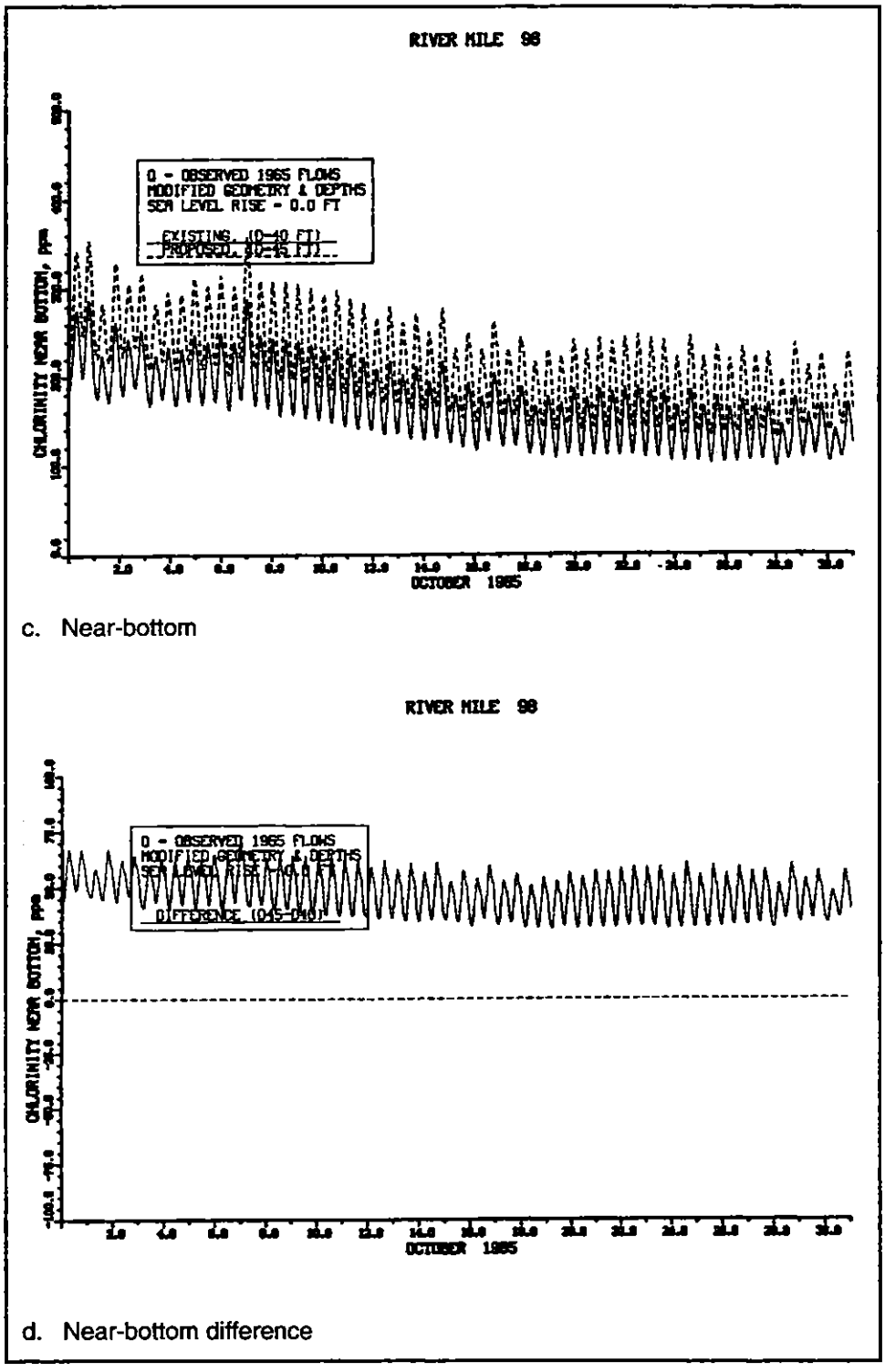

Figure 76. (Concluded)

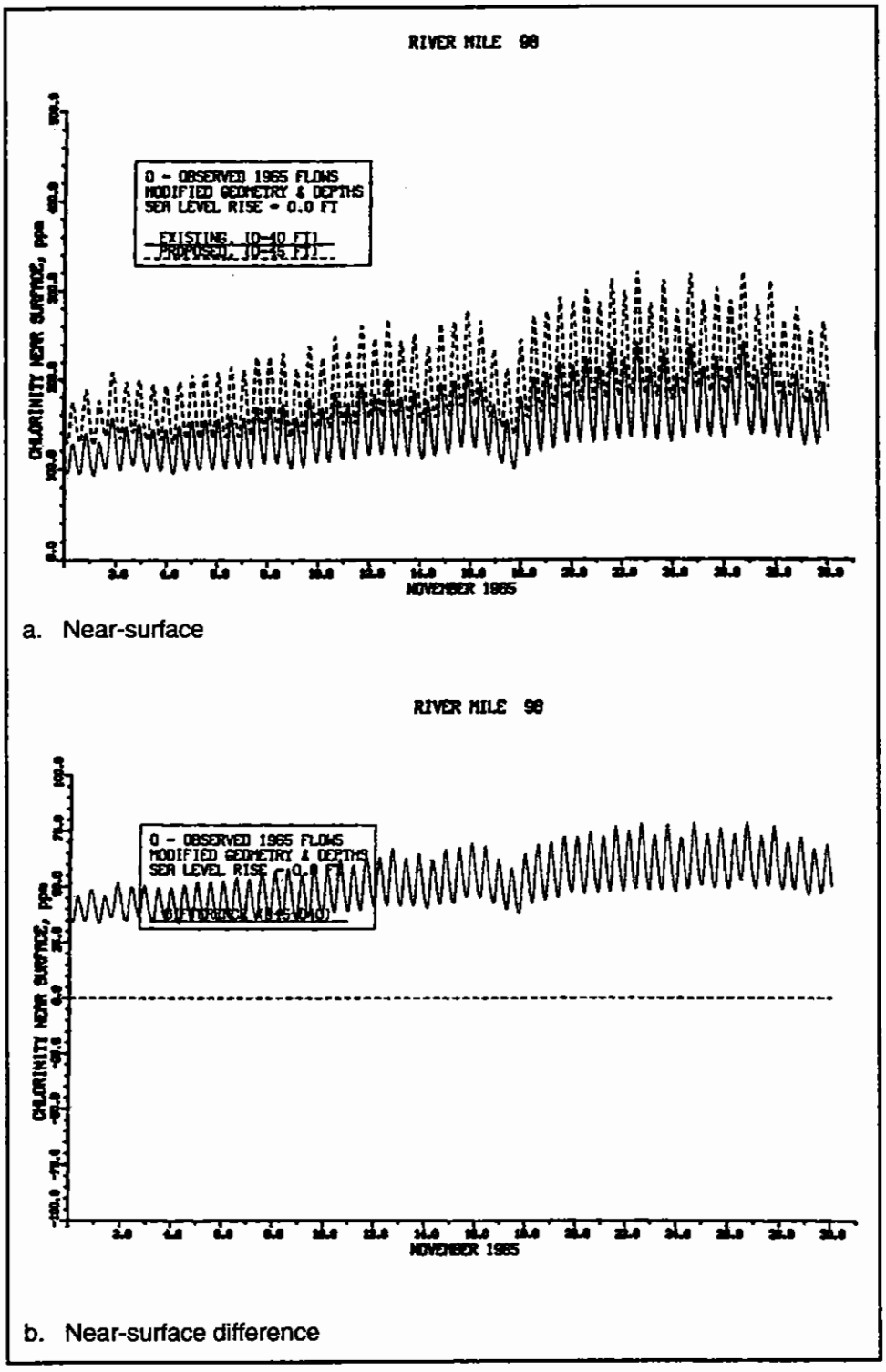

Figure 77. Impact of channel deepening on chlorinity at RM 98 for November 1965 (Continued)

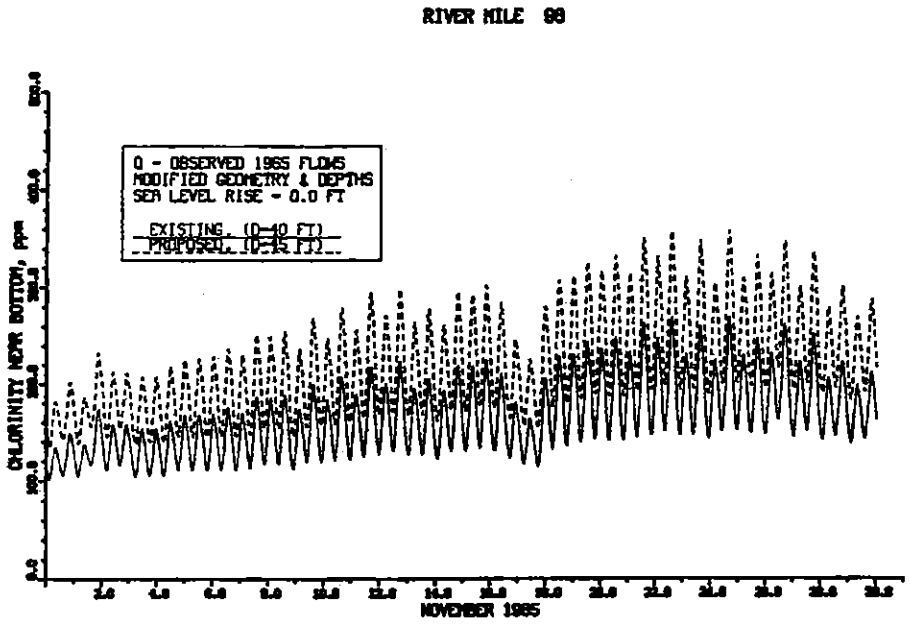

c. Near-bottom

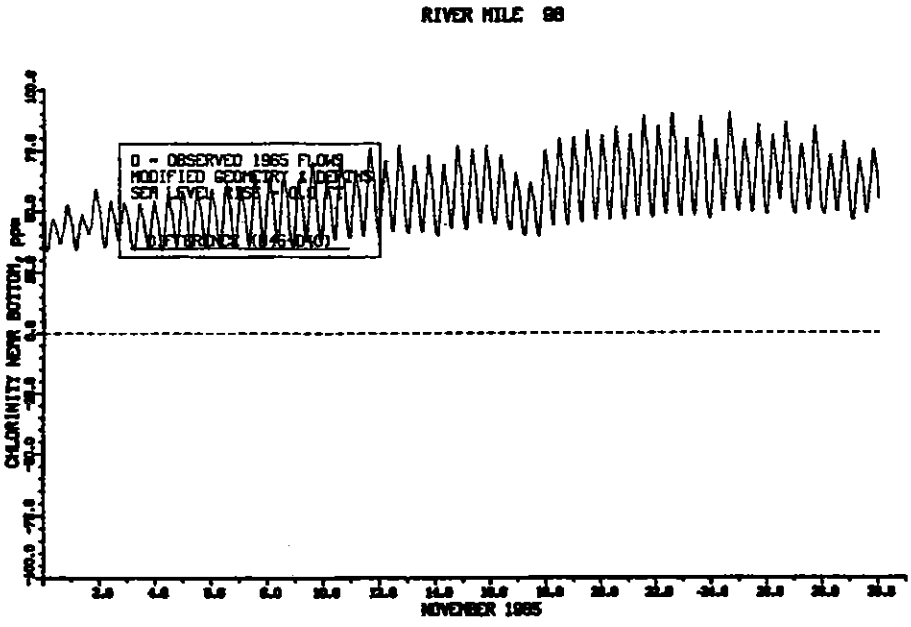

d. Near-bottom difference

Figure 77. (Concluded)

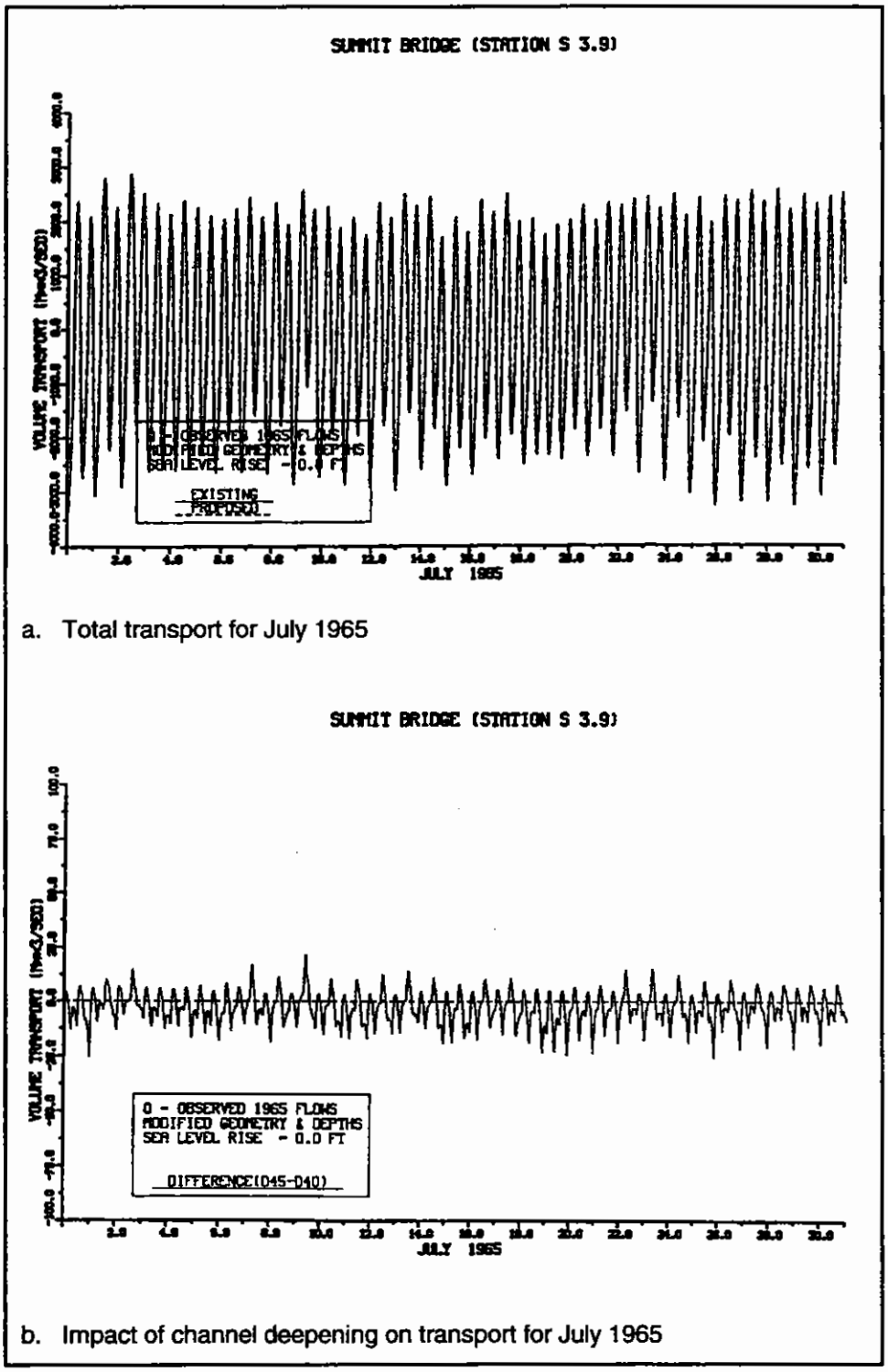

a. Total transport for July 1965

b. Impact of channel deepening on transport for July 1965

Figure 78. Volume transport through the C&D Canal (Sheet 1 of 3)

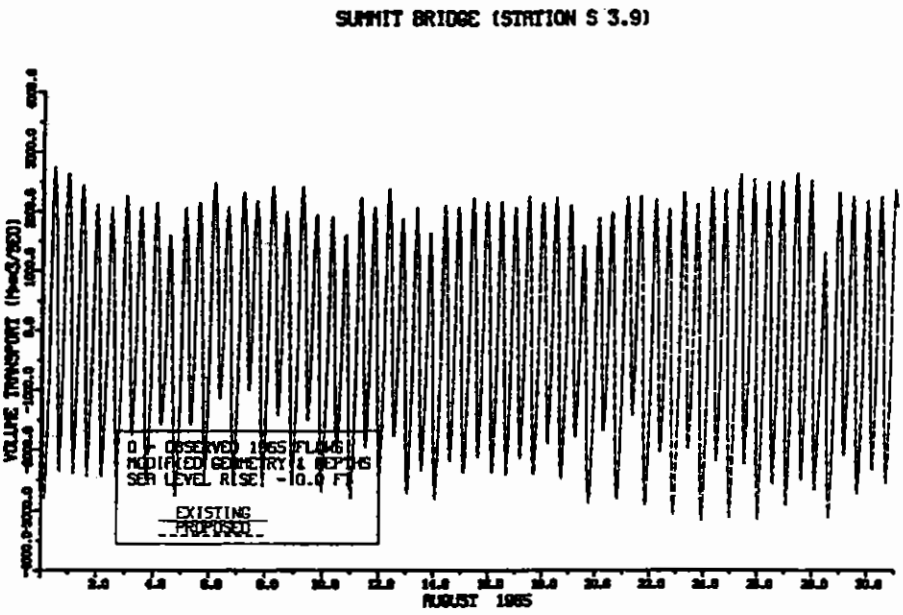

c. Total transport for August 1965

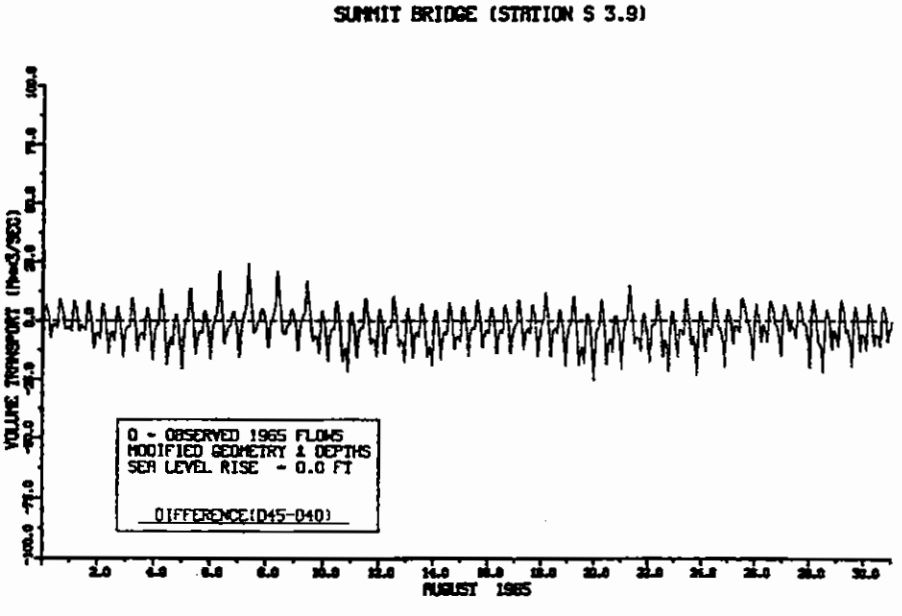

d. Impact of channel deepening on transport for August 1965

Figure 78. (Sheet 2 of 3)

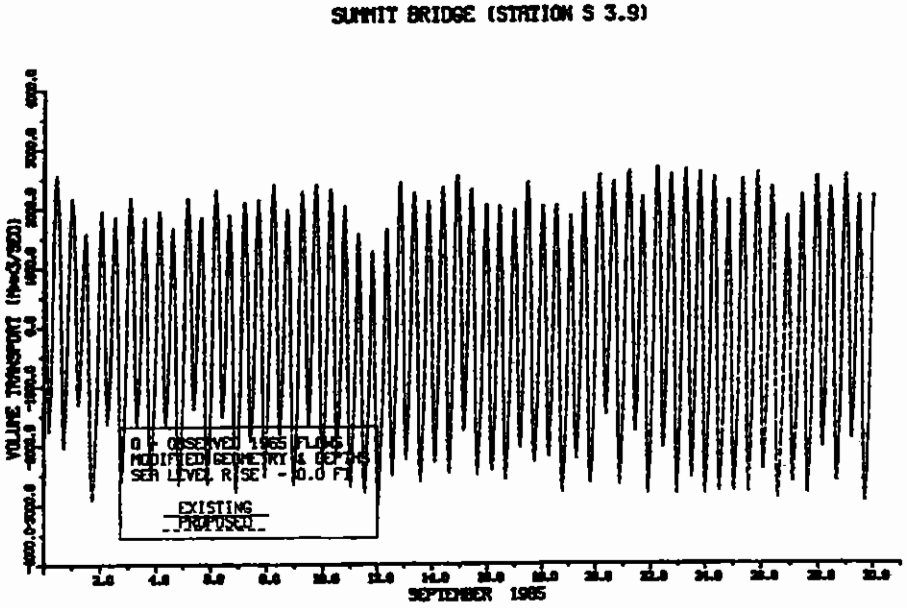

e. Total transport for September 1965

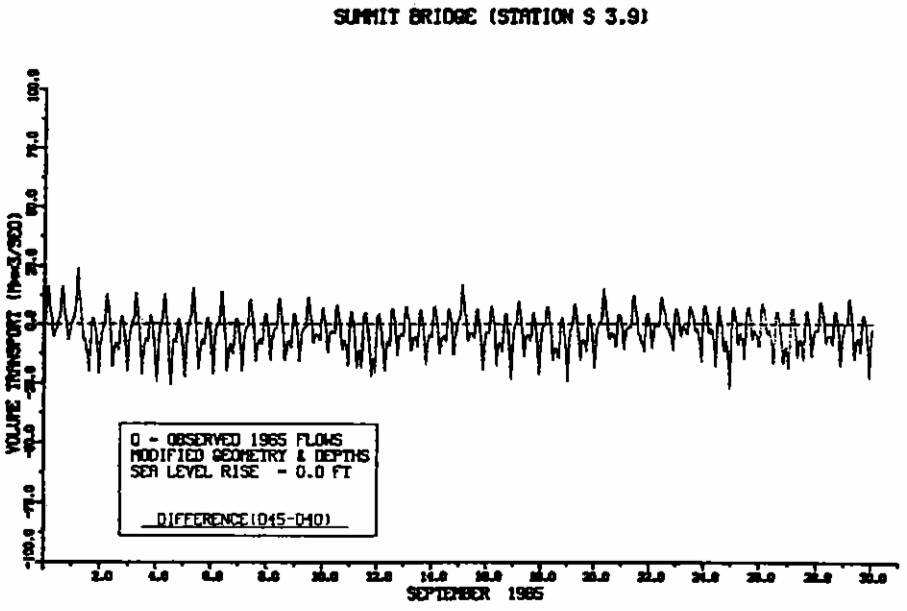

f. Impact of channel deepening on transport for September 1965

Figure 78. (Sheet 3 of 3)

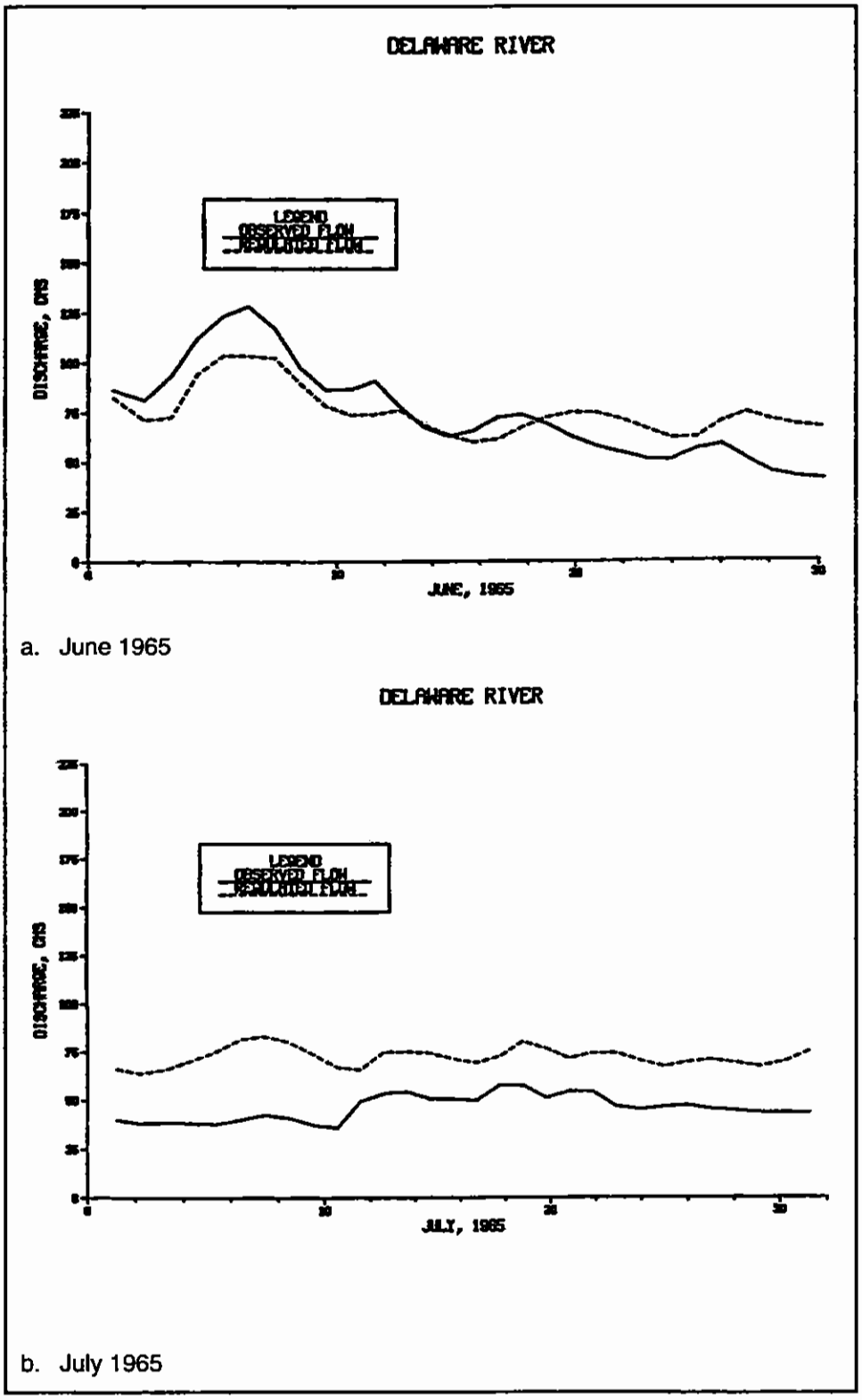

a. June 1965

b. July 1965

Figure 79. Comparison of actual and regulated freshwater inflow on the Delaware River (Sheet 1 of 3)

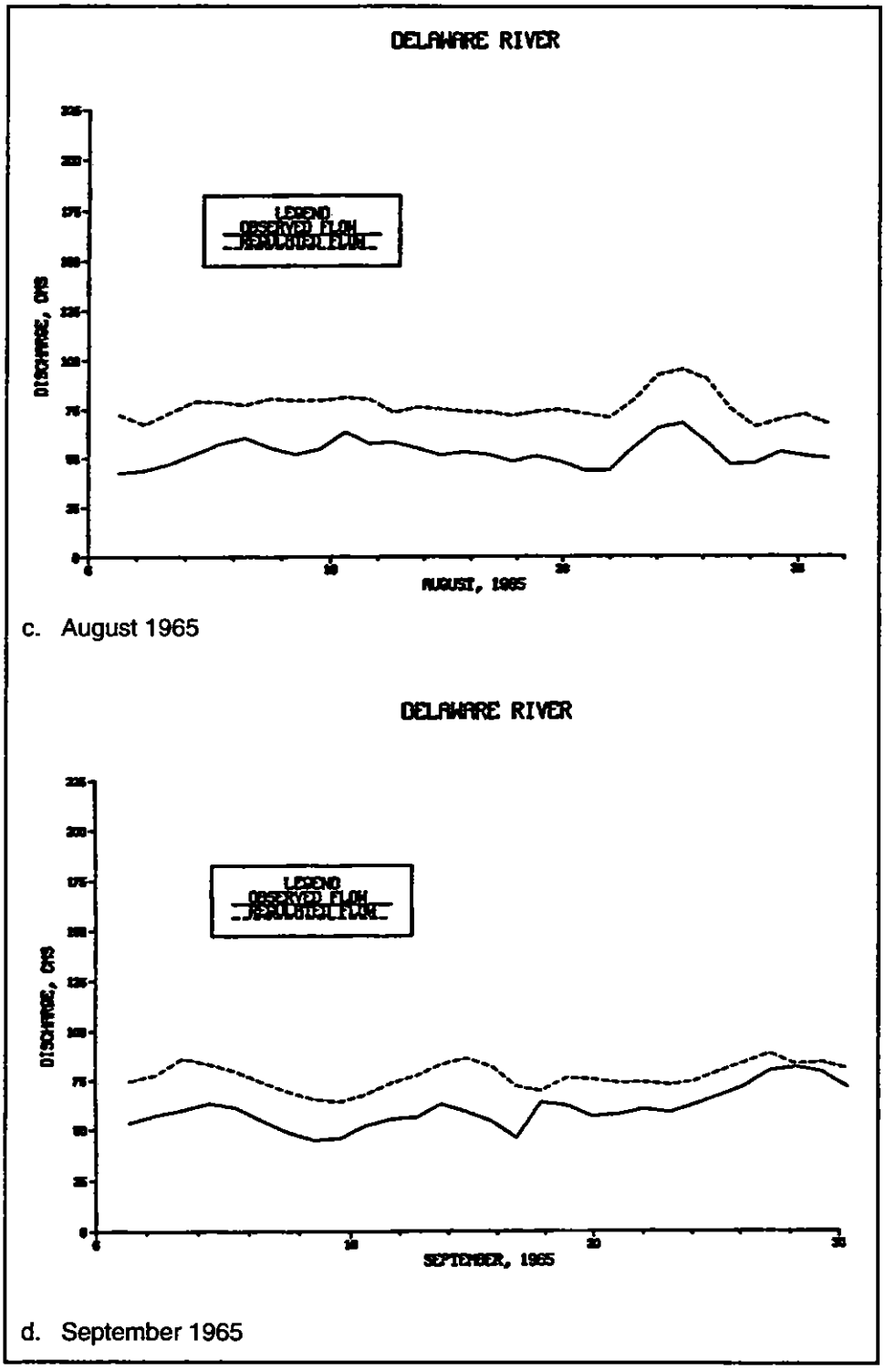

Figure 79. (Sheet 2 of 3)

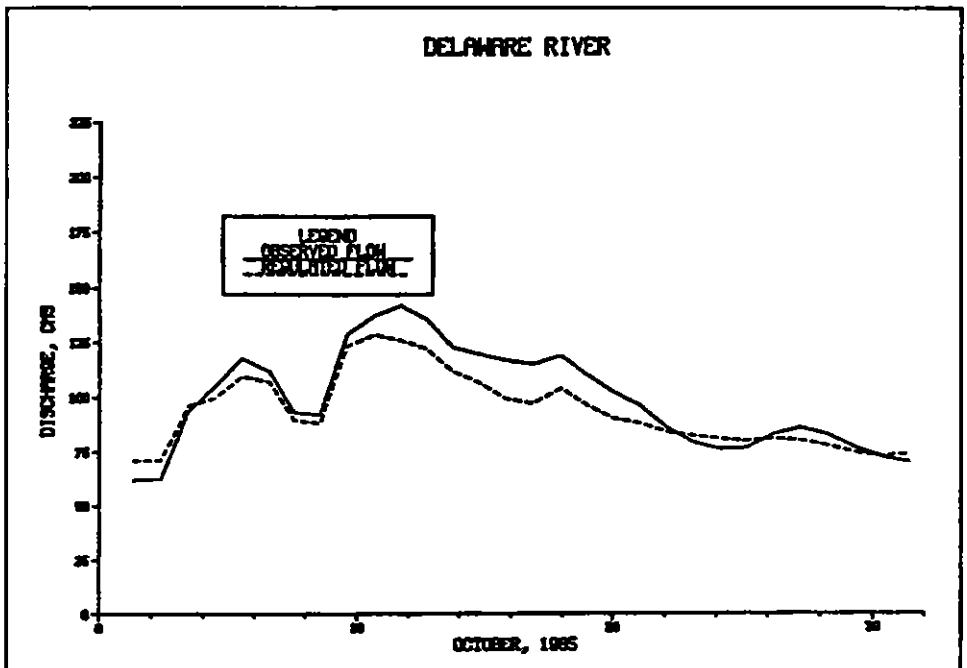

e. October 1965

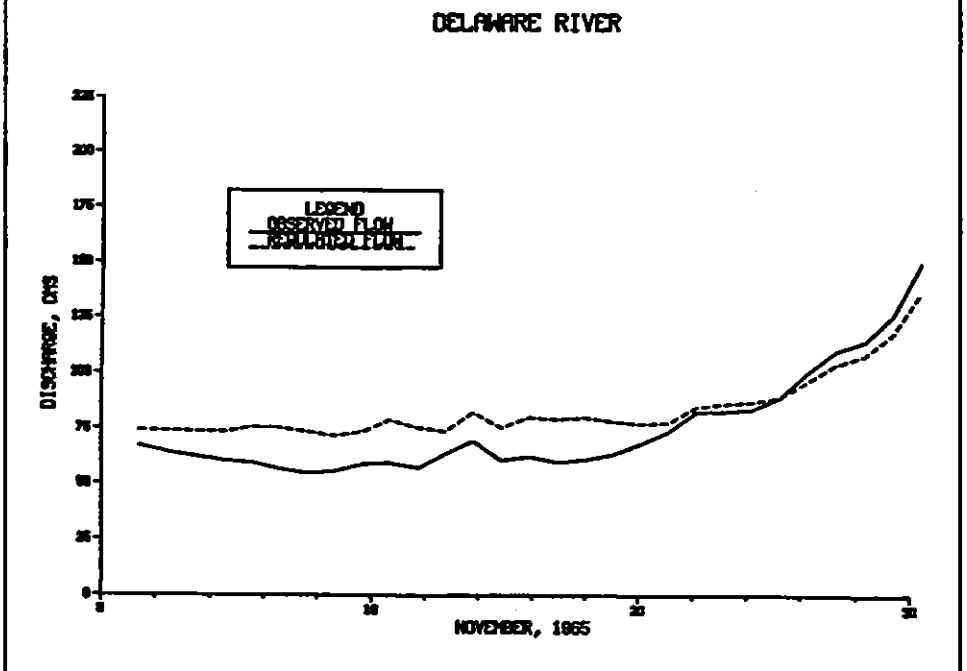

f. November 1965

Figure 79. (Sheet 3 of 3)

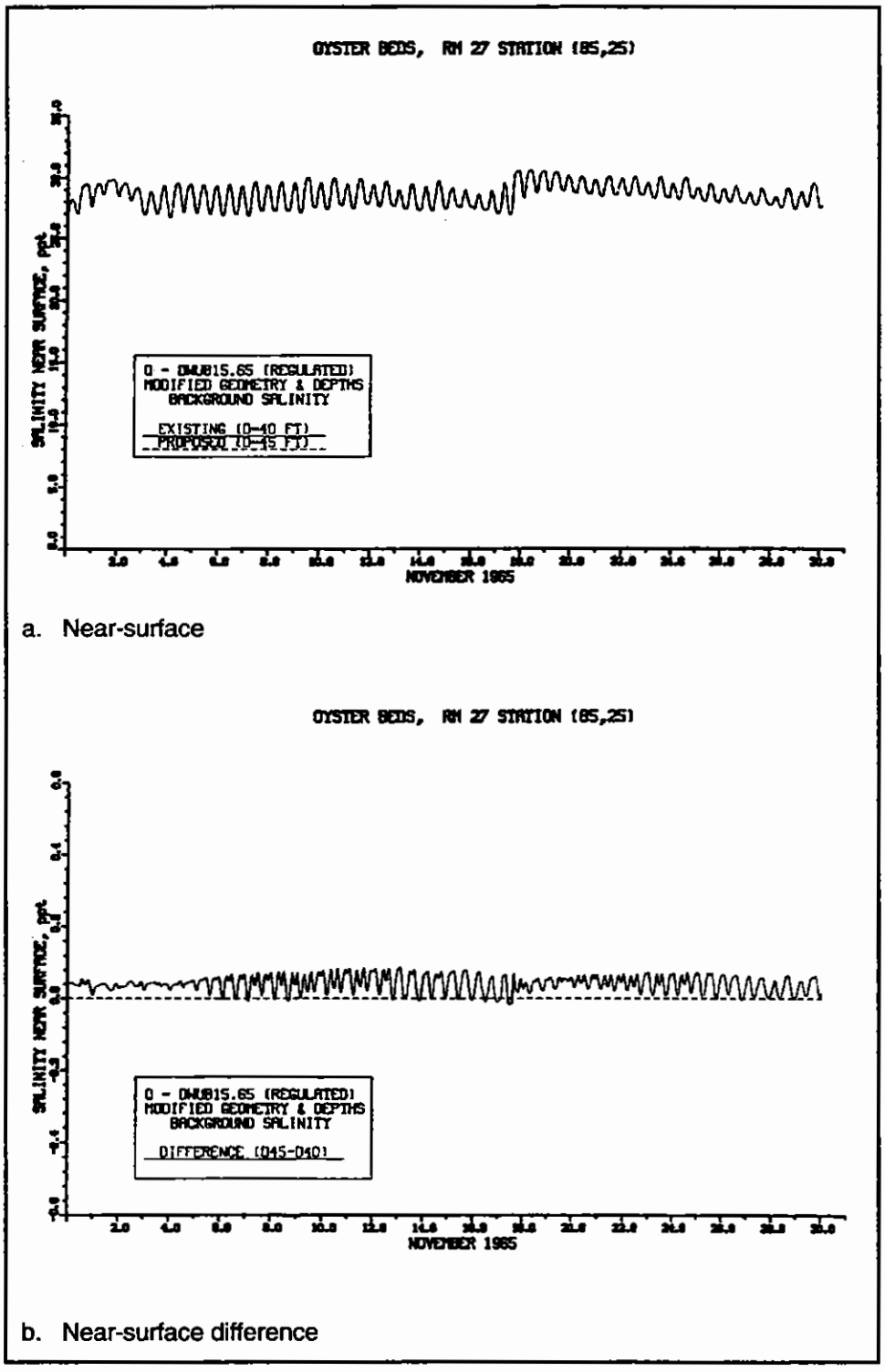

Figure 80. Impact of channel deepening on salinity at RM 27 Station (85,25) for regulated inflow (continued)

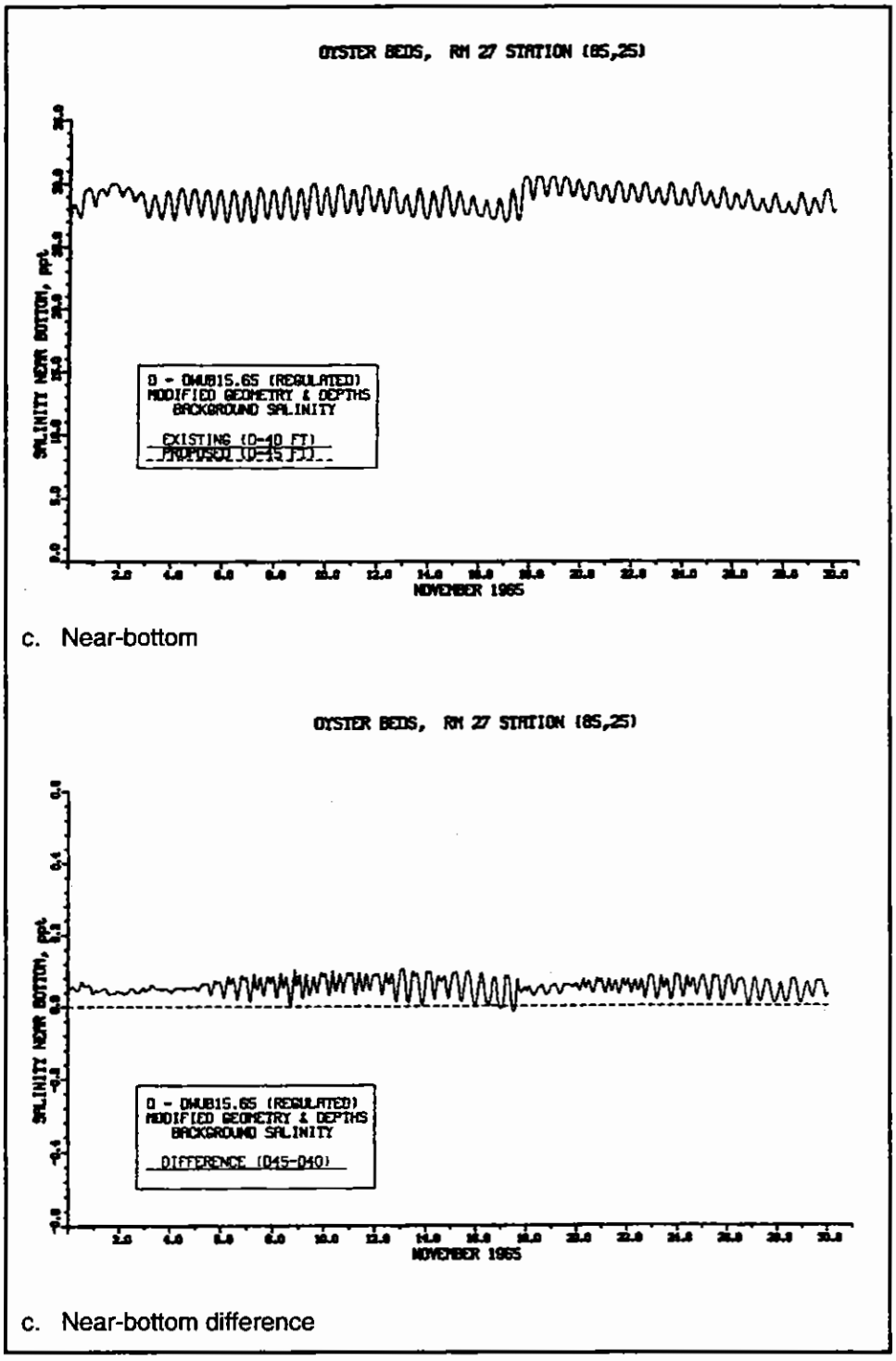

Figure 80. (Concluded)

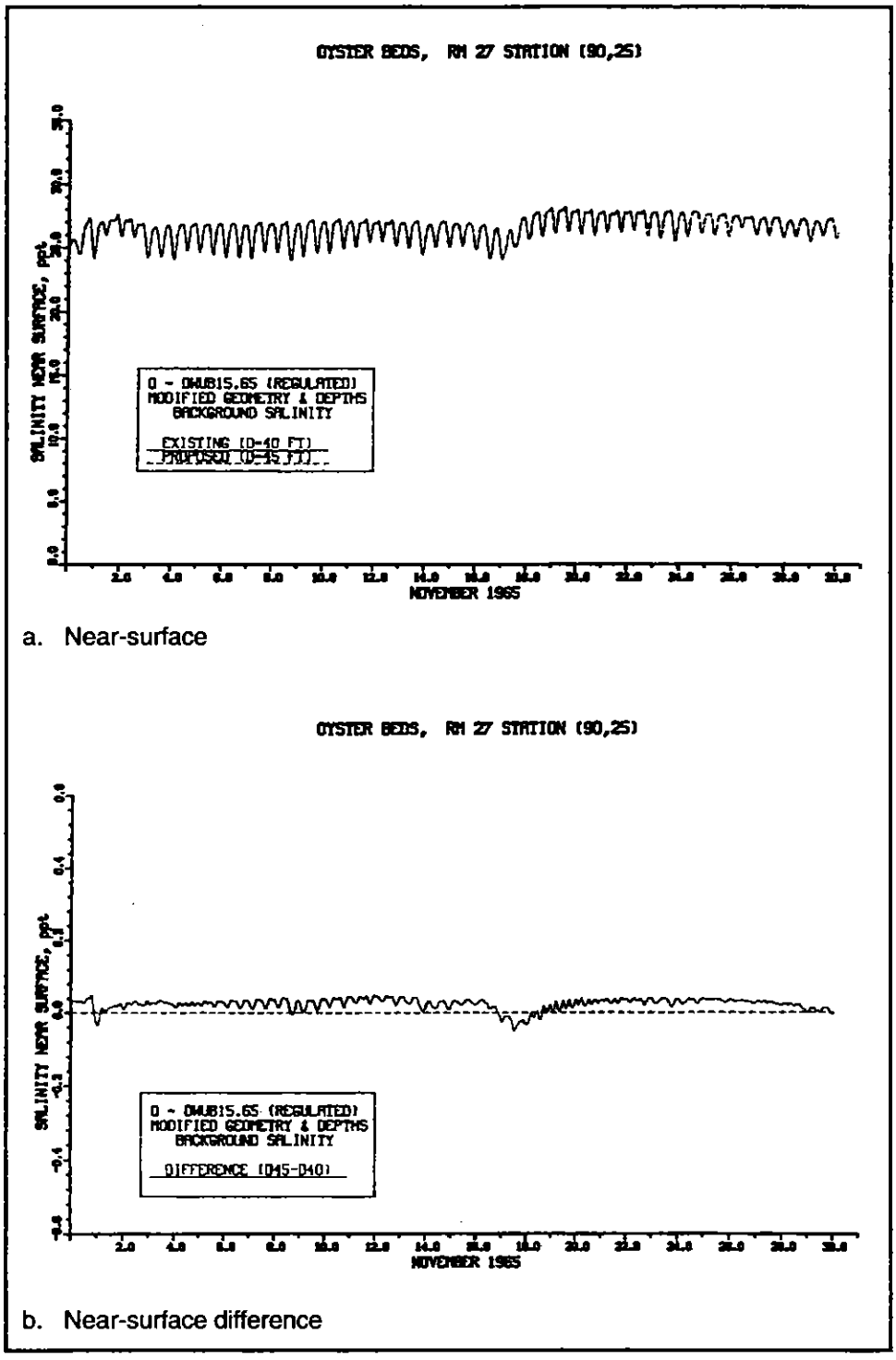

Figure 81. Impact of channel deepening on salinity at RM 27 Station (90,25) for regulated inflow (continued)

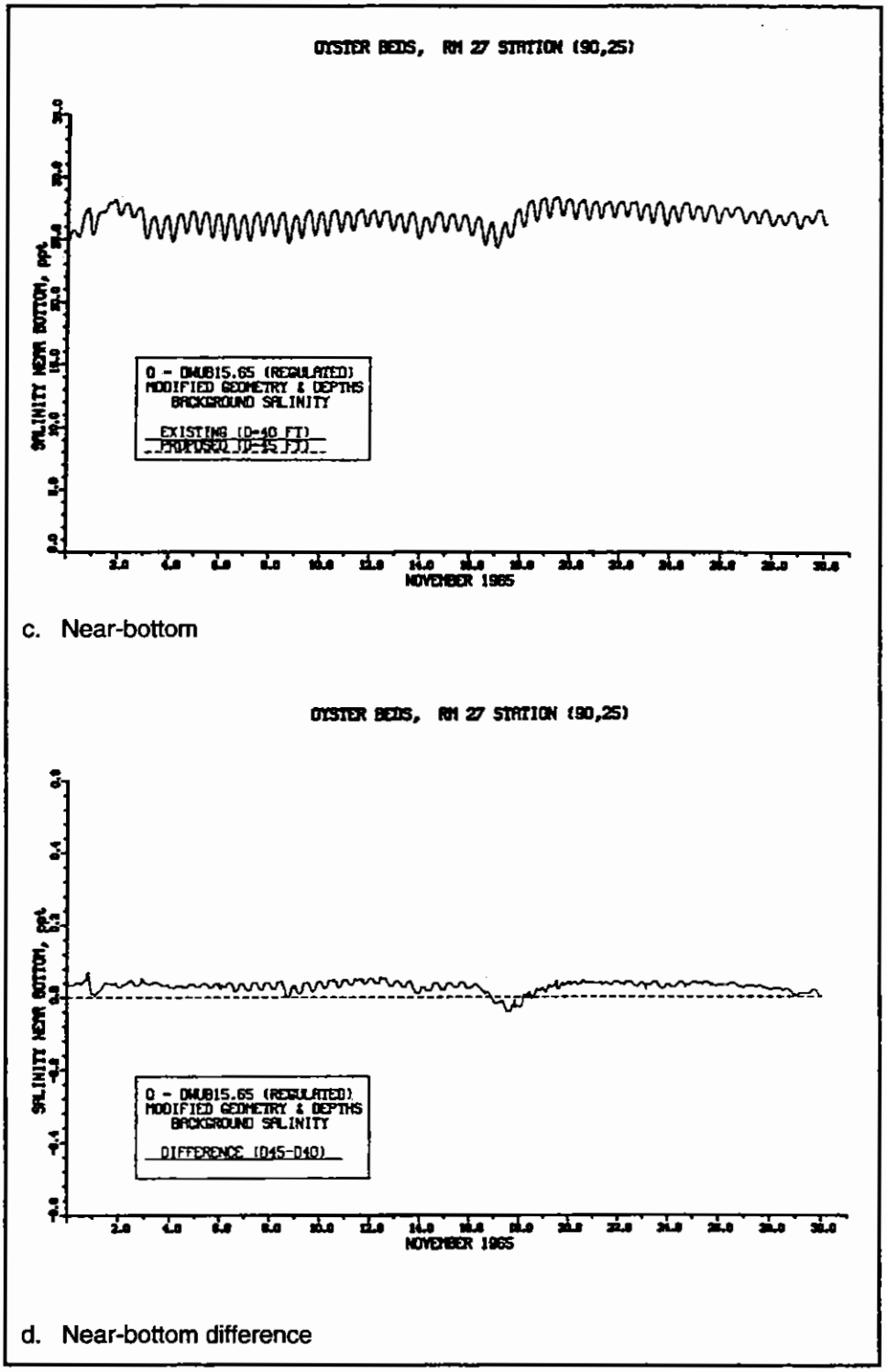

c. Near-bottom

d. Near-bottom difference

Figure 81. (Concluded)

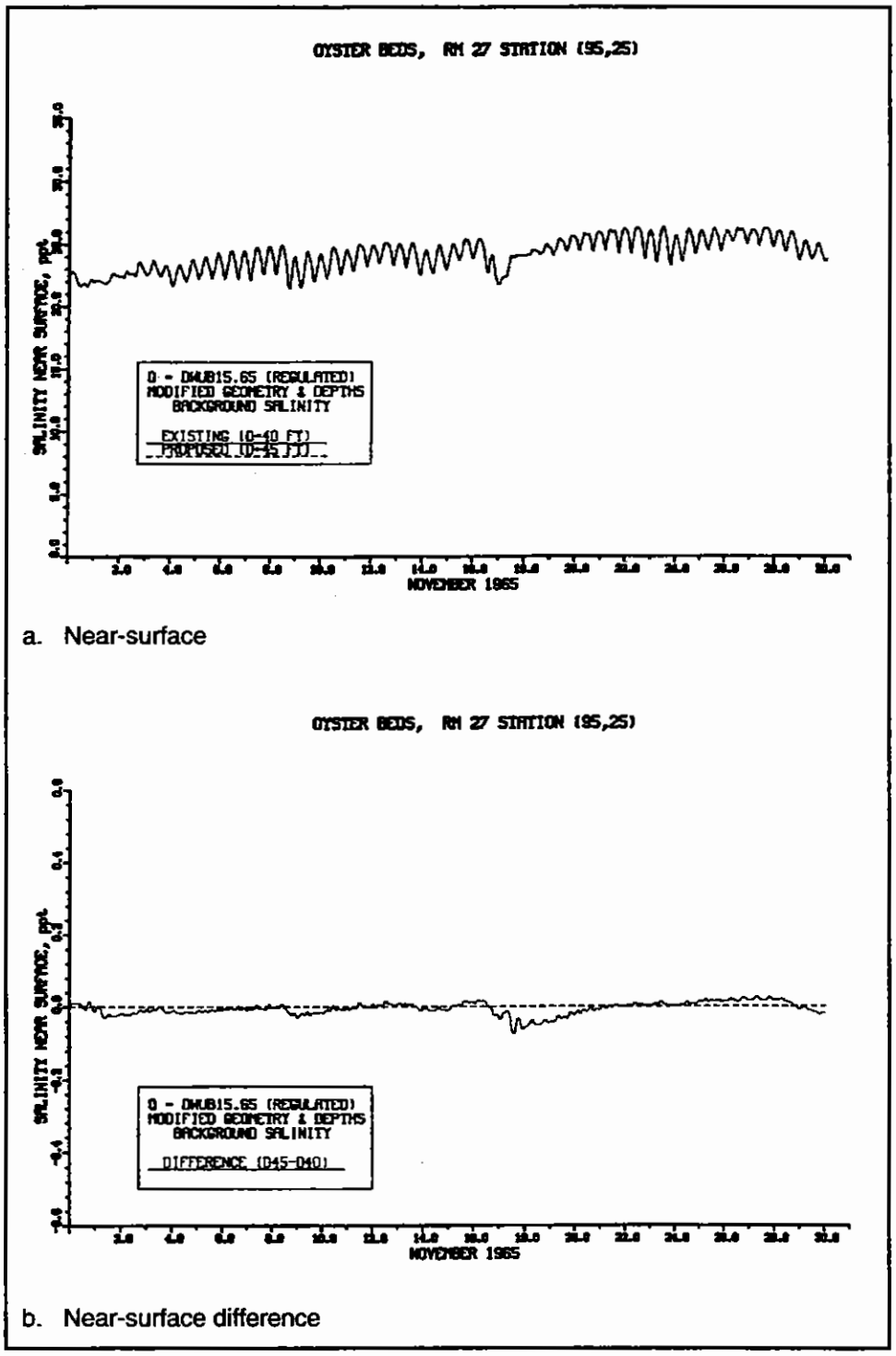

Figure 82. Impact of channel deepening on salintiy at RM 27 Station (95,25) for regulated inflow

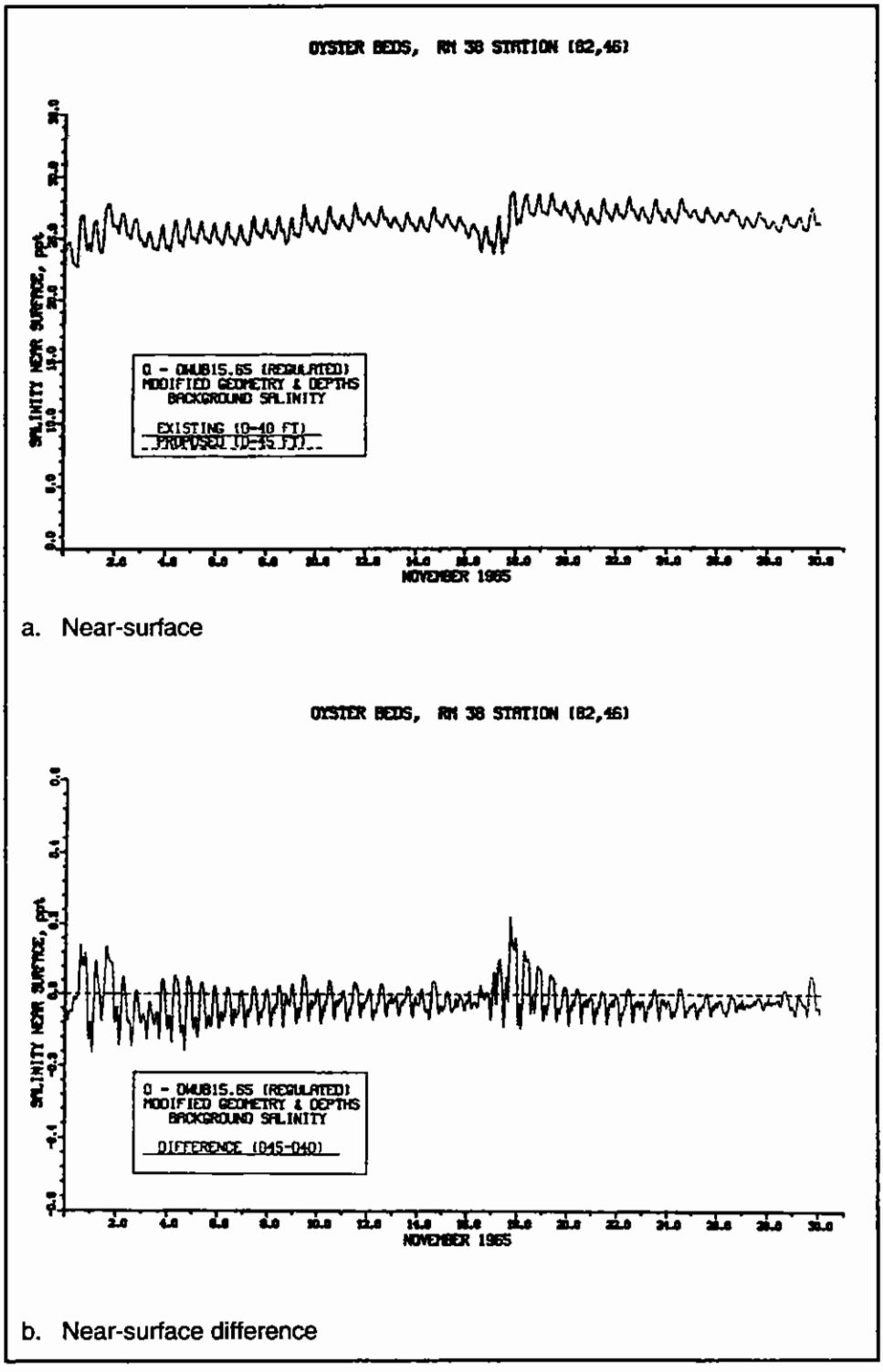

Figure 83. Impact of channel deepening on salinity at RM 38 Station (82, 46) for regulated inflow

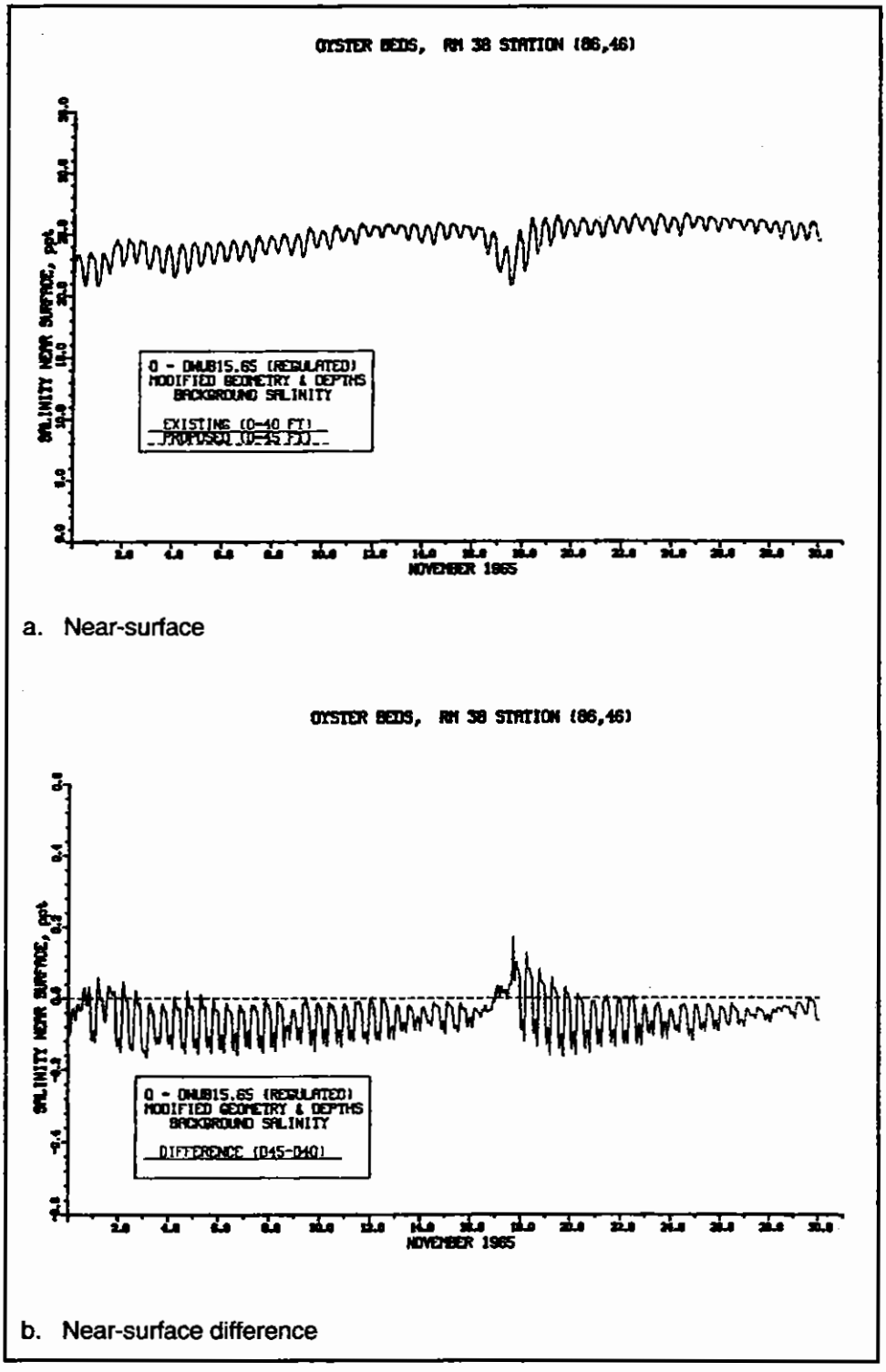

Figure 84. Impact of channel deepening on salinity at RM 38 Station (86,46) for regulated inflow (continued)

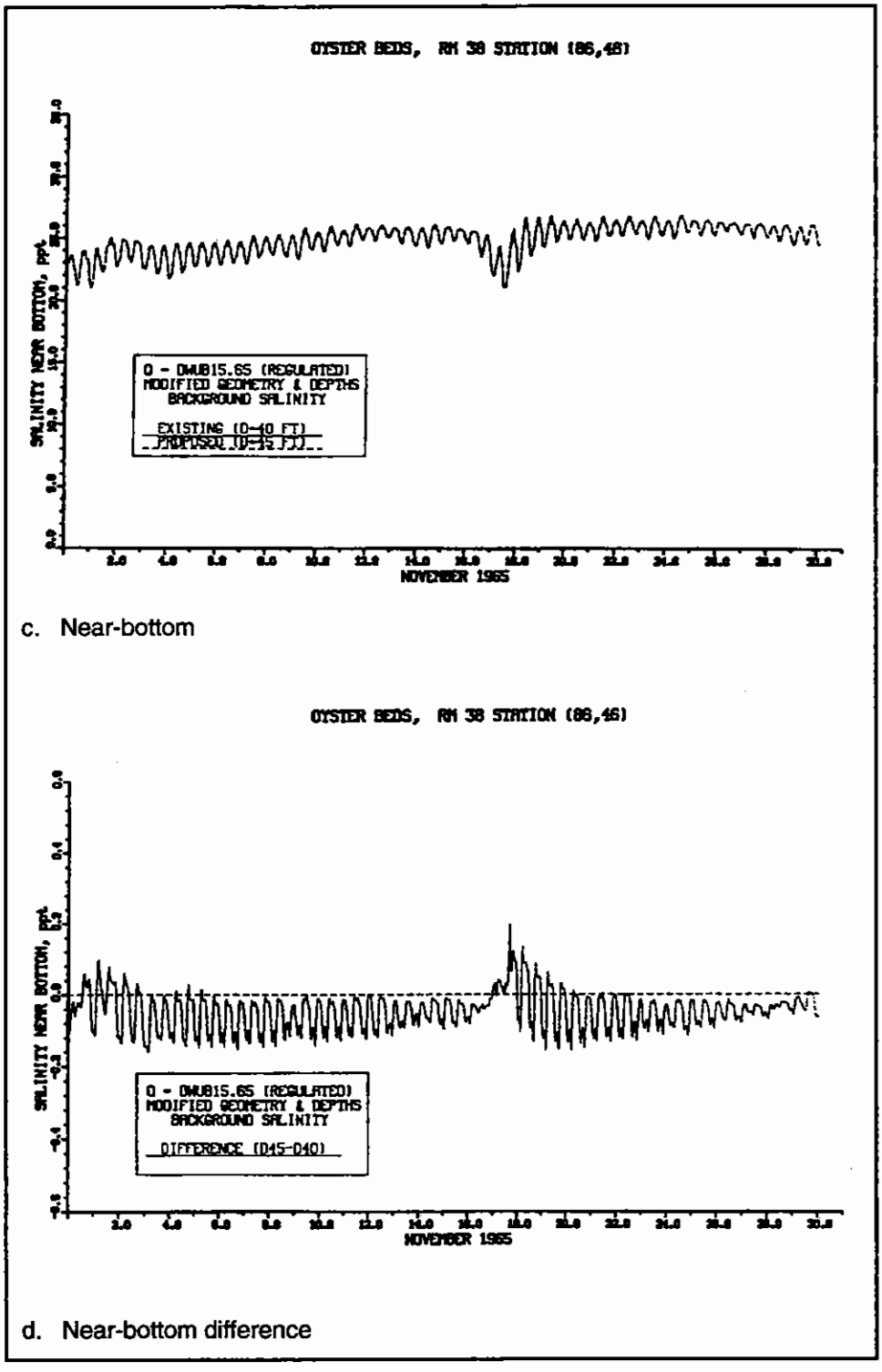

c. Near-bottom

d. Near-bottom difference

Figure 84. (Concluded)

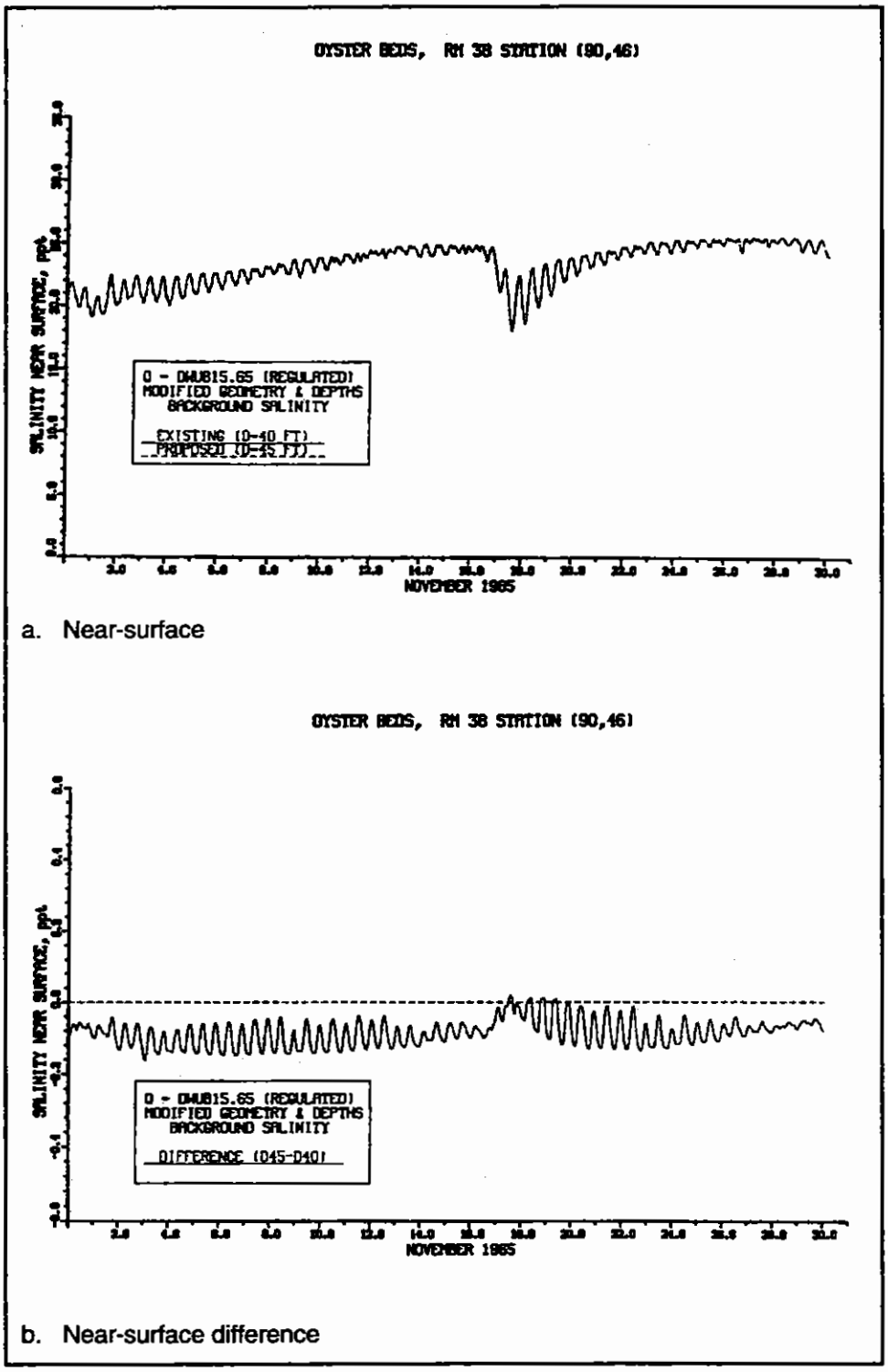

Figure 85. Impact of channel deepening on salinity at RM 38 Station (90,46) for regulated inflow

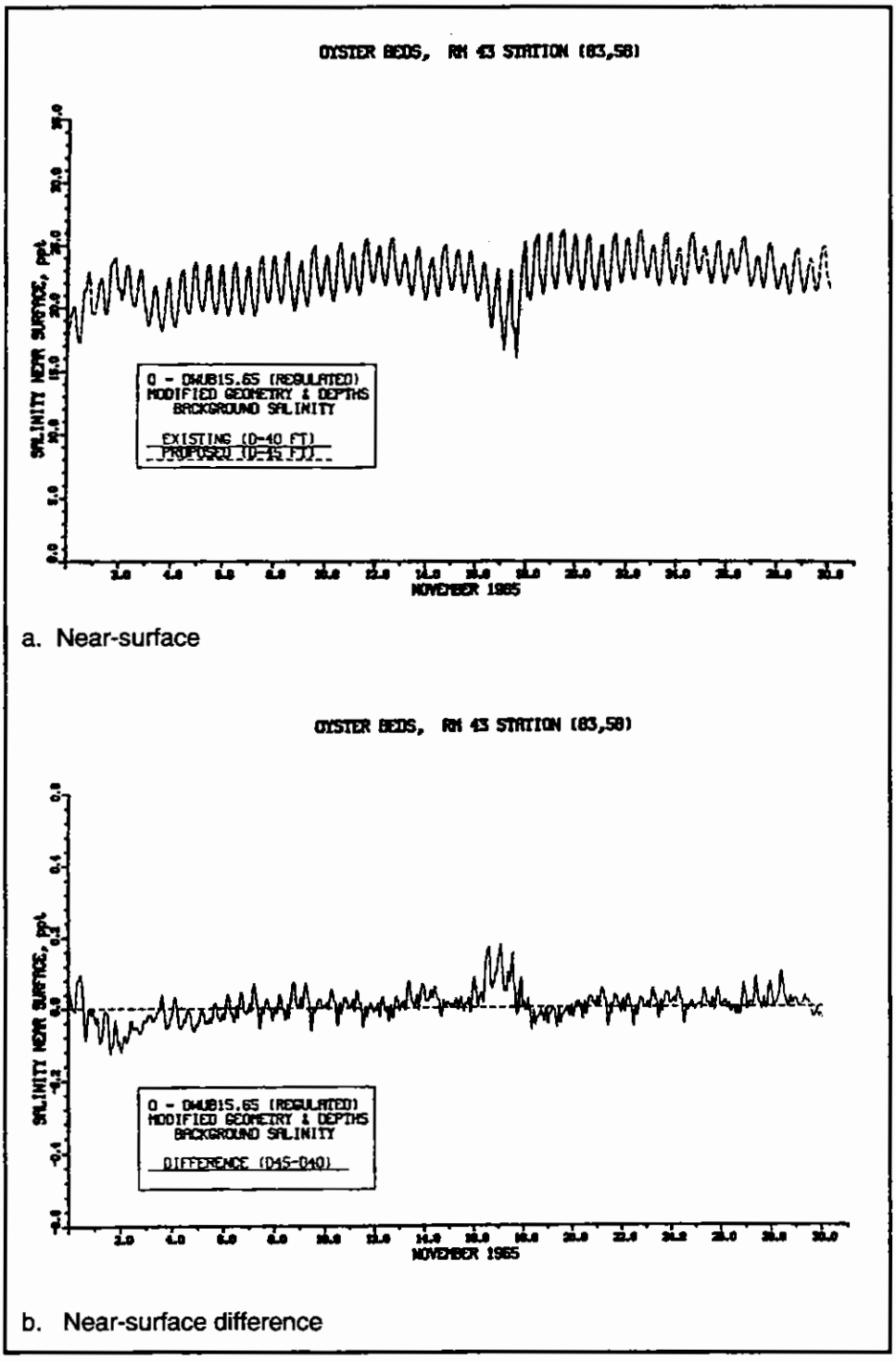

Figure 86. Impact of channel deepening on salinity at RM 43 Station (83, 58) for regulated inflow (continued)

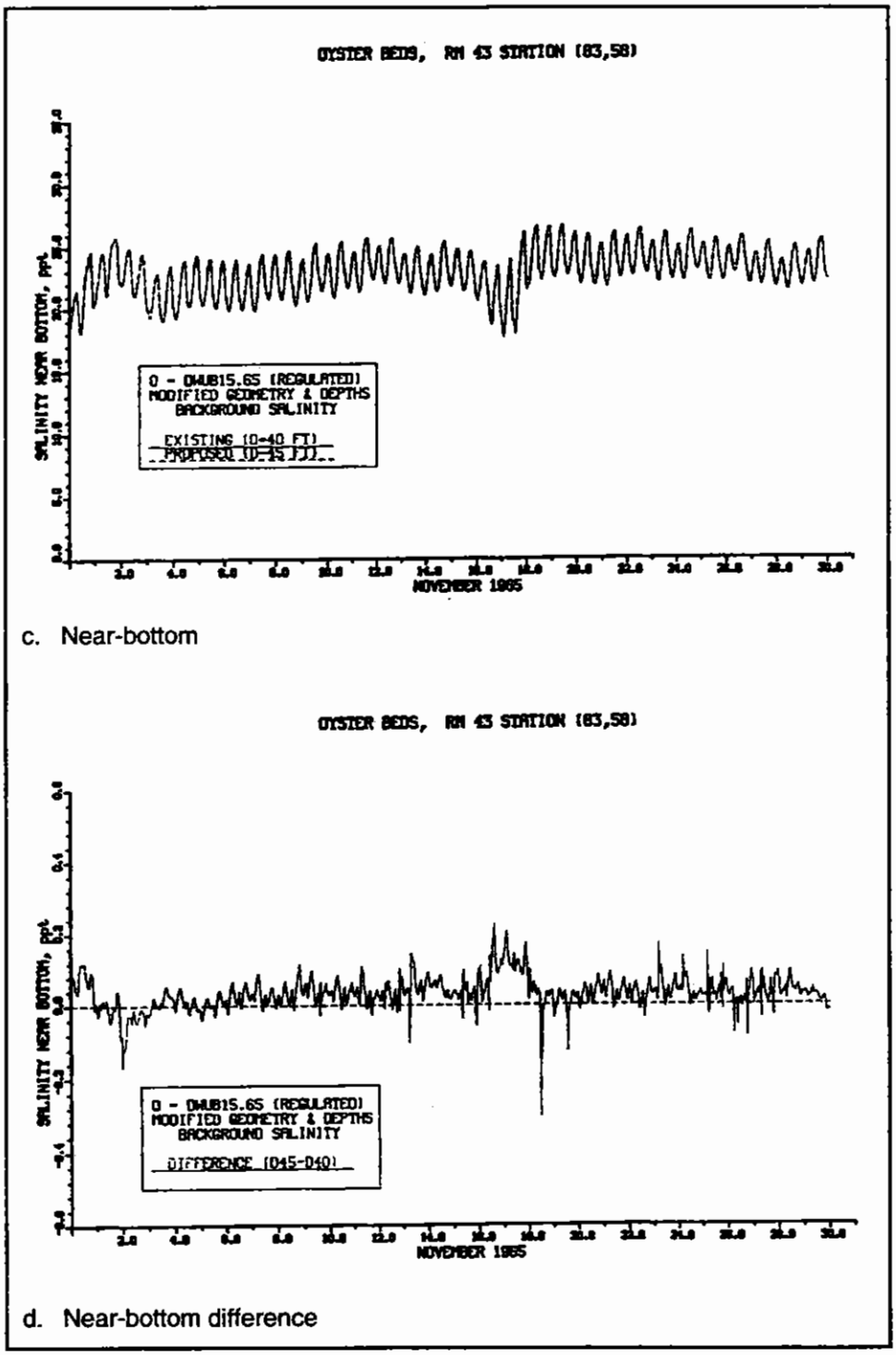

Figure 86. (Concluded)

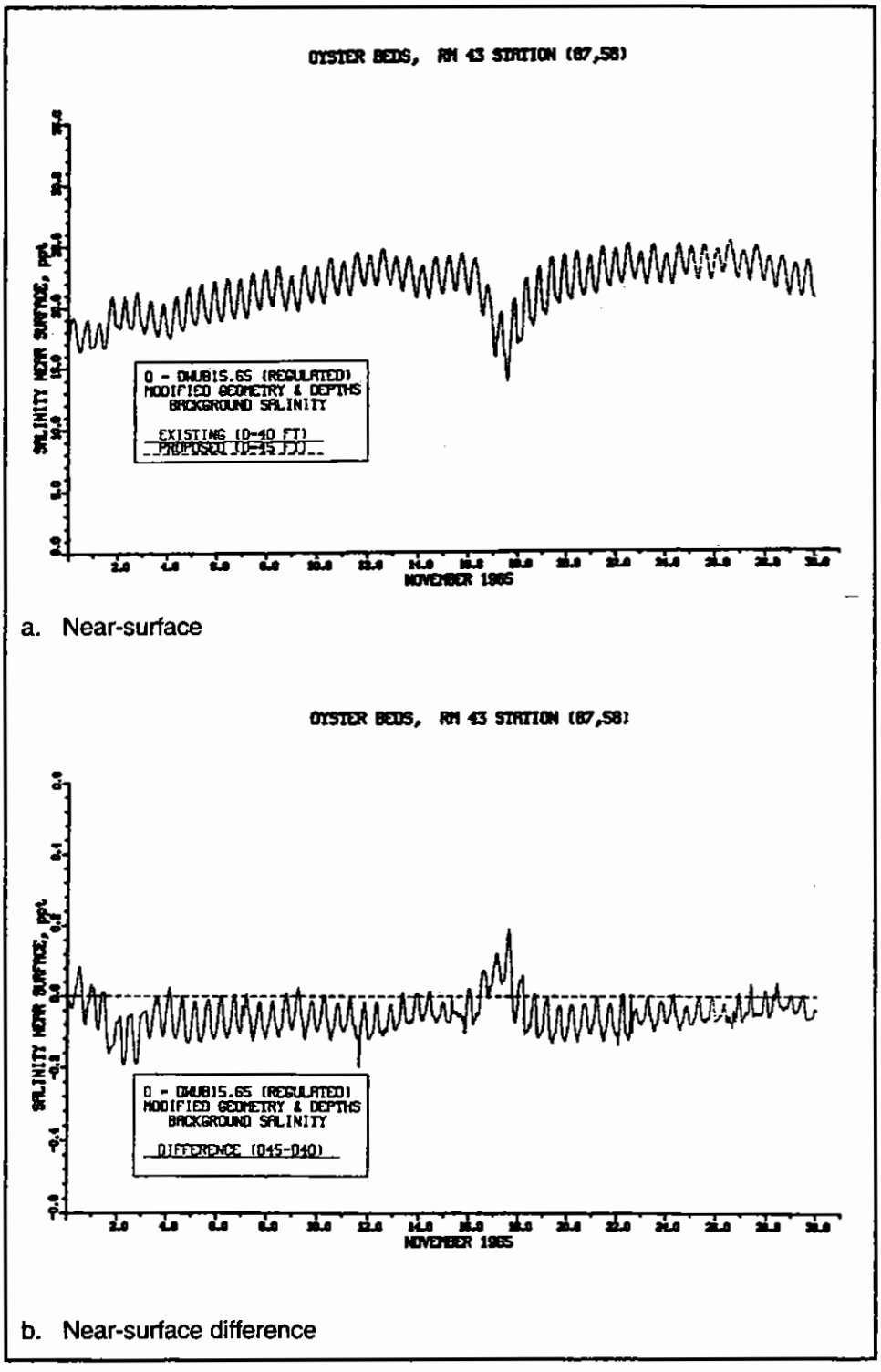

Figure 87. Impact of channel deepening on salinity at RM 43 Station (87,58) for regulated inflow (continued)

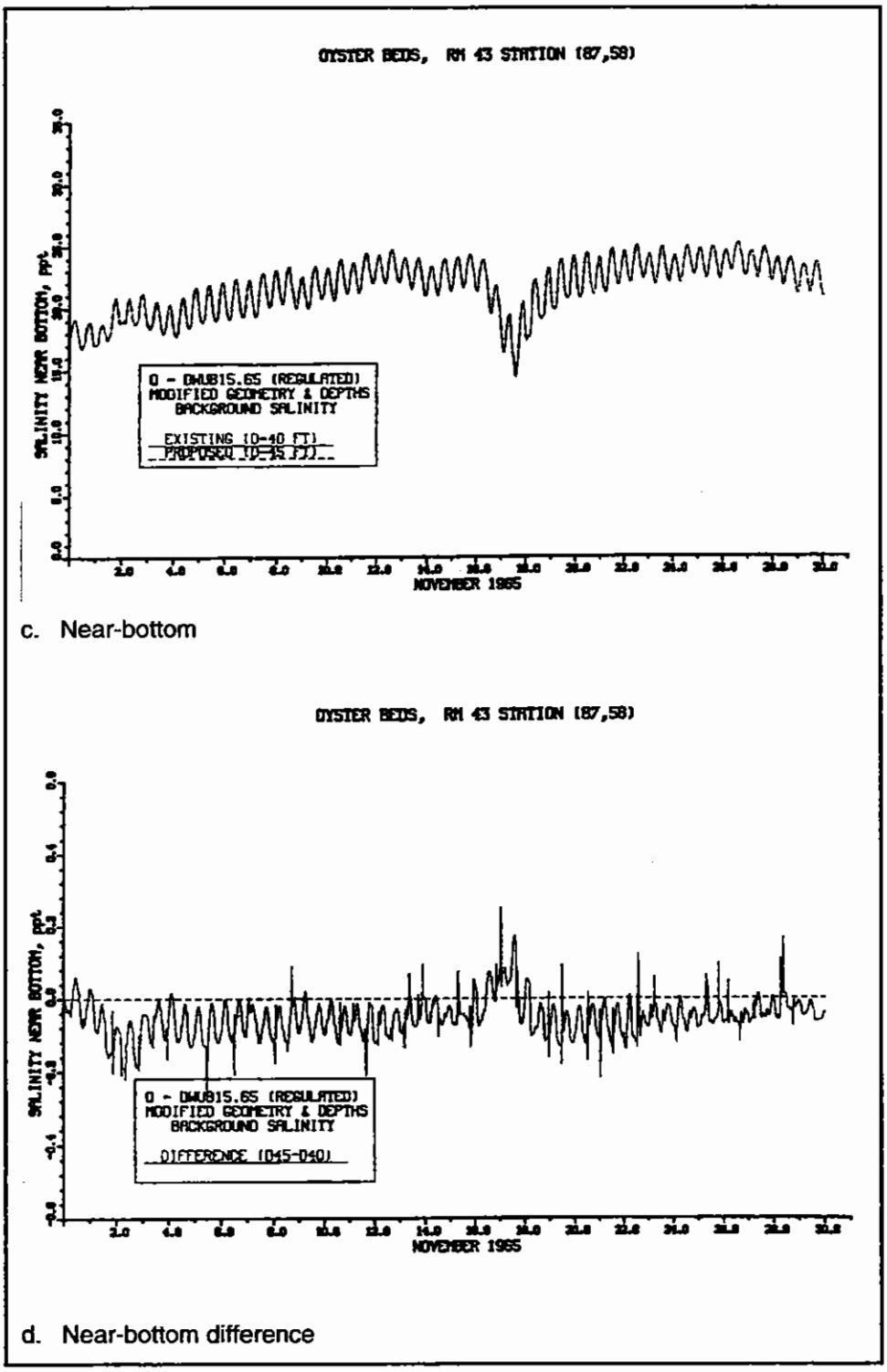

Figure 87. (Concluded)

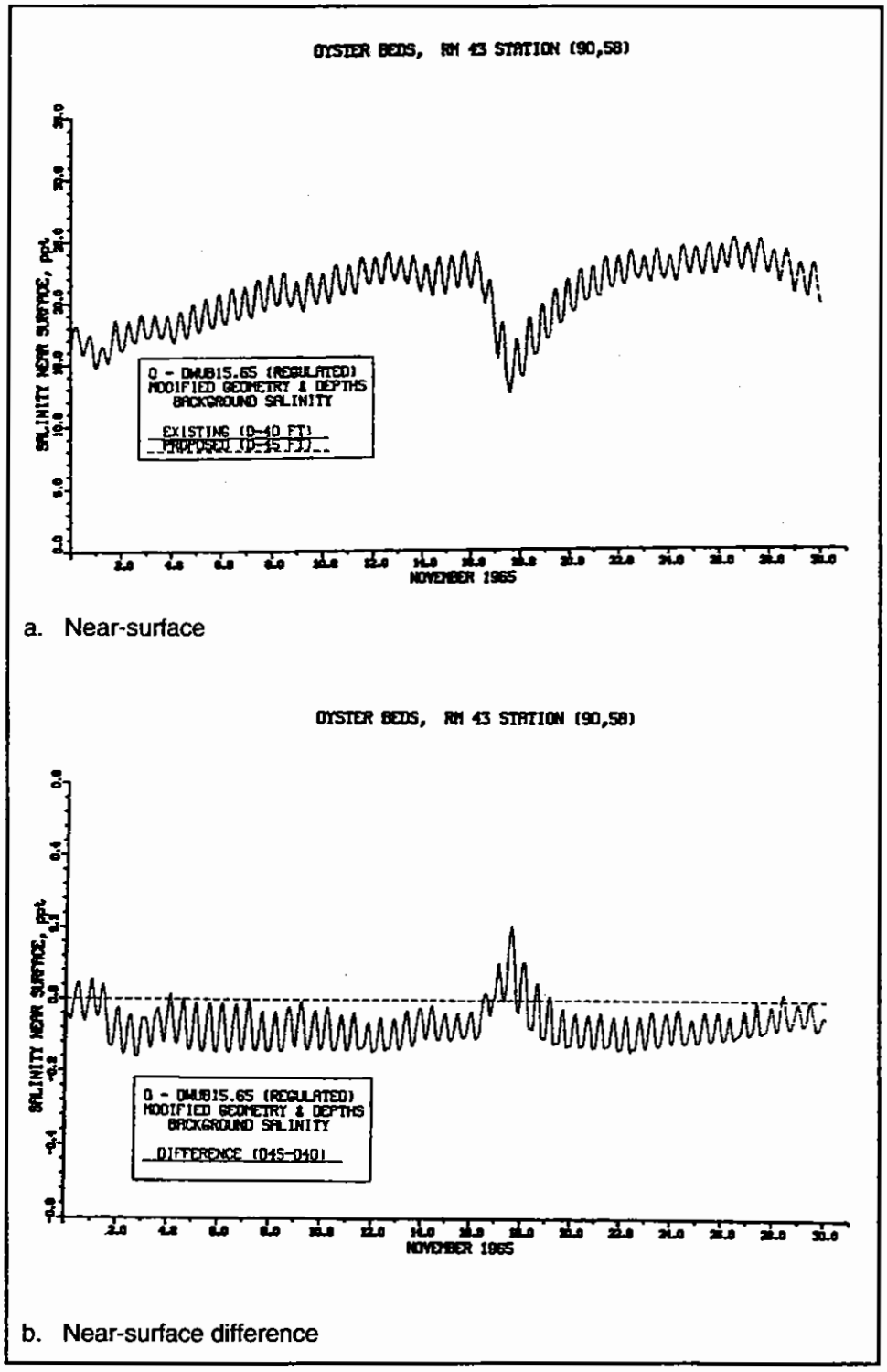

Figure 88. Impact of channel deepening on salinity at RM 43 Station (90,58) for regulated inflow (continued)

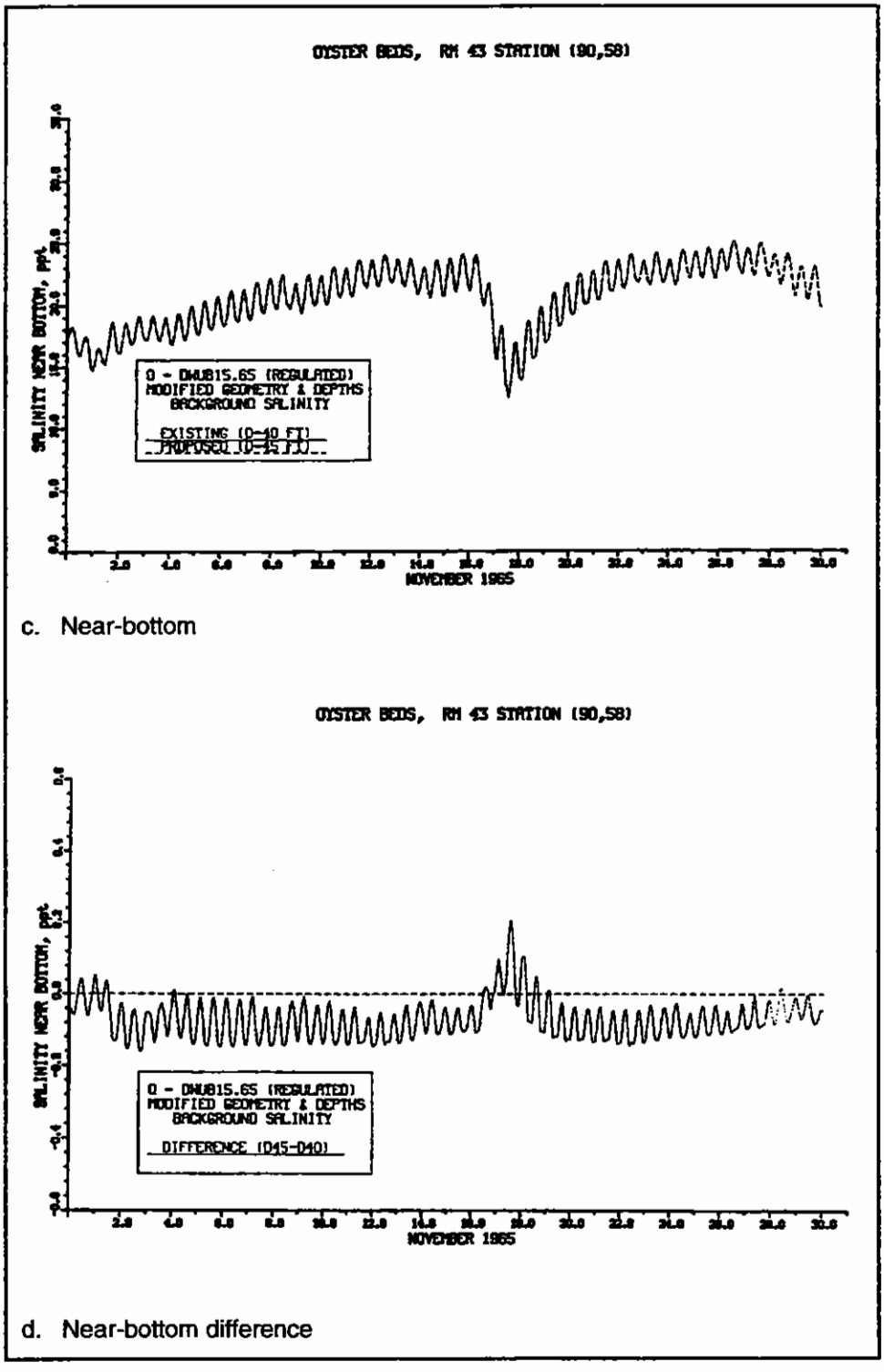

Figure 88. (Concluded)

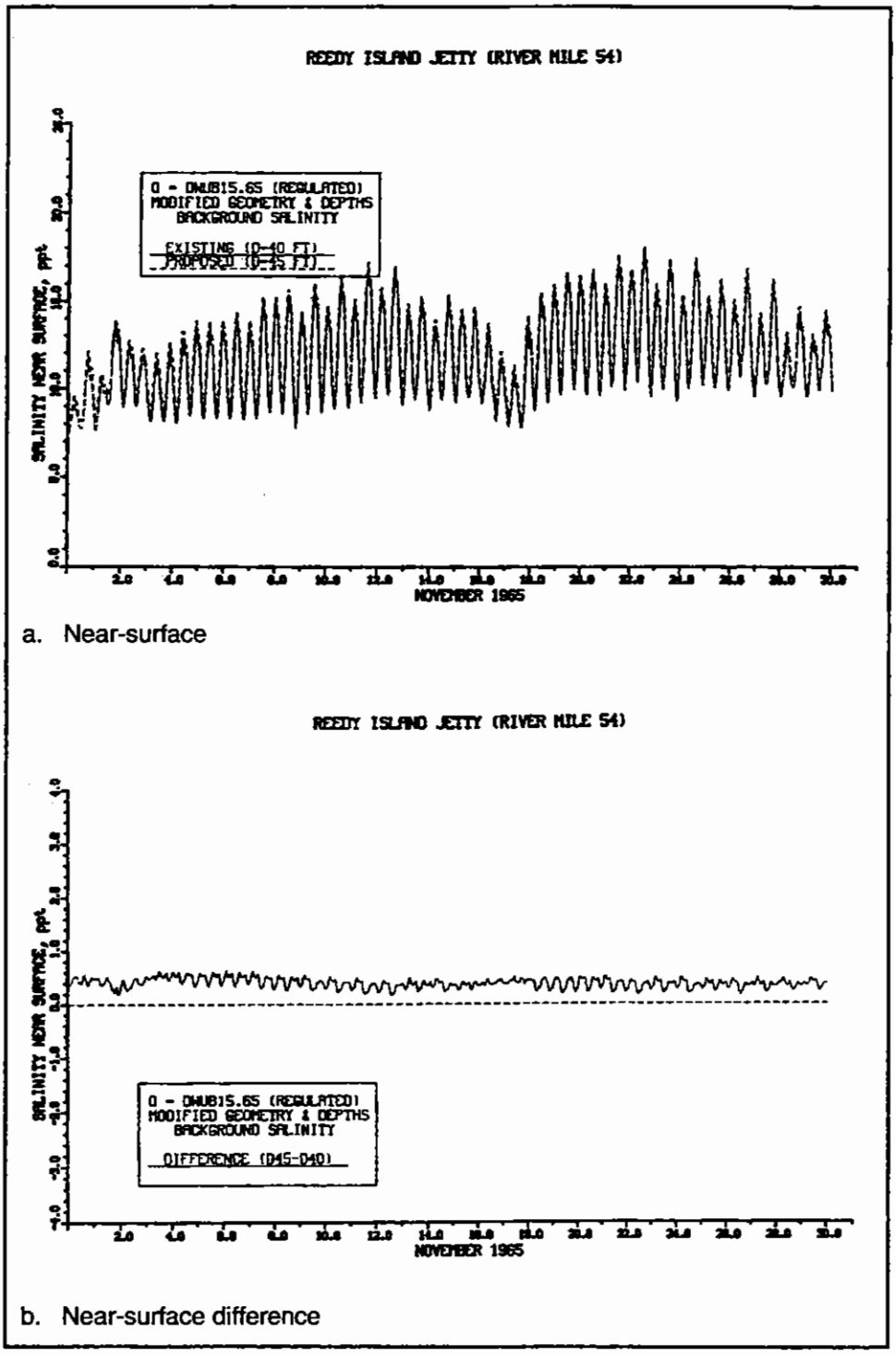

Figure 89. Impact of channel deepening on salinity at RM 54 for regulated inflow (continued)

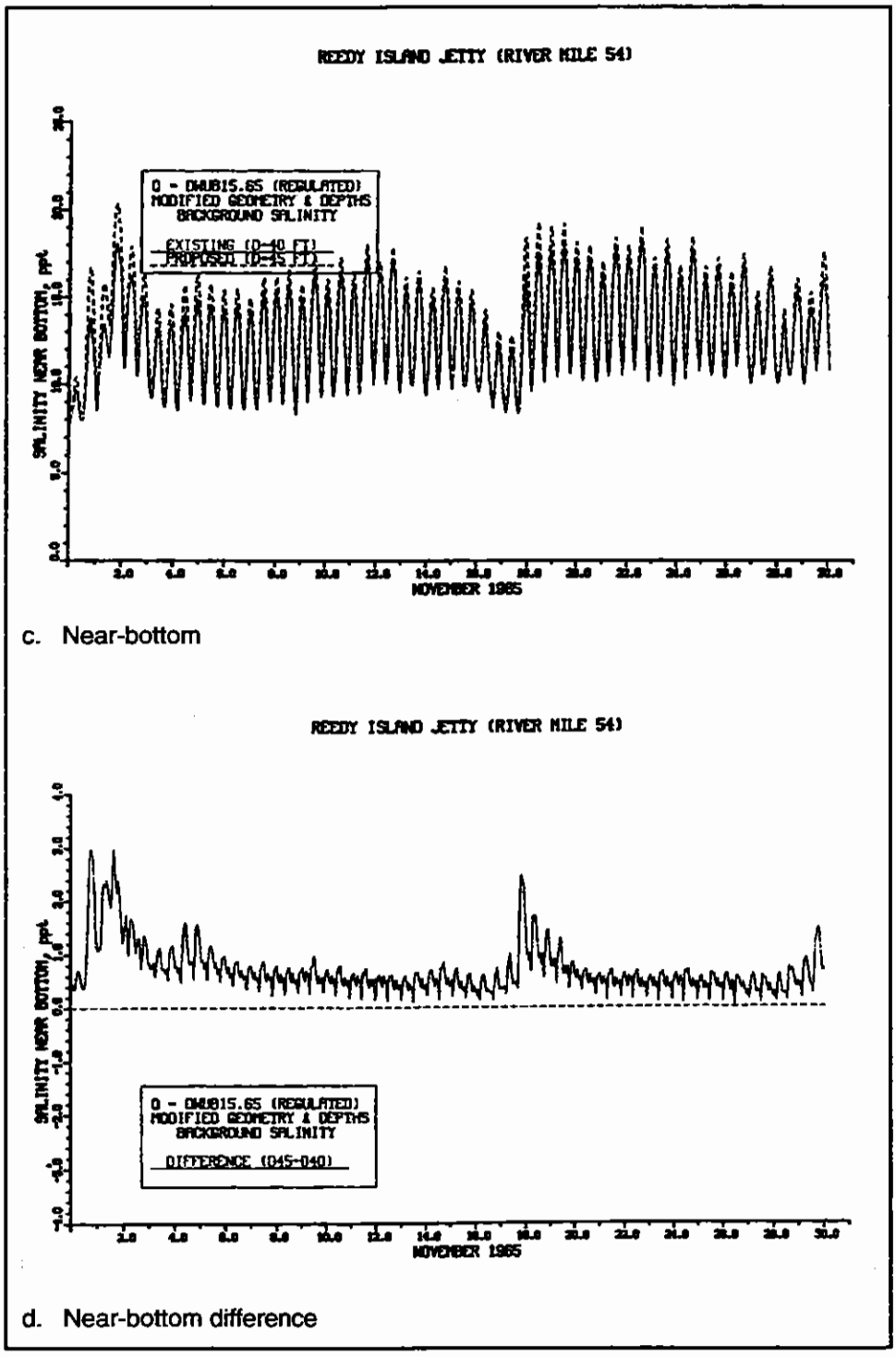

Figure 89. (Concluded)

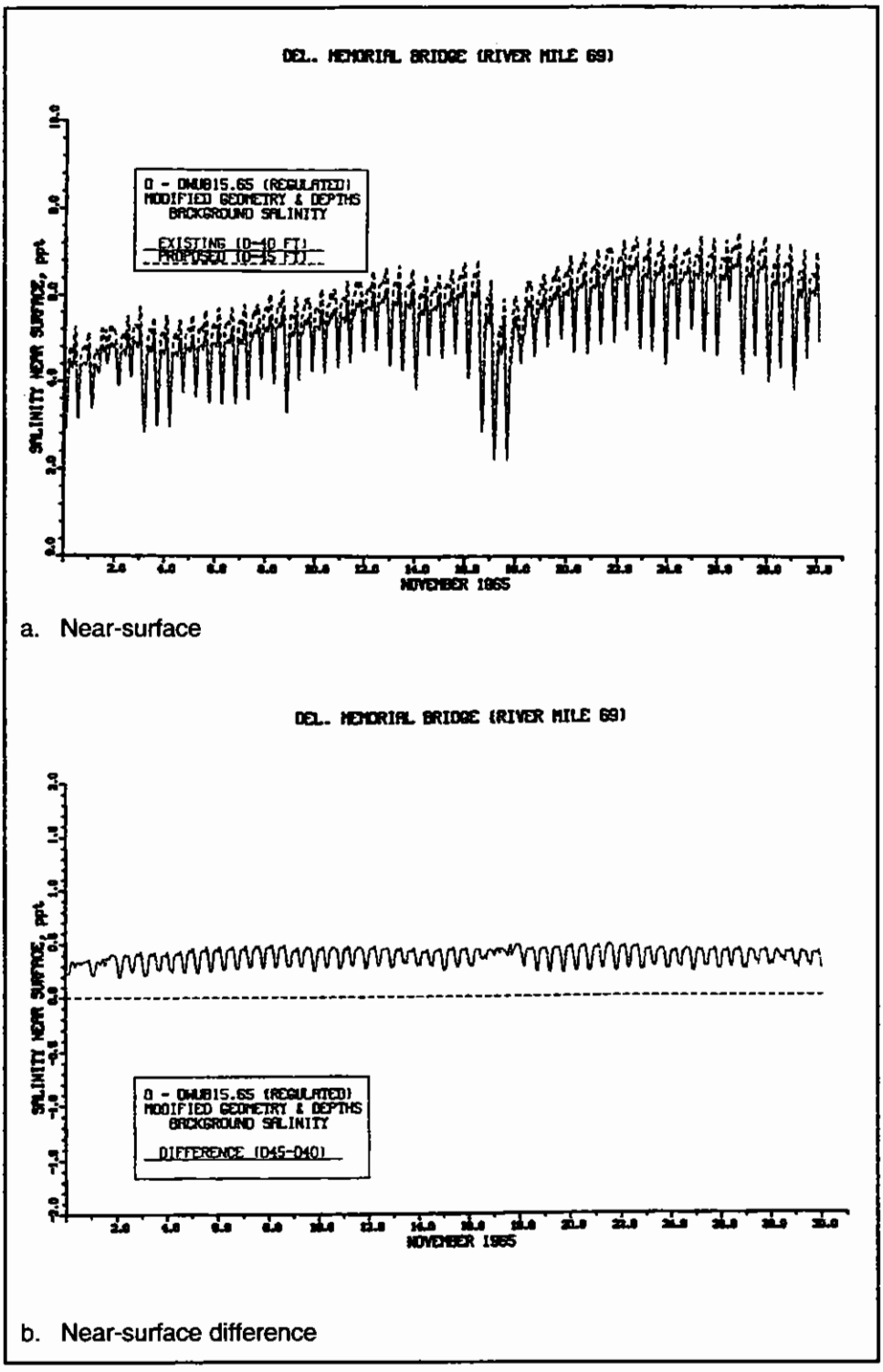

Figure 90. Impact of channel deepening on salinity at RM 69 for regulated inflow (continued)

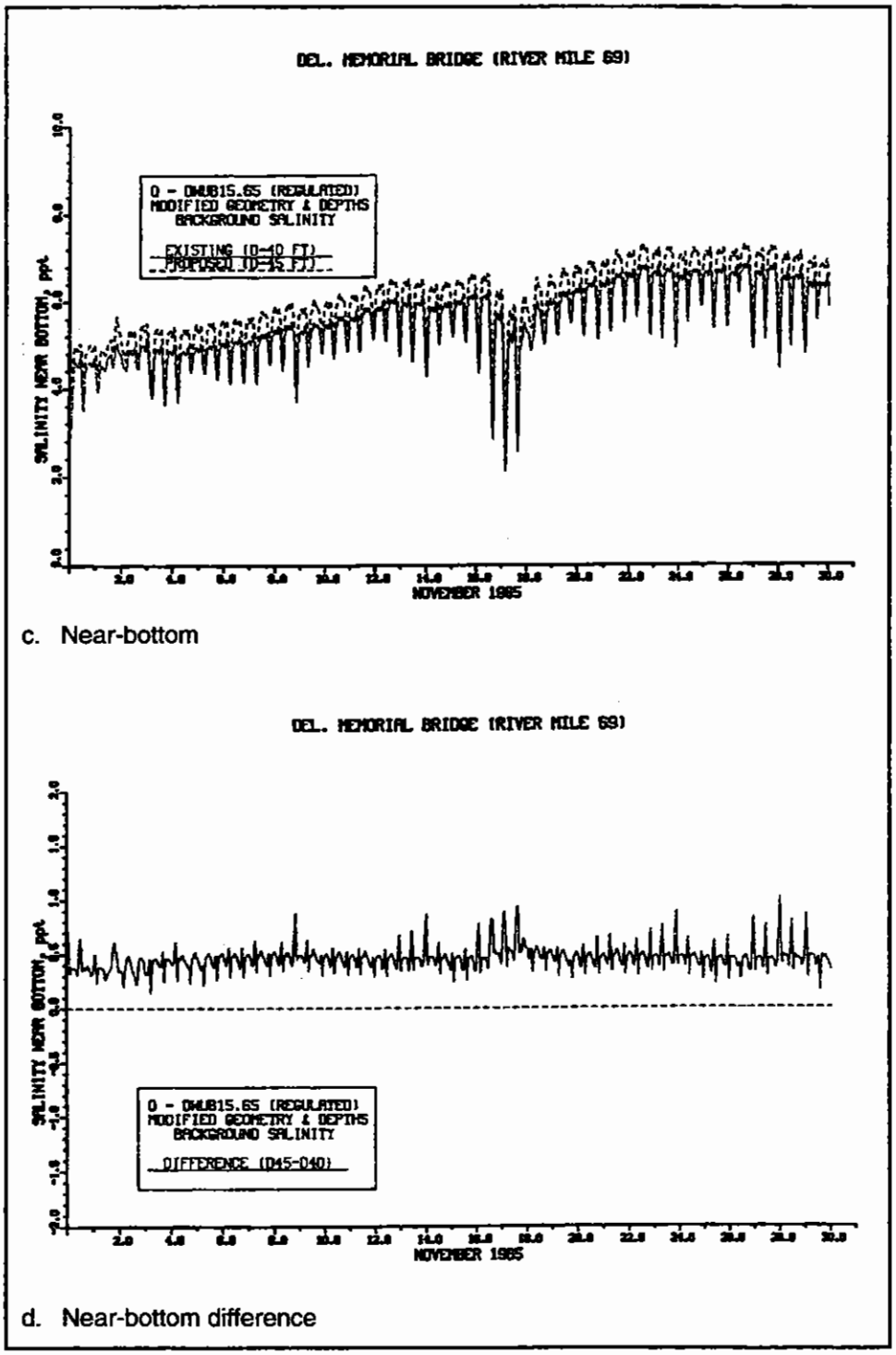

Figure 90. (Concluded)

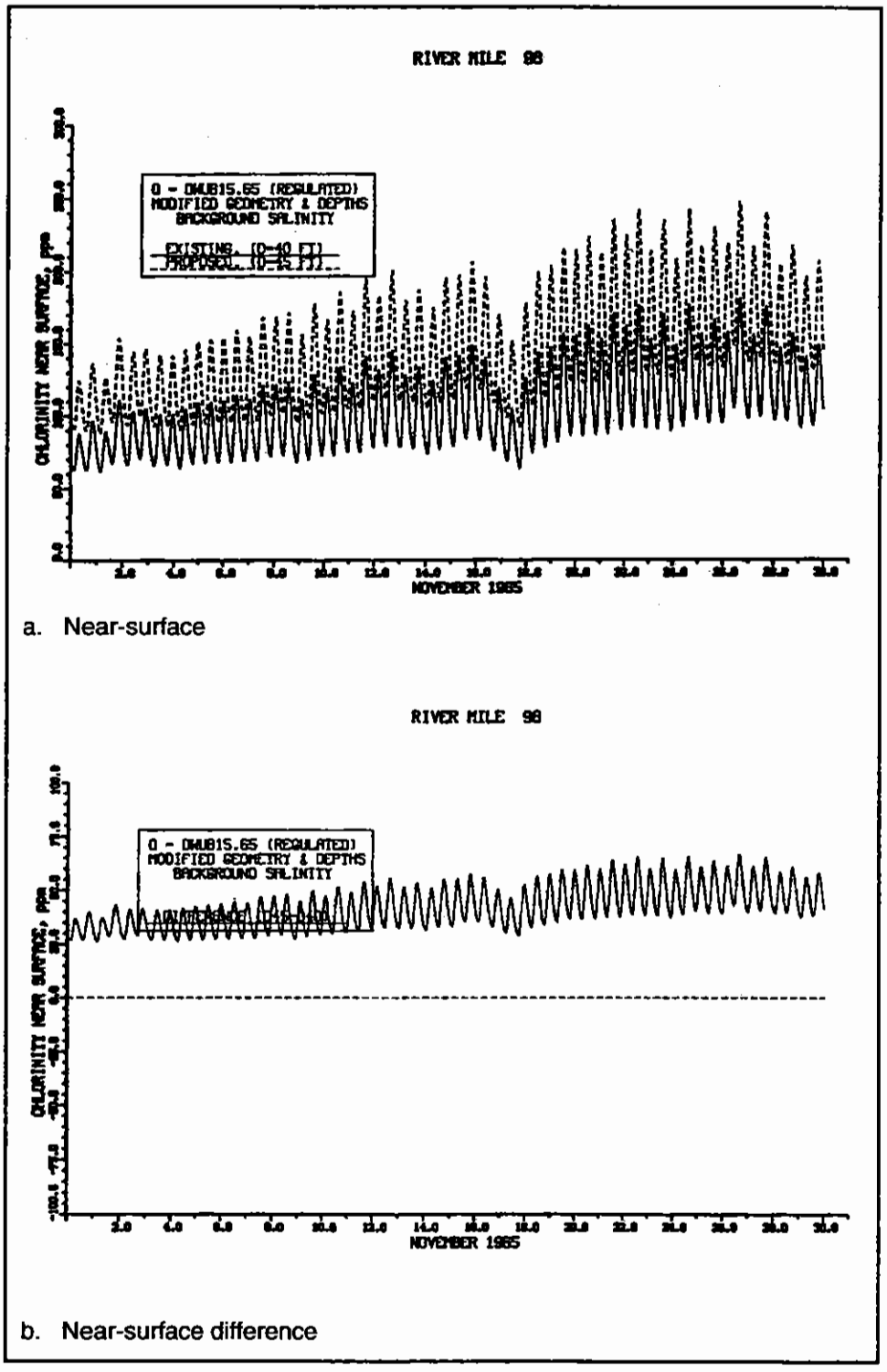

Figure 91. Impact of channel deepening on salinity at RM 98 for regulated inflow (continued)

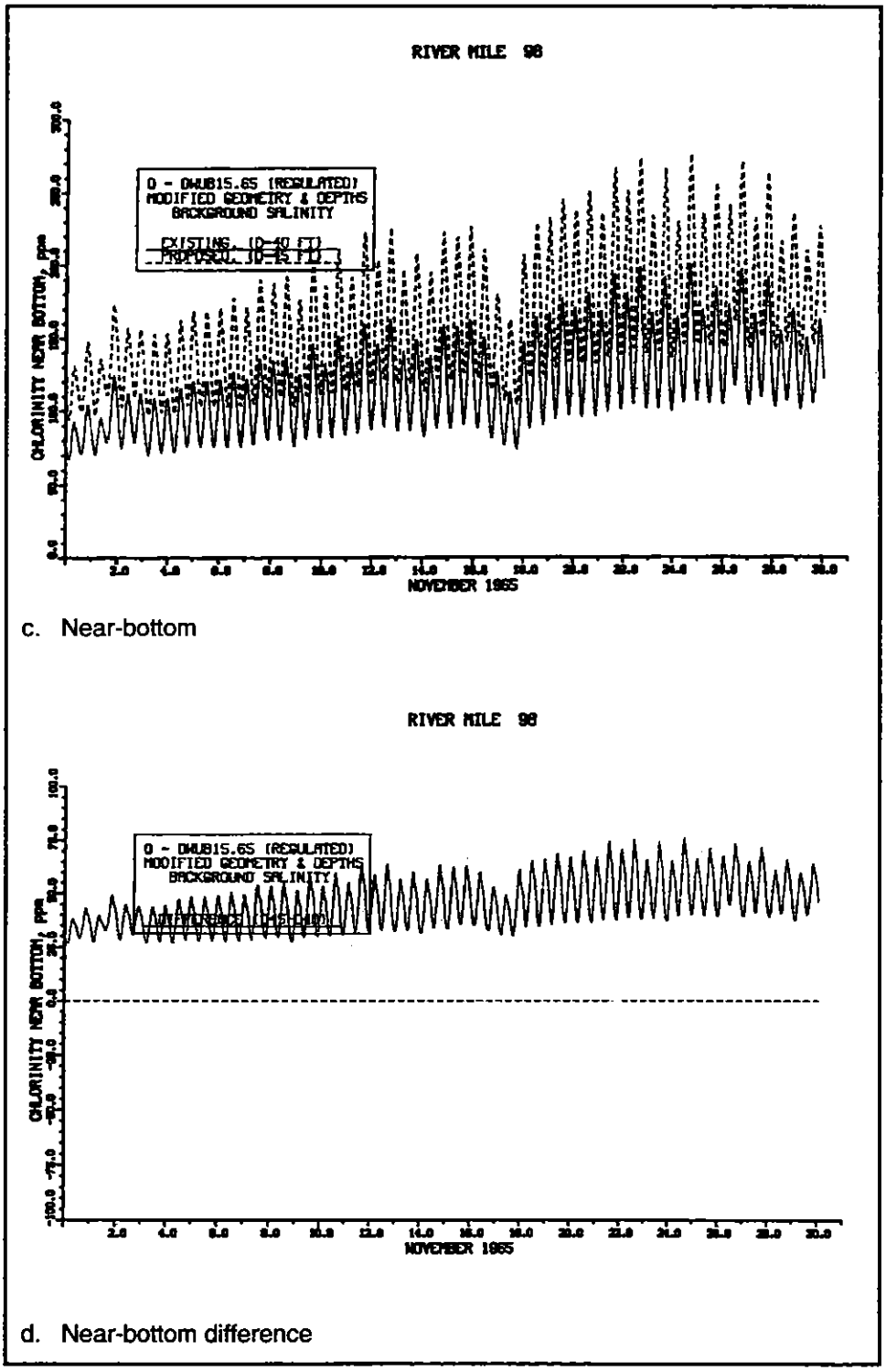

Figure 91. (Concluded)

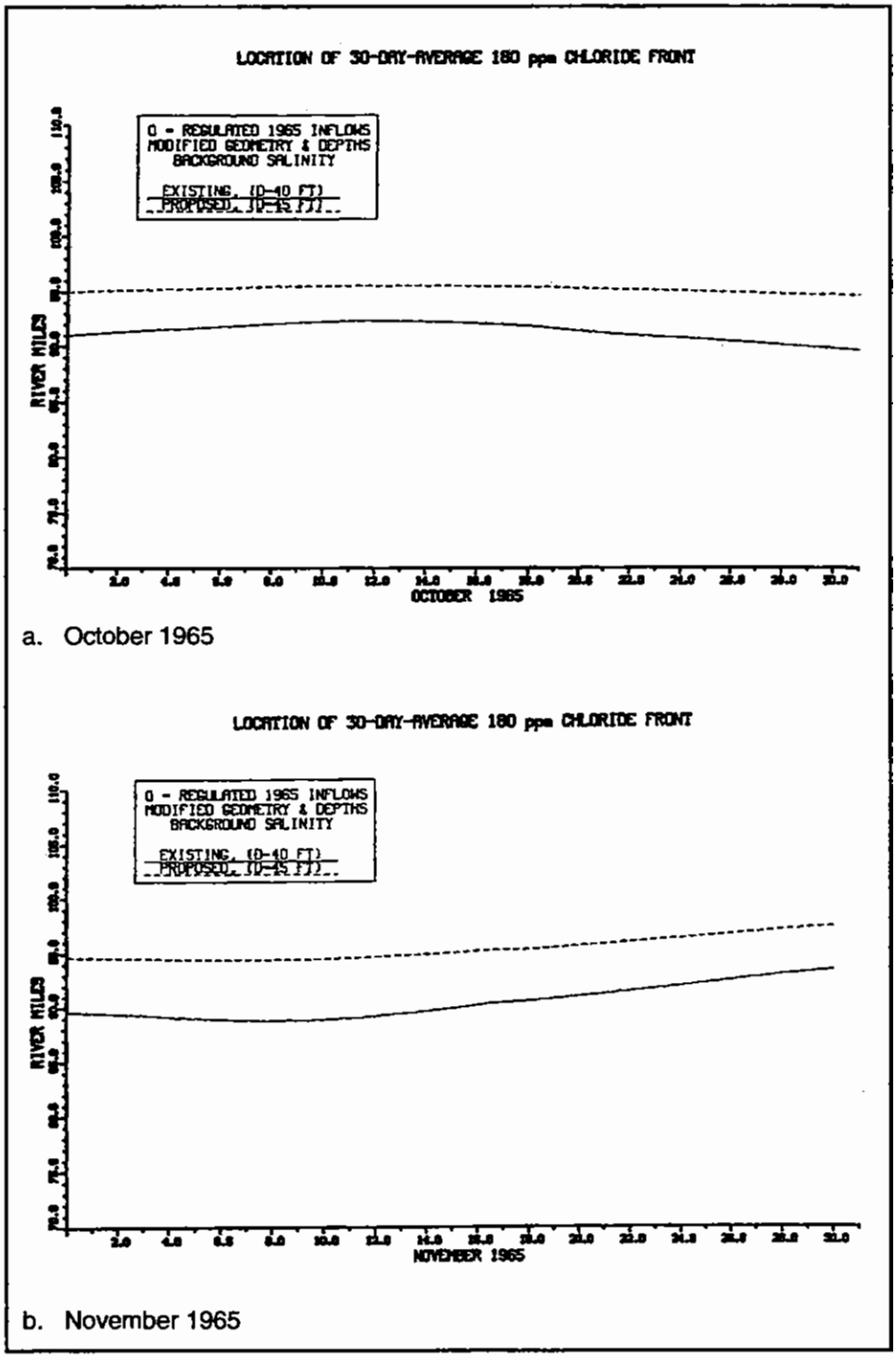

Figure 92. Location of 30-day average 180-ppm chloride for regulated inflow

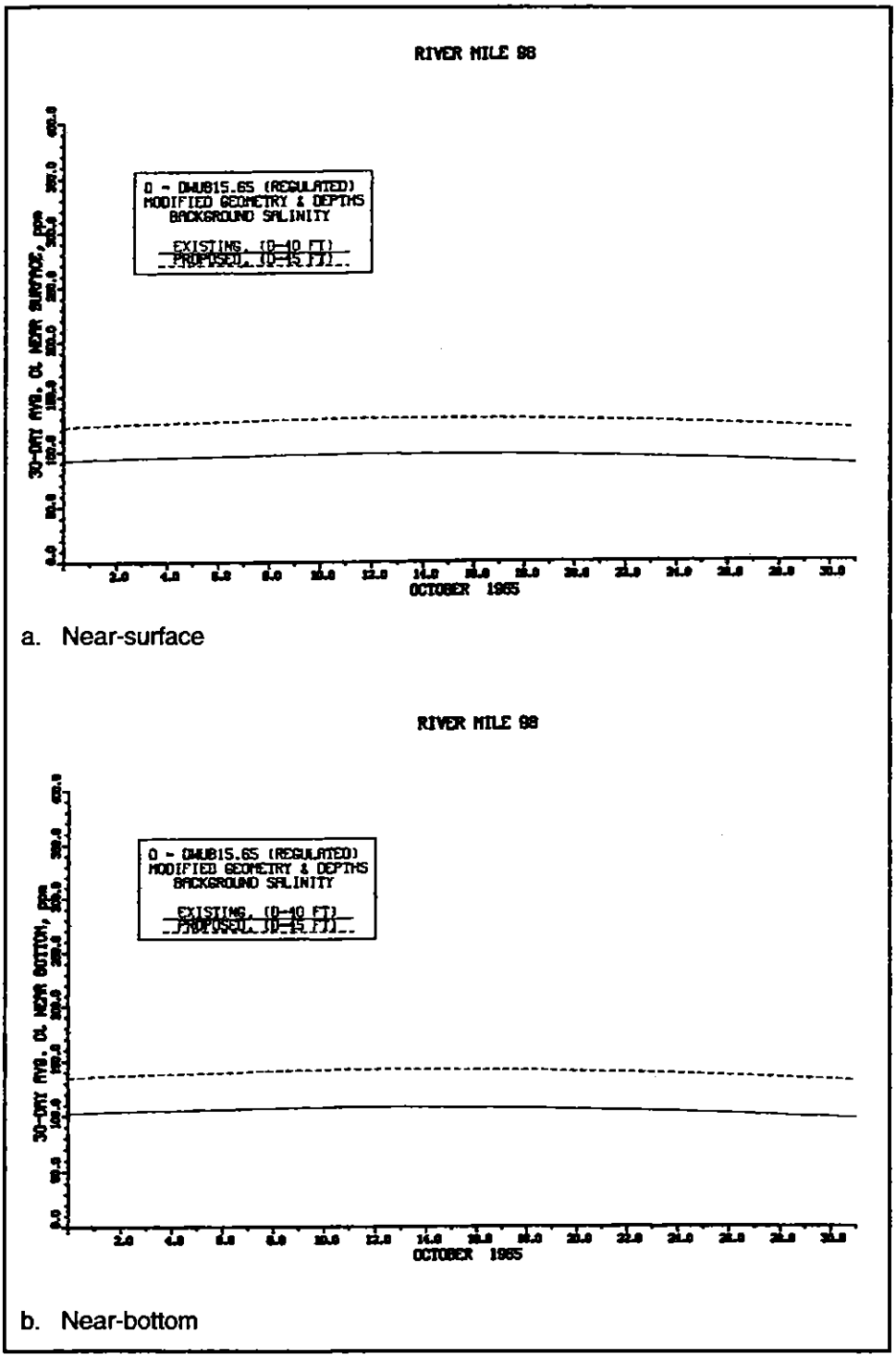

Figure 93. 30-day average chlorides at RM 98 for regulated inflow for October 1965

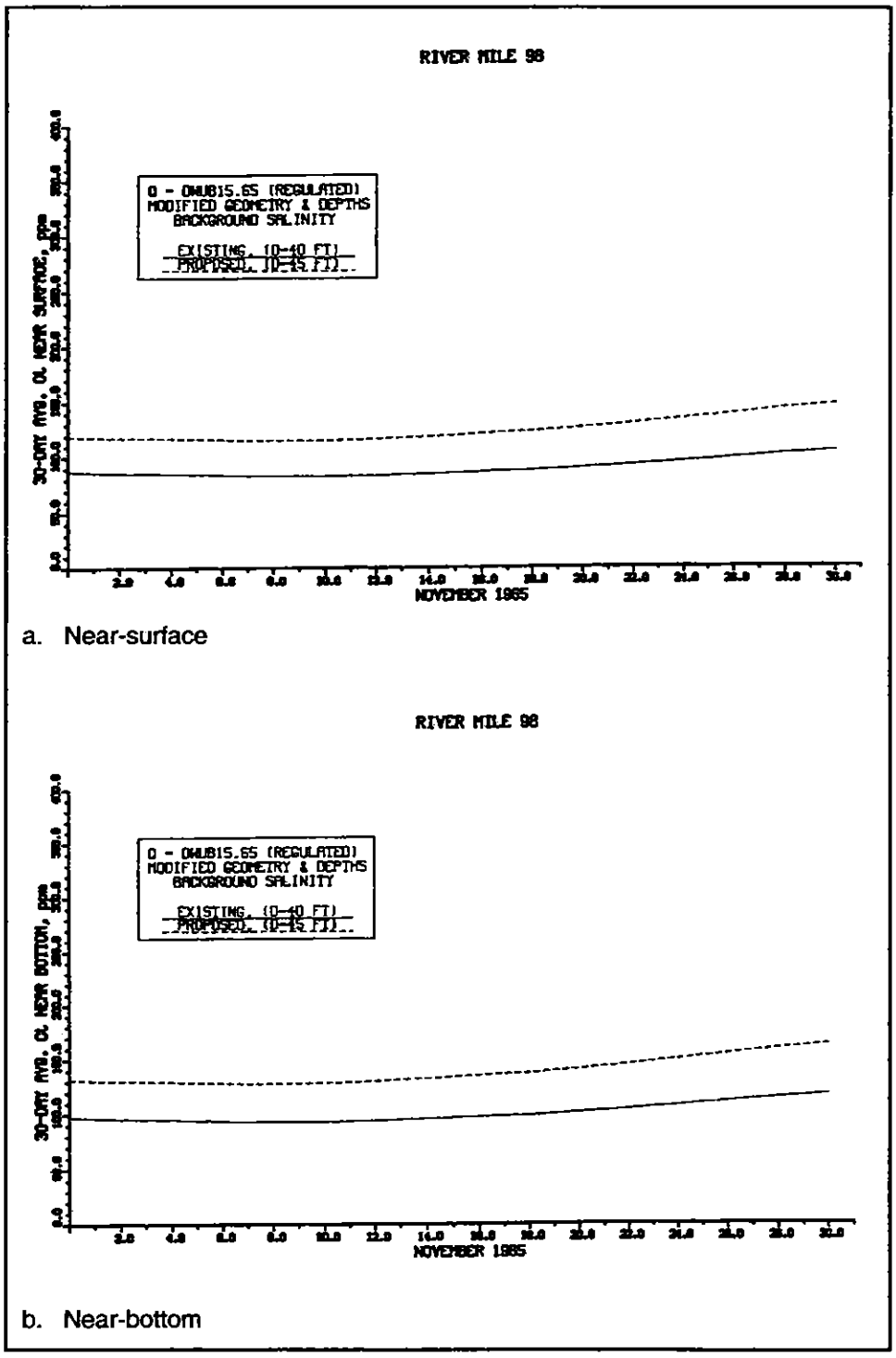

Figure 94. 30-day average chlorides at RM 98 for regulated inflow for November 1965

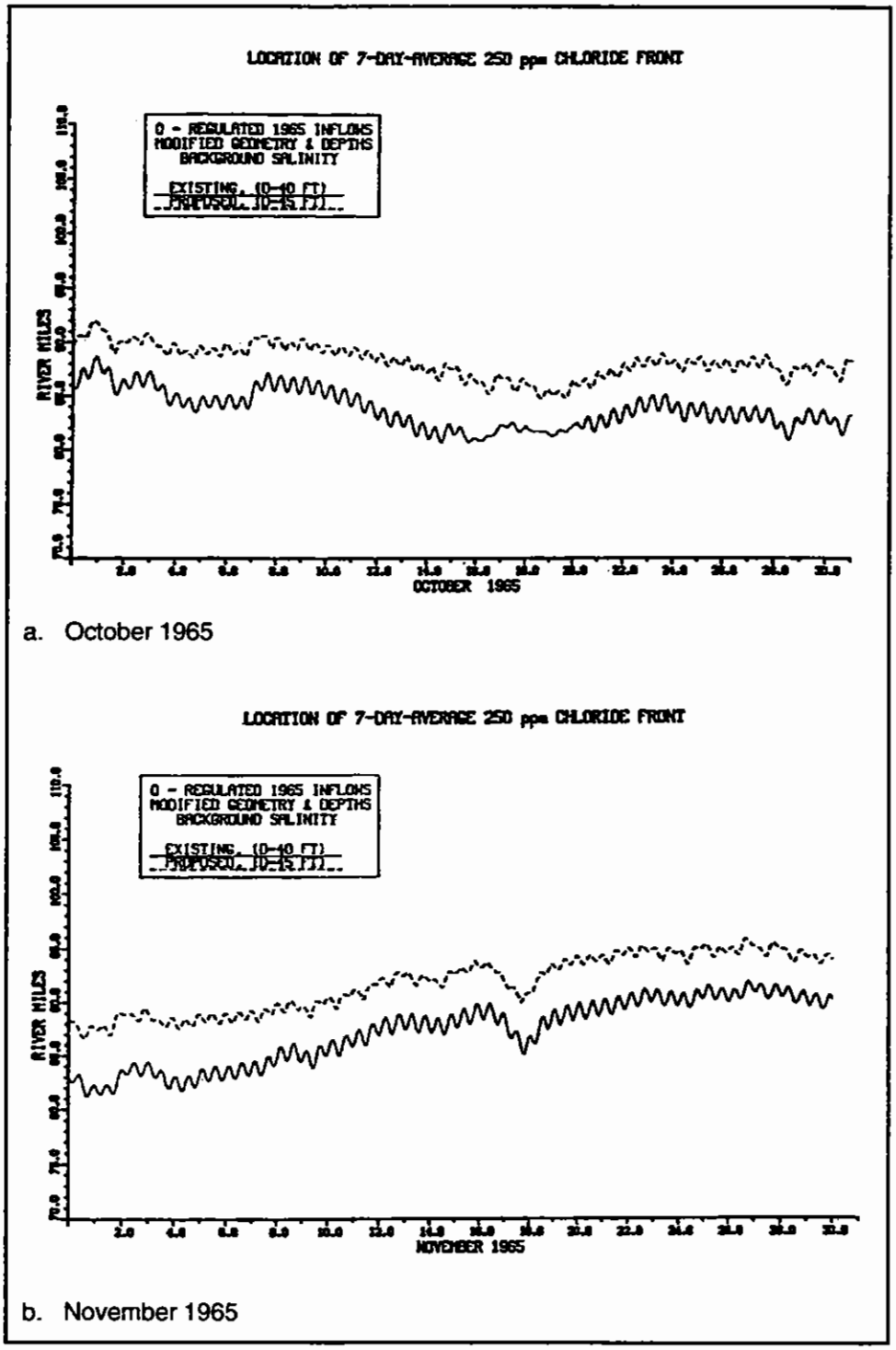

Figure 95. Location of 7-day average 250-ppm chloride for regulated inflow

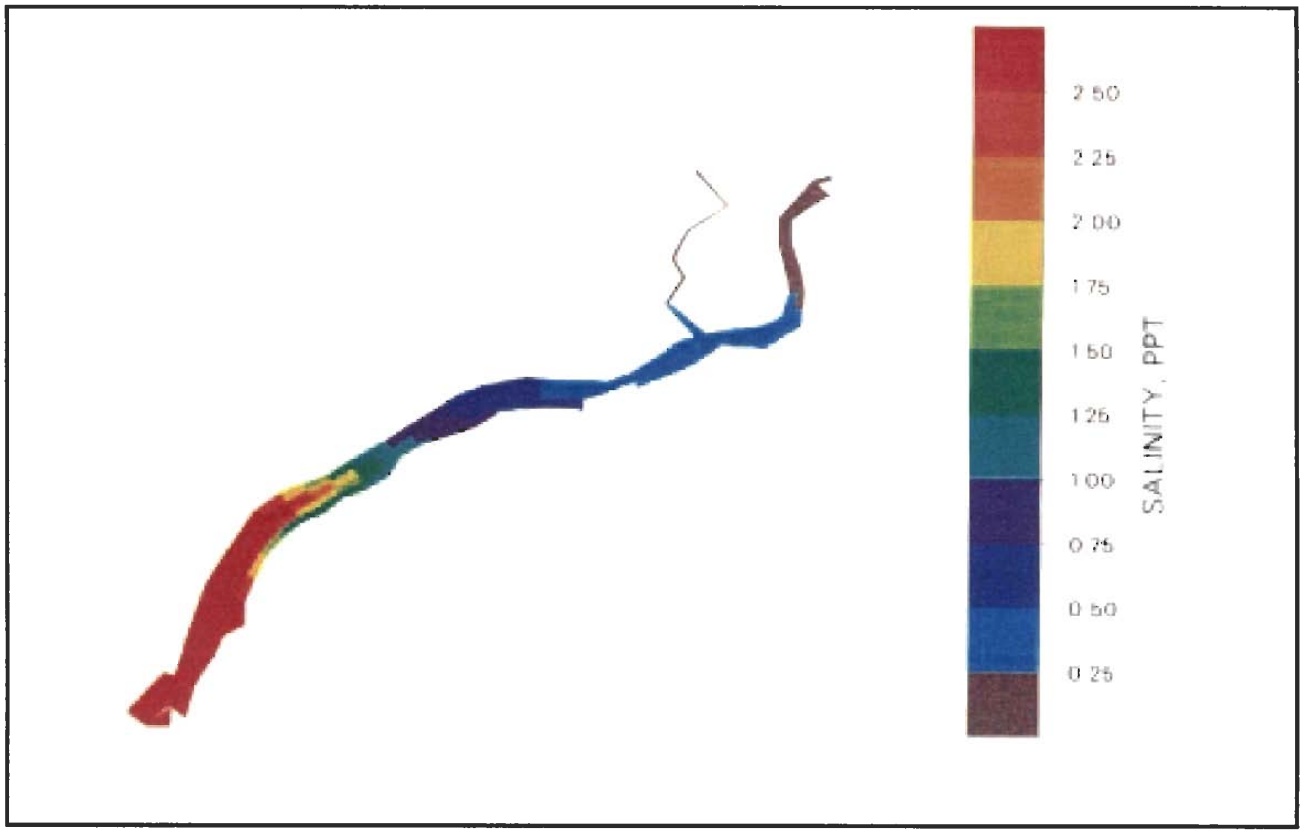

a. Near-surface for 40-ft (12.20-m) channel

Figure 96. Monthly averaged 0.25-ppt isohaline for November 1965 for regulated inflow (continued)

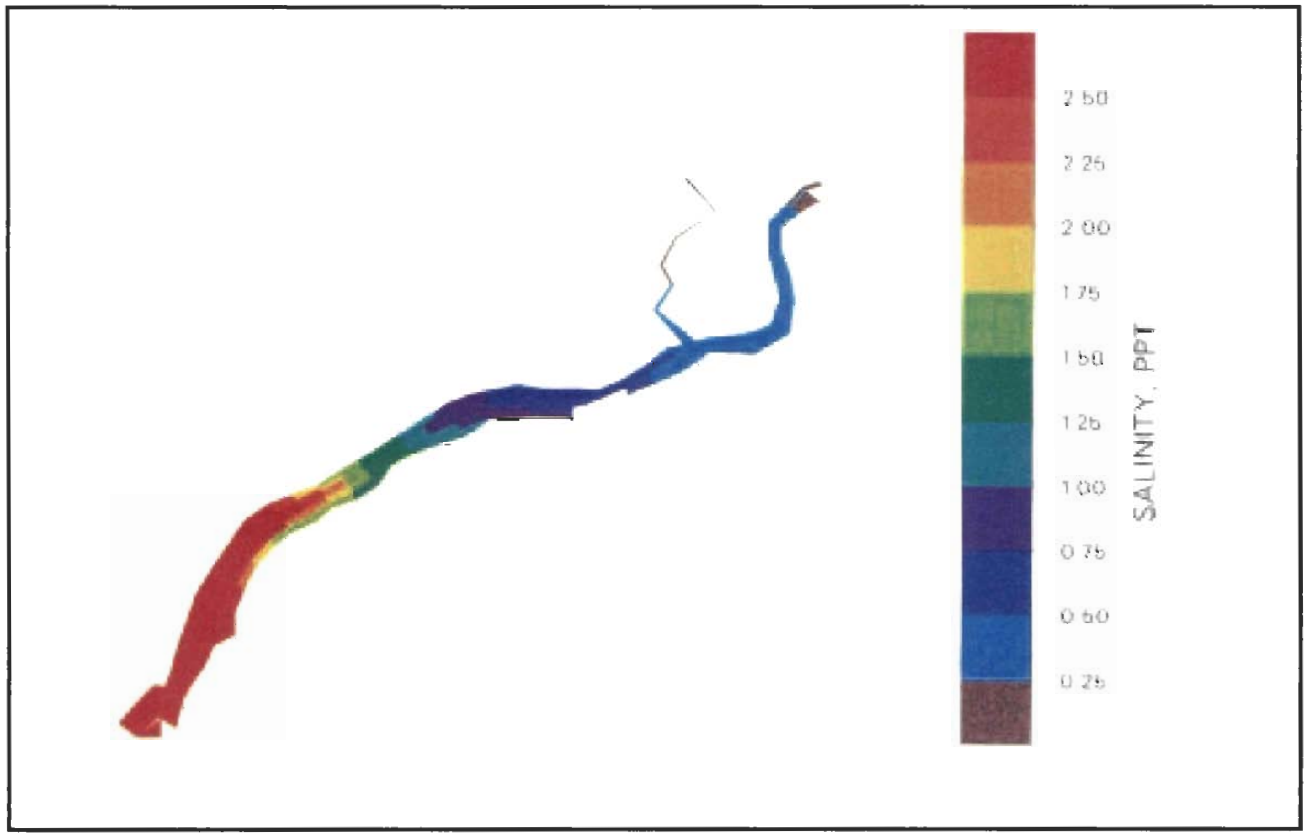

b. Near-surface for 45-ft (13.72-m) channel

Figure 96. (Concluded)

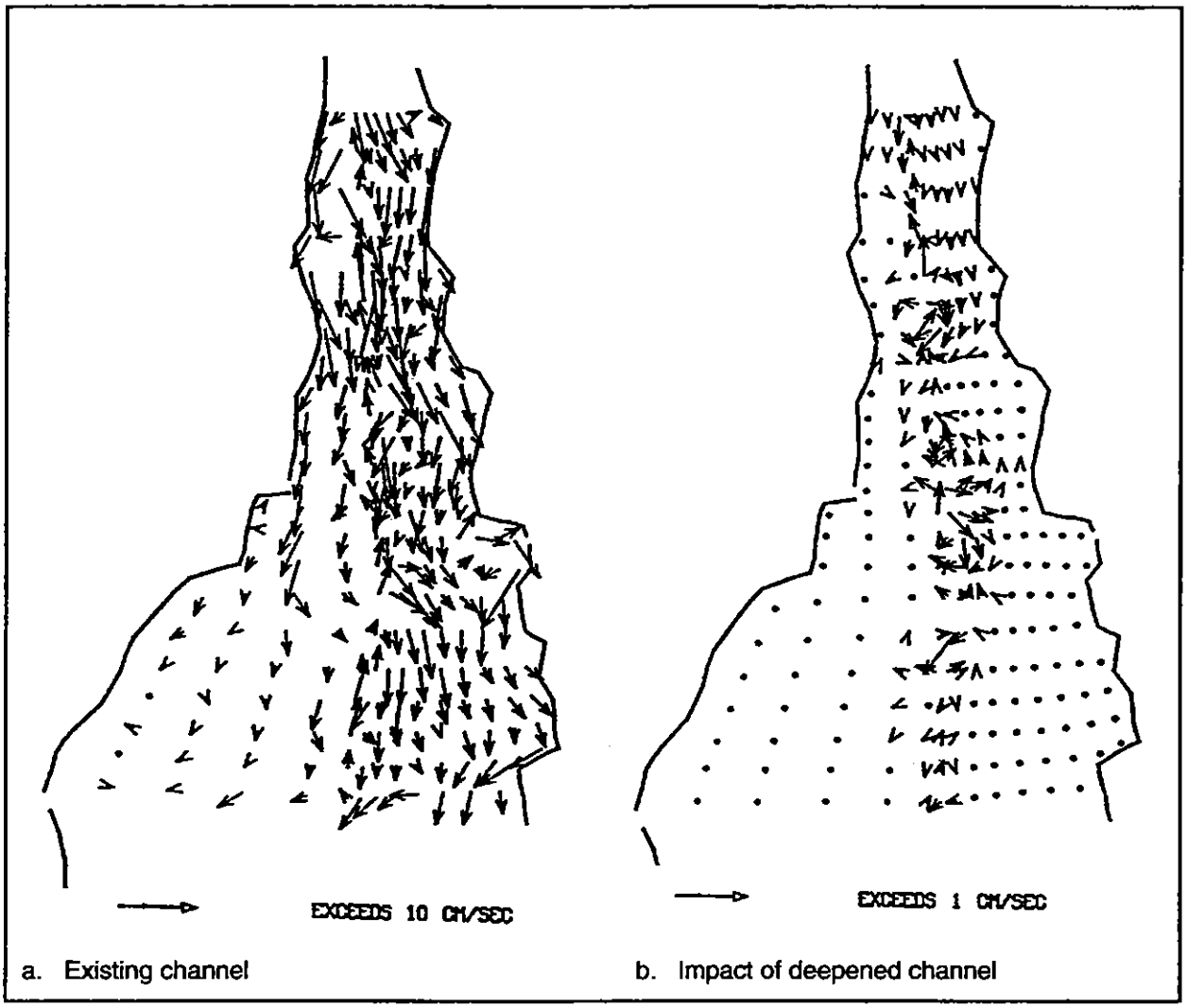

a. Existing channel

b. Impact of deepened channel

Figure 97. Residual near-surface currents for October 1965 for regulated inflow

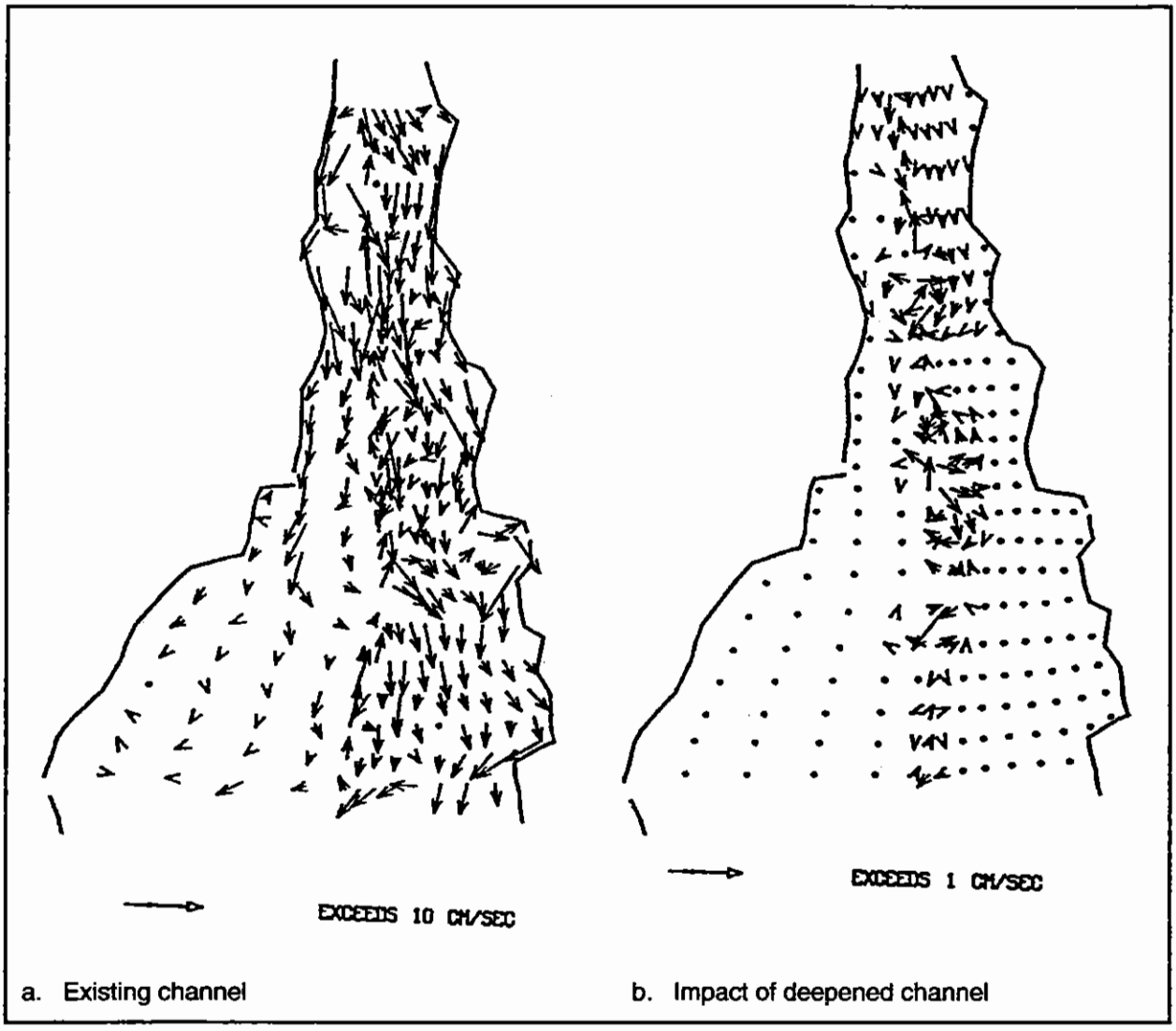

a. Existing channel

b. Impact of deepened channel

Figure 98. Residual near-surface currents for November 1965 for regulated inflow

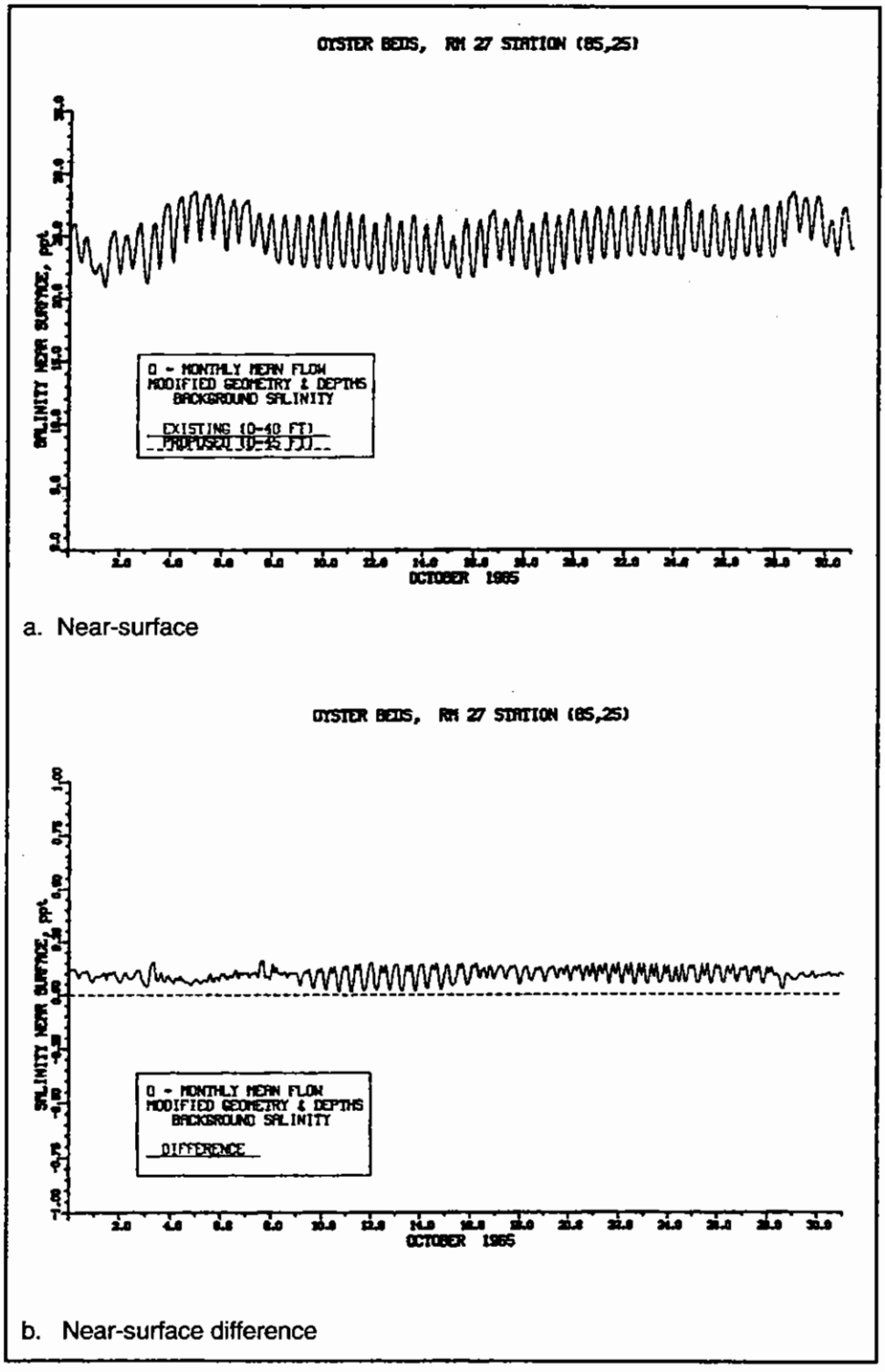

Figure 99. Impact of channel deepening on salinity at RM 27 Station (85,25) for monthly averaged inflow for October

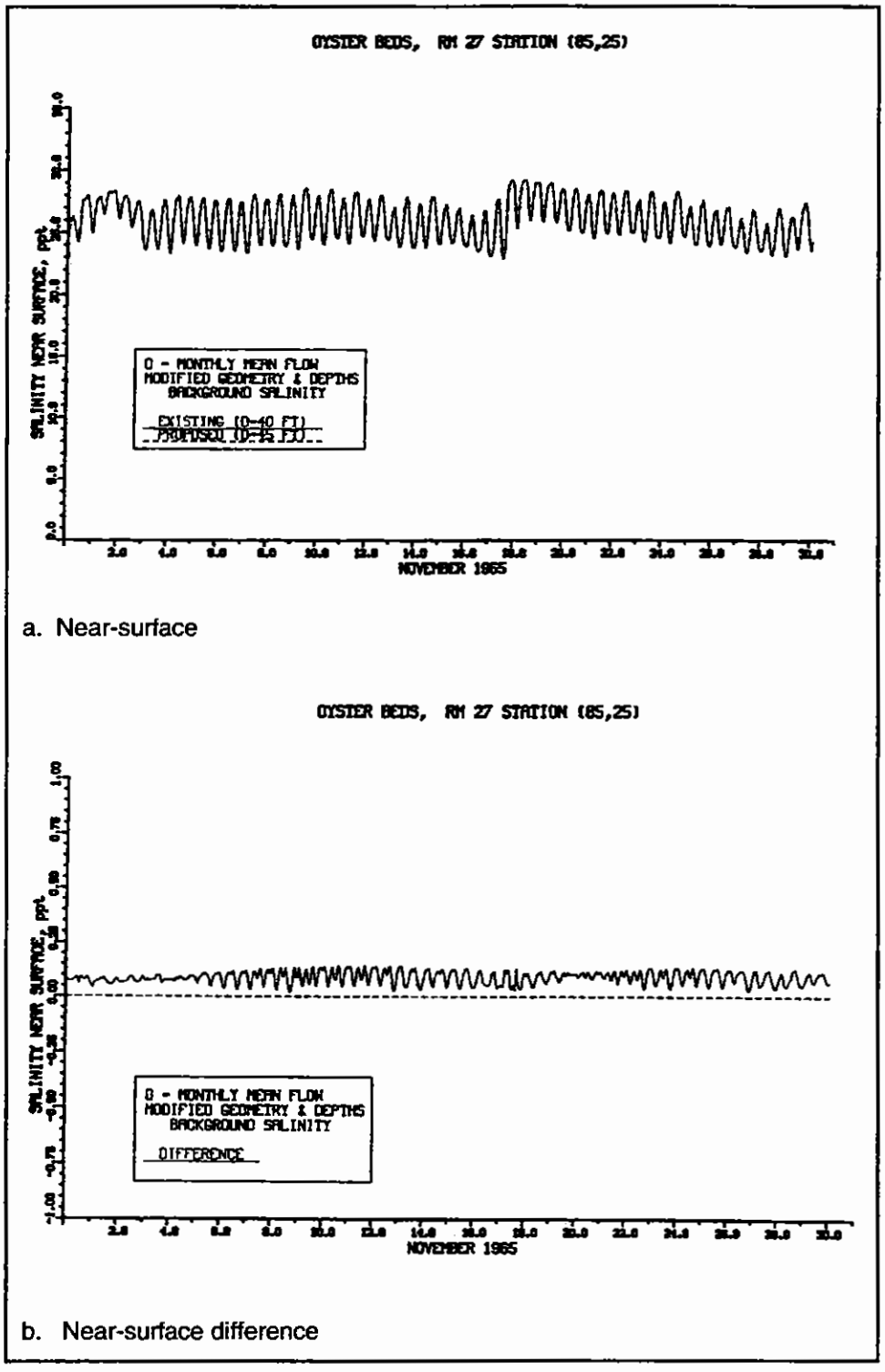

Figure 100. Impact of channel deepening on salinity at RM 27 Station (85,25) for monthly averaged inflow for November

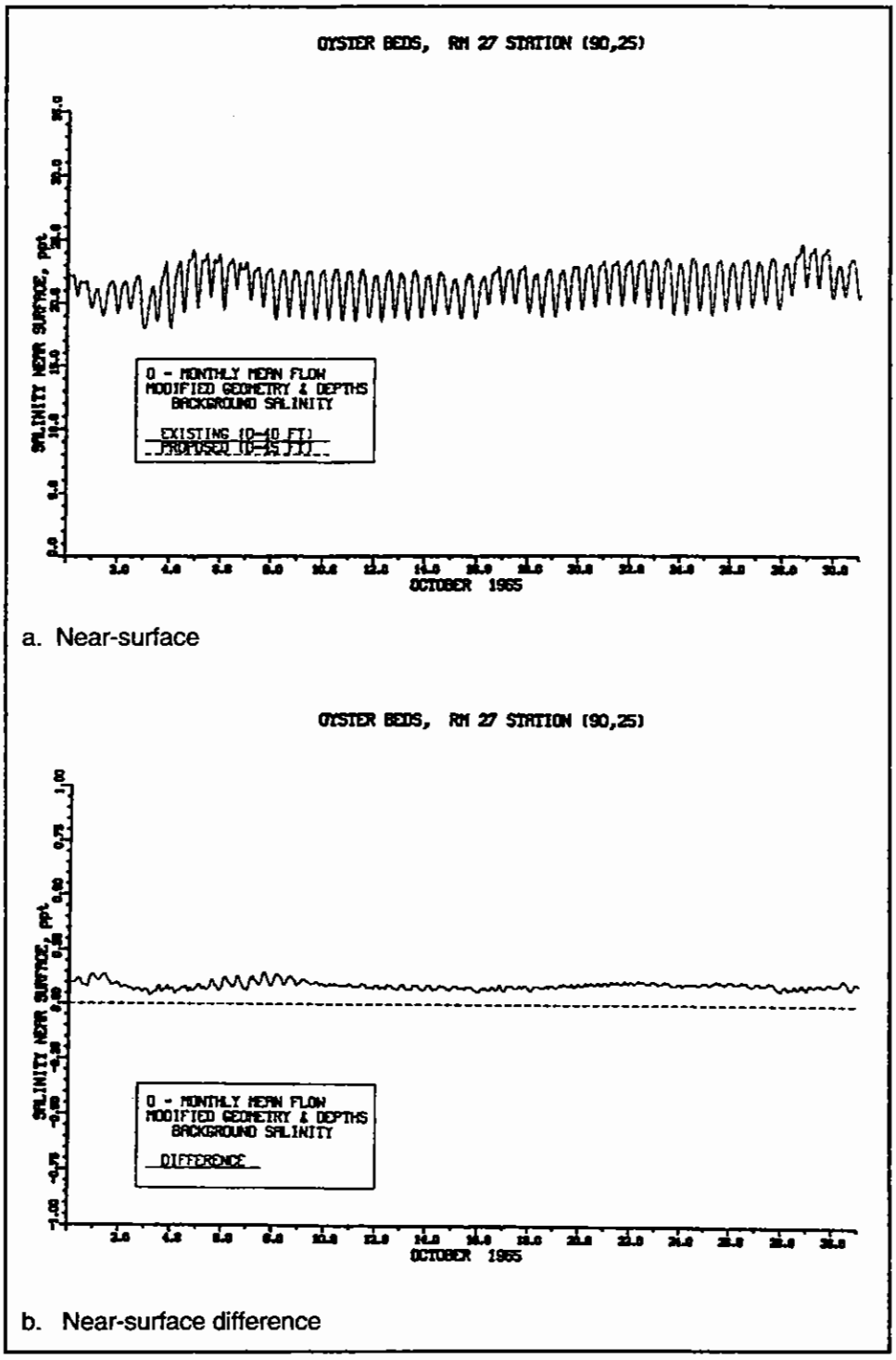

Figure 101. Impact of channel deepening on salinity at RM 27 Station (90,25) for monthly averaged inflow for October

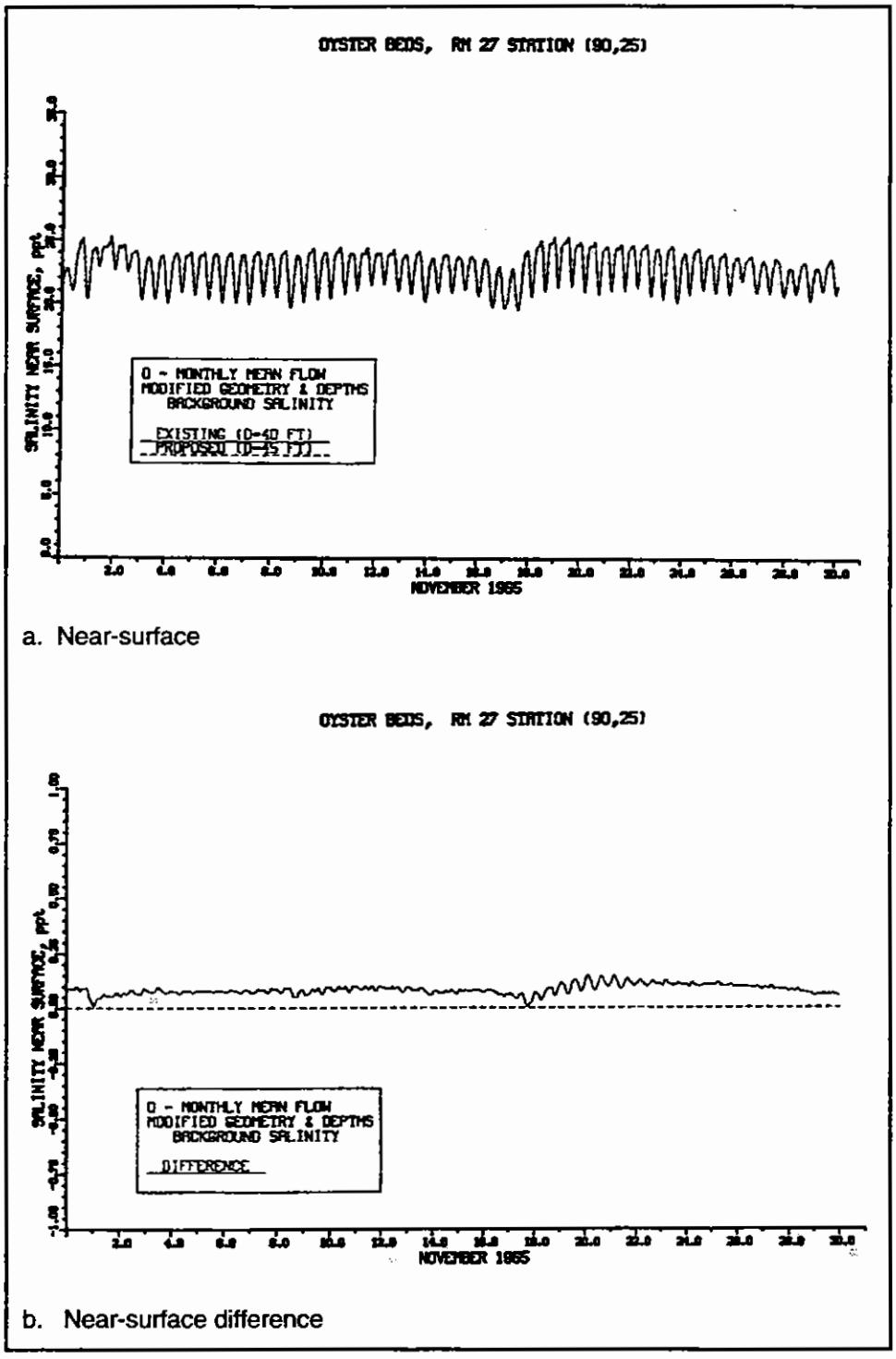

Figure 102. Impact of channel deepening on salinity at RM 27 Station (90,25) for monthly averaged inflow for November

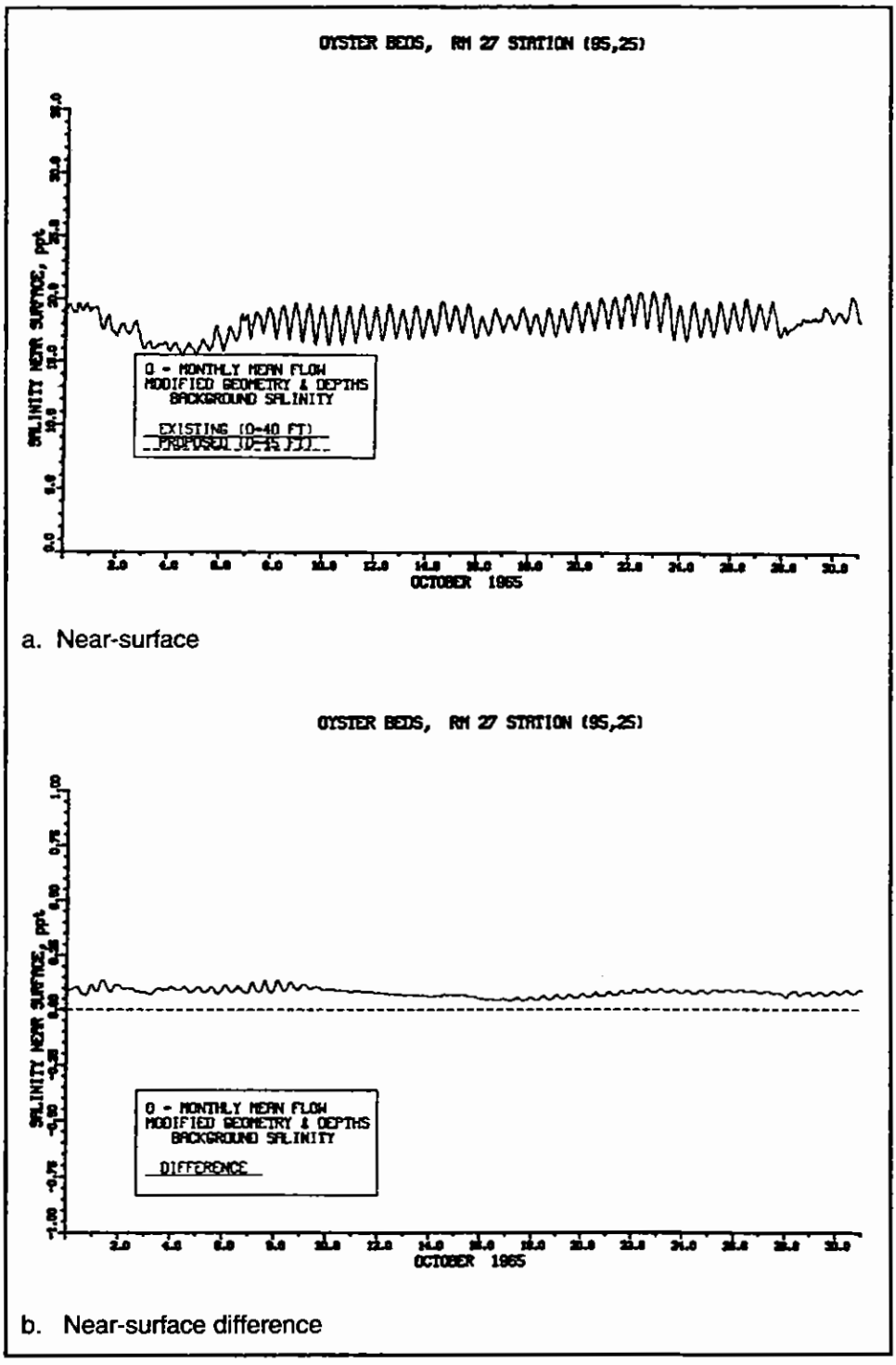

Figure 103. Impact of channel deepening on salinity at RM 27 Station (95,25) for monthly averaged inflow for October

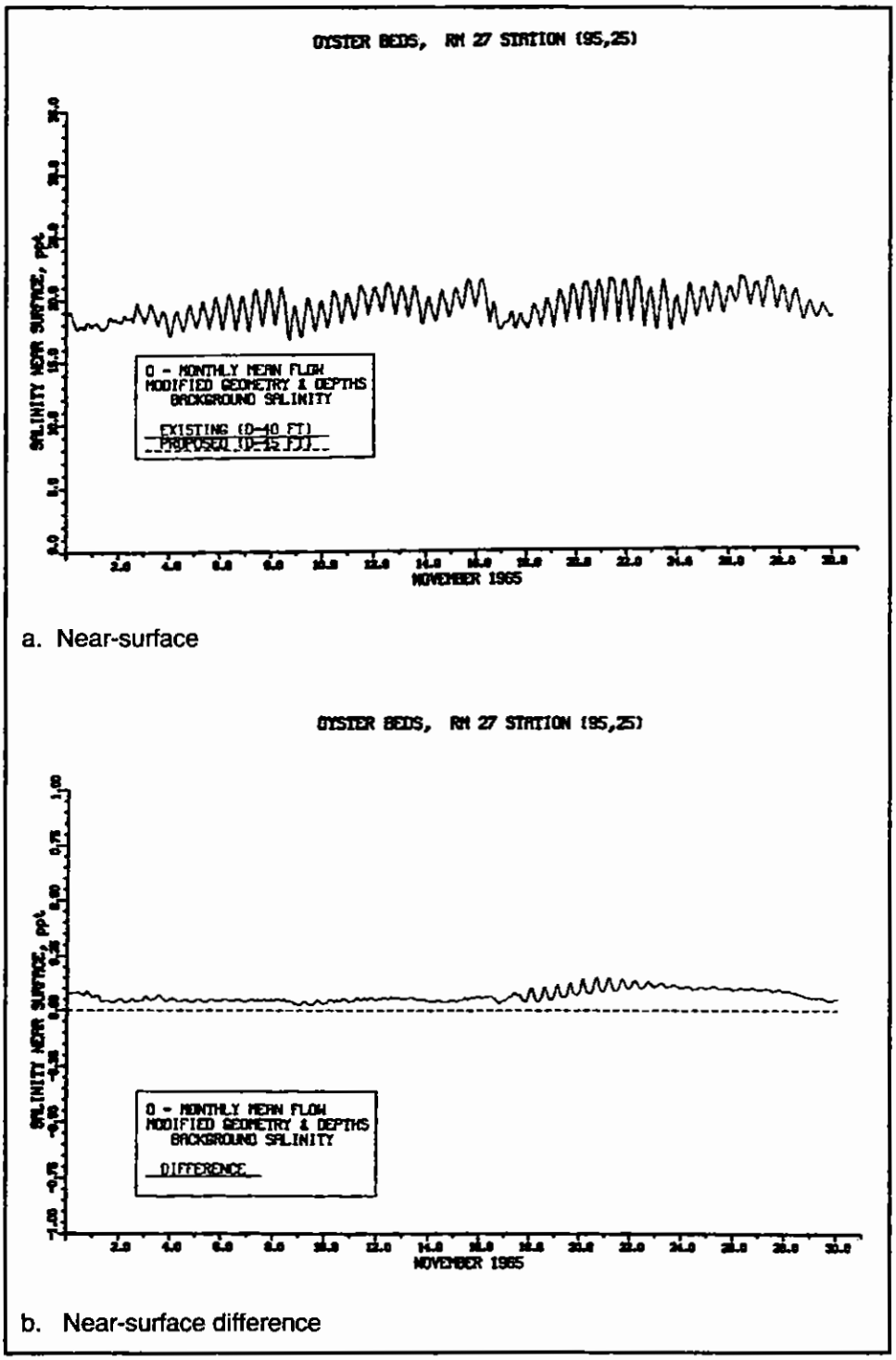

Figure 104. Impact of channel deepening on salinity at RM 27 Station (95,25) for monthly averaged inflow for November

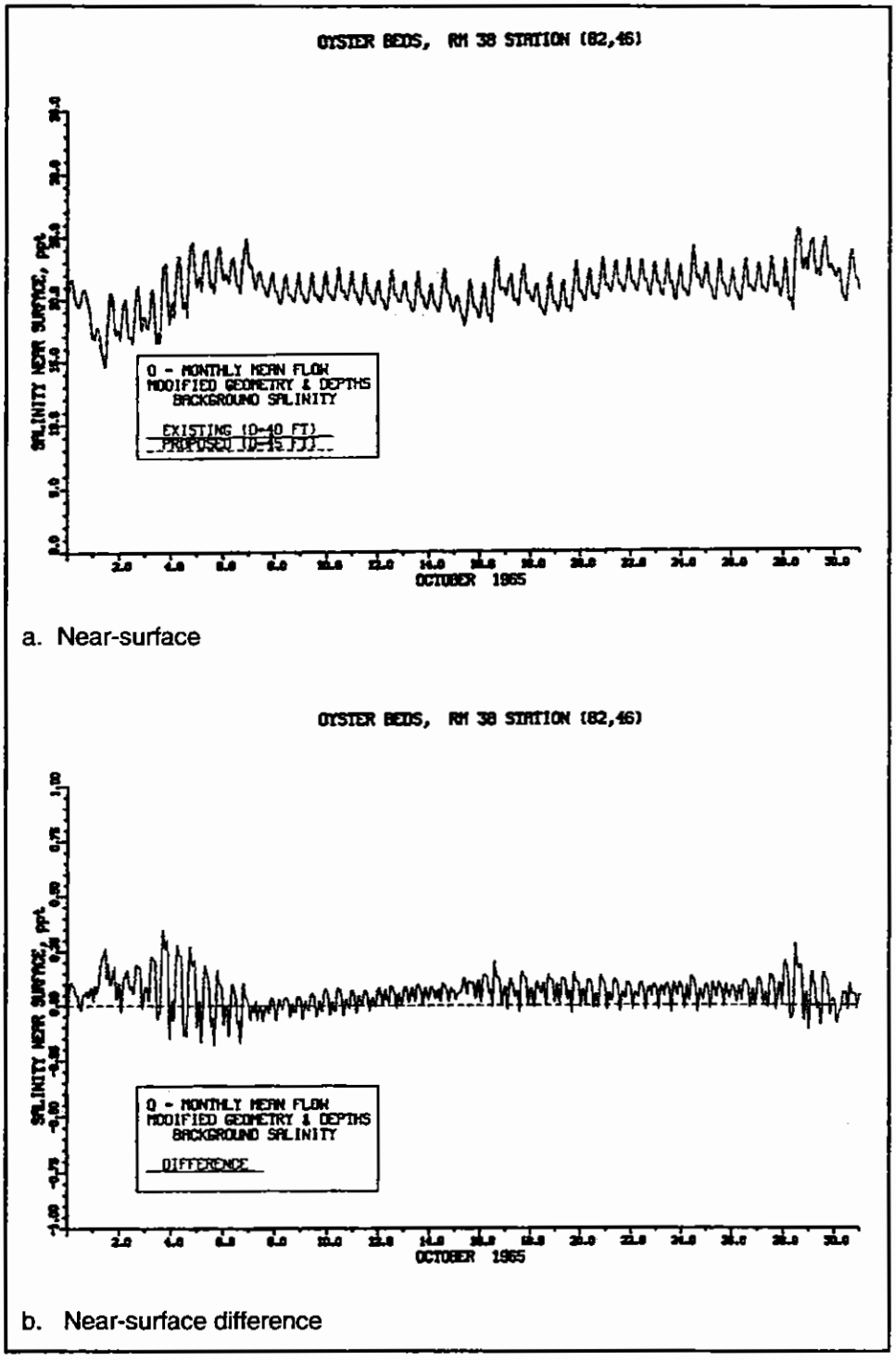

Figure 105. Impact of channel deepening on salinity at RM 38 Station (82,46) for monthly averaged inflow for October

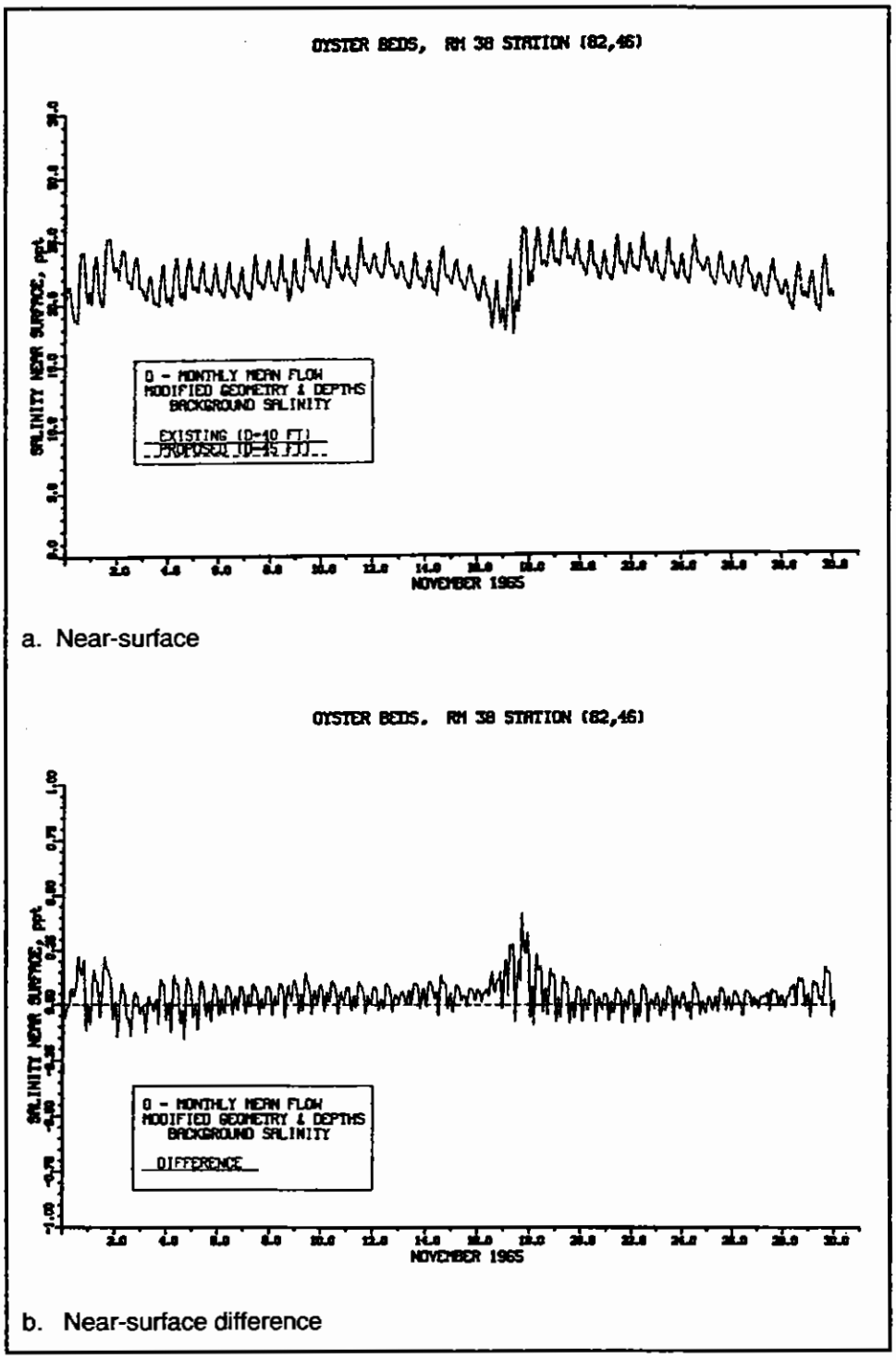

Figure 106. Impact of channel deepening on salinity at RM 38 Station (82,46) for monthly averaged inflow for November

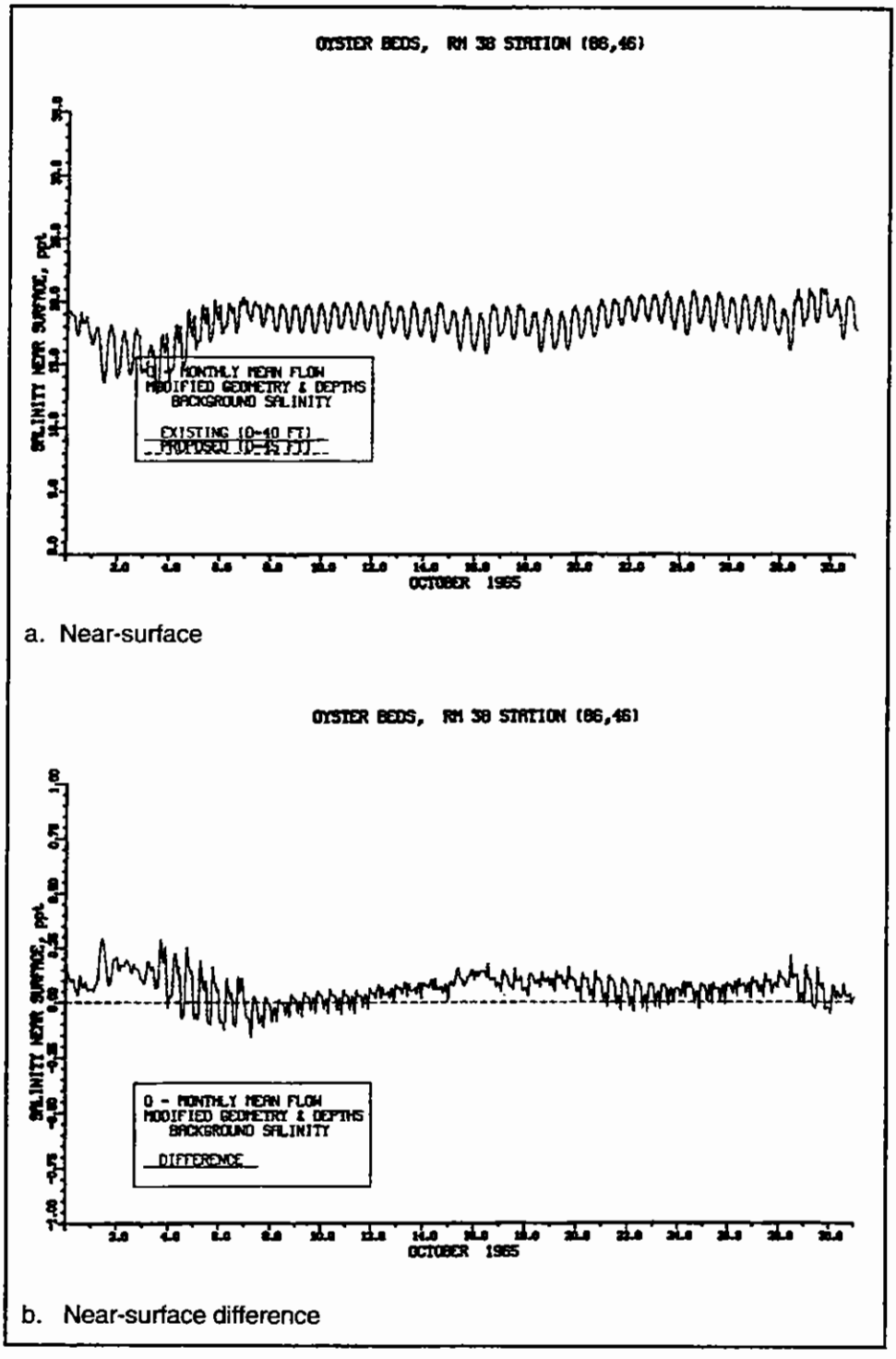

Figure 107. Impact of channel deepening on salinity at RM 38 Station (86,46) for monthly averaged inflow for October

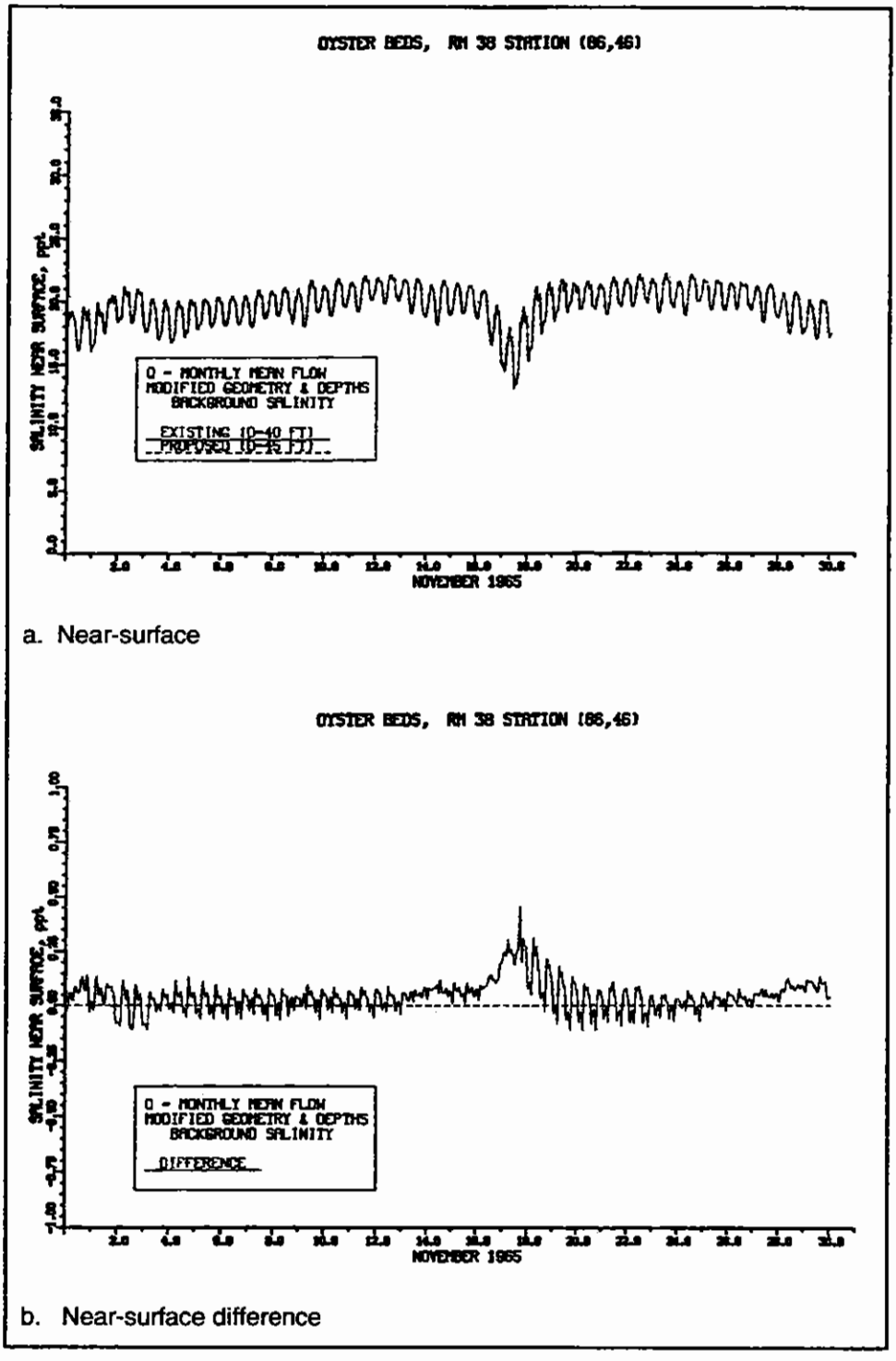

Figure 108. Impact of channel deepening on salinity at RM 38 Station (86,46) for monthly averaged inflow for November

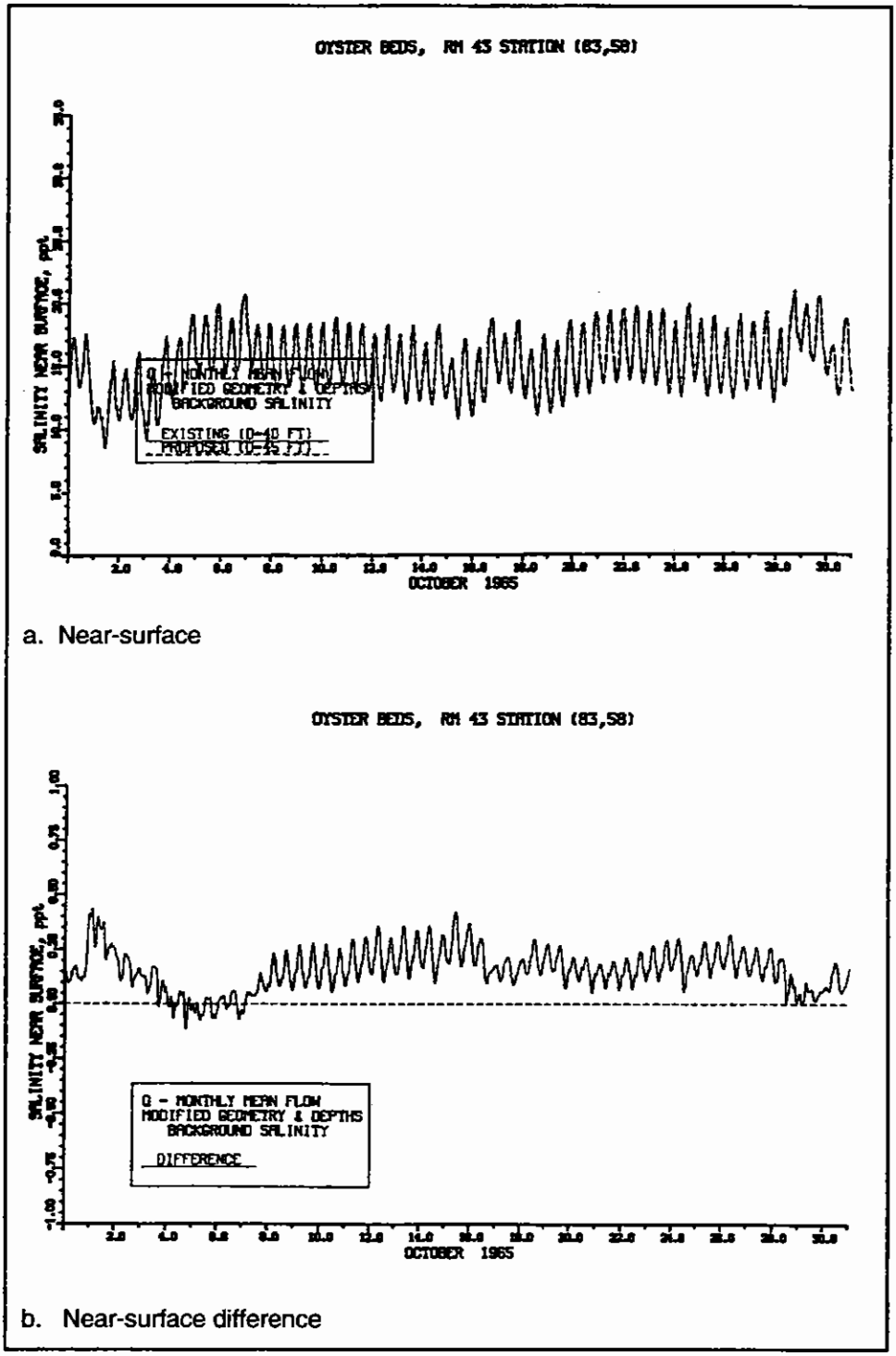

Figure 109. Impact of channel deepening on salinity at RM 43 Station (83,58) for monthly averaged inflow for October

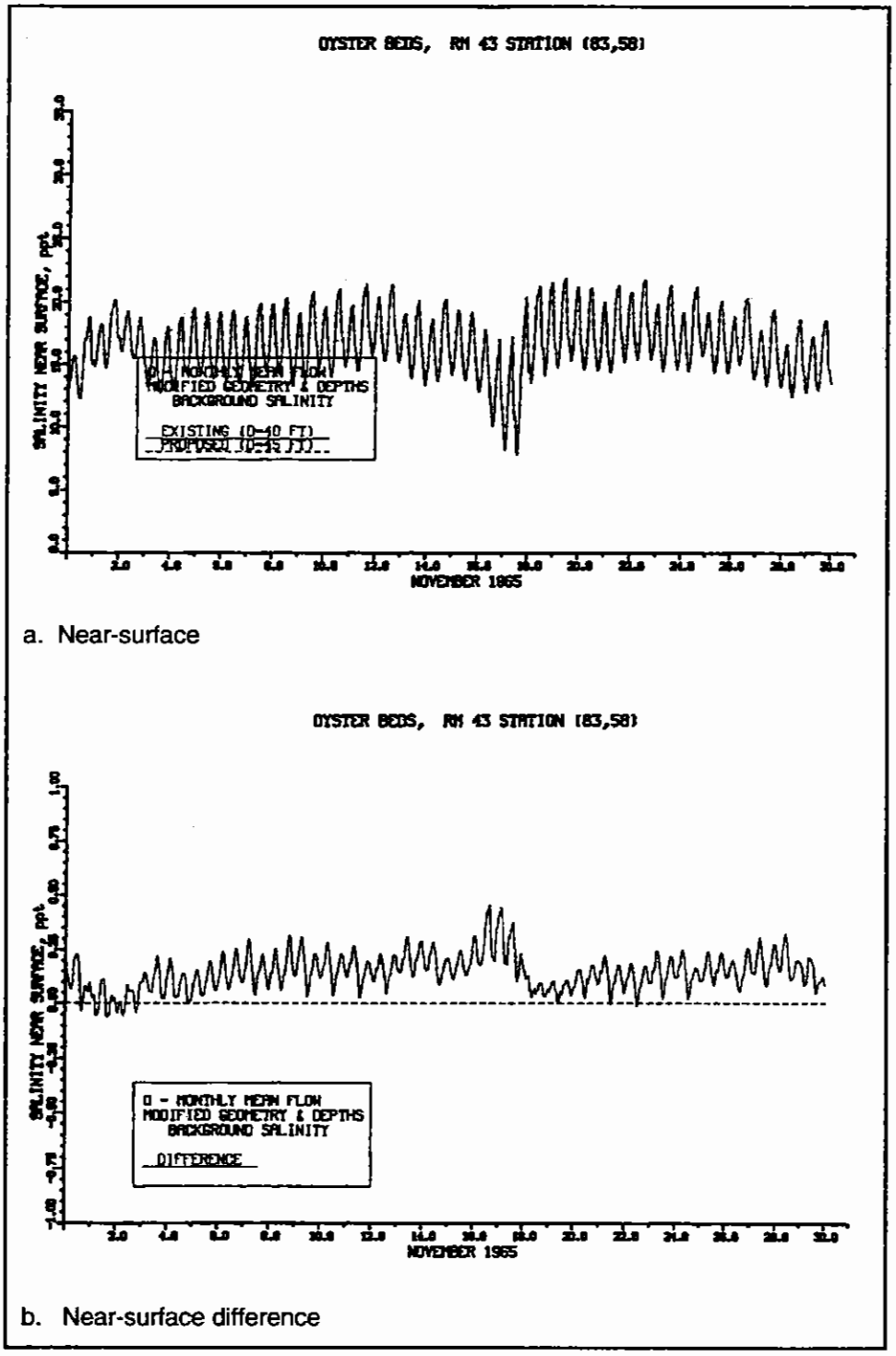

Figure 110. Impact of channel deepening on salinity at RM 43 Station (83,58) for monthly averaged inflow for November

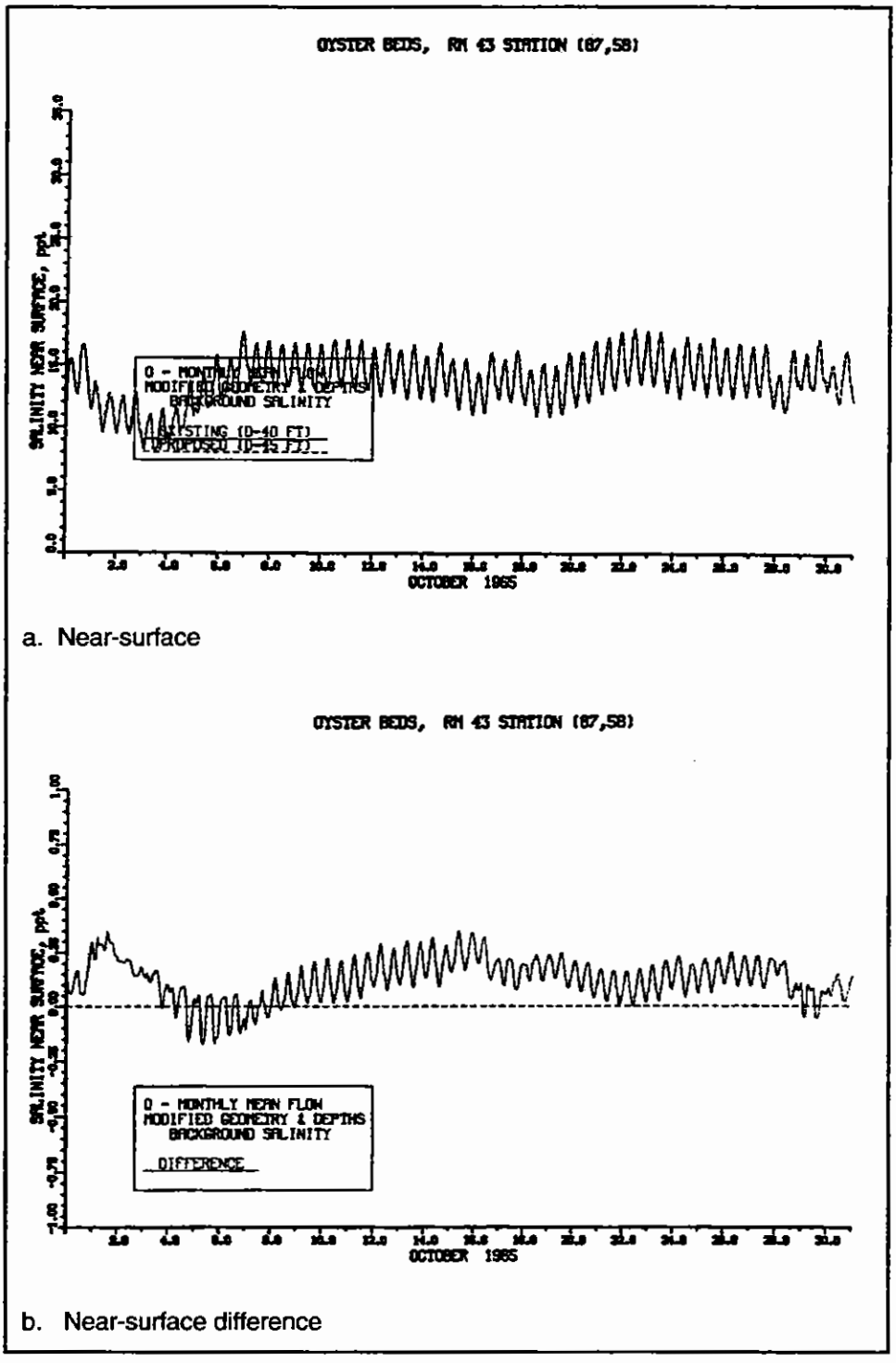

a. Near-surface

b. Near-surface difference

Figure 111. Impact of channel deepening on salinity at RM 43 Station (87,58) for monthly averaged inflow for October

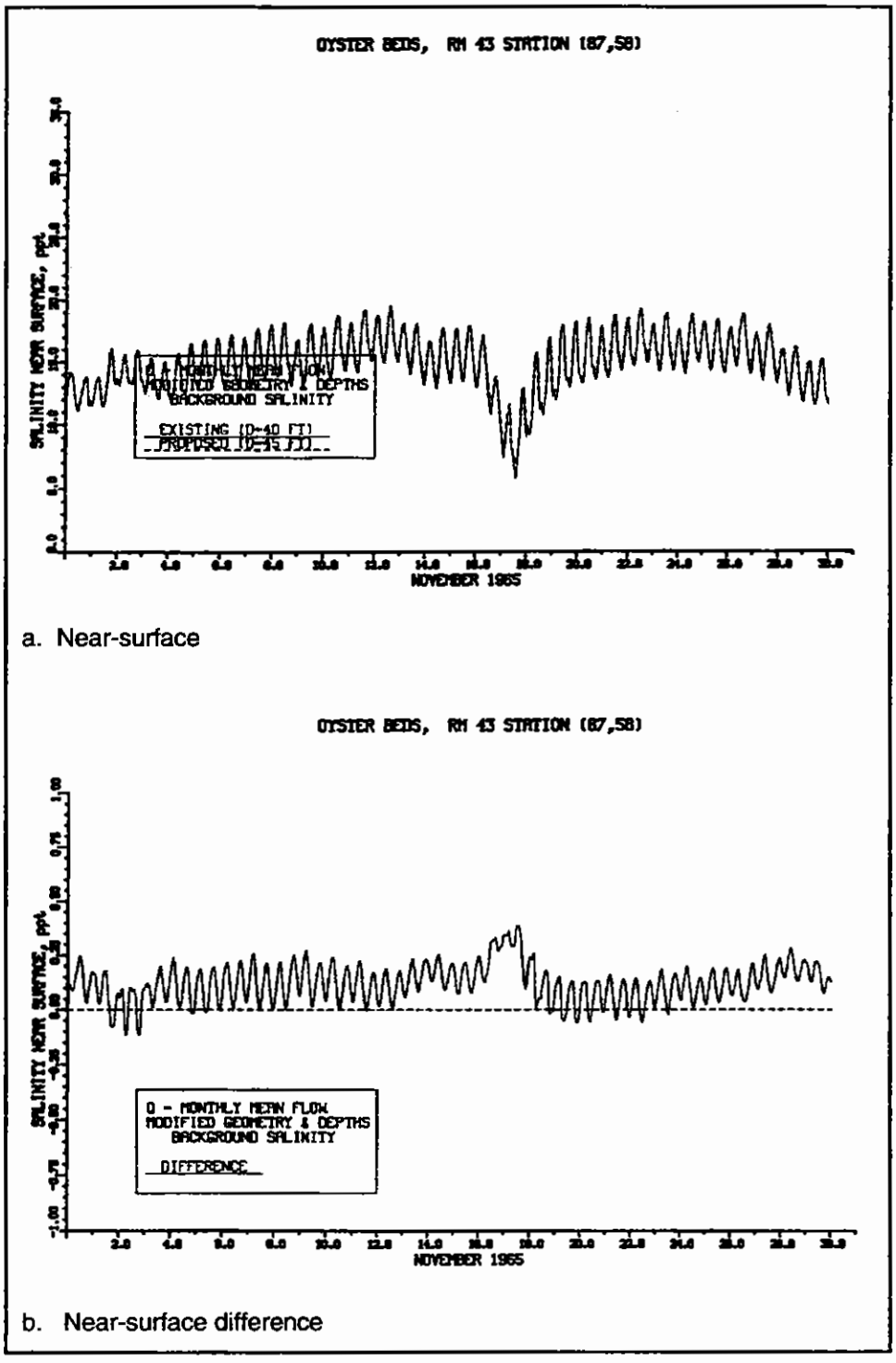

Figure 112. Impact of channel deepening on salinity at RM 43 Station (87,58) for monthly averaged inflow for November

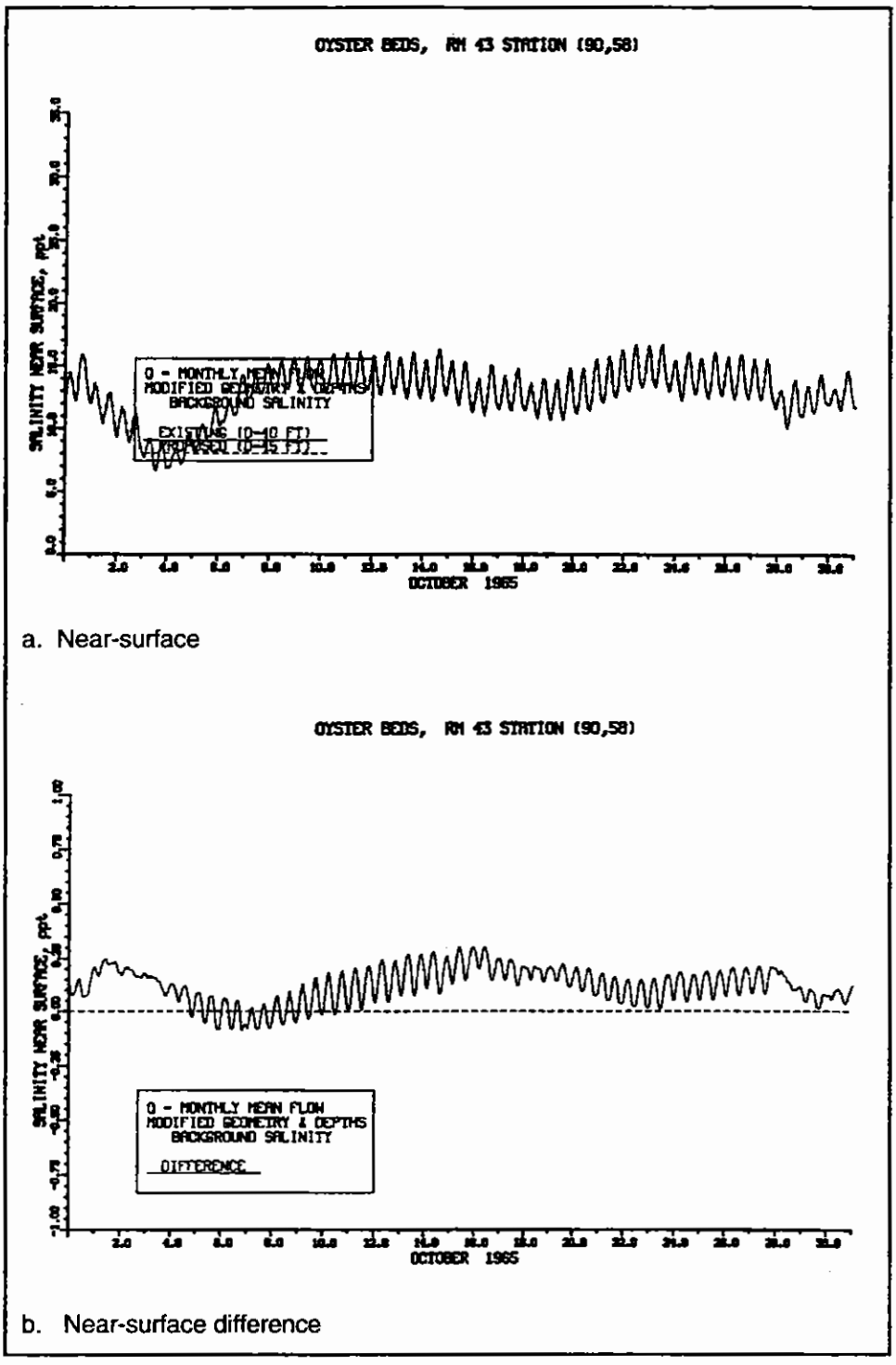

Figure 113. Impact of channel deepening on salinity at RM 43 Station (90,58) for monthly averaged inflow for October

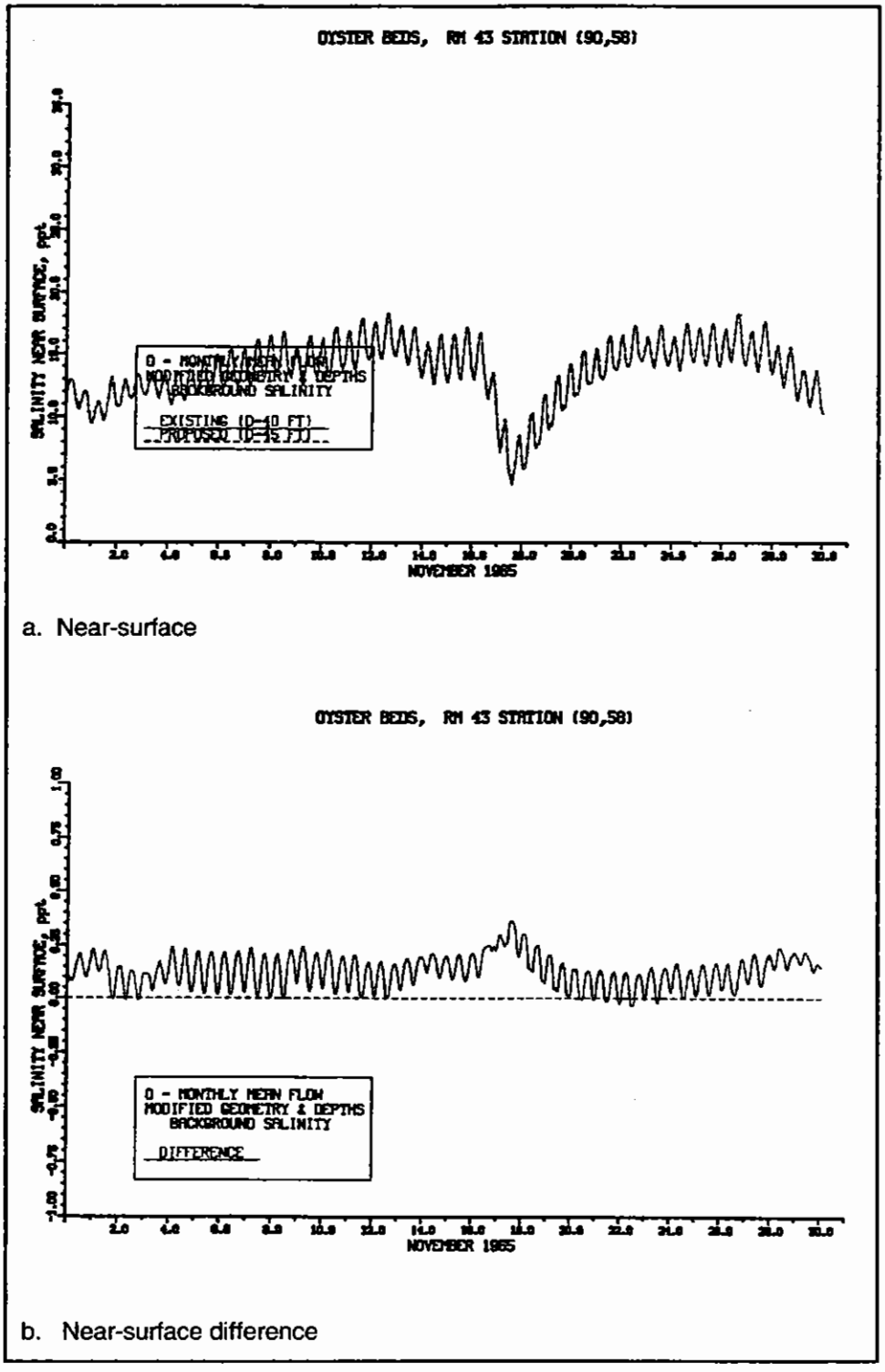

a. Near-surface

b. Near-surface difference

Figure 114. Impact of channel deepening on salinity at RM 43 Station (90,58) for monthly averaged inflow for November

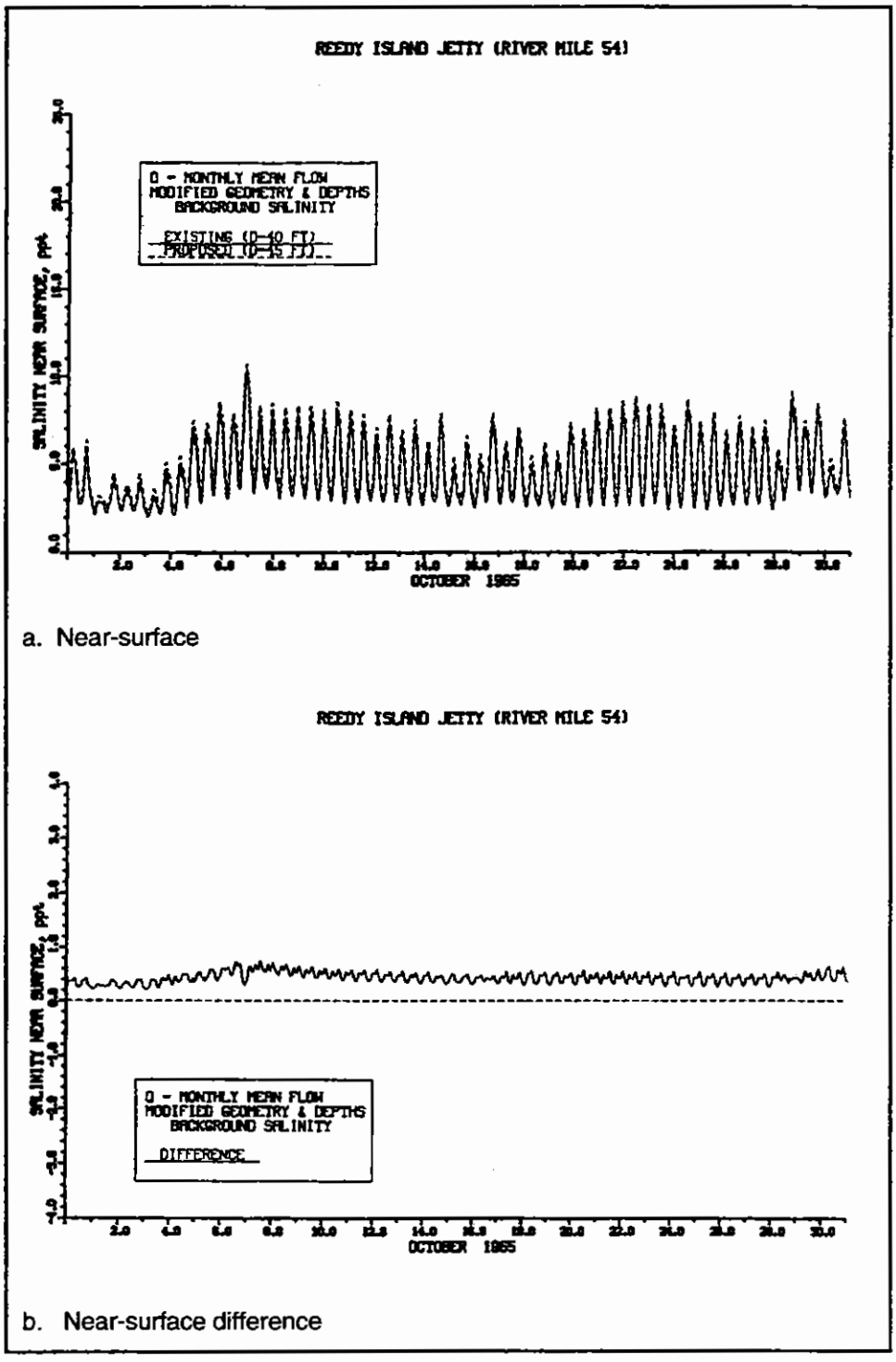

Figure 115. Impact of channel deepening on salinity at RM 54 for monthly averaged inflow for October (continued)

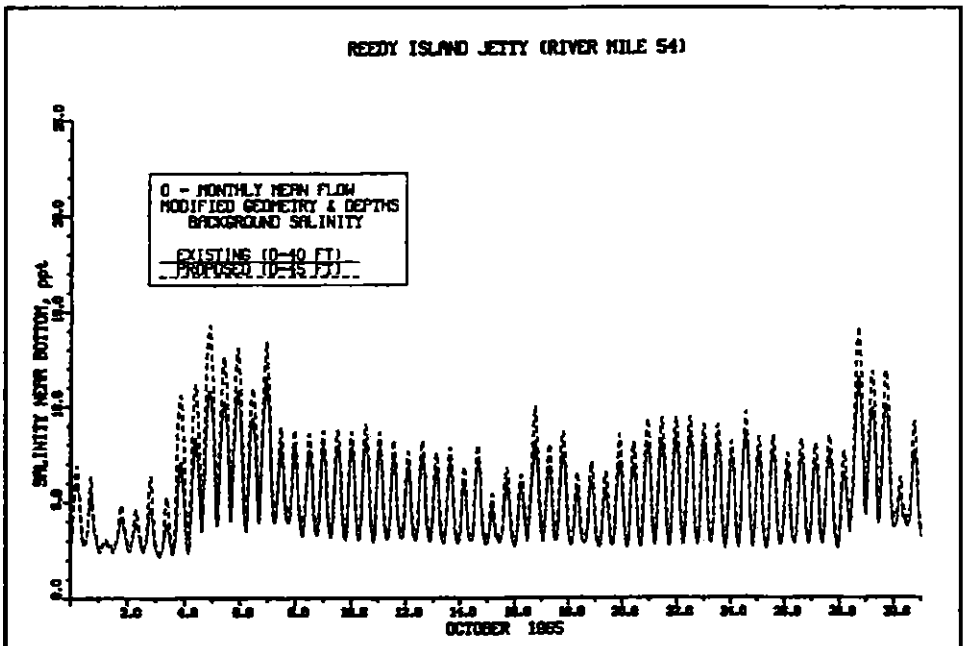

c. Near-bottom

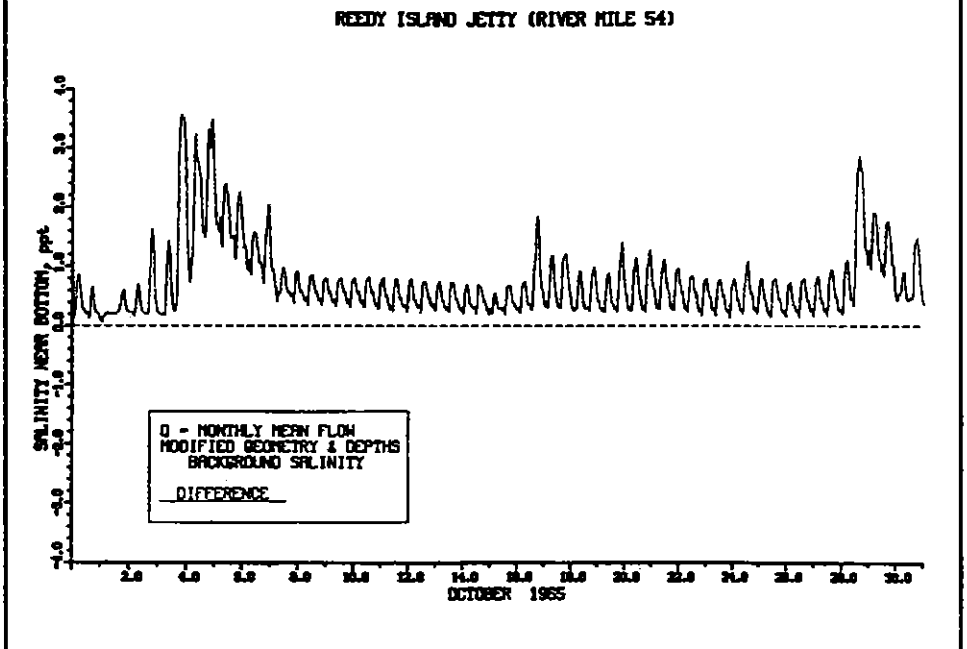

d. Near-bottom difference

Figure 115. (Concluded)

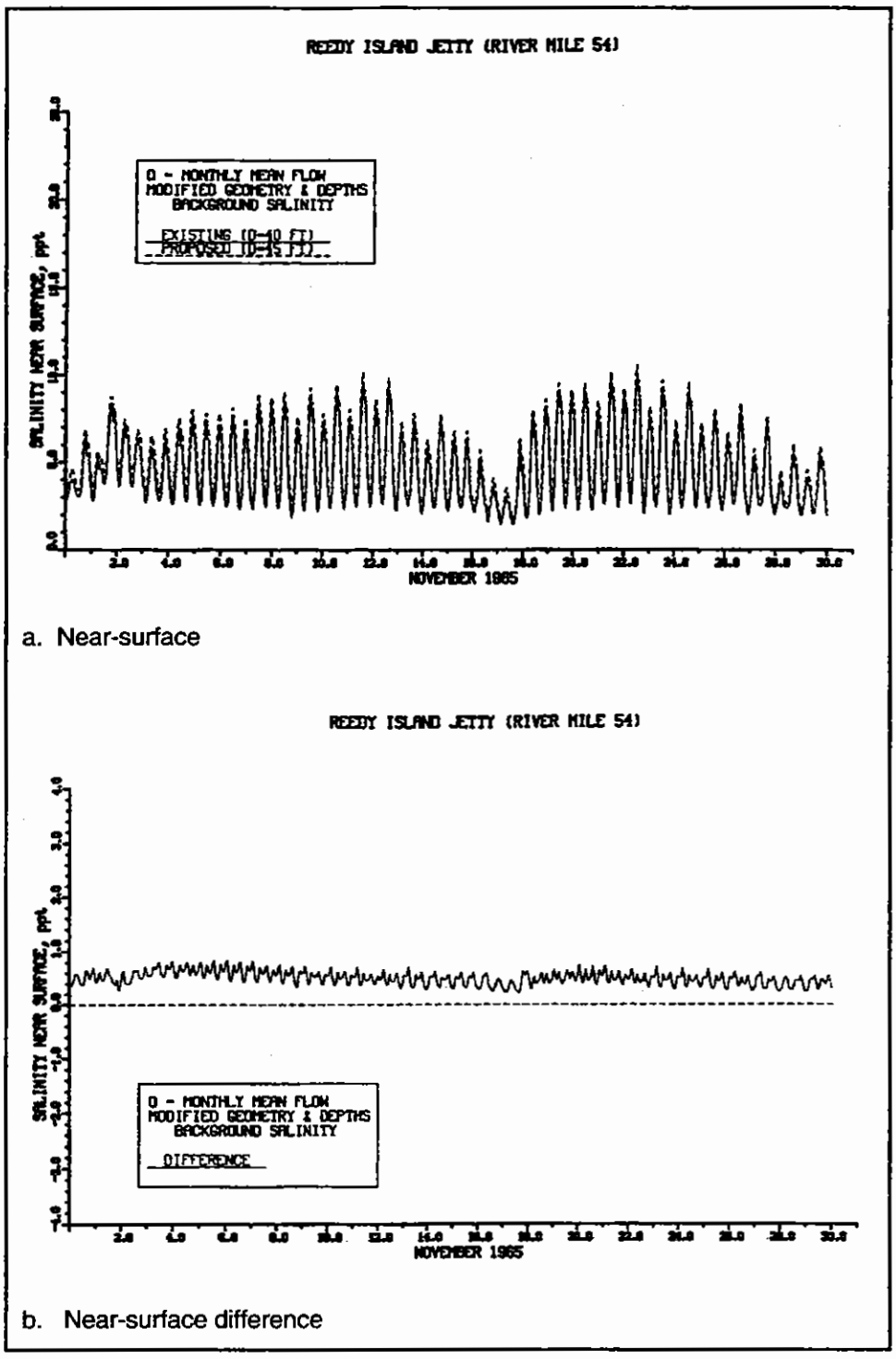

Figure 116. Impact of channel deepening on salinity at RM 54 for monthly averaged inflow for November (continued)

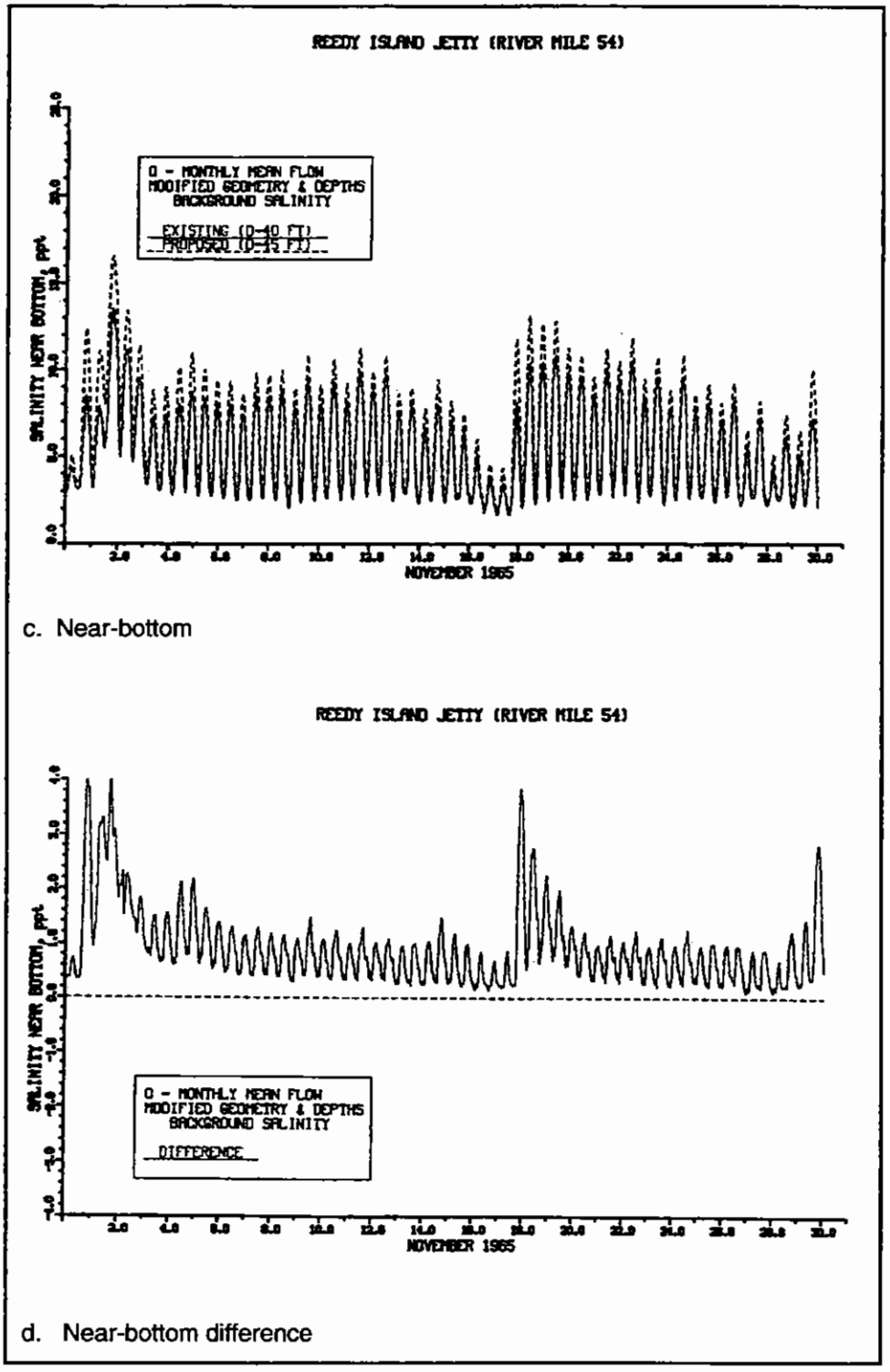

c. Near-bottom

d. Near-bottom difference

Figure 116. (Concluded)

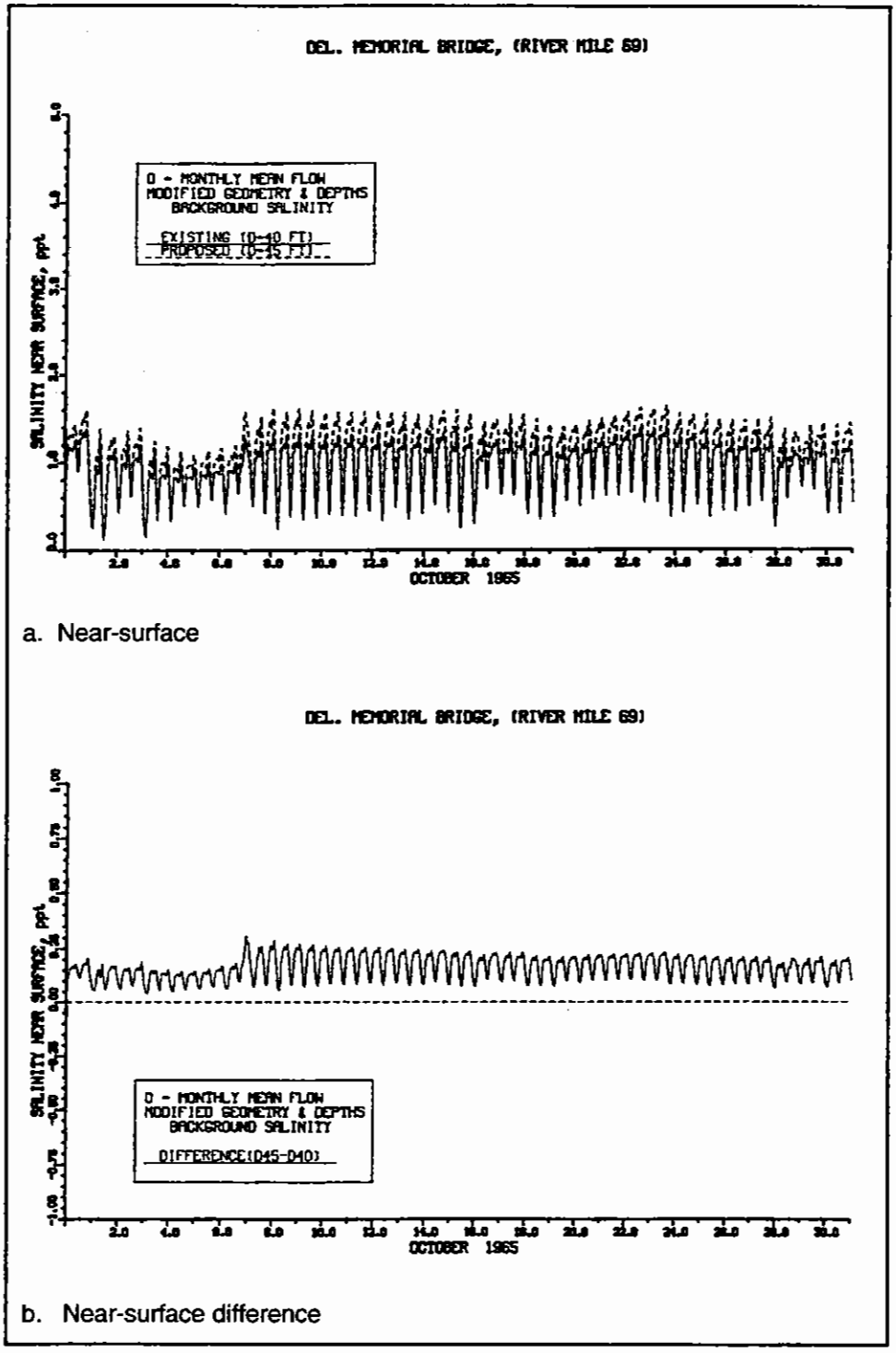

Figure 117. Impact of channel deepening on salinity at RM 69 for monthly averaged inflow for October (continued)

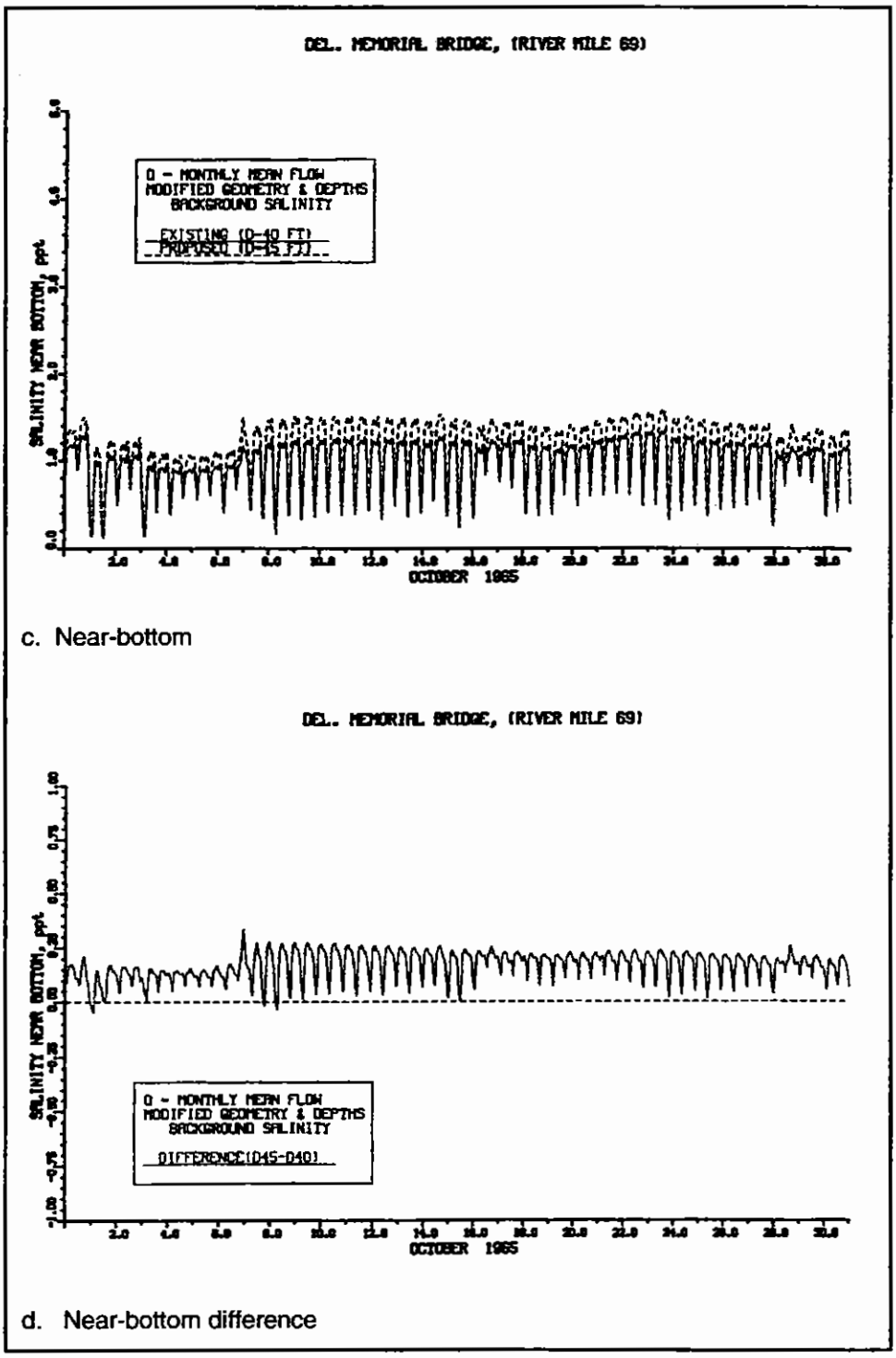

Figure 117. (Concluded)

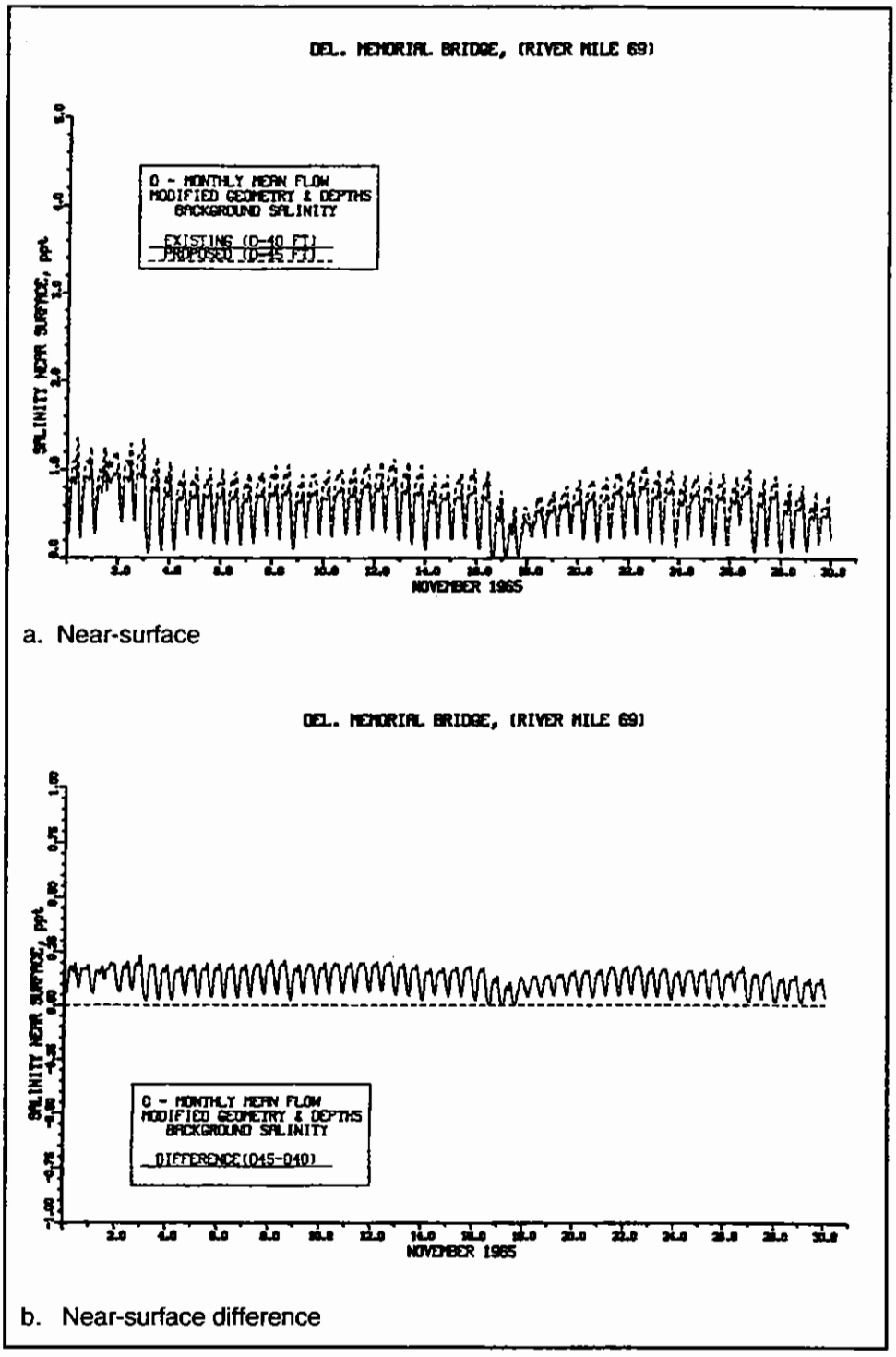

Figure 118. Impact of channel deepening on salinity at RM 69 for monthly averaged inflow for November (continued)

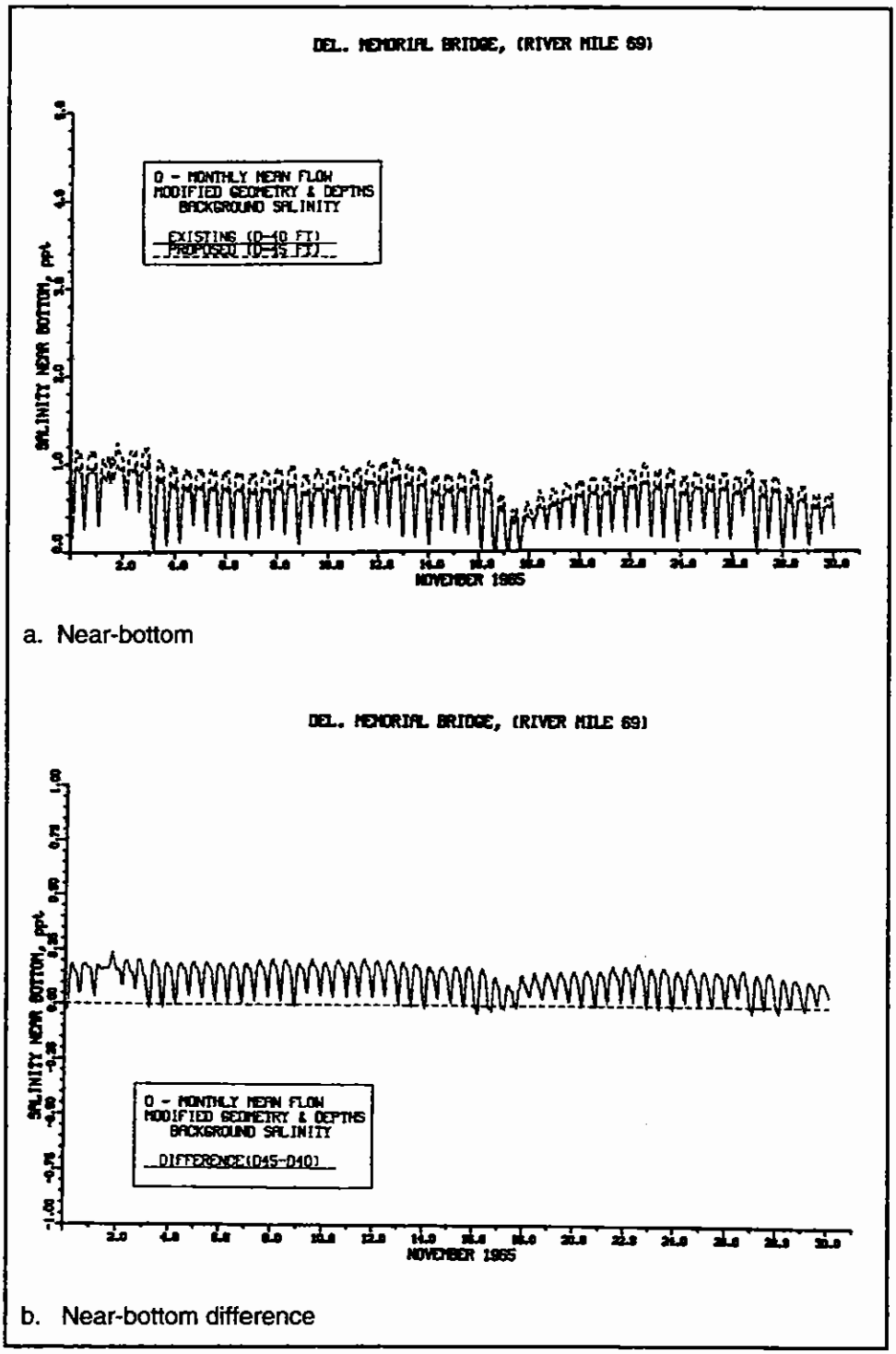

Figure 118. (Concluded)

a. Near-surface for 40-ft (12.20-m) channel

Figure 119. Monthly averaged 0.25-ppt isohaline for November for monthly averaged inflow (continued)

b. Near-surface for 45-ft (13.72-m) channel

Figure 119. (Concluded)

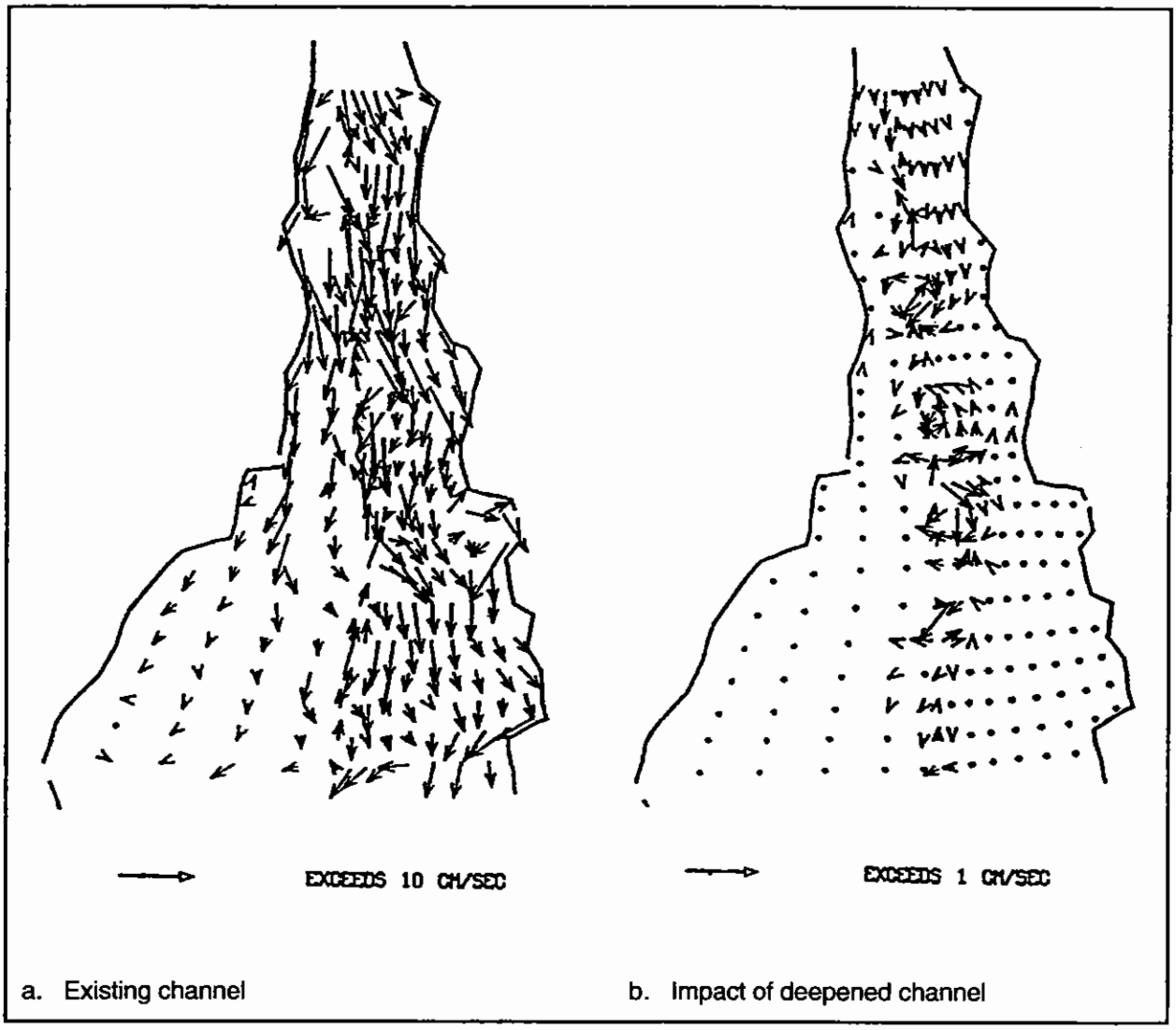

Figure 120. Residual near-surface currents for October for monthly averaged inflow

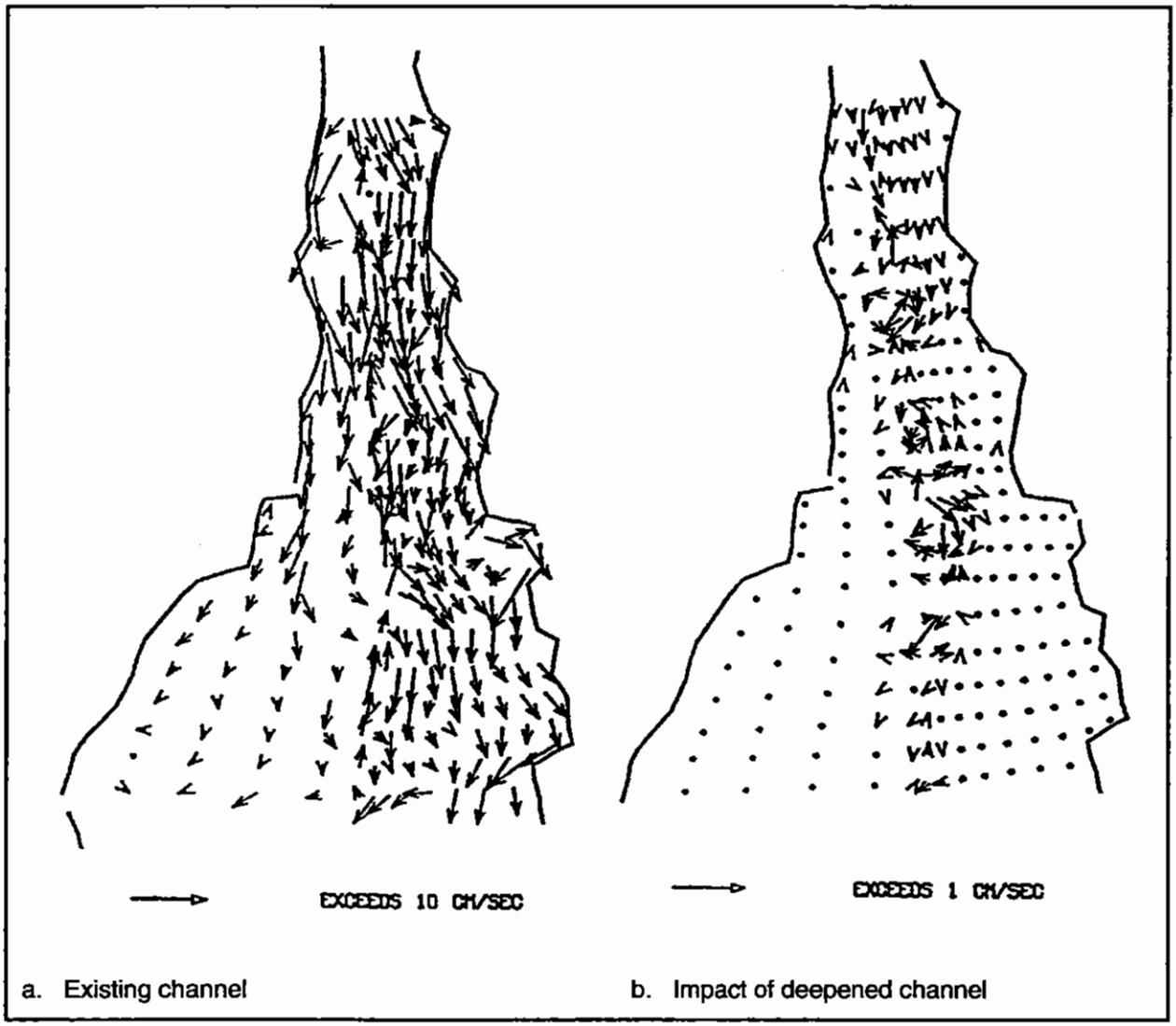

Figure 121. Residual near-surface currents for November for monthly averaged inflow

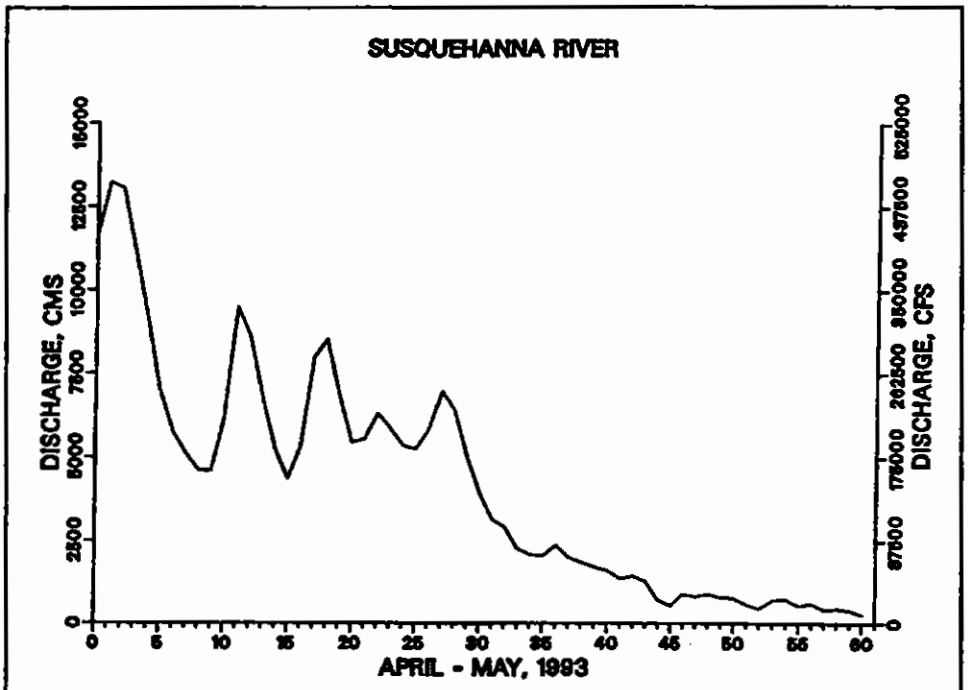

a. Susquehanna River

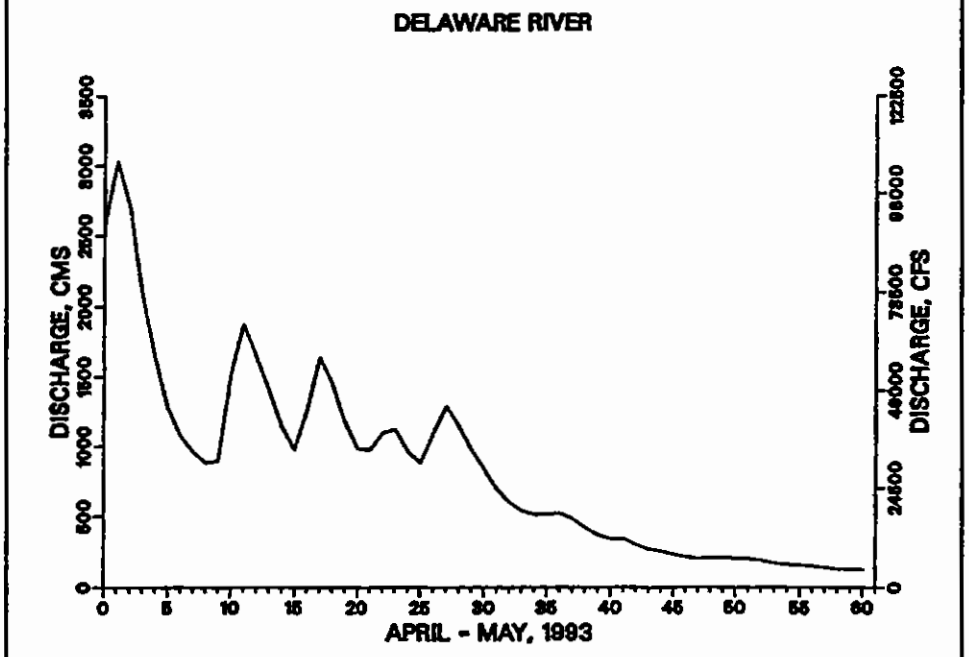

b. Delaware River

Figure 122. Freshwater inflows for April-May 1993 (continued)

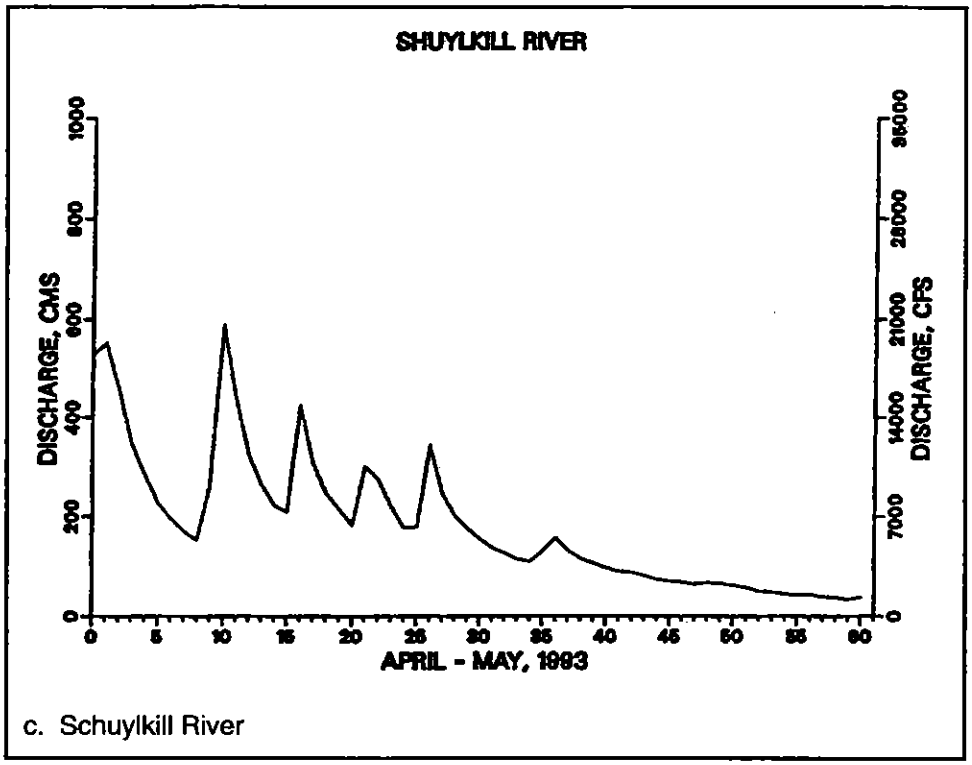

c. Schuylkill River

Figure 122. (Concluded)

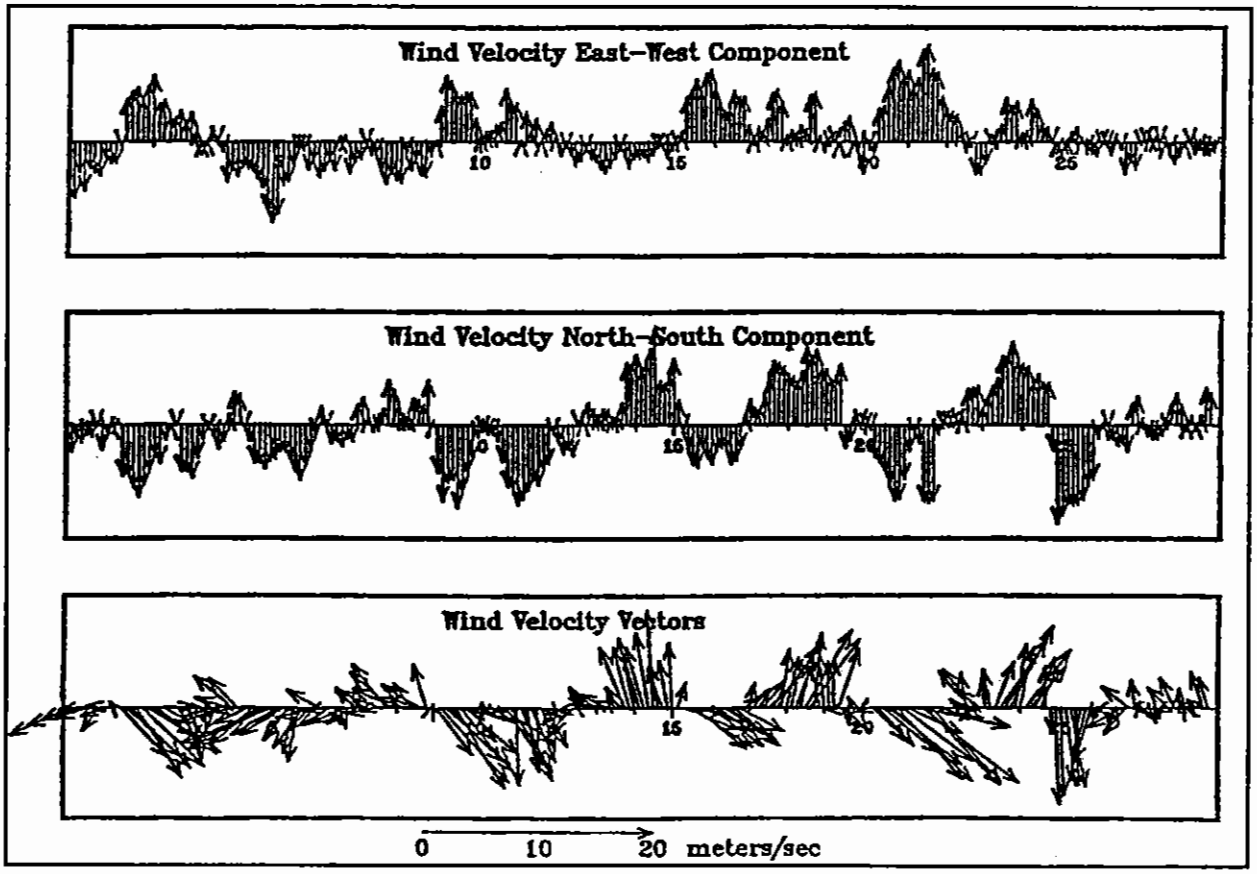

Figure 123. Average wind for May 1993

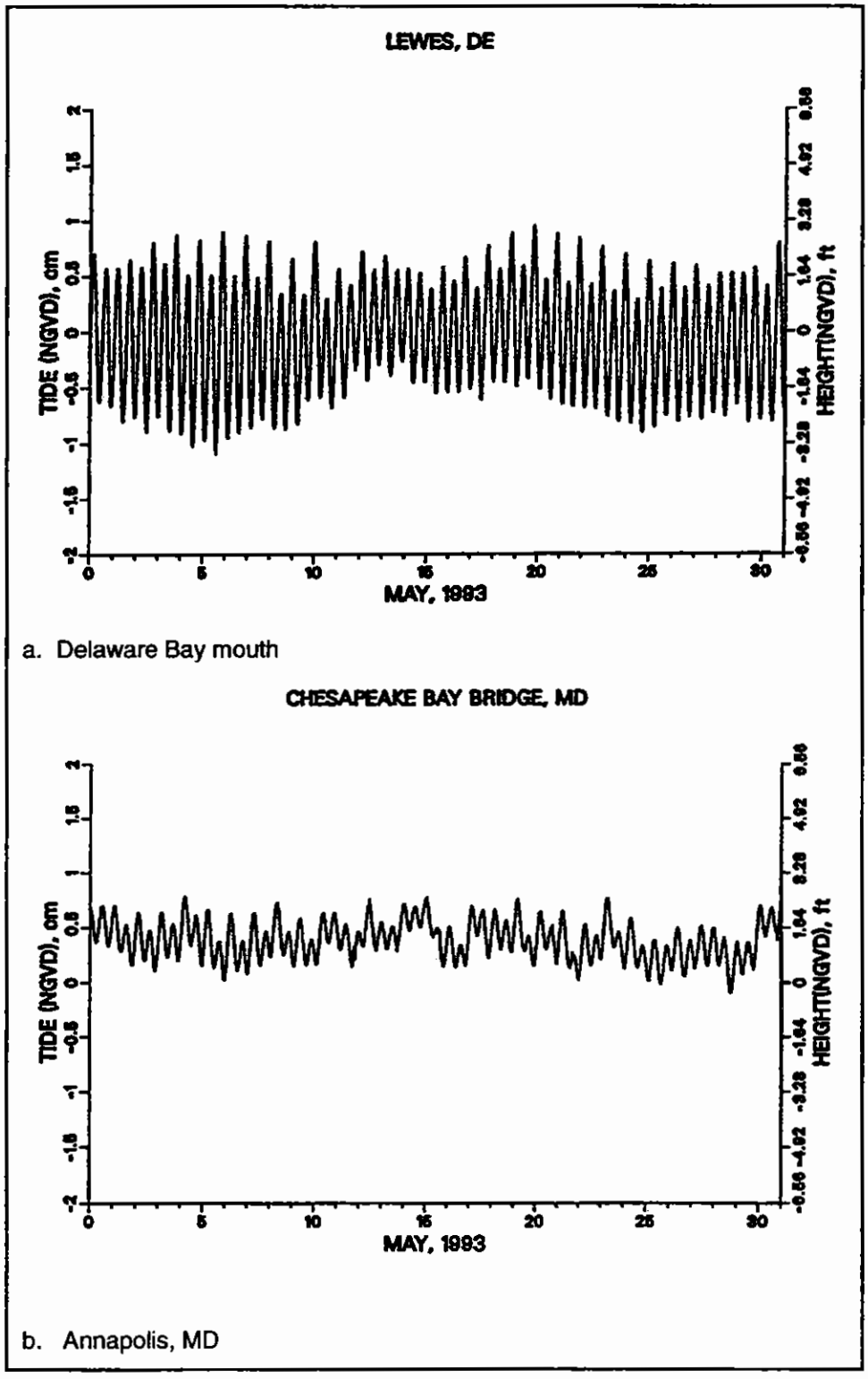

Figure 124. Boundary tides for May 1993

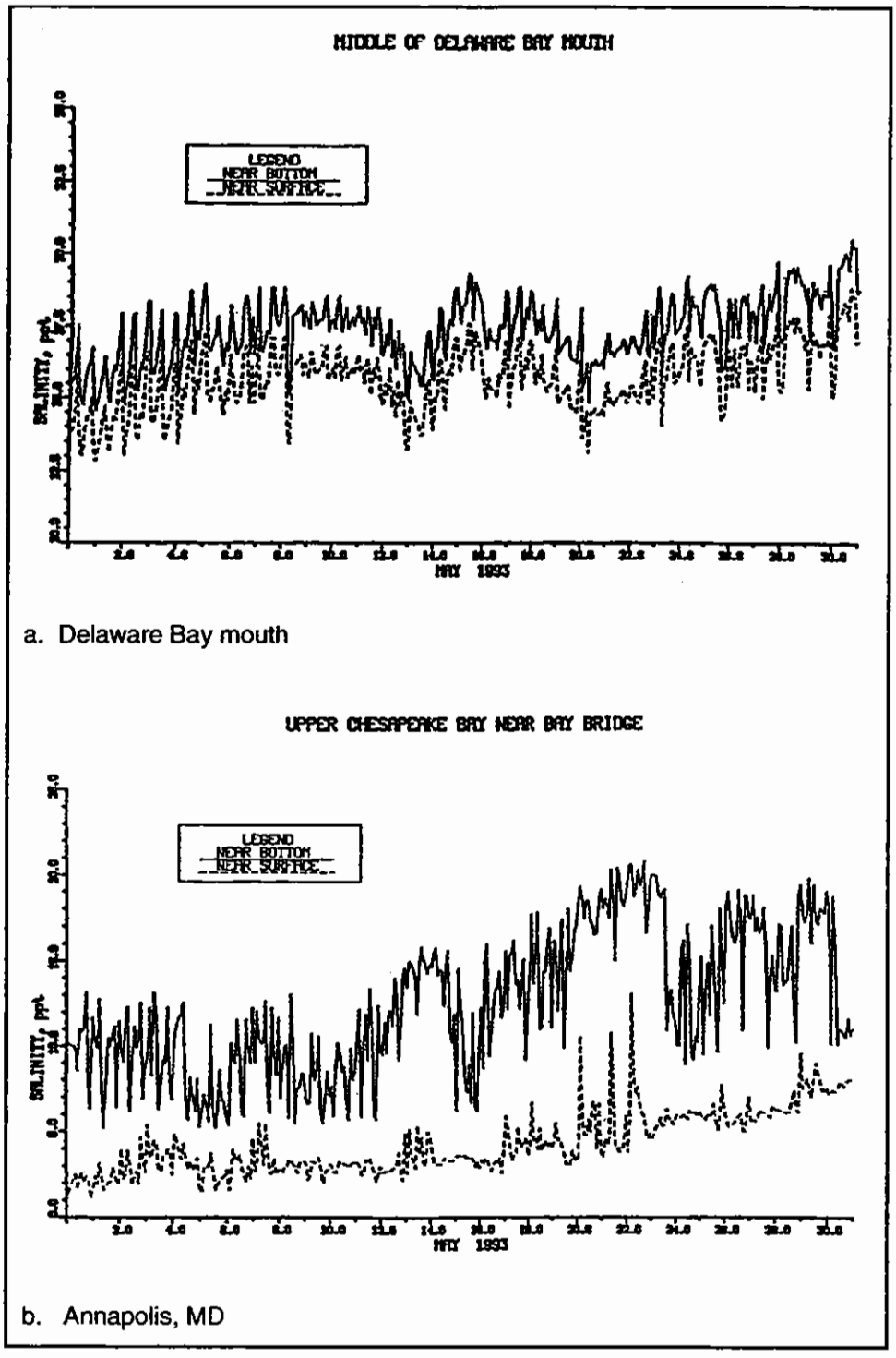

Figure 125. Boundary salinity for May 1993

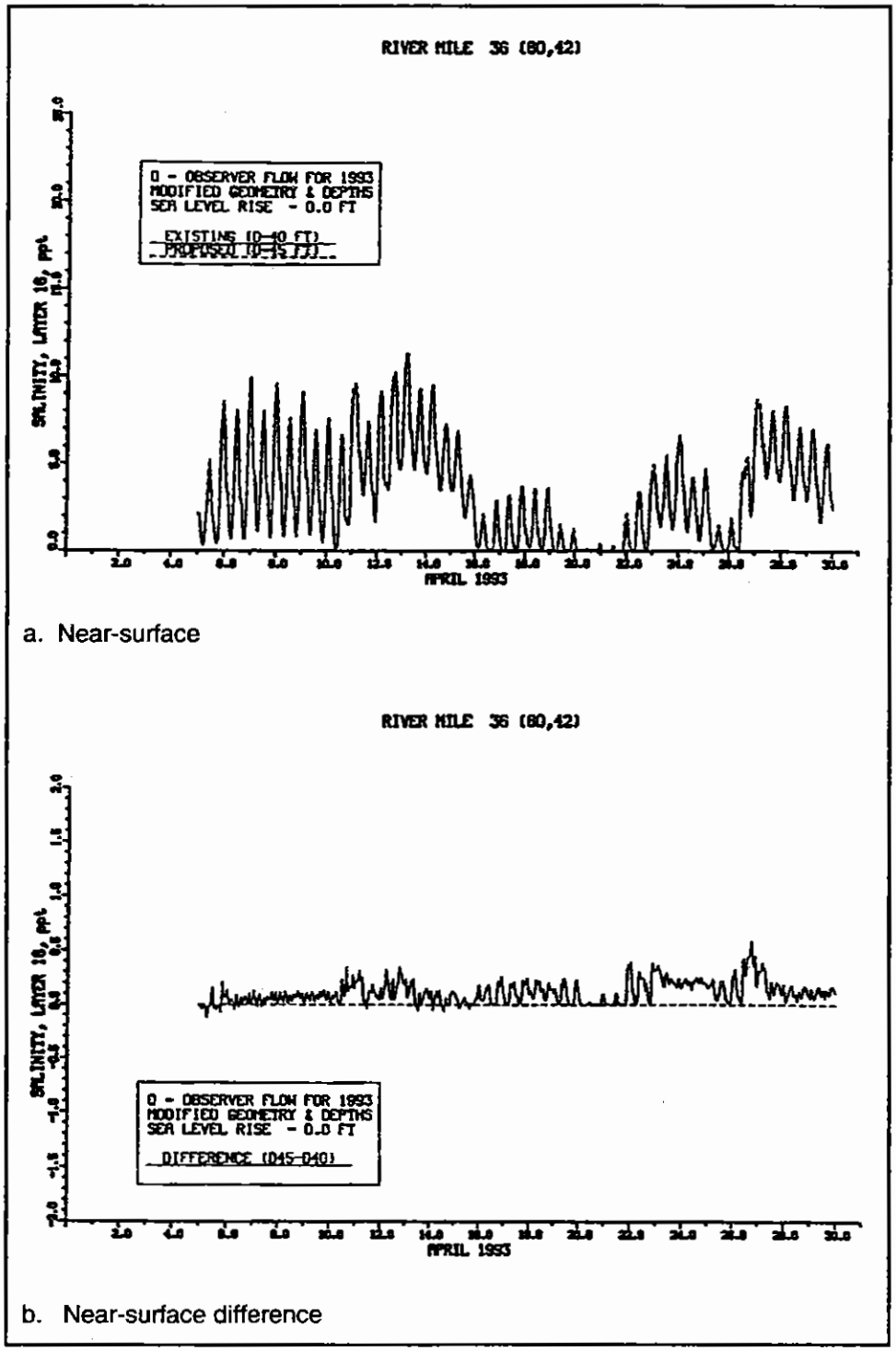

Figure 126. Impact of channel deepening on salinity at RM 36 for April 1993 (continued)

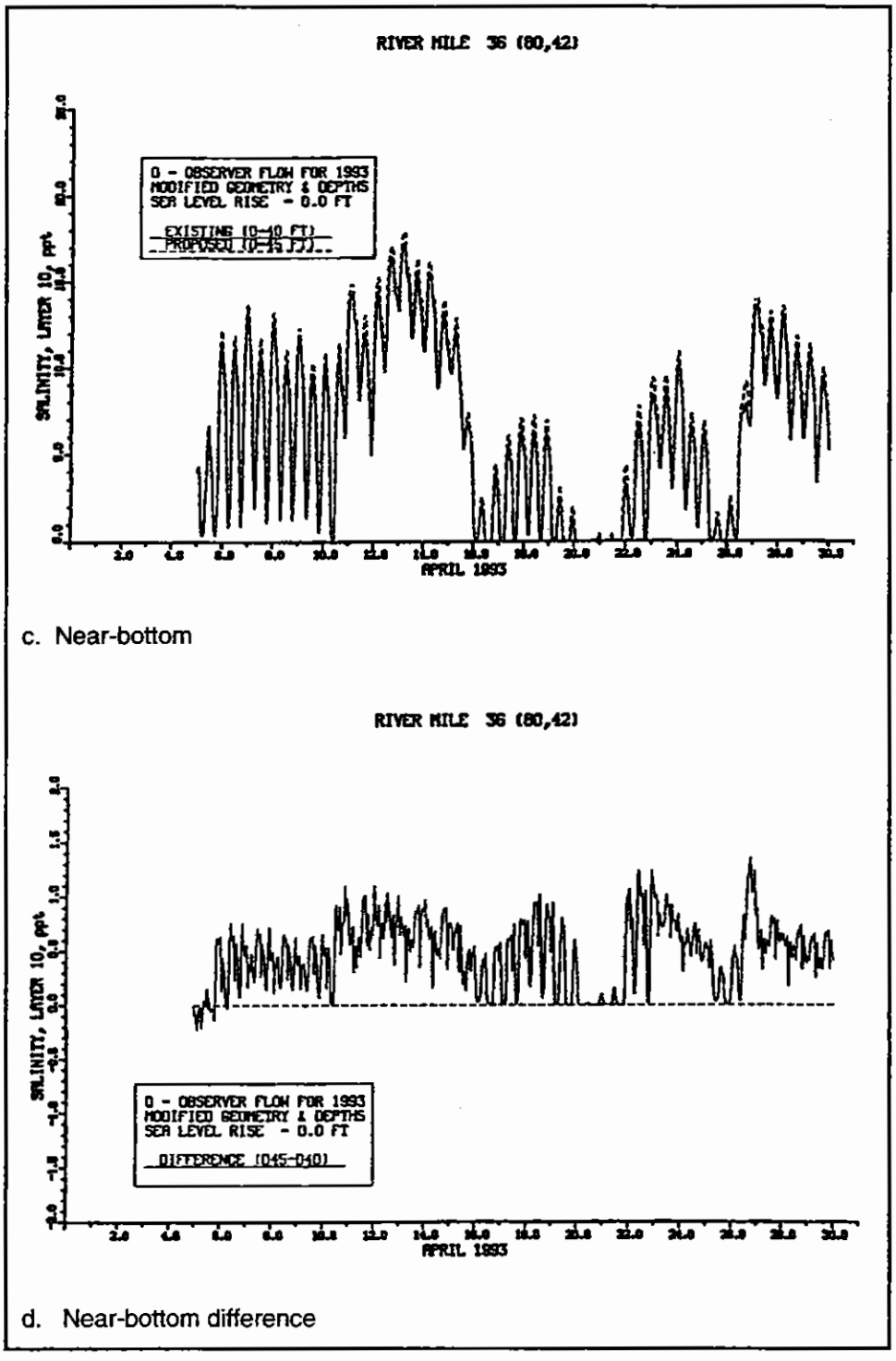

Figure 126. (Concluded)

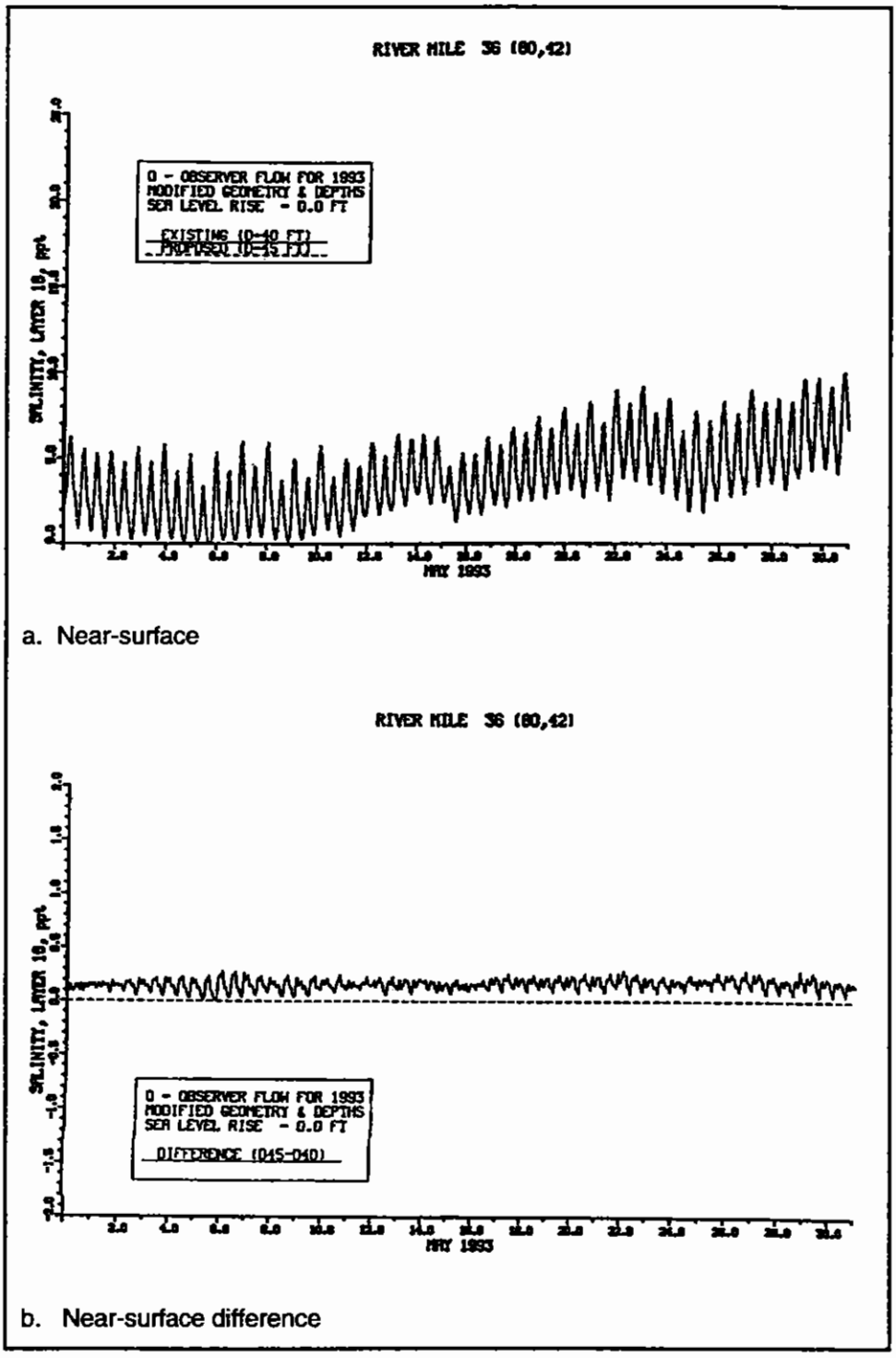

Figure 127. Impact of channel deepening on salinity at RM 36 for May 1993 (continued)

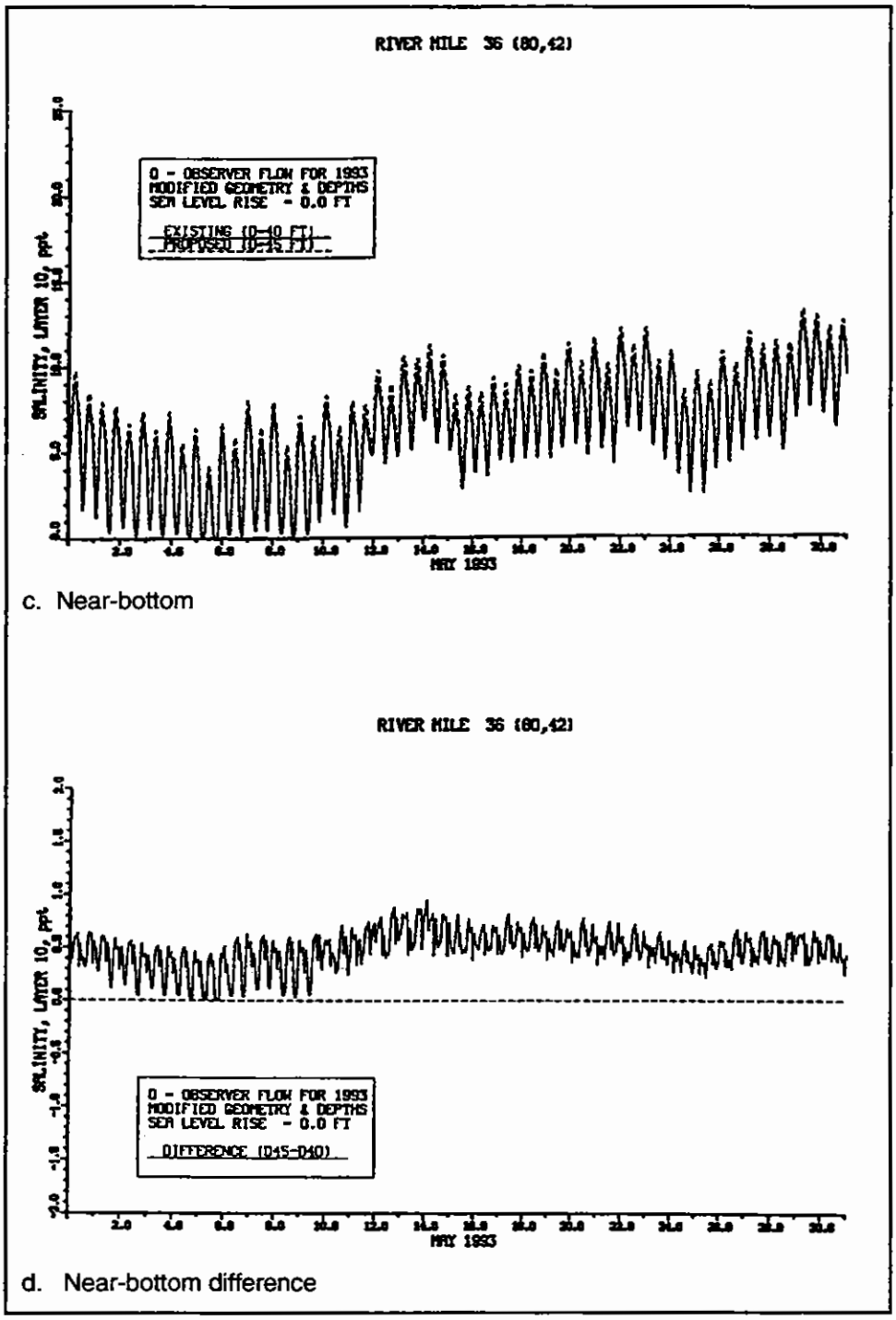

Figure 127. (Concluded)

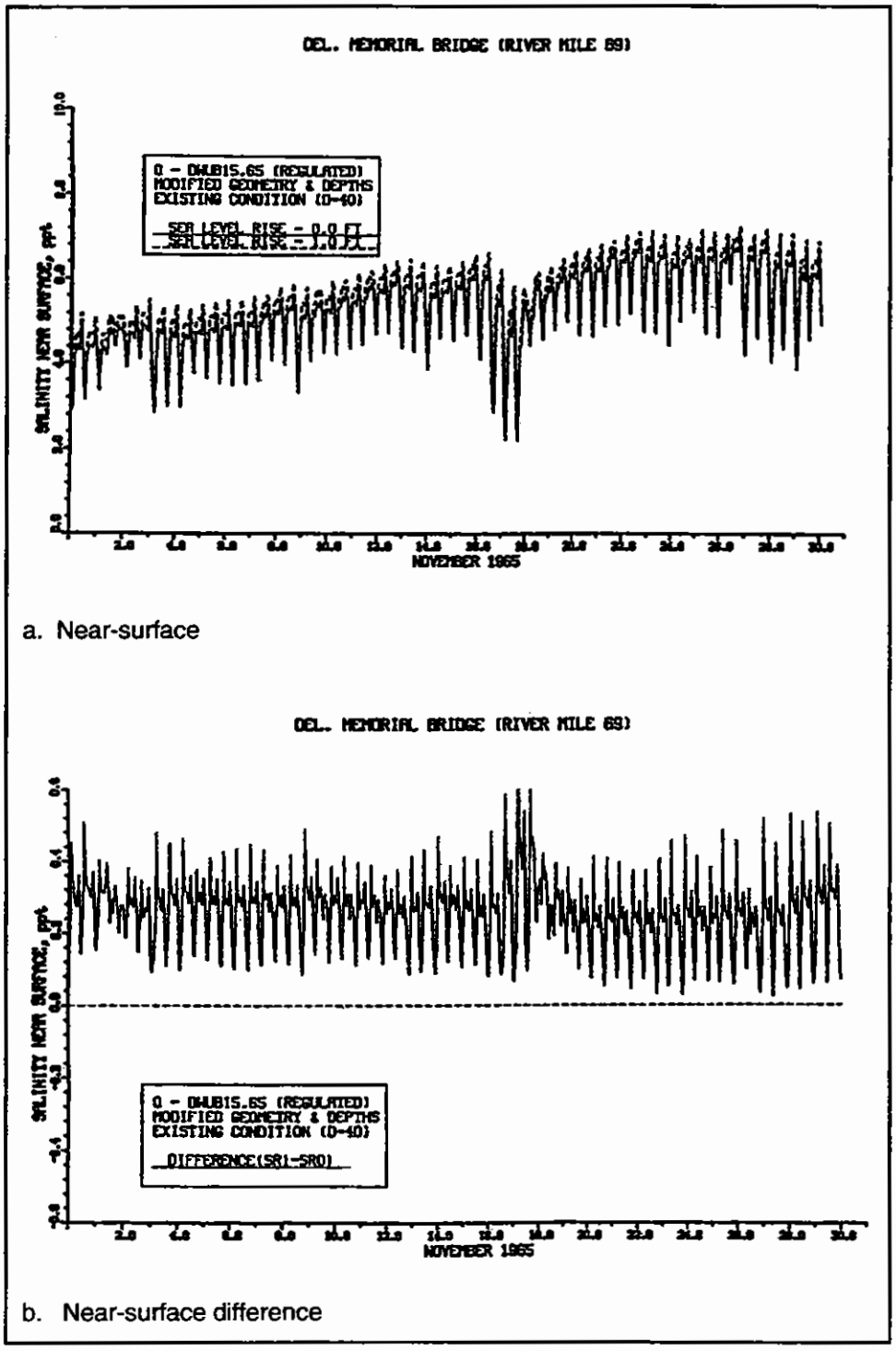

Figure 128. Impact of 1.0-ft (0.30-m) sea level rise on salinity at RM 69 for November 1965 for regulated inflow (continued)

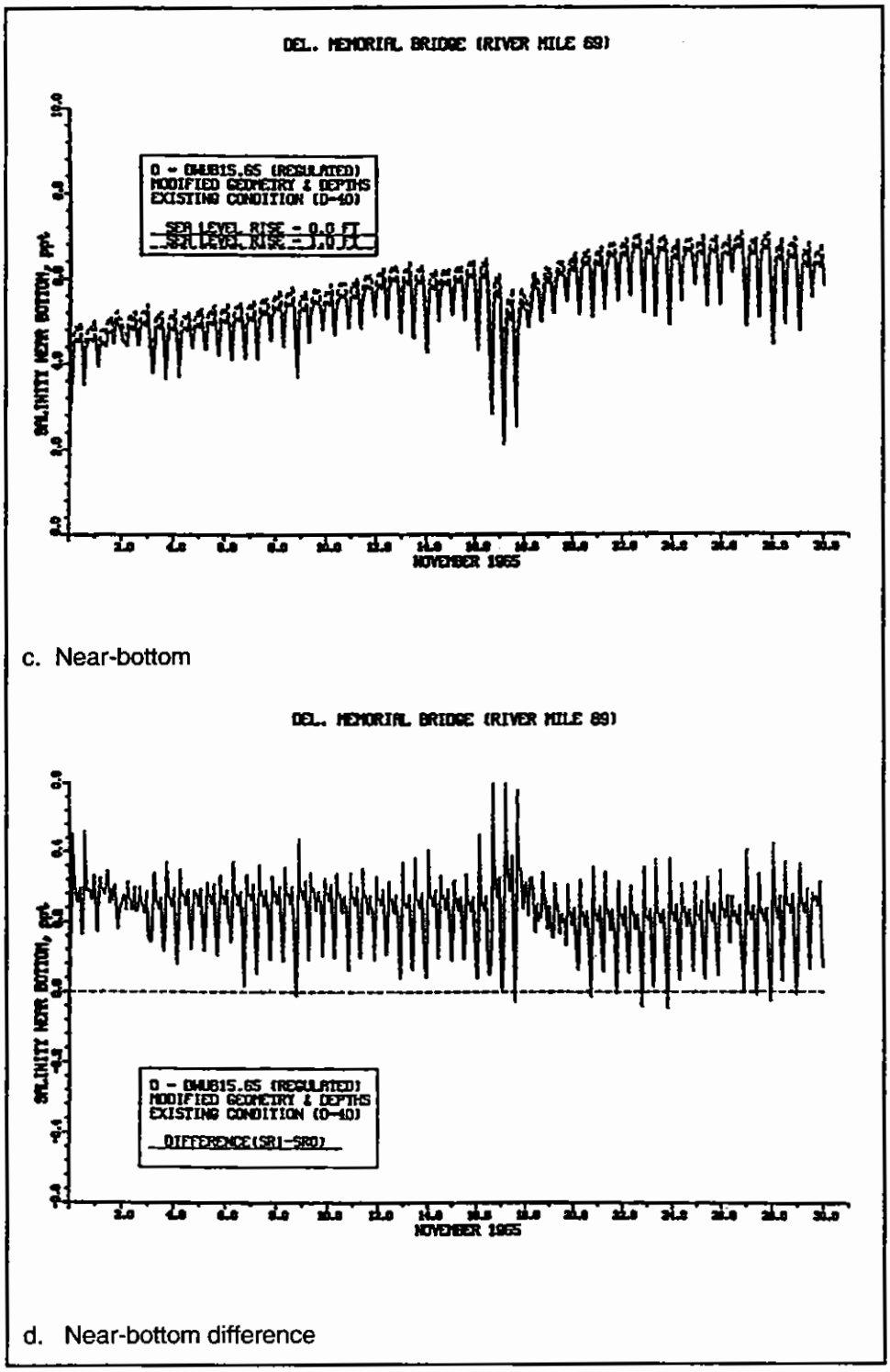

c. Near-bottom

d. Near-bottom difference

Figure 128. (Concluded)

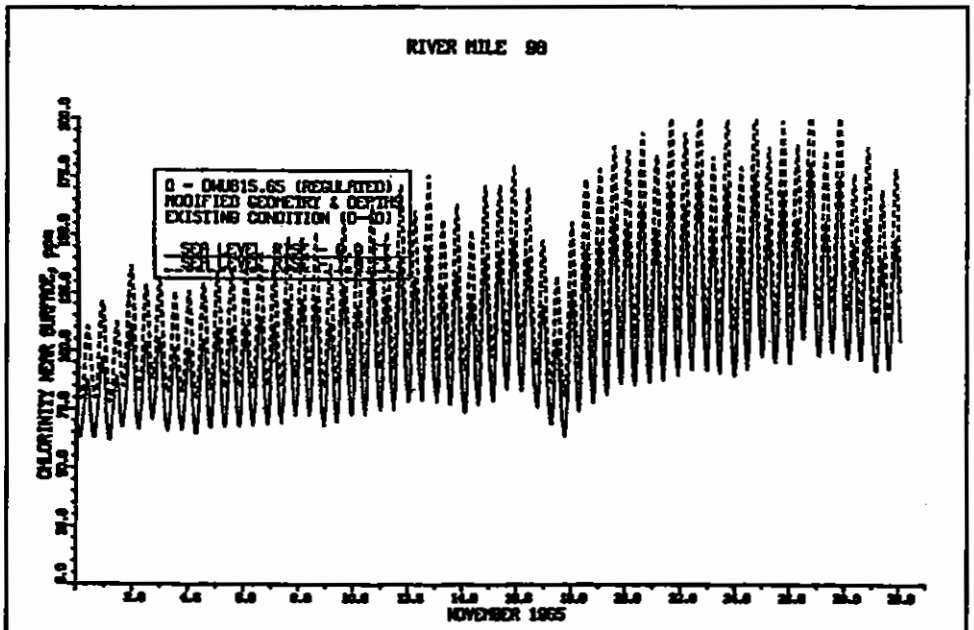

a. Near-surface

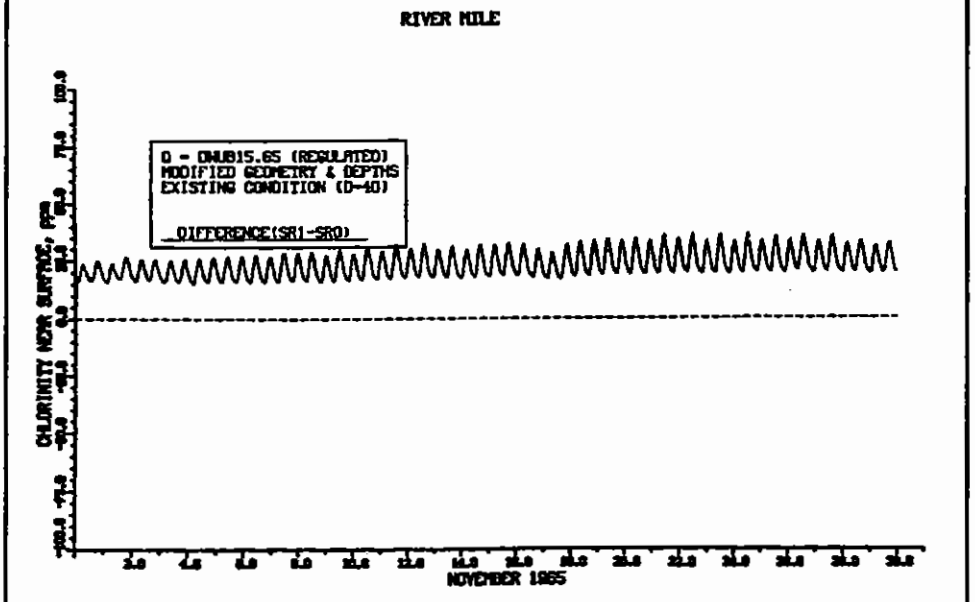

b. Near-surface difference

Figure 129. Impact of 1.0-ft (0.30-m) sea level rise on chlorinity at RM 98 for November 1965 for regulated inflow (continued)

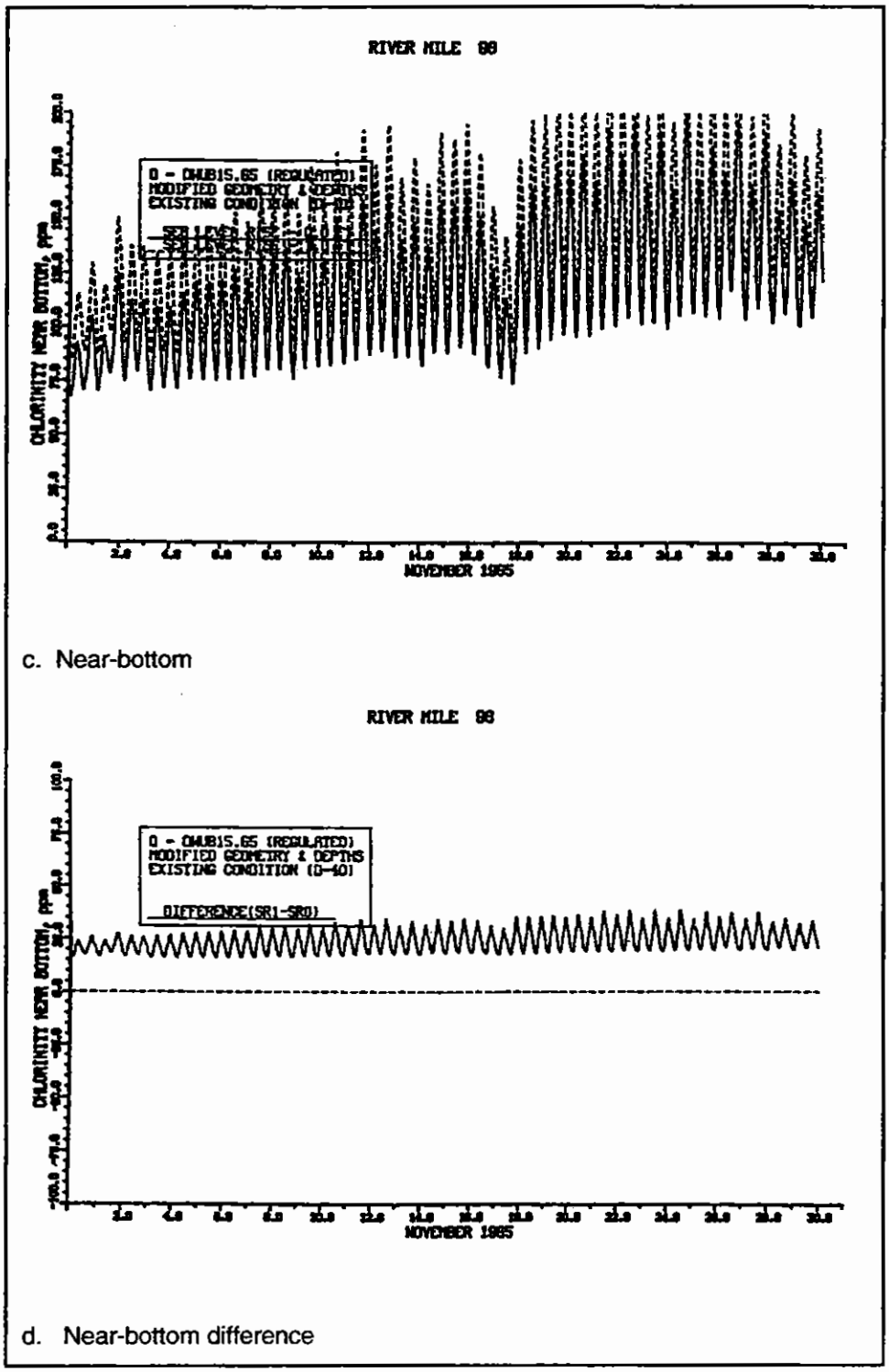

Figure 129. (Concluded)

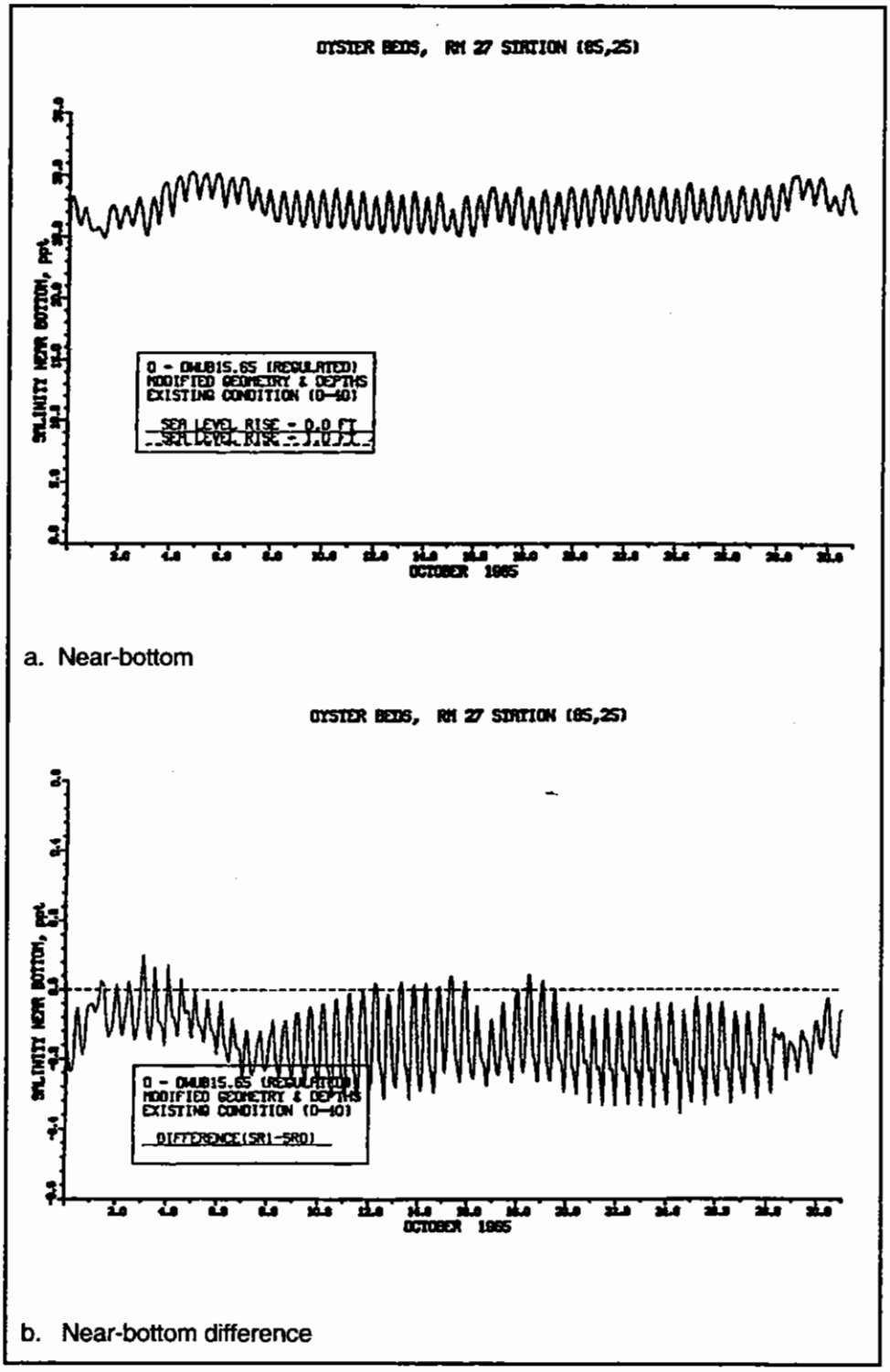

Figure 130. Impact of 1.0-ft (0.30-m) sea level rise on salinity at RM 27 Station (85,25) for October for regulated flow

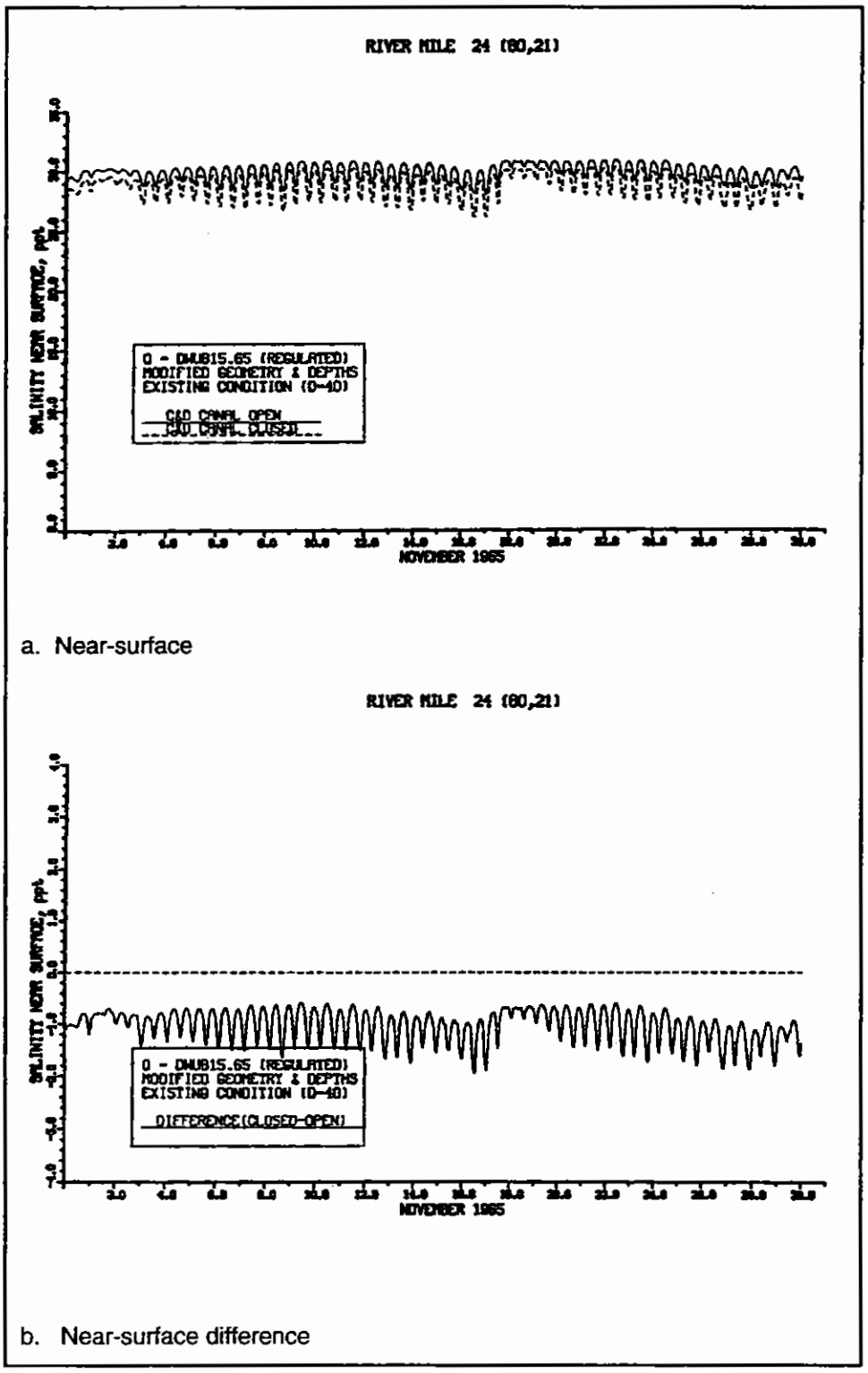

Figure 131. Impact of closing the C&D Canal on salinity at RM 24 for November for regulated inflow (continued)

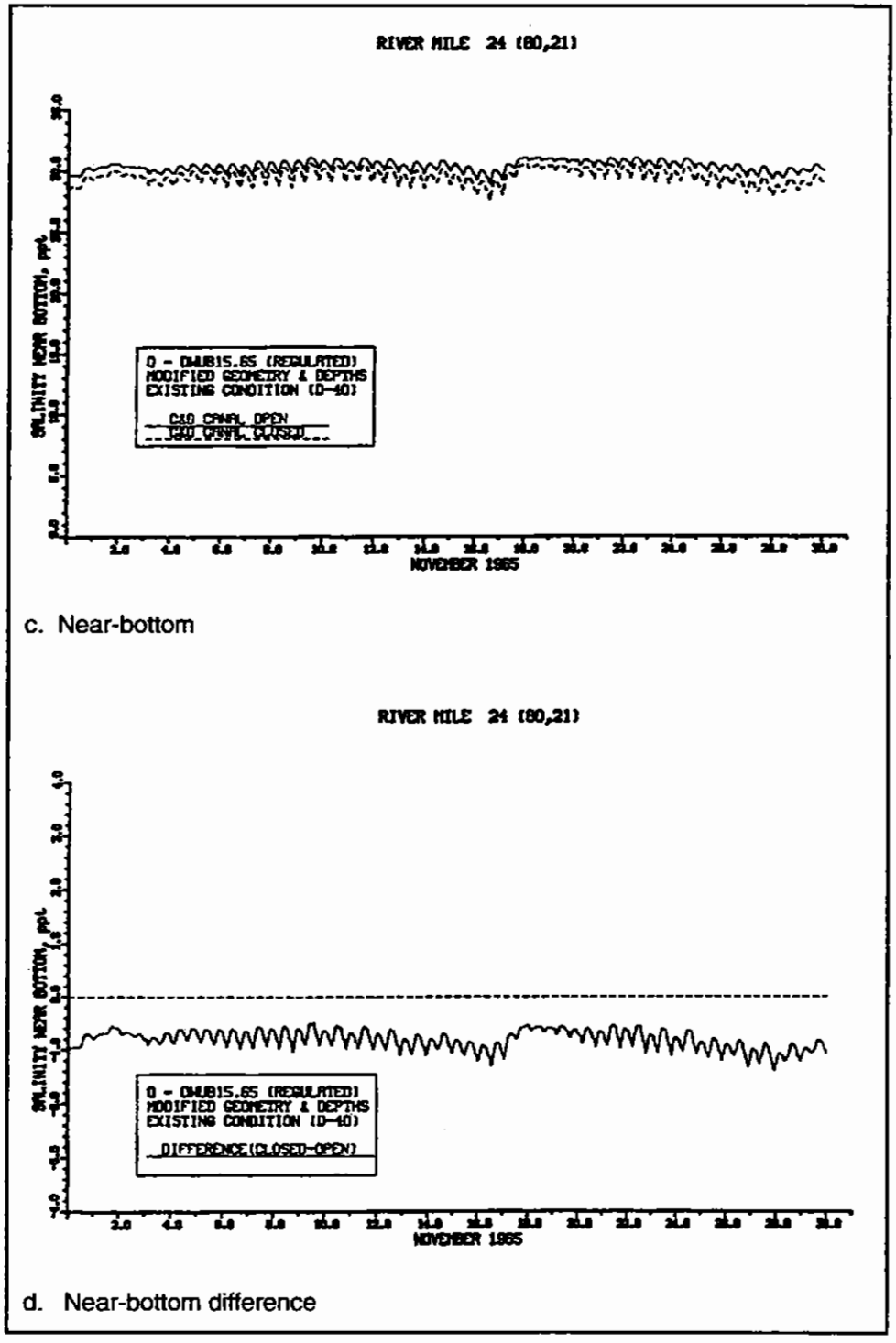

c. Near-bottom

d. Near-bottom difference

Figure 131. (Concluded)

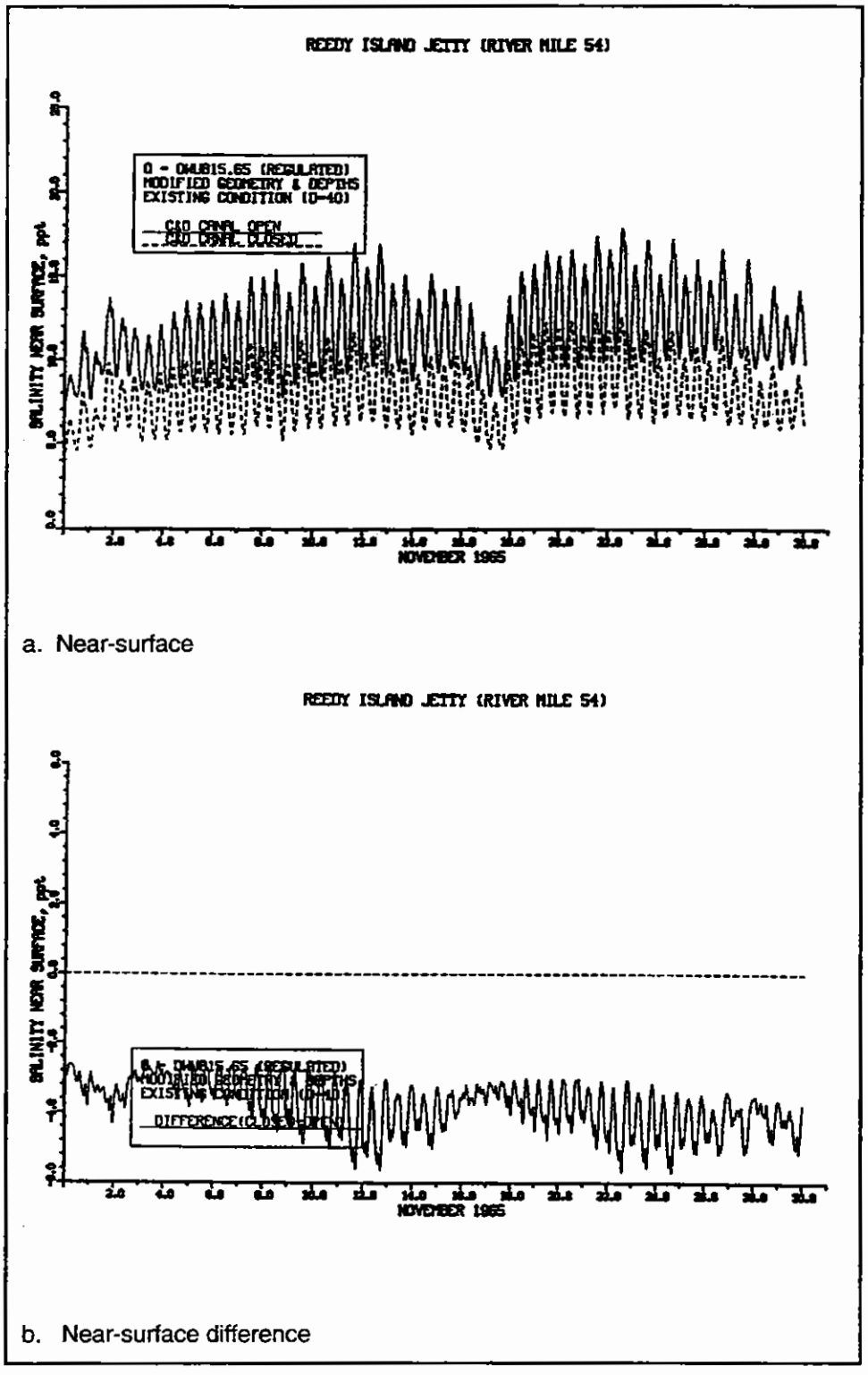

Figure 132. Impact of closing the C&D Canal on salinity at Reedy Island Jetty for November for regulated inflow (continued)

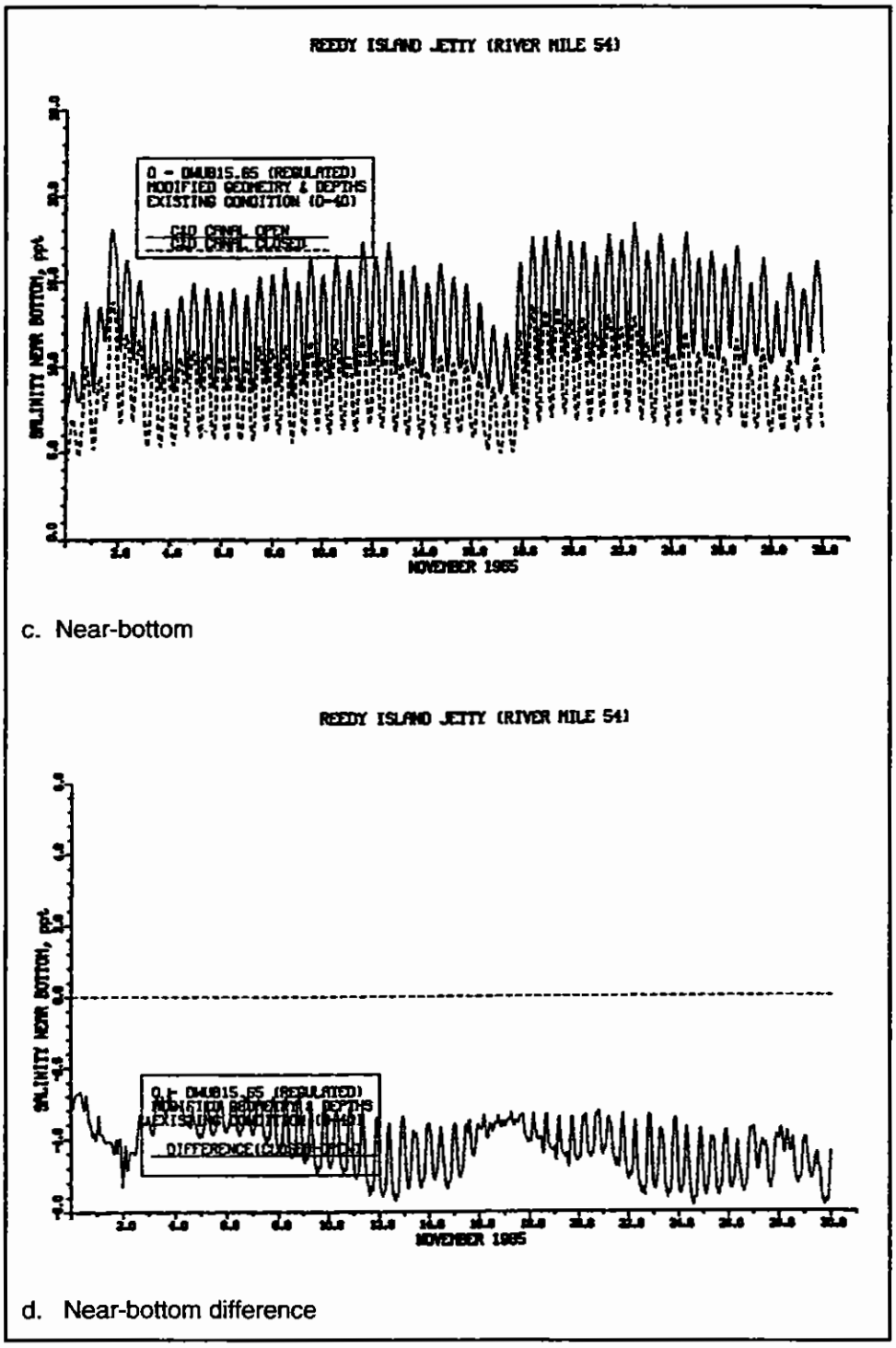

c. Near-bottom

d. Near-bottom difference

Figure 132. (Concluded)

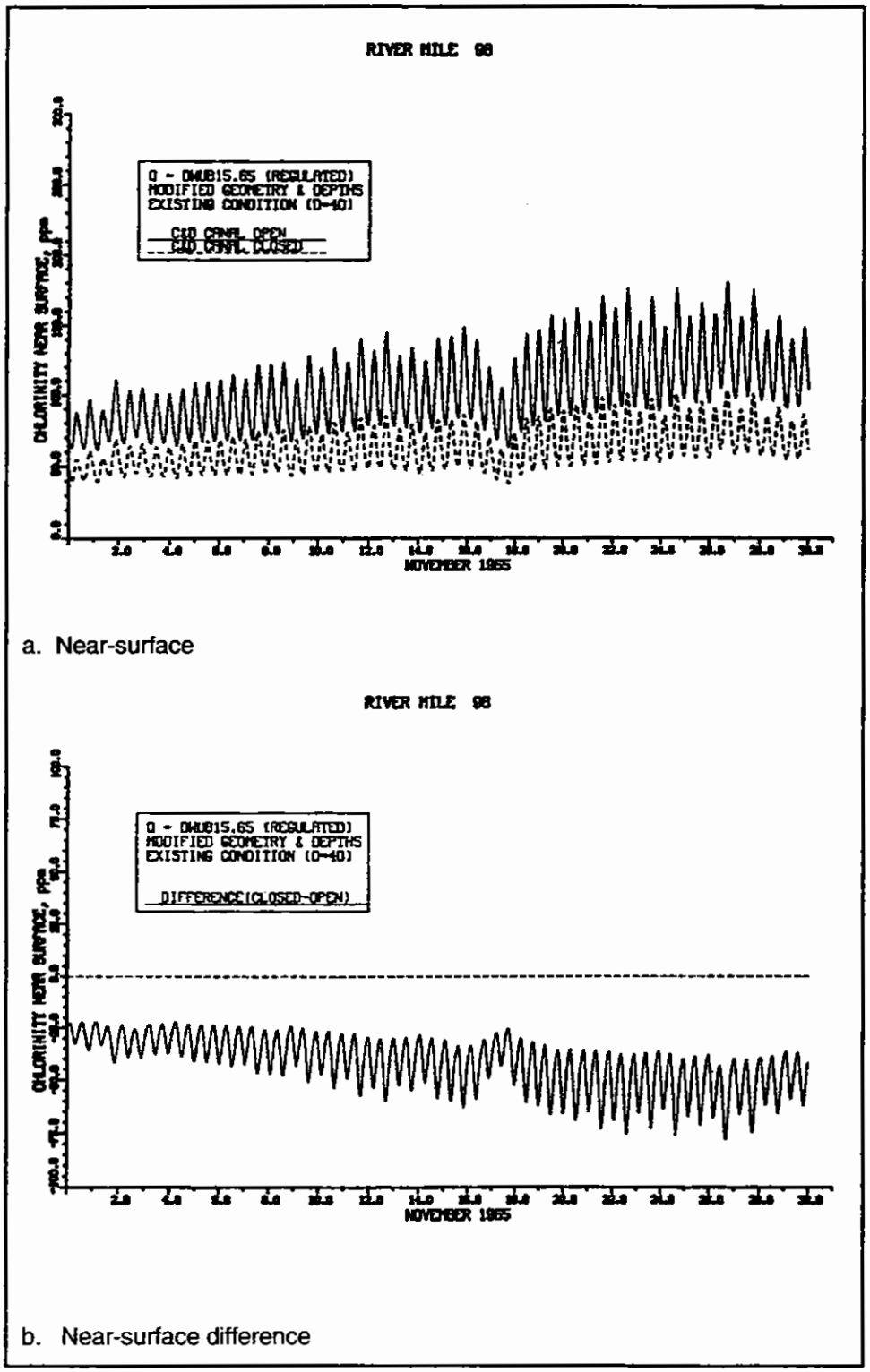

Figure 133. Impact of closing the C&D Canal on chlorinity at RM 98 for November for regulated inflow (continued)

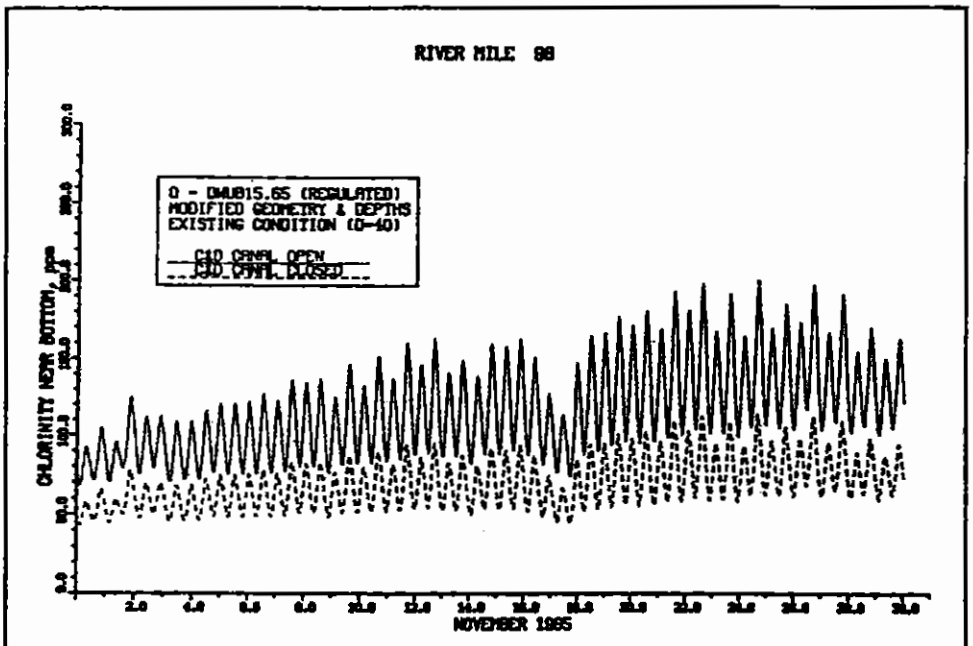

c. Near-bottom

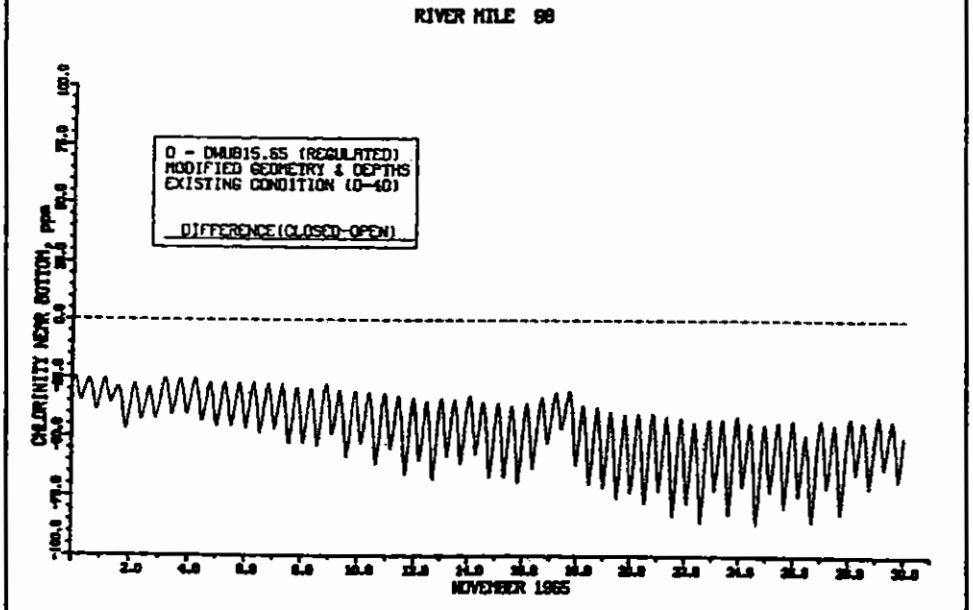

d. Near-bottom difference

Figure 133. (Concluded)

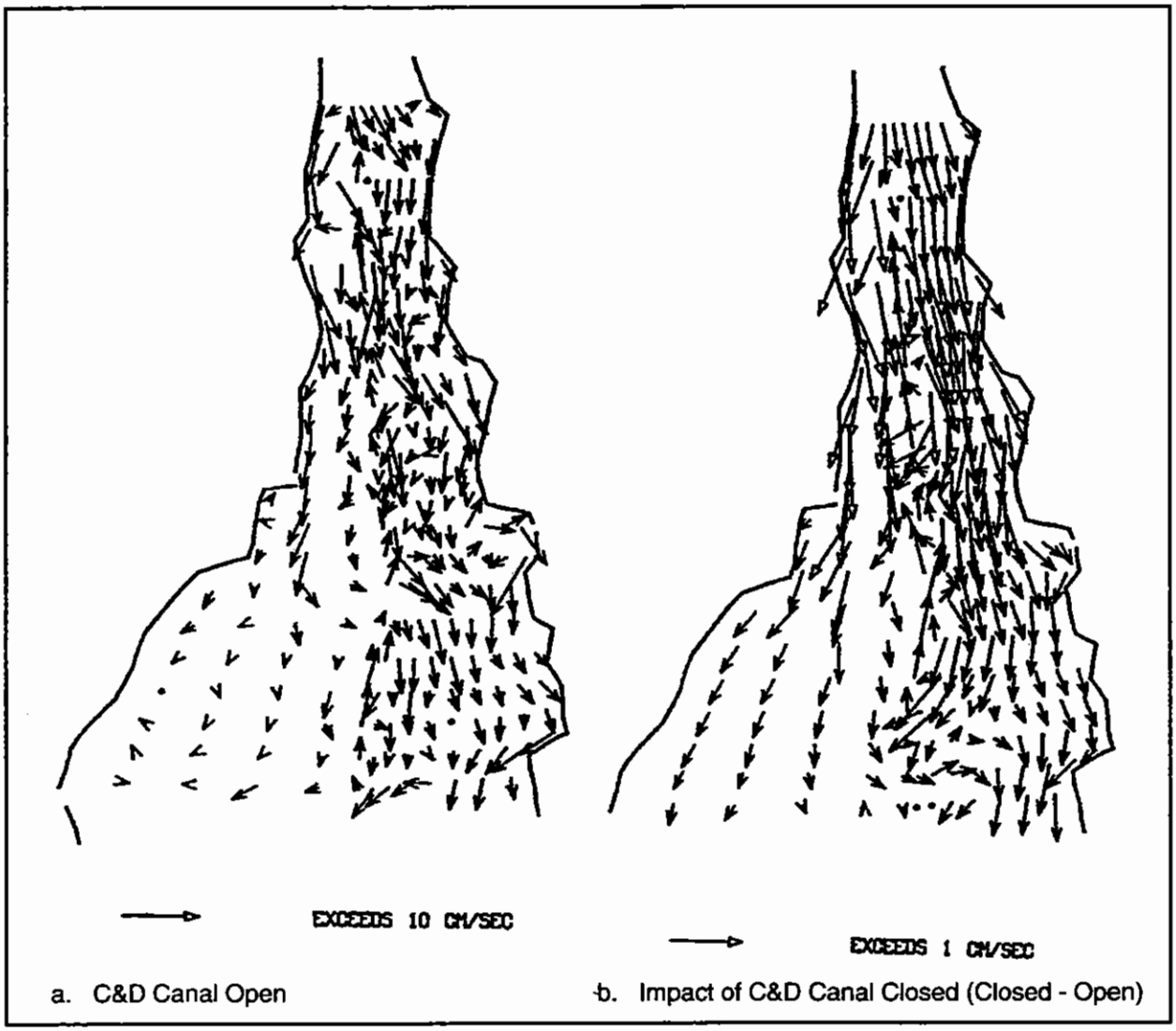

Figure 134. Impact of closing the C&D Canal on near-surface residual currents in lower Delaware Bay for November for regulated inflow

Appendix A
Notation

A_H, K_H	Horizontal turbulent eddy coefficients
A_v, K_v	Vertical turbulent eddy coefficients
C	Surface drag coefficient
C_d	Bottom friction coefficient
E_H	Lateral Ekman number
E_v	Vertical Ekman number
g	Gravitational acceleration
f	Coriolis parameter defined as $2\Omega sin\ \phi$ where Ω is the rotational speed of the earth and ϕ is latitude
F_r	Froude number
Fr_D	Densimetric Froude number
h	Thickness of an internal layer
H	Total depth
J	Jacobian of transformation
k	von Karman constant
K	Surface heat exchange coefficient
N	Brunt-Vaisala frequency
p	Pressure

Pr_H	Lateral Prandtl (Schmidt) number
Pr_v	Vertical Prandtl (Schmidt) number
Ri	Richardson number
R_o	Rossby number
S	Salinity
t	Time
T	Temperature
T_e	Equilibrium temperature
T_o	Typical value for temperature
$\bar{u}$, $\bar{v}$	Contravariant components of Cartesian velocity
$\bar{u}_1$, $\bar{v}_1$	Horizontal velocity components next to the bottom
u, v, w	Velocities in x-, y-, and z-directions
u', v', w'	Turbulent velocity fluctuations
U, V	Unit flow rates in x- and y-directions
U_{ij}, V_{ij}	U- and V-points in the horizontal directions of a unit cell of a numerical grid
$\overline{V}$, $\overline{U}$	Vertically integrated contravariant unit flows
W	Wind speed
z_o	Bottom roughness height
ζ	Water-surface elevation
ζ_{ij}	Water-surface elevation at center of a unit cell in the horizontal direction of a numerical grid
Λ	Macroscale of turbulence
ρ	Density
ρ_o	Typical value for water density

τ_s, τ_b	Surface and bottom shear stresses
τ_x^w, τ_y^w	Wind stress in x- and y-directions

REPORT DOCUMENTATION PAGE

Form Approved
OMB No. 0704-0188

1. AGENCY USE ONLY *(Leave blank)*	2. REPORT DATE	3. REPORT TYPE AND DATES COVERED
	September 1998	Final report

4. TITLE AND SUBTITLE
Assessment of Channel Deepening in the Delaware River and Bay; A Three-Dimensional Numerical Model Study

5. FUNDING NUMBERS

6. AUTHOR(S)
Keu W. Kim, Billy H. Johnson

7. PERFORMING ORGANIZATION NAME(S) AND ADDRESS(ES)
U.S. Army Engineer Waterways Experiment Station
3909 Halls Ferry Road
Vicksburg, MS 39180-6199

8. PERFORMING ORGANIZATION REPORT NUMBER
Technical Report CHL-98-29

9. SPONSORING/MONITORING AGENCY NAME(S) AND ADDRESS(ES)
U.S. Army Engineer District, Philadelphia
Wannamaker Building
100 Penn Square East
Philadelphia, PA 19107-3390

10. SPONSORING/MONITORING AGENCY REPORT NUMBER

11. SUPPLEMENTARY NOTES
Available from National Technical Information Service, 5285 Port Royal Road, Springfield, VA 22161.

12a. DISTRIBUTION/AVAILABILITY STATEMENT
Approved for public release; distribution is unlimited.

12b. DISTRIBUTION CODE

13. ABSTRACT ***(Maximum 200 words)***

A three-dimensional numerical hydrodynamic model has been applied to the Upper Chesapeake Bay-C&D Canal-Delaware River and Bay system. The purpose of the study was to assess the impact of channel deepening in the Delaware River and Delaware Bay on salinity intrusion and circulation. To aid in the modeling study, a field data collection effort was conducted from October 1992 through September 1993. These data were used in the model validation phase of the study as well as to provide boundary conditions for some production runs.

For assessing the impact of channel deepening during low-flow periods, the drought of record that occurred during 1965 was selected to be simulated. Model results for the flow regulation plan of the Delaware River Basin showed that salinities would be slightly increased at Philadelphia with a 1.52-m increase in the depth of the navigation channel, but they would still be below what are considered critical values.

Impacts of channel deepening on salt intrusion for both average and high-flow conditions are also presented. In addition, the numerical model was used to assess the impact of sea level rise and of closing the C&D Canal.

14. SUBJECT TERMS

C&D Canal	Hydrodynamics
Chesapeake Bay	Navigation
Chlorinity	Numerical model
Delaware Bay	Salinity

15. NUMBER OF PAGES
224

16. PRICE CODE

17. SECURITY CLASSIFICATION OF REPORT	18. SECURITY CLASSIFICATION OF THIS PAGE	19. SECURITY CLASSIFICATION OF ABSTRACT	20. LIMITATION OF ABSTRACT
UNCLASSIFIED	UNCLASSIFIED		

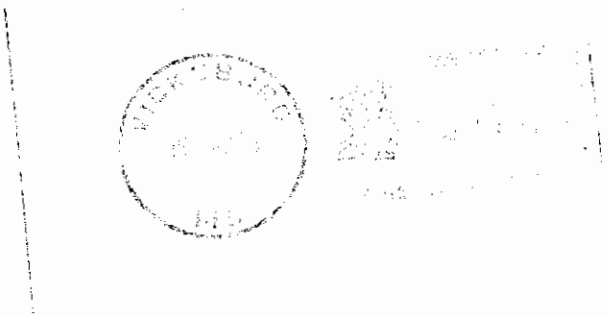

DEPARTMENT OF THE ARMY
WATERWAYS EXPERIMENT STATION, CORPS OF ENGINEERS
3909 HALLS FERRY ROAD
VICKSBURG, MISSISSIPPI 39180-6199

Official Business

SPECIAL
FOURTH CLASS
BOOKS/FILM

1216/L56/ 1
COMMANDER
USAE DISTRICT, PHILADELPHIA
ATTN: C/HYDRAULICS & HYROLOGY BRANCH
WANAMAKER BLDG
100 PENN SQUARE EAST
PHILADELPHIA PA 19107-3390